UAB
Universitat Autònoma de Barcelona

Insights into the functional role of Cytosolic Carboxypeptidases 1 and 6: from interactomics to cell biology

Sergi Rodriguez Calado

PhD program of Biotechnology

2022

Insights into the functional role of Cytosolic Carboxypeptidases 1 and 6: from interactomics to cell biology

Doctoral thesis presented by Sergi Rodriguez Calado
for the degree of PhD in Biotechnology from the
Universitat Autònoma de Barcelona

Thesis supervised by Prof. Julia Lorenzo Rivera

Sergi Rodriguez Calado

Dra. Julia Lorenzo Rivera

Le but de la discussion ne doit pas être la victoire, mais l'amélioration.

- *Joseph Joubert*

A tots aquells que m'heu acompanyat, fent el camí més planer

TABLE OF CONTENTS

TABLE OF CONTENTS

ABBREVIATIONS

ABBREVIATIONS

+TIP	Plus-end tracking protein
2-PMPA	2-(phosphonomethylpentanedioic acid
5'FU	5'fluorouridine
Ac	Acetylation
ACE	Angiotensin-converting enzyme
ActD	Actinomycin D
AGTPBP1	ATP/GTP-1 binding protein
Am	Polyamination
AP	Affinity purification
Arm	Armadillo-like
Asf-1	Anti-silencing function 1
ATCC	American type culture collection
BAP1	Ubiquitin carboxyl-terminal hydrolase
BcCCP	*Burkholderia cenocepacia* cytosolic carboxypeptidase
bCPA	Bovine carboxypeptidase A
BioID	Proximity-dependent biotin identification
BirA	Biotin ligase
bp	Base pair
BrdU	5-bromo-2'deoxyuridine
BSA	Bovine serum albumin
CB	Cajal bodies
CBB	Centriole and basal body
CCP	Cytosolic carboxypeptidase
CCP1	Cytosolic carboxypeptidase 1
CCP2	Cytosolic carboxypeptidase 2

CCP3	Cytosolic carboxypeptidase 3
CCP4	Cytosolic carboxypeptidase 4
CCP5	Cytosolic carboxypeptidase 5
CCP6	Cytosolic carboxypeptidase 6
cGAS	Cyclic GMP-AMP synthase enzyme
CLIP170	Cytoplasmatic linker protein 170
CONDCA	Childhood-onset neurodegeneration with cerebellar atrophy
CP	Carboxypeptidase
CPA1	Carboxypeptidase A1
CPE	Carboxypeptidase E
CSAP	Cilia and spindle-associated protein
Ct	C-terminal
DAPI	4',6-diamidino-2-phenylindole
DFC	Dense fibrillar component
DGKζ	Diacylglycerol kinase ζ
DMEM	Dulbecco's modified eagle's medium
DNA	Deoxyribonucleic acid
DNAJC7	DnaJ homolog subfamily C member 7
DOX	Doxorubicin
EC	Enzyme commission
FC	Fibrillar component
FDR	False discovery rate
FECD8	Fuchs endothelial corneal dystrophy 8
GC	Granular component
GFP	Green fluorescence protein
GO	Gene ontology

GTP	Guanosine triphosphate
HMGB	High mobility group proteins
hnRNA	Heterogeneous nuclear RNA
HP1α	Heterochromatin protein 1α
HRP	Horseradish peroxidase
IFT	Intraflagellar transport system
IL-7Rα	Interleukin-7 subunit alfa
IP	Immunoprecipitation
JS	Joubert syndrome
KO	Knockout
MAP	Microtubule-associated protein
MCP	Metallocarboxypeptidase
MLCK1	Myosin light chain kinase
mRNA	Messenger RNA
MS	Mass spectrometry
MT	Microtubule
MTOC	Microtubule organising centre
MW	Molecular weight
NAP	Nucleosome assembly protein
NAP1L1	Nucleosome assembly protein 1-like 1
NAP1L4	Nucleosome assembly protein 1-like 4
NC-IUBMB	Nomenclature Committee of the International Union of Biochemistry and Molecular Biology
NCP	Nucleosome core particle
NES	Nuclear export sequence
NLS	Nuclear localisation sequence
NNA1	Axotomy-induced nuclear nervous system protein

NOR	Nucleolar organizing regions
Np	Nucleoplasmin
NP-40	Nonidet-P40
Nt	N-terminal
P	Phosphorylation
PaCCP	*Pseudomonas aeruginosa* cytosolic carboxypeptidase
PBS	Phosphate buffered saline
PC	Purkinje cells
pcd	Purkinje cell degeneration
PCM1	Pericentriolar matrix protein 1
PCR	Polymerase chain reaction
PDB	Protein data bank
PEI	Polyethyleneimine
PLA	Proximity ligation assay
PML	Promyelocytic leukaemia
POI	Proteins of interest
PolyE	Polyglutamylation
PPI	Protein-protein interaction
PTM	Post-translational modification
PVDF	Polyvinylidene difluoride
RA	Retinoic acid
RARRES1	Retinoic acid receptor responder 1
rDNA	Ribosomal DNA
RNA	Ribonucleic acid
RNAi	RNA interference
RP75	Retinitis pigmentosa-75

RPGRORF15	X-linked retinitis pigmentosa GTPase regulator
Rpm	Revolutions per minute
rRNA	Ribosomal RNA
RT	Room temperature
SDS-PAGE	Sodium dodecyl sulphate polyacrylamide gel electrophoresis
SEM	Standard deviation of the mean
Shh	Sonic hedgehog
snoRNP	Nucleolar ribonucleoprotein
snRNP	Small nuclear ribonucleoprotein
SVBP	Small vasohibin-binding protein
TBF	TATA binding factor
TRAFD1	TRAF-type zinc finger domain-containing protein 1
TTLD	Transthyretin-like domain
TTLL	Tyrosine ligase-type protein
UBF	Upstream binding factor
VDAC1	Voltage dependent anion channel
WT	Wild type
αTAT1	α-tubulin acetyl transferase
γ-TuRC	*γ-tubulin ring complex*

LIST OF FIGURES AND TABLES

LIST OF FIGURES

LIST OF TABLES

ABSTRACT

ABSTRACT

Proteases are presumed to regulate nearly every biological function, as they represent a considerable percentage of the genome; nevertheless, little is known about the *in vivo* biological roles for many proteases. This is especially true for cytosolic carboxypeptidases, which have suggested functions and implications but are often unknown in terms of their true biological activities and implication in complex cellular processes. The present thesis work reports on the general functional characterisation of CCP1 and CCP6, two deglutamylating enzymes members of the M14D subfamily of metallocarboxypeptidases which have been related with relevant cellular processes. Thus, our research has specifically focused on determining the functional role of CCPs under a biomedical point of view, trying to arise new insights into their implication in health and disease. Cell biology studies, CRISPR/Cas9 knockout generation, high-resolution imaging, and enzymatic activity assessing were all carried out with this goal in mind. Furthermore, a proteomic technique was developed and applied for the study of the carboxypeptidase interactomic landscape.

This thesis work is composed by three interconnected chapters were the cytosolic carboxypeptidases 1 and 6 are functionally characterized.

In the first chapter we aimed for the general characterisation of human CCP1, first focusing on how cells are affected by its loss of activity. CCP1 is the largest member of the CCP family, being the one with the largest number of predicted domains. The elucidation organelle-specific functional roles have long been a factor that has contributed significatively to the study of CCPs. In this chapter have determined general considerations of CCP1 regarding its functional role using the knocking out of the gene in specific cell lines, focusing on its implications in general deglutamylation processes, describing its subcellular localisation, and its specific nuclear functional role.

The second chapter was aimed for the identification of the human CCP1 and CCP6 interactomic landscapes under a biomedical point of view. Unveiling the protein-protein interactions can reveal how they are involved in different processes, providing hints or aid in determining their implication in disease. In this chapter the interactomic landscapes of CCP1 and CCP6 were generated from *in vitro* human cells, identifying new potential interactors and substrates which have allowed us to gain insight into their functional role.

Abstract

The proteomic work performed in this chapter was performed at the Bioscope Group (Universidade Nova de Lisboa, Portugal) headed by Professor Jose Luis Capelo under Dr. Hugo Santos surveillance.

In last chapter we aimed for the characterisation of the conserved N-domain of cytosolic carboxypeptidases, focusing on CCP6 as the minimal CCP expression unit. This characteristic domain is conserved along the evolutionary line, being present in all identified CCPs, but not in other metallocarboxypeptidases. Although an extensive work has been conducted to describe the conserved catalytic domain, little is known about the N-domain and its implication in CCP activity. At present, the only information regarding the N-domain has been obtained from *Caenorhabditis elegans*. In this chapter, we evaluated the effects of this point mutation on the enzymatic activity of human CCP6 while assessing their implications in protein stability, subcellular localisation, and substrate specificity. The experimental work of this chapter was performed in collaboration with Paula Alfonso.

The knowledge and results obtained from this work are the basis of the following book chapters:

Rodriguez-Calado, S., Aviles, F.X., Lorenzo, J. (2022) Cytosolic carboxypeptidase 1. In *Handbook of proteolytic enzymes* (4th ed., chapter 272). Academic Press, Elsevier. Accepted and pending for publication.

Rodriguez-Calado, S., Fricker L.D., Aviles, F.X., Lorenzo, J. (2022) Cytosolic carboxypeptidases 2, 3, 4 and 6. In *Handbook of proteolytic enzymes* (4th ed., chapter 274). Academic Press, Elsevier. Accepted and pending for publication.

Chapter 1. Introduction

1.1 Proteases

A protease is an enzyme that catalyses the hydrolysis of a peptide bond, irreversibly cleaving proteins. They are ubiquitous in nature, being widely distributed among all kingdoms of living organisms as well as viruses (Rawlings & Salvesen, 2013). The complete composite of proteases is defined as the protease degradome, representing about 2% of the genome in higher organisms (Rani et al., 2012). The human genome currently comprises 588 proteolytic enzymes or homologues, forming the second largest enzyme family only after transcription factors (Puente et al., 2005).

Proteolytic enzymes can act as precise modifiers because proteolysis constitutes a type of post-translational modification (PTM) that affects proteins from its synthesis to its degradation. For example, they process newly synthesized proteins to convert them to their active biological forms as they require the removal of the signal peptide. This process, at its time, is also precisely controlled since many proteases are catalytically inactive when synthesized and need to be proteolytically activated at a biologically appropriated time and place (Barrett, 2000). In addition, terminating protein function is also vital to the cell. For instance, the hydrolysis of proteins with signalling functions is needed to keep biological signals fitting an appropriate time and place (Barrett, 2000)

Proteases can regulate the function of proteins by controlling their intra- or extracellular localisation, their activation/deactivation, converting the receptor agonists to antagonists and exposing cryptic neoproteins (López-Otín & Overall, 2002). Their role in posttranslational modifications affect key metabolic reactions that interfere in cell proliferation, cell death, cell signalling, DNA replication, protein catabolism, tissue remodelling, wound healing and immune response among others (King et al., 2014).

Due to their great relevance in living beings, deficiencies or dysregulations of the protease's activity can lead to important human pathologies such as cardiovascular and inflammatory diseases, cancer, osteoporosis, and neurological disorders (Dollery & Libby, 2006; Freije et al., 2003; Murphy & Nagase, 2008; Nalivaeva et al., 2008; Turk, 2006; Varela et al., 2005). Moreover, many infectious microorganisms, viruses and parasites use proteases as virulence factors. In that way, many proteolytic enzymes are an important focus of attention for pharmaceutical industry being currently target of 5-10% of all developing drugs (Meghwanshi et al., 2020).

Even though their ubiquity and conserved structure, they require highly selective drugs to modulate their behaviour. For instance, extracellular secreted proteases are involved in roles ranging from blood pressure regulation (angiotensin-converting enzyme, ACE), blood coagulation (thrombin and factor Xa) and blood glucose regulation (dipeptidyl peptidase 4) (Bond, 2019). These proteases are the target of therapeutics such as the blood pressure drugs lisinopril (Prinivil; Merck & Co.) and aliskiren (Tekturna/Rasilez; Novartis/Speedel), and rivaroxaban (Bayer) (Khan et al., 2020). Intracellular proteases are also popular therapeutic targets in mammalian systems, owing to their involvement in viral infection, cancer, and neurodegeneration. For example, tipranavir (Aptivus; Pfizer/Boehringer Ingelheim) targets the HIV protease (Flexner et al., 2005), and bortezomib (Velcade; Milennium) is a proteasome inhibitor used for the treatment of multiple myeloma and mantle cell lymphoma (Robak & Robak, 2019).

1.1.1   Classification of proteases

Due to the great relevance of proteases to biology and medicine and having into account the high complexity of degradomes in living beings, it is necessary to stablish a standardization system for their classification and nomenclature. The current classification

uses three criteria to fit proteolytic enzymes based on their catalytic type, the type of catalytic reaction catalysed and their structural homology (Rawlings & Barrett, 1999).

1.1.1.1 Catalytic type

The hydrolysis catalysed by peptidases requires a nucleophile attack and is accomplished by means of covalent catalysis and general acid-base catalysis as main mechanisms. To adapt to the wide range of conditions found in complex organisms, proteases use different catalytic mechanisms. Thus, based on the nature of the nucleophilic group participating in the reaction, proteolytic enzymes are classified in seven different classes: aspartic, glutamic, metallo, cysteine, serine, threonine and asparagine as well as a group of unknown mechanism (Table 1.1) (Rawlings et al., 2011; Rawlings & Salvesen, 2013; Turk, 2006).

TABLE 1.1. CATALYTIC TYPE OF PROTEASES AND SELECTED EXAMPLES

MECHANISM	CATALYTIC TYPE	EXAMPLES
ACID-BASE CATALYSIS	Aspartic	Pepsin, Cathepsin E
	Glutamic	Aspergilloglutamic peptidase
	Metallo	Carboxypeptidase A, Thermolysin
COVALENT CATALYSIS	Cysteine	Papain, Cathepsin K
	Serine	Trypsin, Prolyl oligopeptidase
	Threonine	Proteasomal subunits
-	Asparagine	Tsh autotransporter
UNKNOWN	Unknown	Collagenase, gpr endopeptidase

1.1.1.1.1 Structural relationships and homology

Regarding the increasing number of peptidases and their complexity, it was necessary to introduce a more complex classification that considered not only their catalytic mechanism, but also their structure and homology. It was in 1993 when Rawlings and Barrett proposed the MEROPS system using the available sequence data (Rawlings, 2020; Rawlings & Barrett, 1993). This methodology first classifies peptidases into families based on the primary structure of the "peptidase unit" (the part responsible for the proteolytic activity) and is composed around a well-characterised founding member. Clans are then formed grouping

families showing evidence of a common origin. Families that contain groups of peptidases differing in their primary structure are divided in subfamilies. Using the MEROPS system, metallocarboxypeptidases are identified with the letter "M" for the metallo- catalytic type and the number "14" for the specific family. More in detail, in the current work we will focus on the M14D subfamily, the cytosolic carboxypeptidases (CCPs). The complete list can be found at the MEROPS database (http://merops.sanger.ac.uk/).

In 1967, Schechter and Bergen proposed a conceptual model to explain peptidase substrate specificity which has been widely accepted to date (Schechter & Berger, 1967). This model describes the presence of subsites or specificity pockets (S) composed by the residues of the active site that are capable of accommodate the lateral chain of a single amino acid of the substrate (P) in each position. Accordingly, the structure of the active site will specifically determine which substrate residues are able to bind. The authors numbered the enzyme's binding sites from S1 to Sn towards the N-terminus of the substrate and S1' to Sn' towards the C-terminus. Analogously, the substrate amino acids accommodate in these binding sites are numbered P1 to Pn and P1' to Pn', where the peptide bound between P1 and P1' is the site of cleaving (Figure 1.1).
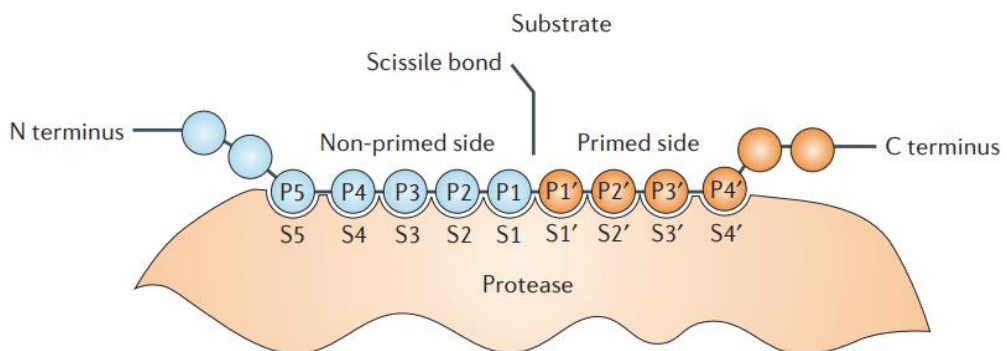
FIGURE 1.1. SCHEMATIC REPRESENTATION OF THE MODEL OF SCHNEIDER & BERGEN. Schematic diagram of a protease binding a peptide substrate. The diagram shows the active site of a protease, in which are represented the locations of its specificity pockets (called S1 to Sn and S1' to Sn'). The enzyme accommodates several residues from the substrate numbered from P1 to Pn and P1' to Pn'. The primed sites correspond to the C-terminal region sequence from the scissile bond and the non-primed side to the N-terminal.

However, the recognition region of the active site of proteases is not a rigid structure. A cooperation model has been described where the binding of one substrate's residue with the subsite enhances the binding of the next residue (Schilling et al., 2011). In exopeptidases, the cleft is likely to be "blind" on one side, no extending beyond S1 for an aminopeptidase or S1' for a carboxypeptidase.

1.1.2   Metallocarboxypeptidases

Regarding the site of cleavage, the focus of this thesis is the carboxypeptidases (CPs), a type of exopeptidases. Carboxypeptidases catalyse the hydrolysis of C-terminal peptide bonds of proteins or peptides releasing a single residue in each hydrolytic cycle. Based on their catalytic mechanism, they are classified into serine-carboxypeptidases (EC 3.4.16), metallo-carboxypeptidases (MCP) (EC 3.4.17) and cysteine-carboxypeptidases (EC 3.4.18) (Rawlings et al., 2004). Metallo-carboxypeptidases englobes a diverse group of CPs which use a coordinated divalent metal ion to catalyse the hydrolysis of peptide bonds. Following the MEROPS classification, a total of six families contains MCPs, although only three of them are found in human beings.

These peptidases are widely characterized and encode for more than 26 genes in the human genome, most of them included into the M14 family, the most numerous in number of enzymes and subfamilies (Fernández et al., 2010).

1.1.2.1   M14 family

The M14 family is composed of four subfamilies based on similarities in their primary amino acid sequence in zinc-binding domains ranging from M14A to M14D (Table 1.2). Between the members of the same subfamily there is a sequential identity of 25-63%, while, in the comparison between two subfamilies, this sequential identity drops to 15-25% (Arolas et al., 2007). Members of the M14 family contain a common CP catalytic domain that houses the active centre of the enzyme with all the residues required for catalysis and substrate binding conserved. In addition, one zinc ion per molecule essential for catalysis is located tetra-coordinated with two His, one Glu and one molecule of water. One of the His and Glu are part of the His-XX-Glu zinc binding motif characteristic of this family, while the third ligand corresponds to a His that is more than 100 residues towards the C-terminus of this motif (Table 1.2).

TABLE 1.2. CLASSIFICATION OF M14 CARBOXYPEPTIDASES

CATALYTIC CLASS	MEROPS FAMILY	REFERENCE PROTEASE	CATALYTIC RESIDUES
Metallo	**M14** Subfamily A	Carboxypeptidase A1 - *H. sapiens*	**HXXE...H**
	M14 Subfamily B	Carboxypeptidase E - *Bos Taurus*	
	M14 Subfamily C	Gamma-D glutamyl-(L)-meso-diaminopimelate peptidase I - *Lysinibacillus sphaericus*	
	M14 Subfamily D	Cytosolic carboxypeptidase 6 - *H. sapiens*	

The M14A subfamily is structurally very uniform, and its members are secreted as zymogens (inactive precursors) with a signal peptide of about 15-22 residues long. They are also known as procarboxypeptidases, as they include a 90-95 residues long region located at the N-terminus of the catalytic domain which blocks the access to the active site of the enzyme, making it latent until further activation (Arolas et al., 2007). However, two mammalian M14A MCPs do not follow this principle; CPA3 that is stored in mast cell granules as an active enzyme (Pejler et al., 2009) and regulates the innate immune responses and mast cell granule homeostasis (Pejler et al., 2009), and CPA6 whose activation occurs in the secretory pathway being secreted in an active form (Lyons et al., 2008). Although they were first defined as digestive enzymes in the gastrointestinal system, many proteases of this subfamily are involved in other processes, such the plasma circulating enzyme CPU (also named thrombin activatable fibrinolysis inhibitor, TAFI) that displays anti-fibrinolytic activity (Declerck, 2011). CPA3 Another noteworthy member is the CPA4 which has been linked to prostate cancer aggressiveness (Ross et al., 2009).

The M14B subfamily is more variable structurally than M14A enzymes and are secreted in an enzymatically active form, not needing zymogen activation. At the C-terminus of the catalytic domain, they contain an 80-90 residues long domain homologue to transthyretin (transthyretin-like domain, TTLD). Generally, M14B metallo-carboxypeptidases favour substrates with a basic C-terminal residue (Arg or Lys) and englobe a broad substrate specificity being primarily secreted or membrane-bound. CPE and CPD play a role in biosynthesis of neuroendocrine peptides at the late secretory pathway and the trans Golgi network respectively (Reznik & Fricker, 2001). Processing of peptide hormones is also

participated by CPN and CPM members, being the CPN the major blood inactivator of potent peptides such as kinins (Vendrell et al., 2000). In constrast, CPZ has been not widely studied, and its exact function is still unknown; it has been proposed that it plays a role in the processing of neuropeptides and growth factors through the interaction with Wnt proteins (Reznik & Fricker, 2001).

The M14C subfamily is composed by a single member, the bacterial enzyme γ-D-glutamyl-(L)-meso-diaminopimelate peptidase I. This enzyme participates in bacterial sporulation playing a role in the metabolism of the bacterial wall peptidoglycan (Guinand et al., 1979).

The M14D has been the last M14 MCP subfamily discovered and was first described by Rodriguez de la Vega and Kalinina simultaneously providing phylogenetic studies (Kalinina et al., 2007; Rodriguez de la Vega et al., 2007). This subfamily is composed by six enzymes named cytosolic carboxypeptidases (CCP1 to CCP6) which share a common catalytic domain, and a N-terminal conserved domain of 150 residues with a β-sandwich fold (Otero et al., 2012). Differently, all the enzymes composing this subfamily show a cytosolic or nuclear localisation instead of being secreted. They act as deglutamylating enzymes, controlling the length of the PTM known as polyglutamylation (Rogowski et al., 2010; Tort et al., 2014). Although polyglutamylation was discovered first in both α and β tubulin (Alexander et al., 1991), later works found a broader spectrum of proteins that could also be affected (van Dijk et al., 2008). It is believed that tubulin polyglutamylation regulates cell functions such as the cell cycle and neuronal differentiation, where CCPs will play a key role as we will be further discussing in this work.

The bovine carboxypeptidase A (bCPA) was the first characterised MCP of the M14 family after its isolation from pancreatic extracts. Its high-resolution structure was elucidated in 1986 by Christianson and Lipscomb (Christianson & Lipscomb, 1986). Bovine CPA presents a zinc coordinated atom with His69, Glu72 and His196, while the fourth ligand is a water molecule (Figure 1.2). The catalysis of the substrate is done by the direct participation of Arg127 and Glu270 (Kilshtain-Vardi et al., 2003); from now on, this will be used as the reference numbering for MCPs of the M14 family.
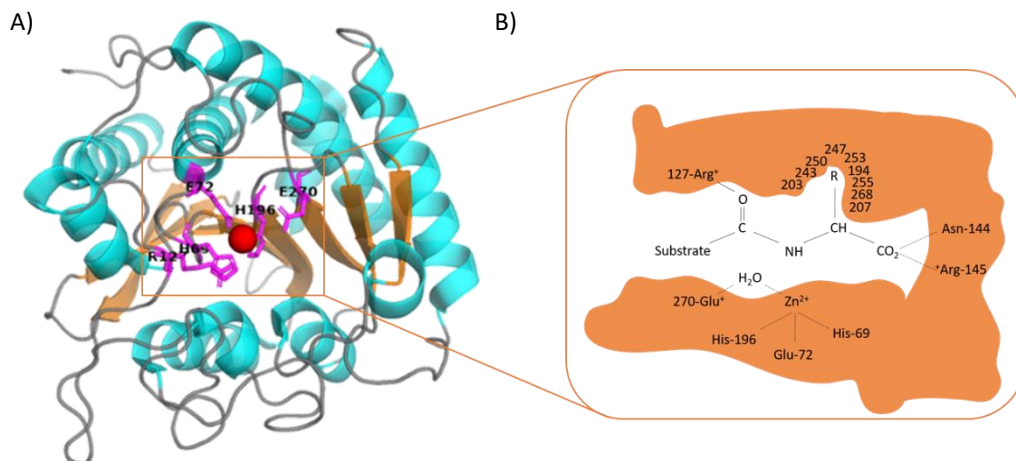
Figure 1.2. Representative structure of the catalytic domain and active site residues of MCPs. (A) Ribbonrepresentation of the three-dimensional structure of the catalytic domain of bCPA (PDB 1M4L). The α-helices and β-strands are shown in orange and cyan, respectively. The sides chains of the main residues involved in zinc binding (H69, E72 and H196) and in the catalytic mechanism (E270 and R127) are depicted in magenta. The metal Zn^{2+} ion is shown as a red sphere. Image generated with PyMOL. **(B)** Scheme of the substrate-binding residues shaping the S1' pocket in the active site of carboxypeptidases from the M14A family. Residues are numbered after active bovine CPA. Adapted from (Tanco et al., 2010).

1.1.3 Cytosolic Carboxypeptidases

The focus of study of this PhD work is the study of CCP1 and CCP6 and their implications in the cell survival processes. As we mentioned before, the M14D subfamily was the last subfamily identified and was first described by our research group (Rodriguez de la Vega et al., 2007). Unlike the other subfamilies, CCPs are intracellular, present both in the cytosol and in other cell compartments (Guinand et al., 1979; Rodriguez de la Vega et al., 2007). The number of genes coding for CCPs is variable, from a single gene in proteobacteria to 32 genes in the hairy protozoan *Paramecium tetraurelia*.

According to the chronological order in which they were discovered, as human genome codes for 6 hCCPs they were named: hCCP1, hCCP2, hCCP3, hCCP4, hCCP5 and hCCP6 (Table 1.3). All human CCPs act as a deglutamylating enzymes, controlling the length of the post-translational modification known as polyglutamylation (Rogowski et al., 2010; Tort et al., 2014).

TABLE 1.3. GENE AND PROTEIN SYMBOLS OF HUMAN CCPs

M14D CLUSTER	HUMAN GENE SYMBOL	PROTEIN SYMBOL
M14D3	AGTPBP1, NNA1	CCP1, AGTPBP1, NNA1
	AGBL1	CCP4, AGBL1
M14D4	AGBL2	CCP2, AGBL2
	AGBL3	CCP3, AGBL3
M14D2	AGBL4	CCP6, AGBL4
	AGBL5	CCP5, AGBL5

1.1.3.1   Cytosolic carboxypeptidase 1

CCP1 (also called axotomy-induced nuclear nervous system protein (NNA1) or ATP/GTP-1 binding protein (AGTPBP1)) was the first discovered and most studied member of the M14D subfamily of MCPs, largely due to the early discovery of the Purkinje cell degeneration (*pcd*) mouse and its well-characterized phenotype (Mullen et al., 1976). It was identified in 2000 by Harris *et al*. in the search for overexpressed mRNAs in the motor neurons of the spinal cord of mice with the sciatic nerve clamped or surgically transected. CCP1 mRNA levels were found to be increased during axogenesis and reinnervation of the axotomized sciatic nerve (Harris et al., 2000).

The CCP1 orthologs are the largest M14D subfamily MCPs, reaching 1,200 residues in length. They contain long N-terminal extensions with highly conserved motifs, presumably related to protein-protein and protein-DNA interaction (Figure 1.3). Furthermore, it contains a nuclear export sequence (NES) that allows its binding to the nuclear export receptor CRM1 and its consequent translocation to the cytoplasm, and a nuclear localisation sequence (NLS) that allows their continuous translocation (Thakar et al., 2013). CCP1 is expressed in most tissues, being especially abundant in the central nervous system and in testis (Kalinina et al., 2007; Tort et al., 2014).

At the subcellular level it is located in the cytoplasm and the nucleus, showing a granular distribution in the nucleus of the interphase and dividing cells. Its nuclear function is unknown, although it could be related to DNA repair processes. Moreover, it has been shown that loss of CCP1 in the *pcd* mouse induces a p53-dependent nucleolar stress, characterised by nucleolar fragmentation, mislocalisation of nucleolin and disfunction of

pre-rRNA processing and mRNA translation (Baltanás et al., 2019). On the other hand, the role of CCP1 in its cytoplasmic localisation is associated with the assembly and elongation of MTs at the centriole and basal body (CBB) level for the formation of the cilia and flagella axoneme, reinnervation and axogenesis, and cell division. In *Caenorhabditis elegans*, the loss of function of Ccpp-1 (homologue to hCCP1) causes the progressive deterioration of the ciliary axoneme that is part of the sensory organs amphidium and fasmidium, suggesting that it is necessary for the maintenance of the structural integrity of the cilia and not for ciliogenesis (Kimura et al., 2010). Furthermore, the reduction of CCP1 expression mediated by RNA interference (RNAi) in human cell lines causes a reduction in the length of cell cilia (J. Kim et al., 2010; Rodríguez de la Vega et al., 2013). Ccpp-1 also regulates the ciliary localisation of the kinesin-3 and polycystin PKD-2 motor proteins in *C. elegans* sensory neurons (O'Hagan et al., 2011). Numerous studies in the ataxic *pcd* mouse due to loss of function of CCP1 indicate that this MCP is essential for the survival and neuronal function of Purkinje cells (PC) of the cerebellum, mitral neurons of the olfactory bulb and certain thalamic neurons, for the prevention of retinal photoreceptor degeneration, spermatogenesis, and sperm motility (Berezniuk et al., 2012; Mullen et al., 1976; Rogowski et al., 2010). Later studies in *pcd* mice, shows that CCP1 promotes mitochondrial fusion and motility to prevent cell death of Purkinje cell neurons (Gilmore-Hall et al., 2019)

In addition, a similar phenotype has been described in sheep due to a mutation in the catalytic domain (R970P) of the ovine CCP1 ortholog, in which the affected sheep have a profound tetraplegia at one week of age (Zhao et al., 2012). In *Caenorhabditis elegans*, the loss of function of Ccpp-1 (homologue to hCCP1) causes the progressive deterioration of the ciliary axoneme, that is part of the sensory organs amphidium and fasmidium, suggesting that it is necessary for the maintenance of the structural integrity of the cilia but not for ciliogenesis (Kimura et al., 2010). Ccpp-1 also regulates the ciliary localisation of the kinesin-3 and polycystin PKD-2 motor proteins in *C. elegans* sensory neurons (O'Hagan et al., 2011). In humans, mutations in the CCP1 gene have been correlated with childhood-onset neurodegeneration with cerebellar atrophy (CONDCA), with a similar phenotype to the ataxic disease in *pcd* mice (Shashi et al., 2018). Furthermore, the reduction of CCP1 expression mediated by RNA interference in human cell lines causes a reduction in the length of cell cilia (Kim et al., 2010; Rodríguez de la Vega et al., 2013).

1.1.3.2   Cytosolic carboxypeptidase 2

The CCP2 orthologs have a size that varies between 400-1000 residues depending on the presence or not of N and C-terminal extensions in the different isoforms of the enzyme. In addition, they contain two well-preserved motifs in the N and C-terminal region (Figure 1.3).

CCP2 is expressed mainly in the testes, trachea, and lung, although it is also detected in the cerebellum, olfactory bulb, and kidney (Kalinina et al., 2007; Tort et al., 2014). At the subcellular level, CCP2 co-localises with γ-tubulin from the centrioles in all phases of the cell cycle and with polyglutamylated tubulin from the basal bodies in ciliated HeLa cells. The major expression of CCP2 in tissues containing mobile hair cells suggests a specialized role for this MCP in the assembly or functionality of the cilia. In 2014, Tort *et al.* demonstrated their importance during the ciliogenesis process. Mice deficient in the Agbl2 gene encoding for CCP2, and the double deficient for the Agbl2 and Agbl3 genes encoding for CCP2 and CCP3, respectively, are viable and do not show obvious phenotypic alterations. However, the double deficient mouse shows increased levels of polyglutamylation in the tubulin of the testes and sperm (Tort et al., 2014). It has recently been shown that the retinoic acid receptor responder 1 (RARRES1) interacts with CCP2, inhibiting its role in tubulin deglutamylation. This inhibition regulates the mitochondrial voltage dependent anion channel (VDAC1), modulating tubulin-mitochondrial interaction, a fundamental regulator of cancer and stem cell metabolism (Maimouni et al., 2019).

Other than tubulin, the interleukin-7 receptor subunit alfa (IL-7Rα) has been identified as a substrate of CCP2. Glutamylation and deglutamylation of this interleukin controls the development of group 3 innate lymphoid cells which promotes lymphoid oncogenesis (Liu et al., 2017).

1.1.3.3   Cytosolic carboxypeptidase 3

CCP3 orthologs range in size from 400-1000 residues depending on the presence or absence of N and C-terminal extensions in the different isoforms of the enzyme. They also contain the two well-conserved motifs present in CCP2 in the N and C-terminal region (Figure 1.3).

CCP3 is primarily expressed in the testes, trachea, and lung, although it is also expressed at moderate levels in the eye, adipose tissue, and kidney (Kalinina et al., 2007; Tort et al.,

2014). In the same way as CCP2, the high expression of CCP3 in tissues containing mobile hair cells suggests an important role for this enzyme in the assembly or functionality of the cilia. The mouse deficient in the *Agbl3* gene coding for CCP3, and the double deficient for the *Agbl2* and *Agbl3* genes coding for CCP2 and CCP3, respectively, are viable mice that do not show obvious phenotypic alterations, although in the latter case the levels of polyglutamylation in tubulin of the testes and sperm are increased (Tort et al., 2014).

Apart from tubulin, the ubiquitin carboxyl-terminal hydrolase (BAP1) has been recently described as a substrate for CCP3. CCP3 deglutamylase activity promotes BAP1 stability, which in turn enhances *Hoxa1* expression leading to hematopoietic stem cells self-renewal (Xiong et al., 2020).

1.1.3.4   Cytosolic carboxypeptidase 4

The orthologs of CCP4 are similar in size and architecture to CCP1, reaching ~1000 residues in length (Figure 1.3). They contain long N-terminal extensions with highly conserved motifs presumably related to protein-protein and protein-DNA interaction.

CCP4 is primarily expressed in the trachea, muscle, and eye, and its mRNA is undetectable in most organs. Its very restricted location suggests a highly specialized function in these tissues (Kalinina et al., 2007; Tort et al., 2014). The role of CCP4 orthologs has been bioinformatically predicted and is associated with the assembly and elongation of MTs at the CBB level for axoneme formation of cilia and flagella. In the zebrafish, an ortholog of the CCP4 gene has been described, but the mRNA corresponding to the expression of the gene has not been detected. The absence of the mRNA coding for CCP4 could be due to the fact that it is expressed at very low levels, in a certain cell type or that it actually corresponds to a pseudogene. In *C. elegans,* there is no CCP4 ortholog, and no *in vivo* functional characterization studies based on reduced expression and/or deficiency of the gene encoding CCP4 have yet been performed in mice.

1.1.3.5   Cytosolic carboxypeptidase 5

The CCP5 orthologs range between 700-800 residues, with an extensive catalytic domain adjacent to a characteristic domain enriched in prolines (Pro-rich domain). It is the only member of the M14 family of MCPs that has two insertions in the catalytic domain, the functional relevance of which is unknown. The smallest has 20 residues in length and is

located in the β2-β3 loop, while the largest has 80 residues and affects the α5-β5 loop (Figure 1.3).

CCP5 is primarily expressed in testes and appears to play an important role in the reproductive physiology of male mice (Kalinina et al., 2007; Tort et al., 2014). It is located in the nucleus of interphase HeLa cells, the mitotic spindle, and the midbody formed during cytokinesis in cell division. The nuclear role of CCP5 is unknown, but its cytoplasmic localisation appears to play an important role in cell division and meiosis during spermatogenesis. Furthermore, its function is also related to motor functions associated with cilia motility and ciliogenesis. Ccp5 is the main deglutamylase in the cilia of zebrafish and plays a very important role in ciliogenesis (Pathak et al., 2014). Reduced expression of the gene encoding CCP5 causes curvature of the fish body, cyst formation in the protonephridium ducts, and hydrocephalus due to enlargement of the cerebral ventricles caused by the paralysis of the cilia of the ependyma and accumulation of cerebrospinal fluid. (Berezniuk et al., 2013; Lyons et al., 2013; H. Y. Wu et al., 2017). The mouse deficient in the *Agbl5* gene encoding for CCP5 is sterile and has restricted involvement of the testes consisting of defective spermatogenesis (Giordano et al., 2019). Finally, another study related to the CCP5-deficient mouse revealed a new role for this MCP in regulating the innate response to viral DNA by controlling the levels of glutamylation of the cyclic GMP-AMP synthase enzyme (cGAS) (Xia et al., 2016).

In humans, it has been observed that CCP5 may have a key role in axoneme polyglutamylation, as the regulation of glutamylation levels is a major contributor for cilia signalling and is necessary for the correct signalling defects in ciliopathies (K. He et al., 2018).

1.1.3.6   Cytosolic carboxypeptidase 6

The CCP6 orthologs make up the M14D subfamily MCPs in simpler eukaryotes, ranging in size from 400-500 residues in length. Basically, they are formed by the N-terminal pro-domain and the CP catalytic domain, with very small extensions at the N and C-terminal of the protein (Figure 1.3).

CCP6 is mainly expressed in the central nervous system, testes and kidney, and its presence is also detectable in the eye and trachea (Kalinina 2007, Tort 2014). It co-locates with the γ-tubulin of the centrioles in the interphase and mitotic cells, and with the golgin

protein GM130 in the Golgi apparatus. In addition, CCP6 has been detected in the basal bodies of NIH-3T3 hair cells (Rodríguez de la Vega et al., 2013).

The ancestral function of CCP6 orthologs is related to the assembly of CBBs and flagellar motility, in addition to a sensory function associated with primary cilia. In *C. elegans* it has been shown that Ccp-6 is required for axogenesis and reinnervation of axons from axotomized neurons (Ghosh-Roy et al., 2012). The mouse deficient in the *Agbl4* gene encoding CCP6 has underdeveloped megakaryocytes and dysfunctional platelets due to defective megakaryopoiesis, causing thrombocytosis and prolonged bleeding times. Consequently, CCP6 has been proposed to be essential in the maturation process of megakaryocytes in the bone marrow (Ye et al., 2014). Another study with the mouse deficient in the *Agbl4* gene revealed a new function for CCP6 related to the regulation of the innate response to viral DNA by controlling glutamylation levels of cGAS. Polyglutamylation of the cGAS viral DNA sensor prevents binding of exogenous DNA to the protein, and therefore CCP6 deficiency increases susceptibility to DNA virus infection (Xia et al., 2016). In addition, CCP6 has been related to Klf4 deglutamylation, playing a critical role in cell reprogramming and early embryonic development in mice (Ye et al., 2018).

In humans, a recent study links CCP6 with cancer, since it has been shown that patients with renal adenocarcinoma have a decrease in the expression of CCP6 that leads to the accumulation of the polyglutamylated DNAJC7 protein. The co-chaperone DNAJC7 represents a new substrate for CCP6 and has been proposed as a blood biomarker for the early detection of kidney cancer (C. Li et al., 2016).

1.1.3.7 Structural domains of CCPs

The human CCP subfamily is formed by monomeric proteins with a molecular weight varying from 58 KDa to 138 KDa that are secreted in their active form and do not contain disulphide bridges or glycosylations in their structure. They share a catalytic carboxypeptidase domain of about 300 residues and a conserved adjacent N-terminal domain of about 150 residues, which is unique to this MCP subfamily and will be further discussed. Members of the M14D subfamily of higher eukaryotes are structurally very heterogeneous and contain additional N-t and C-t domains and extensions (Figure 1.3). Most do not share homology with other known domains and have hardly been characterized.

Some of these N-terminal and C-terminal domains and extensions may have a regulatory role in the specific localisation in certain cellular structures and in the interaction with other proteins or nucleic acids to perform their function (Rodríguez de la Vega et al., 2013). For instance, CCP1 and CCP4 share an armadillo-like (Arm) domain at the N-terminus that could be implicated in protein/protein interaction or protein/nucleic acid interaction (Madhurantakam et al., 2012).

Bacterial CCPs are simpler and more structurally uniform than eukaryotic CCPs. They basically consist of the CP catalytic domain, the adjacent N-terminal pro-domain of about 150 residues and a few small N-terminal and C-terminal extensions. However, although the CCP of *Pseudomonas aureginosa* (PaCCP) is a monomeric protein, the bacterial CCPs of *Shewanella denitrificans*, *Burkholderia mallei*, and *Burkholderia cenocepacia* (BcCCP) are oligomeric proteins. Besides, some bacterial CCPs show a secreting peptide signal at their N-terminal end which suggests that they could be secreted to the extracellular matrix, whereas eukaryotic CCPs do not contain any SP, confirming their intracellular location.
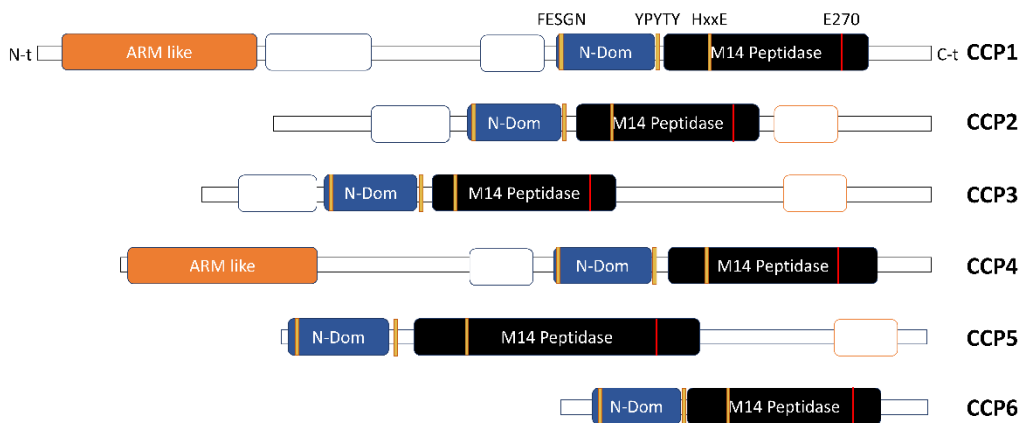
FIGURE 1.3. SCHEMATIC REPRESENTATION OF THE DOMAIN STRUCTURES OF M14D SUBFAMILY MEMBERS IDENTIFIED IN HUMANS. All members of the M14 subfamily of MCPs contain a carboxypeptidase M14 catalytic domain (Peptidase M14, shown in dark blue) and an N-terminal domain (N$_T$-Pro, shown in blue). Furthermore, all members have additional domains in the N-terminal and/or C-terminal region.

1.1.3.7.1   Carboxypeptidase catalytic domain

Cytosolic carboxypeptidases display a typical carboxypeptidase catalytic domain particular of the M14 peptidases. Although mammalian CCPs' structure has not yet been elucidated in a high-resolution format, structural modelling based on bacterial CCPs structures are capable to suggest their folding (Otero et al., 2012; Rimsa et al., 2014). These models suggest the catalytic domain display the typical M14 fold containing an α/β/α sandwich structure with an antiparallel β-sheet of eight strands (Figure 1.4A). Regarding the active site, the zinc atom is penta-coordinated with two His residues (H69 and H196), one Glu residue (E72) and a water molecule, sharing the same conformation described in A/B and N/E MCPs subfamilies (Figure 1.4B). Other conserved residues include R127 and E270 which are responsible to the bind to the carbonyl bond of the cleavage site and to transfer a proton from the water molecule to the leaving amine, respectively in other MCPs. In addition, they also share the NPDG motif, which presumably plays a role in the structure or interaction of the catalytic domain (Otero et al., 2012).
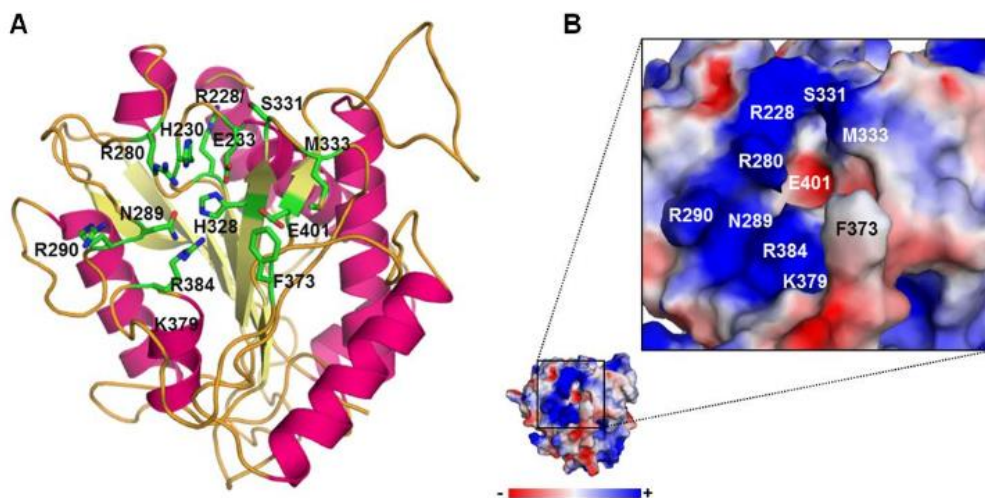
FIGURE 1.4. ANALYSIS OF KEY RESIDUES OF THE ACTIVE CENTRE OF HUMAN CCP6. (A) Cartoon representation of the CP catalytic domain of hCCP6, showing the set of identical amino acids in the M14 family MCPs (HXXE + R + NR + H + Y (F) + E), numbered according to their position in the amino acid sequence of hCCP6. The α-helices and β-strains are shown in magenta and yellow, respectively. Amino acids are represented in bars, and carbon atoms are colored green, nitrogen blue, oxygen red, and sulfur yellow. (B) Representation of the surface electrostatic potential of the catalytic domain of hCCP6 shown as a colour gradient, including red (-60 KbT/ec), white (0 KbT/ec) and blue (+60 KbT/ec). The basic residues are indicated in blue and the acids in red. Both figures have been generated with PyMOL.

TABLE 1.4. CONSERVED RESIDUES OF HCCPs.

		bCPA	hCCP1	hCCP2	hCCP3	hCCP4	hCCP5	hCCP6
Zinc binding site		His69	His920	His462	His364	His804	His252	His230
		Glu72	Glu923	Glu465	Glu367	Glu807	Glu255	Glu233
		His196	His1017	His558	His460	His901	His434	His328
Catalysis		Arg127	Arg970	Arg512	Arg414	Arg854	Arg303	Arg280
		Glu270	Glu1102	Glu630	Glu534	Glu986	Glu516	Glu401
Substrate binding		Asn144	Asn979	Asn521	Asn423	Asn863	Asn312	Asn289
		Arg145	Arg980	Arg522	Arg424	Arg864	Arg313	Arg290
		Tyr248	Phe1075	Phe604	Phe508	Phe959	Phe479	Phe373
S1' specificity pocket		Ser194	Asp1015	Asp556	Asp458	Asp899	Asp432	Asp326
		Leu203	Val1025	Ile566	Ile468	Val909	Cys442	Gly336
		Gly207	Gly1029	Gly570	Gly472	Gly913	Gly446	Gly340
		Ile243	Met1070	Phe599	Phe503	Met954	Phe474	Tyr368
		Ile247	Ser1074	Asn603	Lys507	Ser958	Asn478	Ser372
		Ala250	Lys1081	Lys610	Lys514	Arg965	Lys495	Lys379
		Gly253	Thr1084	Thr613	Thr517	Thr968	Ser498	Thr382
		Ile255	Arg1086	Arg615	Arg519	Arg970	Arg500	Arg384
		Thr268	Thr1100	Thr628	Thr532	Thr948	Thr514	Thr399

A further analysis of the putative binding site shows the presence of an asparagine and an arginine at positions 144 and 145 of the S1' site, which bind to C-terminal carboxylate group of the substrate. Additionally, all six hCCPs conserve an arginine in position 255 (I255 for bCPA) which determine the specificity of substrate for the subfamily; the basic nature of this residue could explain the preference of an acidic substrate. Furthermore, the presence of a lysine or an arginine equivalent to position 250 in the active bCPA would also contribute to promoting a basic environment that facilitates the preference for acidic residues (Table 1.4, Figure 1.4) (García Guerrero, 2017).

1.1.3.7.2   N-terminal pro-domain

Members of the M14D subfamily contain a conserved N-terminal domain adjacent to the characteristic catalytic carboxypeptidase domain which do not show neither structural nor sequential homology to any other domain of known proteins (Rodriguez de la Vega et al., 2007). Folding and structure of this domain in mammals has been inferred from structures of the bacterial CCPs of the microorganisms *P. aeruginosa* (PDB:4A37), *B. cenocepacia* (PDB:4B6Z), *B. mallei* (PDB:3K2K) and *S. denitrificans* (PDB:3L2N), as any 3D structures have not been yet obtained for any mammalian CCP. Observing the obtained bacterial structures, the N-terminal pro-domain is about 100 residues long and has a β-sandwich fold consisting of a total of 9 β-strands, structure never described before in any other protein. In addition, it contains three highly conserved motifs that could participate in its correct folding or substrate recognition.
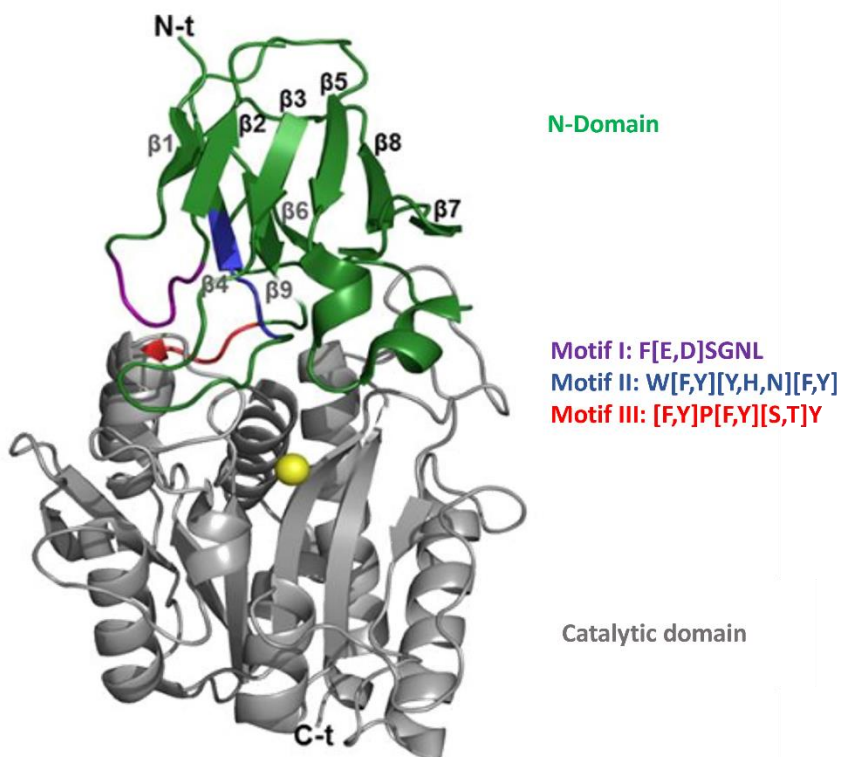
FIGURE 1.5. THREE-DIMENSIONAL STRUCTURE OF THE CCP OF PSEUDOMONAS AERUGINOSA. Cartoon representation of the structure of the PaCCP (PDB: 4A37) showing the catalytic domain CP (gray) and the N-domain (green). The N-domain motifs are shown in purple (motif I), blue (motif II) and red (motif III). The secondary structure elements in the N-domain are numbered. The catalytic zinc ion is shown as a yellow sphere. Image generated with PyMOL.

Motif I (F[E,D]SGNL) is the closest one to the N-terminal end, located in the loop between the chains β1 and β3. Motif II (W[F,Y][Y,H,N][F,Y]) is located 60 residues away from motif I as part of the β4-chain and contributes significantly to the formation of the hydrophobic nucleus together to other aromatic residues. Motif III ([F,Y]P[F,Y][S,T]Y) is located at the C-terminal end of the pro-domain and represents the end of this domain before the catalytic CP domain (Figure 1.5) (Rimsa et al., 2014).

The orientation of the N-terminal pro-domain with respect to the catalytic domain partially blocks the entrance to the active centre, leaving a small open channel accessible to the solvent. Multiple conserved residues in the N-terminal pro-domain of bacterial and eukaryotic CCPs are in direct contact through polar, hydrophobic, and van der Waals interactions with the catalytic domain CP (Otero et al., 2012).

1.1.3.7.3   Arm-like domain

The Arm-like domain is only present in two members of the human CCP family, hCCP1 and hCCP4 (Figure 1.3). This domain consists of a multi-helical fold comprising two curved layers of alpha helices arranged in a regular right-handed superhelix, where the repeats that make up this structure are arranged about a common axis (Groves & Barford, 1999). These superhelical structures present an extensive solvent-accessible surface that is well suited to binding large substrates such as proteins and nucleic acids. They also have been found as key molecule for nuclear import by the recruitment of nuclear localisation sequences to importin-α in a classical import pathway of cargo molecules to the nucleus (Pumroy & Cingolani, 2015). The presence of this domain could be key for the nuclear localisation of CCP1 and should have a role in its nuclear function by its nucleic acid binding properties.

1.1.3.8   Catalytic function

Human CCPs have been shown to catalyse the cleavage of genetically encoded glutamine at the C-terminal as well as post-translationally added polyglutamate side chains of proteins (phenomena known as polyglutamylation) (Berezniuk et al., 2012; Rogowski et al., 2010). However, for their bacterial counterparts PaCCP and BcCCP, no substrates have been identified to date *in vivo* or *in vitro* despite multiple efforts, and their possible role in the bacterial cell is unknown. The best-known functional relationship with CCPs is related to tubulin. CCPs catalyse the excision of genetically encoded Glu at the C-terminal end of

detyrosinated α-tubulin, generating Δ-2 and Δ3-tubulin. In addition, as PTM, CCPs also catalyse the deglutamylation of the lateral chain of glutamic acid (poly-E) of the subunits α- and β-tubulin (Figure 1.6).
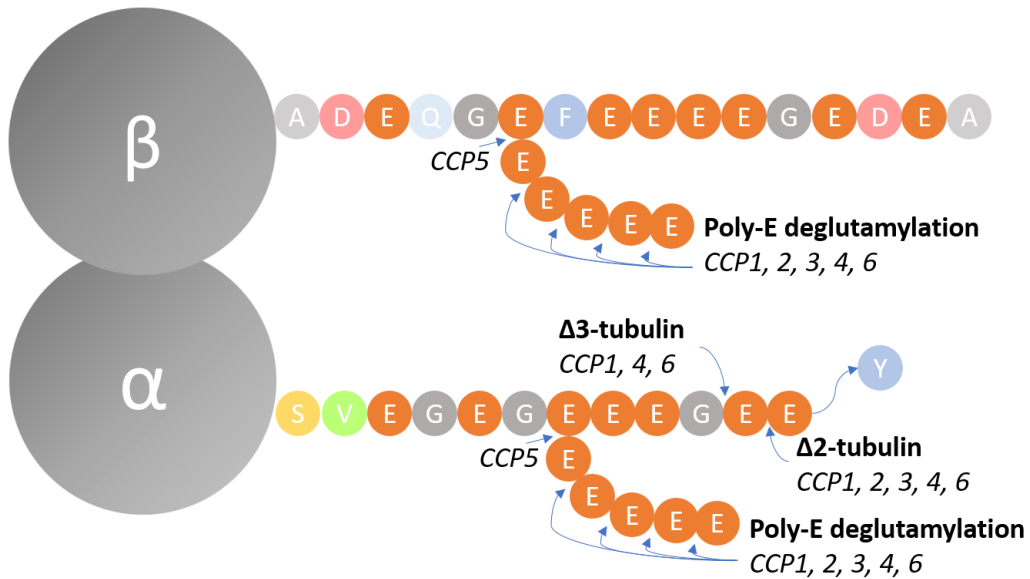
FIGURE 1.6. SCHEMATIC REPRESENTATION OF THE PTMS CATALYSED BY THE MCPS OF THE M14D SUBFAMILY. CCPs are tubulin deglutamylases with different substrate specificities that catalyse the elimination of post-translationally generated Glu side chains in the C-terminal tail of the α- and β-tubulin subunits, and the Glu genetically encoded at the C-terminal end of the detyrosinated α-tubulin, generating Δ2- and Δ3-tubulin. CCP5 is the only enzyme capable of removing the first Glu from the branch point of the poly-E side chain. The Tyr cleaved by vasohibin proteins at the C-terminal end of the α-tubulin is represented as a blue circle. Amino acids are indicated in a letter code and coloured according to their biochemical properties. The C-terminal sequence of α- and β-tubulin corresponds to the isotypes βIa and βIIb, respectively.

In addition to tubulin, some CCPs also act on other substrates with extensions of C-terminal acidic residues encoded in their primary sequence, such as myosin light chain kinase (MLCK1) and high mobility group proteins (HMGB) among many other potential substrates that have not yet been evaluated (Rogowski et al., 2010; Tanco et al., 2015; Tort et al., 2014). Recent studies demonstrate that hCCP1 and mCCP3 are capable of hydrolysing C-terminal Asp as well, revealing a new deaspartilase activity not described to date for members of this subfamily (Tort et al., 2014).

1.1.3.8.1   *Deglutamylation*

Polyglutamylation is a PTM present in the microtubules (MT) of the mitotic spindle, neuronal axons, centrioles, basal bodies, and axonemes of cilia and flagella. The presence of deglutamylase enzymes like the CCPs in these intracellular locations modulate the glutamylation levels of MTs and the generation of Δ2- and Δ3-tubulin, regulating the interaction between MTs and their interactor proteins, axogenesis, the stability of the centrosome and other processes related with cell division and the sensory and motor functionality of cilia and flagella (Rogowski et al., 2010).

Although all CCPs catalyse essentially the same reactions, they have been shown to differ in their preferences for poly-E lateral chain length and kinetic (H. Y. Wu et al., 2015):

CCP1, CCP4 and CCP6 catalyse the formation of Δ2- and Δ3-α-tubulin and the deglutamylation of post-translationally generated poly-E long chains in the C-terminal region of α- and β-tubulin (Figure 1.6). Furthermore, they are also capable of hydrolyse genetically encoded Glu in the primary C-terminal sequence of the MLCK1 and telokin proteins (Rogowski et al., 2010). Specifically, CCP1 has a preference for long poly-E chains (≥3 consecutive Glu), although it can also hydrolyse extensions of ≥2 Glu at the C-terminus of its substrates. Recently, Tanco et al. have identified five new potential substrates for CCP1, including ribosomal proteins, HMGB, and transcription and translation factors, that point to a possible role for CCP1 in the process of transcription and remodelling of chromatin according to its nuclear localisation. All these proteins contain variable length extensions of consecutive acidic residues in their C-terminal region, demonstrating the ability of CCP1 to hydrolyse Asp C-terminal residues, albeit less efficiently than Glu (Tanco et al., 2015). On the other hand, CCP4 is specifically capable of hydrolysing ≥2 C-terminal Glu from its substrates, without showing any preference for chain length (H. Y. Wu et al., 2015).

CCP2 and CCP3 catalyse the formation of Δ2-α-tubulin and the deglutamylation of post-translationally generated poly-E long chains in the C-terminal region of α- and β-tubulin (Figure 1.6). Tort et al. demonstrated its ability to catalyse the deglutamylation of the C-terminal region of MLCK1 and telokin, anticipating a mild aspartilase activity in CCP2 (Tort et al., 2014). While *in vitro* deglutamylation assays in the presence of C-terminal modified telokins with different extensions and combinations of C-terminal acidic residues

demonstrated that CCP3 is capable of hydrolysing Glu and Asp with the same efficiency and preference, thus demonstrating a new enzymatic activity for the M14D subfamily different from deglutamylation for the first time (Tort et al., 2014).

On the other hand, Kimura *et al.* in 2010 were the first to demonstrate that CCP5 specifically hydrolyses the first branched Glu of the post-translationally generated poly-E chain in the C-terminal region of α- and β-tubulin. CCP5 is the only CCP capable of hydrolysing the isopeptide bond formed between the γ-carboxyl group of the branching point Glu and the amino group of the branching Glu (Rogowski et al., 2010) (Figure 1.6).

1.1.3.9   Related pathologies

Mutations in CCP1 were first identified as the cause of the cerebellar ataxia of the *pcd* mouse and have been later related with a similar neuron disease in sheep (Zhao et al., 2012). In humans, several deficiencies of unknown cause have been genetically mapped to the regions comprising the CCPs, such as spastic paraplegia 19 and 41, spinocerebellar ataxia 32, primary ciliary dyskinesia 8, essential hereditary tremor 2 and dystonia 9 (Baird & Bennett, 2013) (Table 1.5). Moreover, three specific human diseases have been related with CCP1, CCP4 and CCP5; the childhood-onset neurodegeneration with cerebellar atrophy (CONDCA) (Shashi et al., 2018), the Fuchs endothelial corneal dystrophy-8 (FECD8) (Riazuddin et al., 2013) and the retinitis pigmentosa-75 (RP75) (Kastner et al., 2015) respectively.

TABLE 1.5. HUMAN CONDITIONS OF UNKNOWN CAUSE THAT MAP TO DEFINED GENETIC REGIONS ENCOMPASSING THE SIX CCPS.

CONDITION	OMIM	BAND INTERVAL	ENCODING GENE
SPASTIC PARAPLEGIA-19	607152	9q33-q34	CCP1, AGTPBP1
SPASTIC PARAPLEGIA-41	613364	11p14.1-p11.2	CCP2, AGBL2
SPINOCEREBELLAR ATAXIA-32	613909	7q32-q33	CCP3, AGBL3
PRIMARY CILIARY DYSKINESIA-8	612274	15q24-q25	CCP4, AGBL1
ESSENTIAL HEREDITARY TREMOR-2	602134	2p25-p22	CCP5, AGBL5
DYSTONIA -9	601042	1p33	CCP6, AGBL4

1.1.3.9.1 Childhood-onset neurodegeneration with cerebellar atrophy (CONDCA)

The CONDCA (OMIM 618276) is a severe autosomal recessive disease affecting the cerebellum, spinal motor neurons and peripheral nerves. Patients with this disorder generally present global development delay, impaired intellectual development, poor or absent speech and motor abnormalities during their first year of life. Brain imaging shows cerebellar atrophy with a variable progression which can lead to a progressive worsening of neurological function and death in childhood. Additionally, features such as microcephaly, eye movement abnormalities, feeding difficulties, ataxia, spasticity and dystonia are constantly observed in patients (Shashi et al., 2018).

Shashi *et al.* related this rare condition to CCP1 in 2018 being the first human disease associated with this CCP. In their study, they show that rare biallelic variants of CCP1 is the cause of CONDCA, with different affectation depending on the mutation of the peptidase. Patients with truncated forms of the protein had more severe phenotypes compared with patients with missense variants. Due to the small number of reported cases, there is not a definitive genotype-phenotype correlation, although all patients showed absence, low expression or catalytically dead forms of CCP1 (Shashi et al., 2018).

1.1.3.9.2 Fuchs endothelial corneal dystrophy-8 (FECD8)

The FECD is the most common genetic disorder of the corneal endothelium. It is a hereditary dystrophy of the corneal endothelium marked by thickening of Descemets membrane and excrescences, called guttae, that typically appear in the fourth or fifth decade of life. Disease progression results in decreased visual acuity as a result of increasing corneal edema, and end-stage disease is marked by painful epithelial bullae (Riazuddin et al., 2013).

Riazudin *et al.* related this disease to CCP4 in 2013. They found a nonsense mutation in the AGBL1 gene that resulted in a premature termination of the protein. This mutation is responsible for the change of the localisation of CCP4, which is predominantly found in the cytoplasm, to a nuclear localisation. Moreover, they also demonstrated that the interaction between CCP4 and the FECD-associated protein TCF4 was diminished in patients (Riazuddin et al., 2013).

1.1.3.9.3   Retinitis pigmentosa-75 (RP75)

The retinitis pigmentosa is the most common retinal dystrophy and it is characterized by progressive loss of rods resulting in tunnel vision (reduced peripheral vision), nyctalopia (night blindness) and changes in the peripheral retina (Patel et al., 2016).

In 2015, Kastner *et al.* identified homozygosity for a missense mutation in the AGBL5 gene in a Turkish family with retinitis pigmentosa. These studies were further corroborated by Patel *et al.* in 2016 after conducting a study implicating 541 patients. Although the loss of function of CCP5 is essential for the development of the disease, the exact involvement of its mutation in causing the symptoms is not yet known (Branham et al., 2016; Kastner et al., 2015; Patel et al., 2016).

1.2   Nuclear compartments

As previously indicated, loss of function of CCP1 causes the *pcd* mouse model. Different alterations occurring in degenerating Purkinje cells have been described (Baltanás, Casafont, Lafarga, et al., 2011; Baltanás et al., 2019; Valero et al., 2006). However, little is known about the possible alterations that take place in the different nuclear compartments of the neuron. In this context, it is assumed that the cell nucleus is organized into structural and functional compartments that are fundamentally involved in: a) the preservation of DNA and its transcription; b) RNA processing and c) ribosome formation. These nuclear compartments include chromosomal territories and interchromatin regions, including the nucleolus (Cremer & Cremer, 2001; Misteli et al., 1997). The organization of nuclear compartments is highly dynamic and reflects the functional state of cells (Lamond and Earnshaw, 1998). In the case of mammalian neurons, the reorganization of nuclear compartments has been observed in response to changes in gene expression associated with physiological and experimental conditions, but also in certain neurodegenerative pathologies (Villagrá et al., 2004; Yamada et al., 2001). Specifically, there is evidence of a relationship between the components of the DNA damage and repair signalling machinery and the pathophysiology of certain human neurodegenerative diseases (Caldecott, 2004; Francisconi et al., 2005; McKinnon, 2004; Paulson & Miller, 2005).

1.2.1   Chromatin territories

Chromosomes are organized in a radial pattern, with some located preferentially on the periphery of the nucleus while others are located in the central area. This radial arrangement allows preferential grouping between neighboring chromosomes (Cremer et al., 2006; Meaburn and Misteli, 2007). Although it is still unknown what factors control this specific organization, it is known that the radial organization of chromosomes depends on the amount of DNA and the transcriptional activity of its different genomic domains (Meaburn and Misteli, 2007). The non-random organization of the genome allows functional compartmentalisation in the nuclear space. The active and inactive regions of the genome are separated, allowing different genes to be transcribed or repressed more efficiently. The portion of DNA that is not transcribed is usually densely folded in the heterochromatin regions, while the transcriptionally active and inducible genes are located in the euchromatin regions (Ferreira et al., 1997; Carvalho et al., 2001).

Chromosomes during interphase were thought to spread throughout the cell nucleus, acquiring a morphology of fine interlaced strands. Today it is known that during the cell cycle each chromosome maintains its individuality, occupying a limited and determined space, known as the chromosomal territory. In general, chromosomal territories comprise the interphase chromosomes and their euchromatin and heterochromatin domains (Cremer and Cremer, 2001; Cremer et al., 2006). The interior of the chromosomal territories is connected by a complex network of channels that allows access to deep sequences of the genome of different regulatory factors (Cremer et al., 2006; Meaburn and Misteli, 2007). Within chromosomal territories, the structural arrangement of DNA is not random. For example, the arms of the chromosomes are as far apart from each other, and the regions of the chromosomes rich in genes are separated from those where they are scarce (Meaburn and Misteli, 2007). This organization probably contributes to the coordinated regulation of different sets of genes. Furthermore, this may reflect that heterochromatin and euchromatin occur in the nucleus as separate and defined domains. In eukaryotic plant cells, chromosomes tend to be polarized with telomeres at one end and centromeres at the opposite end. In contrast, in eukaryotic cells of animals, specifically mammals, each chromosome acquires a specific location with respect to the center of the nucleus (Meaburn and Misteli, 2007).

Euchromatin is made up of loose chromatin regions that retain a nucleosomal configuration that allows transcription. Its structural configuration is in the form of 30 nm fibers or looped domains. Heterochromatin has generally been classified as facultative and constitutive. Constitutive heterochromatin contains repeating DNA sequences that are not transcribed and that correspond to centromeric and telomeric regions. Facultative heterochromatin is one that can be transcribed but is temporarily or indefinitely silenced. It contains inactive genes whose expression is not required to maintain the phenotype or functionality of a specific cell type. The degree of heterochromatinization depends on cellular metabolism and its maintenance is subject, to a great extent, to the recruitment of silent genes (Lamond and Earnshaw, 1998; Spector, 2001; Carmo-Fonseca, 2002; Cremer et al., 2004, 2006; Dillon, 2006). Purkinje cells have a large nucleus in which the chromatin appears uniformly dispersed, although some aggregates appear in the periphery, near the nuclear envelope (Herndon, 1963; Khan, 1993). This euchromatic state indicates a high availability of chromatin domains "open" and therefore accessible for transcription. This coincides with the high metabolic and functional activity exhibited by PCs (Womack and Khodakhah, 2002; Swensen and Bean, 2003; Davie et al., 2008).

The ratio of heterochromatin to euchromatin is related to various modifications in nucleosomal histone. Euchromatin is generally enriched in hyperacetylated histones H3 and H4 (Hendzel et al., 1998; Görisch et al., 2005). Heterochromatin is characterized by the presence of hypoacetylated histone H3, trimethylated in lysine 9 and monomethylated in 27 and by the presence, also, of trimethylated histone H4 in lysine 20 (H4-K20-3Me; Peters et al., 2003; Rice et al., 2003; Kourmouli et al., 2004). It is considered that the trimethylation of histone H3 favours its interaction with structural proteins of heterochromatin, such as HP1α (heterochromatin protein 1α), which contribute to the maintenance of the high level of condensation of this type of chromatin (Lachner et al., 2001; Nielsen et al., 2001; Jiang et al., 2004; Maison and Almouzni, 2004; Misteli, 2005). The presence of these modifications in histones and the appearance of certain molecules (such as HP1α) serve as cytological markers of the different types of chromatin and their functional status. At present it is accepted that the chromatin configuration in neurons is very dynamic and capable of being structurally and functionally remodelled very quickly. Furthermore, changes in chromatin conformation may be necessary for the protection of the genome against various types of

stress and for the expression of genes in response to cellular stress (Pena et al., 2000; Navascués et al., 2008).

1.2.1.1   Chromatin structure

Eukaryotic cells contain about two meters of DNA which must be physically organized and compacted into a nucleus with a micrometre-scale diameter (Rocha & Verreault 2008). This compaction is achieved synergistically by the arrangement of DNA with specific proteins. This combination of protein and DNA is known as chromatin. The global and local compaction/de-compaction of chromatin are essential for all the cellular processes that involves DNA, such as DNA replication, DNA transcription or chromatin sorting during cell division, thus throughout the cell cycle the extent of chromatin compaction is in dynamic equilibrium (Figure 1.7) (Horn 2002).
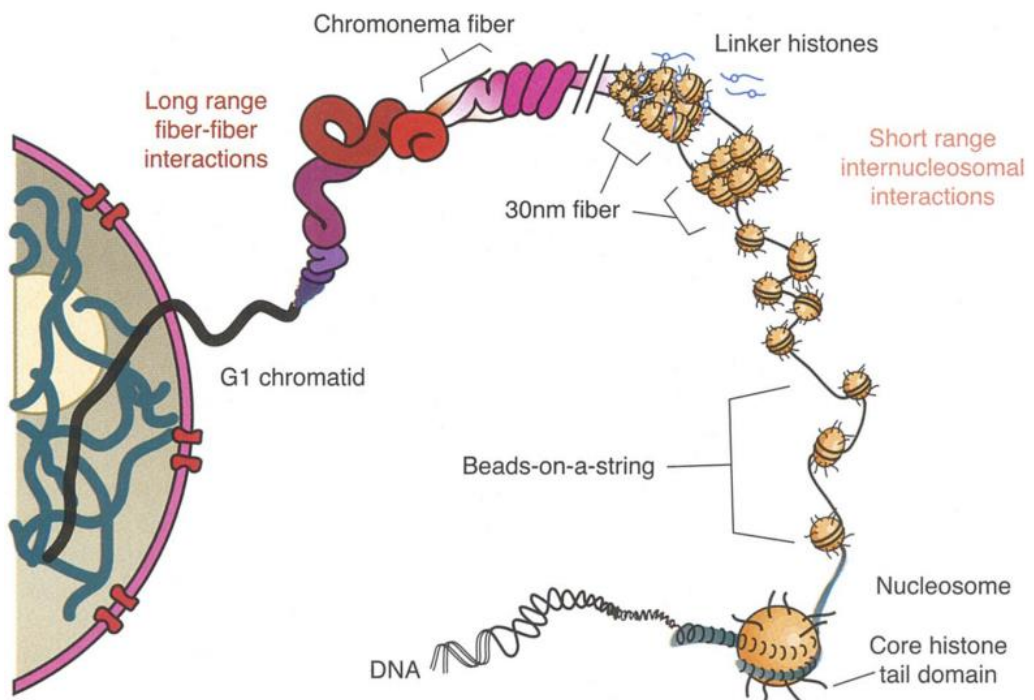
FIGURE 1.7. SCHEMATIC REPRESENTATION OF THE MULTIPLE STAGES OF CHROMATIN FOLDING. Figure from (Horn 2002).

The chromatin is compacted in a hierarchical fashion through several degrees of compaction. The first stage of compaction occurs when double stranded DNA wraps around a core of histone proteins, forming a structure known as the nucleosome core particle (NCP)

or nucleosome (Olins, A & Olins, D 1974). The remaining DNA between two NCPs, known as linker DNA, is protected by a linker histone, whose recruitment to NCPs results in a complex known as the chromatosome (Simpson 1978). Thousands of nucleosomes are organized as such on a continuous DNA helix, in linear strings separated by 10 to 60 base pairs (bp) of linker DNA in the genome (Hansen 2002). This "beads-on-a-string", to which this linear nucleosomal array is referred in the literature, fibre may be considered to constitute the lowest function unit of chromatin (Horn 2002; Hansen 2002).

The second level of compaction is accomplished through histone tail-mediated nucleosome-nucleosome interaction, which promotes the formation of a 30 nm wide fibre (Horn 2002). Two models have been proposed to explain the organization of this 30 nm fibre structure: (a) the 'one-start' (solenoid) model, which consists of consecutive nucleosomes interacting with each other and following a helical trajectory via torsion of the linker DNA; and (b) the 'two-start' (zigzag) model, characterized by two rows of nucleosomes which form a two-start helix so that alternate nucleosomes become interacting partners with relatively straight linker DNA (Woodcock & Ghosh 2010; Luger et al. 2012). Even though the prevailing view is that the 30 nm fibre is organized in a 'heteromorphic' fibre in vitro in a more energetically favourable conformation, and both models may coexist in the genome (H. Wong et al. 2007; Grigoryev et al. 2009). However, this model remains controversial, as it has not yet been proven to reflect the true chromatin structure in vivo (Fussner et al. 2012).

A third level of compaction arises from the histone tail-mediated association of individual 30 nm fibres, which produces a tertiary structure known as 'chromonema' fibres (Figure 1.7) (Horn 2002). The ultimate level of compaction results in the higher structural organisation of the highly recognizable X-shaped chromosomes observed at metaphase (Figure 1.7) (Woodcock & Ghosh 2010).

1.2.1.1.1   The nucleosome core particle: structure and assembly

The NCP is the elemental repeat unit of all known eukaryotic chromatin structures (Oudet et al. 1975; Finch et al. 1977). However, although the structure of the NCP itself is well characterized (Luger, Mäder, et al. 1997; Davey et al. 2002), the mechanisms of its assembly and dynamics in vivo are not yet well understood.

The NCP consists of a histone octamer (one tetramer of histones H3/H4 and two dimers of H2A/H2B) around which 147 bp of DNA are wrapped in 1.7 turns of a tight, flat, and left-handed super-helix (Figure 1.8) (Luger, Mäder, et al. 1997). The central 80 bp of the nucleosomal DNA are organized by a heterotetramer of histones H3/H4, whereas the peripheral 40 bp of DNA on each side are bound more loosely by the H2A/H2B dimers (Figure 1.8) (Ransom et al. 2010). The penultimate 10 bp of DNA are coordinated by the amino(N)-terminal -helix of histone H3 (Figure 1.8) (Ransom et al. 2010).
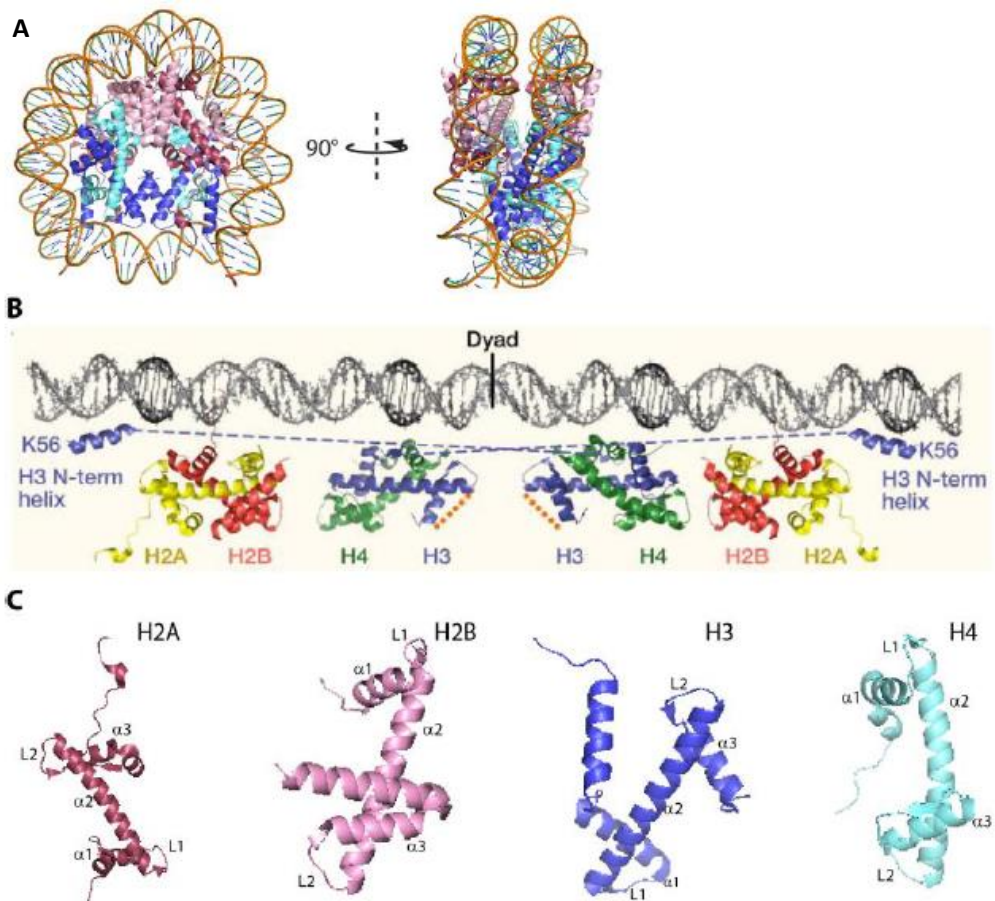
FIGURE 1.8. NUCLEOSOME STRUCTURE. (A) Nucleosome core particle structure (PDB Code: 2NQB), front and side views. (B) Unravelling of the nucleosomal DNA to indicate which region of the DNA is organized by which histone proteins. Dashed lines indicate the H3-H3 dimerization interface involved in H3/H4 tetramerization. Figure from (Ransom et al. 2010). (C) Histone-fold domain of H2A, H2B, H3, and H4 (PDB Code: 2NQB). Histone H2A is coloured in red, H2B in pink, H3 in blue, and H4 in cyan.

The four core histone proteins (H2A, H2B, H3, and H4), which constitute the histone octamer, share a highly similar structural motif named the 'histone-fold' domain in their central regions (Figure 1.8). This domain is formed of three helices connected by two interspersed loops, an arrangement denoted as 1-L1-2-L2-3 in Figure 1.8, and is characteristic of this class of proteins. Due to complementary internal packing, H3 and H2A form crescent-shape heterodimers exclusively with H4 and H2B respectively through their histone fold domains. In the nucleosome core particle, the two H3/H4 heterodimers interact though a 4-helix bundle formed exclusively by the two juxtaposed H3 histone folds thus constituting the heterotetramer (Figure 1.8). Each H2A/H2B heterodimer interacts with the heterotetramer through a second, homologous 4-helix bundle between H2B and H4 histone folds. For more details refer to (Luger, Mäder, et al. 1997).

Histones are small and highly basic proteins that have an intrinsic affinity for the negative charge of DNA (Kornberg & Thomas 1974). Histone tails are found at the N-terminal end of the histone-fold domain and can extend outside of the nucleosome (Luger, Mäder, et al. 1997a). These tails are extremely basic due to the high proportion of lysine and arginine that they contain, and their post-translational modifications can modulate nucleosome assembly or disassembly (Luger & Richmond 1998).

The assembly of the NCP is thought to be a two-step process guided by histone chaperones in cooperation with ATP-dependent remodelling factors, and histone modification enzymes (Mello & Almouzni 2001; Ransom et al. 2010; Haushalter & Kadonaga 2003). First a tetramer of H3/H4 is deposited onto the DNA to form an intermediate known as the tetrasome (Figure 1.8) (Smith & Stillman 1991). Secondly, an H2A/H2B heterodimer is initially deposited unilaterally on the tetrasome, forming the hexasome (Figure 1.8); followed by a second H2A/H2B heterodimer from the other side of the central H3/H4 heterotetramer thus constituting the final NCP (Figure 1.8) (Nakagawa et al. 2001). Disassembly likely occurs as a reversal of this series of events.

1.2.1.2 Histone chaperones

The association of histones and DNA in vitro under physiological conditions leads to the rapid formation of insoluble aggregates (Tyler 2002), thus additional factors must be required for the establishment of biologically relevant histone-DNA assemblies, such as

chromatin. It has been described in the literature that the presence of additional acidic proteins, which could attenuate the charge of the histones, precludes aggregation and ensures the formation of chromatin by the regular and ordered deposition of histones on DNA (Akey & Luger 2003). Such acidic factors are known as histone chaperones. These chaperones associate with histones upon their synthesis, escort them into the nucleus, and modulate their specific association with DNA during essential processes in the cell such as DNA replication, DNA repair or transcription (Avvakumov et al. 2011; Eitoku et al. 2008; Rocha & Verreault 2008). Additionally, they are involved in histone storage which prevents their non-productive aggregation with DNA (Akey & Luger 2003). Lastly, specialized histone chaperones mediate the assembly of histone variants into the nucleosome (Campos & Reinberg 2010; Henikoff & Ahmad 2005).

The affinity and specificity for H3/H4, H2A/H2B, and linker histones varies among different classes of histone chaperones, and it is principally the variation in these attributes that determines the functional specialisation of the chaperones. For example, Anti-silencing function 1 (Asf1) interacts specifically with the core histones H3/H4 (Natsume et al. 2007; English et al. 2006), while Nucleoplasmin (Np) preferentially binds the core histones H2A/H2B (Ramos et al. 2010), thus both may be considered highly specific chaperones. Additionally, Chaperone for H2A.Z/H2B 1 (Chz1) and Death domain-associated protein (DAXX) are two histone chaperones that interact specifically with histone variants H2A.Z and H3.3, respectively (Luk et al. 2007; Elsässer et al. 2012). Conversely the histone chaperone Nucleosome assembly protein 1 (Nap1) has been reported to bind to all core histones (H2A/H2B and H3/H4) as well as the linker histone H1 (McBryant et al. 2003; Kepert et al. 2005; Park et al. 2005), meaning that Nap1 interacts with histones with considerable promiscuity.

Furthermore, histone chaperones also bind other factors in addition to their histone partners to form complexes that participate in other cellular functions such as DNA replication, DNA repair, and transcription (Zlatanova et al. 2007).

1.2.1.2.1   *Nucleosome assembly proteins*

Nap1 was the first nucleosome assembly protein identified in HeLa cells as a histone chaperone that facilitates nucleosome assembly by binding to two histones pairs: H2A/H2B

and H3/H4 (Ishimi et al. 1987). Orthologues of Nap1 were subsequently identified in other organisms, such as *Saccharomyces cerevisiae* (Ishimi & Kikuchi 1991), *Drosophila melanogaster* (Ito et al. 1996), *Xenopus levis* (Steer et al. 2003), *Arabidopsis thaliana* (Zhu et al. 2006), and *Plasmodium* (Gill et al. 2009; Gill et al. 2010). Members of the Nap family can be classified into (a) Nap1 proteins (or NAP1L1 in higher eukaryotes), (b) Nap1-like proteins (Nap1-L2 through Nap1-L6) in metazoans, including the yeast homolog Vacuolar sorting-associated protein 75, and (c) SE Translocation proteins (Park & Luger 2006a; Hansen et al. 2010).

1.2.1.2.2   Nap1 proteins

Nap1 regulates around 10% of genes in *S. cerevisiae*, according to a genome-wide expression study (Ohkuni et al. 2003). In vitro, Nap1 interacts with all four core histones (H2A/H2B, H3/H4), but only with H2A/H2B dimers in vivo (McQuibban et al. 1998; Ito et al. 1996; Mosammaparast et al. 2001). As a result, Nap1 is mostly thought of as an H2A/H2B-specific chaperone that conducts a variety of activities linked to this job. By interacting with the karyopherin Kap114, Nap1 is implicated in the nuclear import of H2A/H2B dimers (but not H3/H4 dimers) (Mosammaparast et al. 2002; Mosammaparast & Pemberton 2004). It is also linked to gene activation, possibly through interactions with transcriptional activators and co-activators like p300 (Ito et al. 2000; Asahara et al. 2002).

1.2.1.2.3   Nap1-like proteins

Nap1-L2 has been shown to play a key function in neural precursor cells, where it may offer histones H3/H4 for acetylation by HAT enzymes (Attia et al. 2007). Nap1-L3 is a brain-specific member of the Nap family that may help regulate brain-specific gene expression by regulating chromatin structure states in collaboration with other factors (Shen et al. 2001). These and other studies suggest that some members of the Nap1-like class have tissue-specific expression and function, which is consistent with the presence of a wide family of proteins in higher eukaryotes.

Isoform evolution is not the only way to produce function variety. Post-translational changes of Nap family members have been demonstrated to impact their localisation throughout the cell cycle. Casein Kinase II (CKII) phosphorylation of Nap1-L4 (also named

Nap2) keeps Nap1-L4/histone complexes in the cytoplasm, whereas dephosphorylation allows it to enter the nucleus with histone cargo intact (Rodriguez et al. 2000).

1.2.1.2.4   Vps75

Vps75 was the most recent member of the Nap family to be discovered. Surprisingly, unlike other Nap proteins, Vps75 prefers to bind histone H3/H4 in its tetrameric state (Selth & Svejstrup 2007). The interaction of Vps75 with the histone acetyltransferase (HAT) Regulation of Ty1 transposition protein 109 (Rtt109) has been postulated as a way for Vps75 to regulate chromatin dynamics (Tang et al. 2008; Berndsen et al. 2008; Kolonko et al. 2010). The Vps75-Rtt109 complex increased both components' acetyltransferase and histone deposition activity, as well as their specificity for histone H3-lysine9 acetylation (H3K9ac) (Berndsen et al. 2008), revealing a HAT-chaperone complex that combines histone modification with nucleosome assembly (Berndsen et al. 2008).

1.2.1.2.5   SET/INHAT/TAF-1

SET (also known as INHAT or TAF-1) is a histone chaperone that binds to histones H3/H4 and dsDNA with preference (Muto et al. 2007). It has been postulated that SET's histone chaperone activity requires DNA binding, which leads to the creation of a pre-nucleosome complex, to which histones are then recruited (Muto et al. 2007). In this case, SET might direct the dsDNA to certain places on the core histones, determining the DNA-winding initiation site (Muto et al. 2007). SET has also been demonstrated to play a crucial function in transcription (Gamble et al. 2005; Seo et al. 2001). By attaching to histones and preventing them from functioning as acetylase substrates, SET substantially inhibits HAT/co-activator-mediated acetylation of core histones and nucleosomes (Seo et al. 2001). "Histone masking" is a term used to describe one of SET's properties (Seo et al. 2001)

1.2.2   Interchromatinc regions

Between the chromosomal territories, and even within a single chromosomal territory, is the interchromosomal or interchromatin space (Cremer et al., 2004, 2006). The space located at the boundary between the interchromatin regions, and the chromosomal territories is known as the perichromatin region (Fakan and van Driel, 2007). In this area there are numerous macromolecular-non-chromatin complexes involved in transcription, splicing, replication and/or DNA repair processes, among others (Lamond and Spector,

2003; Misteli, 2005). The compartments or structures of the interchromatic regions are very dynamic and their structural and spatial organization is mainly related to the processes that regulate the expression of the genome (Misteli, 2001; Fakan and van Driel, 2007). The interchromatic regions include: a) the nucleolus, the place of formation of ribosomal units, b) the perichromatin fibrils, which represent the morphological expression of the process of transcription and maturation of heterogeneous nuclear RNAs (hnRNA) or pre-mRNA, c) the aggregates of interchromatic granulations, where the hnRNA maturation factors are assembled and stored, d) and the Cajal bodies (CB), which are nuclear organelles involved in the biogenesis of small nuclear (snRNP) and nucleolar (snoRNP) ribonucleoproteins (Carvalho et al., 1999; Lamond and Spector, 2003; Raska et al., 2004; Cioce and Lamond, 2005). These snRNPs and snoRNPs are not required for the processing of hnRNA (unmatured mRNA and, therefore, with all its introns) and pre-rRNA, respectively (Carvalho et al., 1999; Cioce and Lamond, 2005).
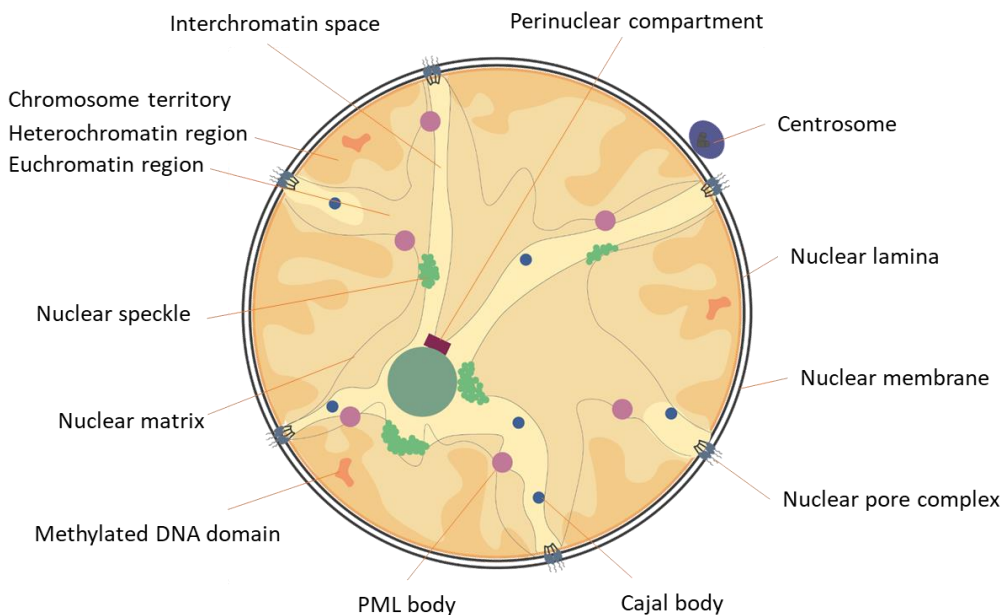
FIGURE 1.9. NUCLEUS COMPARTIMENTALISATION. The cell nucleus includes the chromosomal territories, made up of interphase chromosomes and their domains of euchromatin and heterochromatin, and the interchromatin regions, including the nucleolus, Cajal's body, PML, speckles, cleavage bodies, sam68 body, polycomb body, perichromatin fibrils, or aggregates of interchromatic granulations, among others.

There are also other bodies that have been characterized by different techniques such as: the OPT domain, the perinucleolar compartment, the cleavage body, the SAM68 nuclear body, the Polycomb body, the Gemini body, the promyelocytic leukemia (PML) body and speckles and paraspeckels, whose functions are not fully understood, although they have been associated with different mRNA processing processes (Huang et al., 1998; Spector, 2001; Fox et al., 2002; Misteli , 2005; Bernardi and Pandolfi, 2007) (Figure 1.9).

1.2.2.1   The nucelolus

The nucleolus is the nuclear organelle where ribosomal DNA (rDNA) is transcribed and where these transcripts are subsequently processed and assembled with ribosomal proteins (Mélèse and Xue, 1995; Gerbi et al., 2003; Sirri et al., 2008). Biochemical studies have shown that the nucleolus is highly dynamic and that its structure is closely linked to its main function; generating ribosomes (Mélèse and Xue, 1995). Recently, other functions in which the nucleolus is involved have been proposed, such as the regulation of mitosis, nuclear export, multiple types of response to stress, and biogenesis and assembly of different types of RNPs (Boisvert et al., 2007; Cmarko et al., 2008). Nucleoli are formed around specific portions of the chromosomes, known as nucleolar organizing regions (NOR), which consist of ribosomal genes, arranged in tandem, that code for rRNA (Carmo-Fonseca et al., 2000; Raska, 2003; Dimario, 2004; Hernández-Verdún and Louvet, 2004; Louvet et al., 2005; HernándezVerdún, 2006; Boisvert et al., 2007). The number of NOR-bearing chromosomes varies between species. In man, only five pairs of acrocentric chromosomes have rDNA, which indicates that diploid cells can have a maximum of 10 nucleoli. Also, the number of copies of ribosomal genes in NORs varies between species. Diploid human cells contain a total of 400 ribosomal genes, which have a high transcription rate, although not all rRNA-encoding genes are active (Hadjiolov, 1985; Cmarko et al., 2008).

Nucleoli are very sensitive to changes in cell growth and metabolic activity, indicating that this structure receives and responds to numerous types of signaling (Boisvert et al., 2007). During interphase, ribosomal genes from more than one NOR normally associate, forming the nucleolus, and rDNA is transcribed into rRNA thanks to RNA polymerase I. During mitosis, rRNA synthesis ceases as a result of phosphorylation of different nuclear and nucleolar factors and the nucleolus disassembles. In other words, nucleologenesis occurs when NOR transcription is reinitiated (Dimario, 2004; Hernández-Verdún, 2006). The

complex process of ribosome biogenesis occurs in different compartments of the nucleolus, easily distinguishable under electron microscopy. These compartments are the fibrillar centers, the dense fibrillar component and the granular component (Figure 1.10). The fibrillar centers are rounded and clear areas made up of fine fibrils of about 300 nm in length (Huang, 2002; Raska, 2003; Derenzini et al., 2006). In the fibrillar centers, mediated by RNA polymerase I, rDNA transcription occurs. In this region, in addition to rDNA, there are some pre-rRNAs (especially in the cortical area), the TATA binding factor (TBF), the upstream binding factor (UBF) and DNA topoisomerase I. However, despite concentrating the machinery required for transcription, it has not been shown that rDNA transcription exists in the fibrillar centers. Most likely, it occurs at the border between the fibrillar center and the dense fibrillar component (Cheutin et al., 2002). The dense fibrillar component is an electrodense region that is located around the fibrillar centers. The first co-transcriptional modifications of pre-rRNAs (47S-45S), such as methylations and pseudouridilations, take place in this nucleolar compartment.
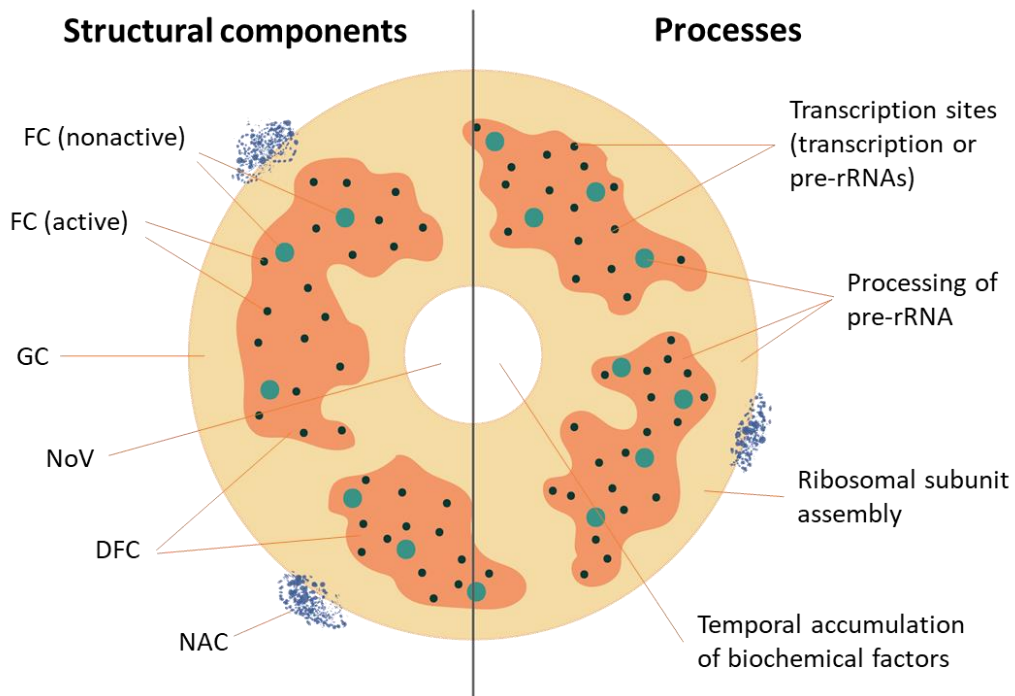
FIGURE 1.10. STRUCTURAL AND FUNCTIONAL DOMAINS OF THE NUCLEOLUS. FC, fibrillar center; DFC, the dense fibrillar component; GC, the granular component; NoV, nucleolar vacuole; NAC, nucleolus-associated chromatin. Nucleolonema is encircled with black lines.

These transcriptional modifications are made by the snoRNPs, among them the best known is U3, which is essential for the formation of 18S rRNA (Borovjagin and Gerbi, 2004; Granneman and Baserga, 2005). Furthermore, proteins such as fibrilarin or B23 have been found in this nucleolar compartment (Boisvert et al., 2007). Surrounding the dense fibrillar component is the granular component, made up of dense granules 15 nm in diameter (Strouboulis and Wolffe, 1996; Raska, 2003; Derenzini et al., 2006). The final maturation of pre-RNPs and the assembly of ribosomal proteins occur in this nucleolar compartment. Here, the 28S and 5.8S rRNAs are assembled with the 5S rRNA, synthesized in foreign nucleolar chromatin domains, constituting the 60S ribosomal subunit (Strouboulis and Wolffe, 1996). On the other hand, the 18S rRNA binds to the 40S ribosomal unit. Finally, the 40S and 60S ribosomal subunits are independently exported to the cytoplasm, where they have just matured to form functional ribosomal subunits (Carmo-Fonseca et al., 2000; Olson et al., 2002; Raska et al., 2004; Olson and Dundr, 2005).

1.2.2.2   Other relevant structures

Perichromatin fibrils are located in the perichromatin regions. They are structural constituents rich in RNPs, with a diameter that varies between 3-20 nm and that are located in the nucleoplasm, normally at the edges of heterochromatin masses, although they can also be observed in euchromatin domains (Fakan, 1994). They represent the morphological expression of hRNA transcription (Nash et al., 1975; Fakan, 1994) and their density is directly related to the level of hRNA synthesis (Fakan, 1994; Puvion-Dutilleul and Puvion, 1996).

Interchromatic granulations are areas in which components of the splicing machinery of pre-mRNAs accumulate. They may appear diffuse through the nucleoplasm or forming aggregates but are rarely associated with condensed chromatin groups (Fakan and Puvion, 1980). These aggregates measure between 0.8-1.5 µm (Thiry, 1995) and are composed of granules that have a diameter of about 20 to 25 nm, which appear to be connected by a subtle network of fibrils of about 10 nm (Thiry, 1995).

Cajal bodies were discovered by Ramón y Cajal (1903) in mammalian neurons. It is a structure found in both plant and animal cells; their size and number depend on the cell type, the phase of the cycle and the transcriptional activity (Lafarga et al., 1991, 2009; Pena et al., 2001; Ciace and Lamond, 2005; Berciano et al., 2007). These nuclear organelles

contain determined splicing factors, the p80 coilin protein (Andrade et al., 1991), snRNP and the motor neuron survival protein (SMN; Matera and Frey, 1998; Carvalho et al., 1999; Gall, 2000). In addition, CB contains the proteins fibrilarin and Nopp140, some snoRNP (Raska et al., 1990; Cioce and Lamond, 2005), and various kinases and transcription factors (Gall, 2000, 2001).

1.3   Microtubules

Microtubules are dynamic polymers composed of α- and β-tubulin heterodimers that form part of the cytoskeleton, providing structure and shape to eukaryotic cells. In the most common form of a MT, tubulin heterodimers polymerise into thirteen protofilaments that laterally align to form a hollow tube. Microtubules take part in key cellular processes such as structural support, morphogenesis, spatial organisation of the cell content, cell polarity, chromosome segregation during cell division, intracellular trafficking, secretion and motility of cilia and flagella (Alberts et al., 2014). Alterations in the functionality of this structure has been associated to pathological processes which include cancer, ciliopathies or neurodegenerative diseases (Chakraborti et al., 2016).

1.3.1   Structure of microtubules

Microtubules in eukaryotes are composed by a heterodimeric protein formed by the subunits α- and β- of tubulin. These α and β subunits are approximately 50% identical at their amino acidic level, having an approximated molecular weight of 50 KDa each. Dimers polymerise into thirteen protofilaments which are added laterally forming a hollow tube with an external diameter of 25 nm. The protofilaments can also associate forming doublets (axoneme of cilia and flagella) or triplets (centrioles or basal bodies). To polymerise, it is required a minim concentration of dimers, phenomena called as *critical concentration*, heat (30-37ºC) and guanosine triphosphate (GTP).

It is important to note that microtubules have a distinct polarity, as their formation is accomplished by the addition of dimers at one or both ends of the forming microtubule. The addition is head-to-tail in the elongation of the protofilaments, generating skewed rows of α and β monomers and causing a global polarity to the microtubule. Due to the orientation of the protofilaments, one end is made up of an α-tubulin ring (the – end) and the opposite end is made up of a β-tubulin ring (the + end). While microtubule elongation can occur at

both the (+) and (−) ends, it is significantly more rapid at the (+) end (Walker et al., 1988). The negative end is usually stabilised by its anchoring to the microtubule organising centres (MTOC). The MTOC are exclusive of eukaryotes and can organise into more complex structures (J. Wu & Akhmanova, 2017).
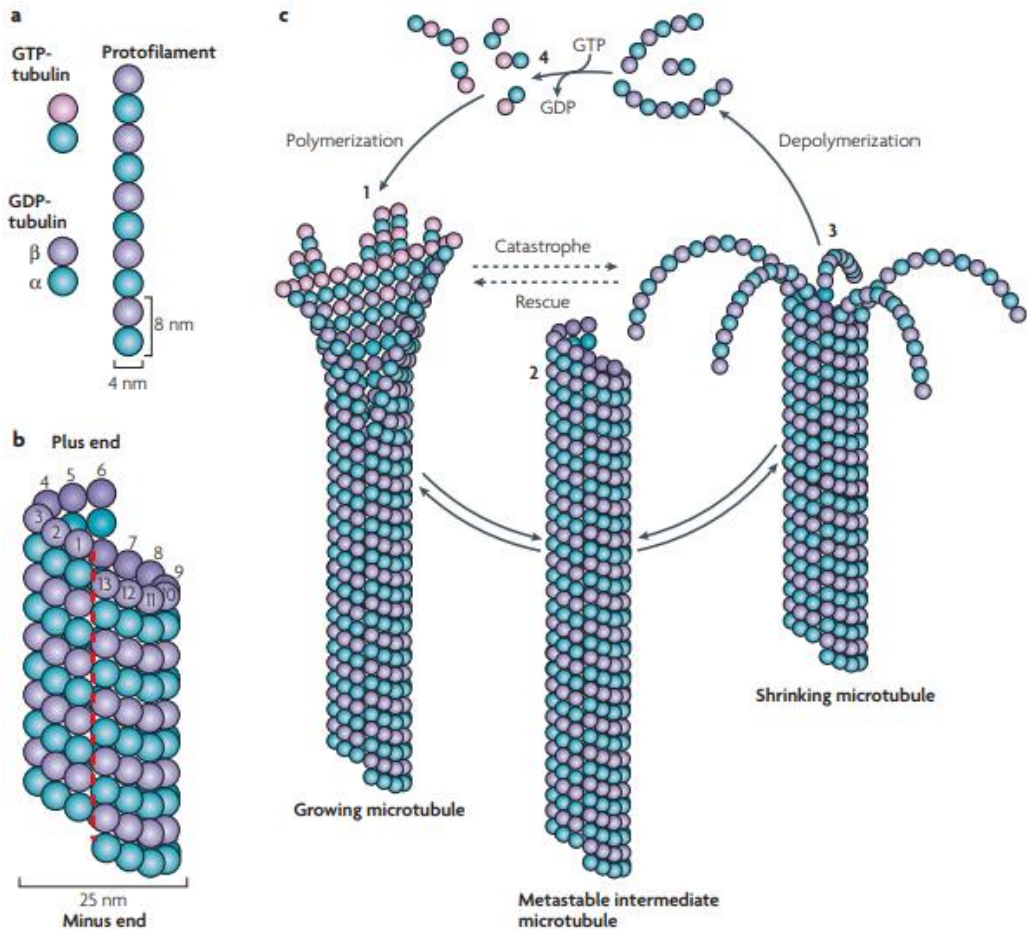
FIGURE 1.11. MICROTUBULE DYNAMIC STABILITY AND STRUCTURE. Microtubules are composed of tubulin heterodimers that are aligned in a polar head-to-tail fashion to form protofilaments. b. The cylindrical microtubule wall typically comprises 13 parallel protofilaments in vivo. The 3-subunit helical pitch generates a discontinuity in B lattice MTs called the seam (red dashed line). c. Assembly and disassembly of microtubules is driven by the binding, hydrolysis and exchange of a GTP on the beta-tubulin monomer (GTP bound to alpha-tubulin is non-exchangeable and is never hydrolysed). Polymerization is typically initiated from a pool of GTP-Tubulin. Once tubulin is incorporated into the MT wall, its GTP is hydrolysed into GDP. The GDP-MT wall is metastable and can stochastically switch to a depolymerization state, releasing GDP-Tubulin in solution. The cycle is completed by exchanging the GDP of the disassembly products with GTP, enabling the tubulin to start a new cycle. (Adapted from Akhmanova & Steinmetz, 2008)

The overall structure of MTs is a pseudo-helix with one turn of the helix containing thirteen tubulin dimers. In the most common architecture, dimers interact with the next one with a vertical offset of three tubulin monomers (Figure 1.11) (Sui & Downing, 2010).

1.3.2   Dynamics of microtubules

Microtubules are very dynamic structures in cells, with an individual half-life of ten minutes. This constant change is due to its continuous process of polymerization and depolymerization. The assembly of its structure proceeds in three different phases, the nucleation, the elongation and the steady state.

Nucleation is the assembly of the first tubulin dimers. Contained in the MTOC, we found the γ-tubulin, another subunit of tubulin, different from α- and β-. The γ-tubulin forms the *γ-tubulin ring complex* (γ-TuRC) which acts as a cap of the (–) end while MTs keep growing on their (+) end (Desai & Mitchison, 1997). Although the centrosome is the primary MTOC in most cells, other cellular structures, like cilia and flagella, have their own MTOC on their base (basal bodies) and the Golgi apparatus has been demonstrated to serve as platform for nucleation (Zhu & Kaverina, 2013)

On the next step, tubulin dimers are added at both ends of microtubules during the elongation. In this phase, both tubulin subunits are attached to a GTP, which plays a structural role in α-tubulin but is eventually hydrolysed to GDP in β-tubulin shortly after assembled. Assembly properties of GDP- and GTP-tubulin are different, as GDP-tubulin is more prone to depolymerisation (Weisenberg 1976).

At the steady state phase, tubulin can be found either forming part of the filaments or soluble in the cytosol. Both forms are in a dynamic equilibrium since continuous GTP hydrolysis is occurring and there is a constant exchange of tubulin subunits forming the soluble tubulin pool (Alberts et al., 2014).

1.3.3   The tubulin code

Microtubules are essential for cell maintenance and survival, as they control shape, division, motility and differentiation among other key processes. Many of their functions are carried by the formation of specific structures as the mitotic and meiotic spindle, ensuring correct cell division, axonemes, the central machines of cilia and flagella, and the neuronal

cytoskeleton, controlling the connectivity and function of neurons (Ishikawa, 2012; Kelliher et al., 2019; Prosser & Pelletier, 2017). MTs are dynamic, alternating between polymerisation and depolymerisation phases. However, MTs in cell compose a highly ordered and controlled structures.
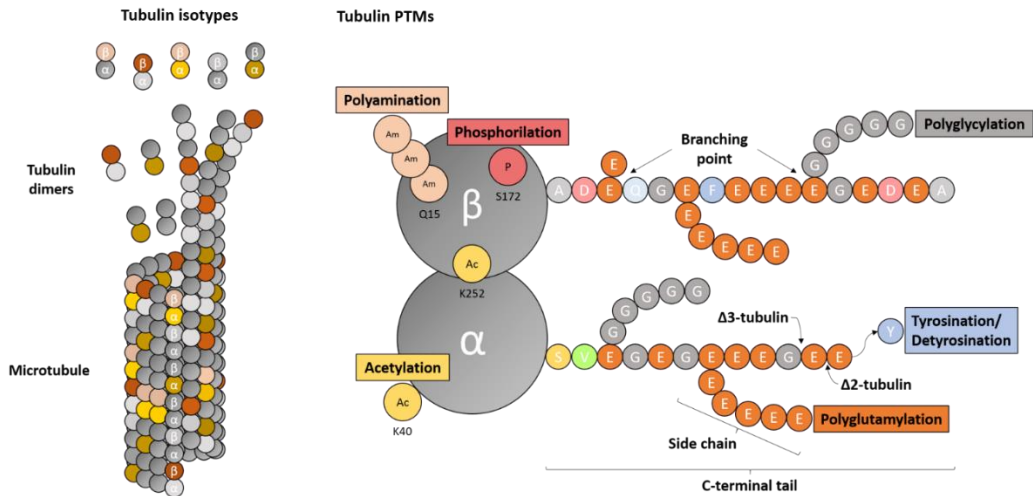
FIGURE 1.12. COMPONENTS OF THE TUBULIN CODE. Tubulin isotypes (α-tubulins, dark grey and brown; β-tubulins, light grey and pink) are encoded by different tubulin genes and can mix during microtubule assembly. Tubulin PTMs are catalysed by a range of enzymes (**TABLE 1.6**) and are located either at the globular, highly structured tubulin bodies (for example, acetylation (Ac), phosphorylation (P) and polyamination (Am)), or at the unstructured C-terminal tails of tubulin (for example, glutamylation, glycylation, tyrosination, detyrosination and removal of glutamate residues to produce Δ2-tubulin and Δ3-tubulin). Polymodifications are initiated by the generation of a branching point, from which side chains are further elongated.

Both diversity of functionally distinct MTs and their precise control emerges from the molecular heterogeneity of tubulin promoted by the expression of different isotypes of α- and β-tubulin and the generation of PTMs in the tubulin heterodimer (Janke & Magiera, 2020). Analogously to the *histone code*, the genetic and chemical complexity of tubulin forms the base of the *tubulin code*. Regarding this concept, specialised enzymes are capable to *write* the code generating PTMs in the C-terminus of tubulin isotypes (Figure 1.12). These PTMs would be then *read* by microtubule-associated proteins (MAPs) to execute the specific cellular functions (Janke & Bulinski, 2011).

1.3.3.1   Tubulin isoforms

The human genome contains nine different genes for each α- and β-tubulin isotype which are highly conserved between them and show little structural variation (Janke & Magiera, 2020). The presence of different isotypes of tubulin subunits into the MTs lattice can serve for two main purposes: affect the assembly, dynamics and mechanical properties of the MTs or affect the interactions between MTs and MAPs. Specialised MTs, such as neuronal ones, are enriched in specific β-tubulin isotypes which are in part responsible for their function (βIIa and βIIb isotypes are enriched in brain and epithelial cells and βIII in specific neuronal cells) (Denoulet et al., 1986). In addition, mutations of a single isotype, have been linked to specific deleterious disorders (Cederquist et al., 2012; Niwa et al., 2013). Nevertheless, not all isotypes are forming part of individual cell type or tissues, as different isotypes can freely mingle into mosaic MTs (Lewis et al., 1985).
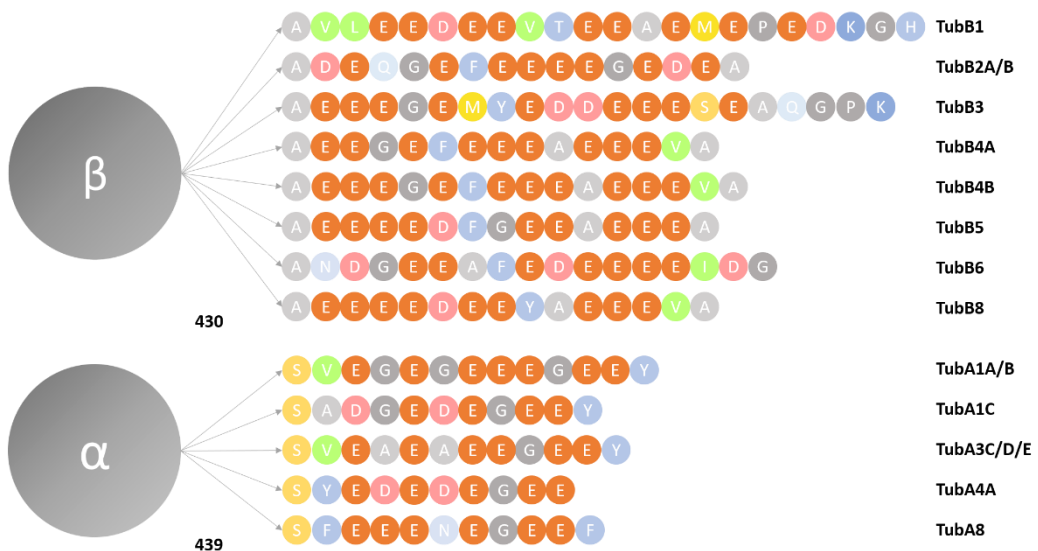
FIGURE 1.13. TUBULIN ISOTYPES. Schematic representation of the tubulin heterodimer showing the amino acid sequence of the C-terminal tails from the last residue included in the compact globular domain of tubulin. Amino acids are indicated in a letter code and colored according to their biochemical properties. The nomenclature of the different isotypes and the genes that encode them are shown on the right of the image.

In addition to α- and β-tubulin (and their respective isotypes), there are other tubulins called γ, δ, ε, δ ε, ζ and κ, which together make up the tubulin superfamily. Γ-tubulin corresponds to the best studied tubulin after α and β-tubulin, sharing a 30% sequential identity. It is located in MTOCs in interphase cells, being a key component for the nucleation

and stability of MTs. In mitotic cells, γ-tubulin is in centrosomes, in MTs of the mitotic spindle, and in the midbody during cytokinesis. The other members of the tubulin superfamily have been poorly described and little or nothing is known about its function or biological relevance (McKean et al., 2001).

1.3.3.2   Post-translational modifications of tubulin

Tubulin is subject to a large range of PTMs (Figure 1.12) that can directly modulate microtubule dynamics. This mechanism is faster than *de novo* synthesis of tubulin subunits and proteosomal degradation, allowing a rapid target and de-target of MTs for specific functions (Verhey & Gaertig, 2007). The most studied PTMs of microtubules are acetylation, phosphorylation, polyamination, polyglutamylation, detyrosination and polyglycylation (Garnham & Roll-Mecak, 2012; McKean et al., 2001).

The complexity of the modifications found in MTs is particularly high in their C-terminal end. Most tubulin isotypes encode a C-terminal tyrosine or phenylalanine (Figure 1.13) which is easily removed and readded (Arce et al., 1975; Hallak et al., 1977). In addition, the presence of a glutamate rich C-terminal end allow the generation of polymodifications, consisting in the addition/removal of a variable number of glutamates (polyglutamylation) (Eddé et al., 1990) or glycines (polyglycylation) (Redeker et al., 1994) as side chains. These type of modifications cause both chemical and structural changes in MTs, modifying their interaction with MAPs and motor proteins (Bodakuntla et al., 2019; Bonnet et al., 2001; Boucher et al., 1994).

A great variety of enzymes have been found to be involved in the different tubulin PTMs (Table 1.6). This thesis will focus on the CCPs family, which is directly involved with deglutamylation processes (Kalinina et al., 2007; Tort et al., 2014), as a counterpart of the action of tubulin tyrosine ligase-type proteins (TTLLs) (Janke et al., 2005; van Dijk et al., 2007).

TABLE 1.6. ENZYMES CATALYSING TUBULIN POST-TRANSLATIONAL MODIFICATIONS (ADAPTED FROM (JANKE & MAGIERA, 2020).

MODIFICATION SITES	FORWARD ENZYMES	REVERSE ENZYMES
Acetylation		
α-Tubulin Lys40	α-Tubulin acetyltransferase 1	Histone deacetylase 6; sirtuin 2
β-Tubulin Lys252	San acetyltransferase	Not known
Methylation		
α-Tubulin Lys40	SET domain-containing protein 2	Not known
Detyrosination		
α-Tubulin C-terminal Ty	Vasohibin proteins	Tubulin–tyrosine ligase
Generation of Δ2-tubulin and Δ3-tubulin		
α-Tubulin penultimate C-terminal Glu residues	Cytosolic carboxypeptidases	No reverse reaction known to date. Tyrosination of Δ2-tubulin is not possible
Glutamylation or polyglutamylation		
α-Tubulin and β-tubulin C-terminal tails (multiple Glu residues can be modified)	Tubulin–tyrosine ligase-like proteins, multiple members in most organisms (9 glutamylases in mammals)	CCPs, multiple members in most organisms (6 deglutamylases in mammals)
Glycylation or polyglycylation		
α-Tubulin and β-tubulin C-terminal tails (multiple Glu residues can be modified)	TTLL proteins, multiple members in most organisms (3 glycylases in mammals)	No reverse reaction or enzymes known
Polyamination		
α-Tubulin and β-tubulin, major modification site β-tubulin Gln15	Transglutaminases	No reverse reaction or enzymes known
Phosphorylation		
β-Tubulin Ser172	Cyclin-dependent kinase 1	Not known
β-Tubulin Ser172	Dual-specificity tyrosine-regulated kinases	Not known
β3-Tubulin Ser444	Not known	Not known
α-Tubulin Tyr432	Spleen tyrosine kinase	Not known
α-Tubulin and β-tubulin Tyr residues	Neuronal proto-oncogene tyrosine-protein kinase SRC	Not known
Ubiquitinylation		
α-Tubulin, major modification site Lys304	Not known	No reverse reaction or enzymes known
Sumoylation		
α-Tubulin (modification site unknown)	Not known	No reverse reaction or enzymes known
Palmitoylation		
α-Tubulin, major modification site Lys376	Not known	No reverse reaction or enzymes known

1.3.3.2.1   Δ2- and Δ3-tubulin

Following detyrosination, additional removal of the penultima glutamic acid generates a form of tubulin called Δ2-tubulin; consequently, a subsequent removal of another glutamic acid on the same chain will generate Δ3-tubulin (Lafanechère & Job, 2000). Thus, Δ2-tubulin generation requires a previous detyrosination, making Δ2-tubulin levels be regulated by the tyrosination/detyrosination cycle. Moreover, Δ2-tubulin is considered to be a non retyrosinable form of α-tubulin being only found in highly stable MTs (Paturle-Lafanechère et al., 1994).

Δ2-tubulin may represent more than 35% of total tubulin in the brain. Given the irreversible nature of this MPT, it has been proposed that the generation of Δ2-tubulin would keep MTs in a state of permanent detyrosination that would protect them against depolymerization (Janke & Kneussel, 2010). Δ2-tubulin is restricted to very stable MTs such as those of the axons of differentiated neurons and the axonems of cilia and flagella. Furthermore, the formation of Δ2-tubulin occurs in the final stages of functional differentiation, in which MTs are excluded from the dynamics of polymerization-depolymerization. Consequently, the generation of Δ2-tubulin seems to have a relevant role in the stability of MTs. The enzymes responsible for the generation of Δ2-tubulin belong to the M14D subfamily of MCPs, the CCPs (Rogowski et al., 2010; Tort et al., 2014).

Aillaud *et al.* confirmed in 2016 the physiological occurrence of αΔ3-tubulin and βΔ4-tubulin (Aillaud et al., 2016). αΔ3-tubulin can be generated by CCP1, CCP4, CCP5 and CCP6 but not by CCP2 and CCP3. It has a specific distribution pattern, localised in the brain in a quantity similar to Δ2-tubulin only around birth. Although no role has been assigned to this form of tubulin, it is expected to have a critical function in neuronal development, resembling tyrosinated-tubulin rather than other truncated variants. On the other hand, βΔ4-tubulin was found ubiquitously in cells and tissues with a constant expression level through the cell cycle and little is known about its generation or biological implications (Aillaud et al., 2016).

Polyglutamylation (poly-E or poly-Glu) is a reversible PTM which generates lateral Glu chains of variable length (1-20, typically 4-6 residues long (Audebert et al., 1993)) to the γ-carboxyl group of any of the gene-encoded glutamates found at the C-terminal end of tubulin and other proteins (Figure 1.14). Tubulin glutamylation was first observed to be increased during neuronal differentiation (Audebert et al., 1993), axonemes of cilia and flagella (Fouquet et al., 1994) and centrioles of mammalian centrosomes (Bobinnec et al., 1998). However, the polyglutamylation is not only restricted to tubulin, as other substrates have been identified (van Dijk et al., 2008). Glutamylation levels in cells are balanced by the action of glutamylases and deglutamylases.

Both the branching point and the elongation processes are carried out by enzymes of the TTLL family (Janke et al., 2005; van Dijk et al., 2007). In mammals, there are nine confirmed polyglutamylases from the TTLL family, with different substrate preference and specificity for initiation or elongation of the Glu chain (van Dijk et al., 2007). In this way, TTLL4, TTLL5, and TTLL7 prefer the initiation reaction, while TTLL6, TTL11, and TTLL13 prefer to catalyse the elongation of the poly-E chain. On the other hand, TTLL5, TTLL6, TTLL11 and TTLL13 preferably act on the α subunit of tubulin, while TTLL4 and TTLL7 act on the β subunit (van Dijk et al., 2007). In neurons, TTLL1 existing in a protein complex is the main glutamylase and catalyse the elongation in the α-subunit (Janke et al., 2005).
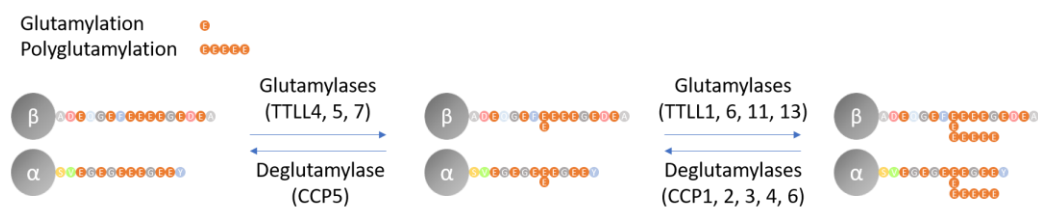
FIGURE 1.14. TUBULIN GLUTAMYLASES AND DEGLUTAMYLASES. The generation of poly-E side chains in the C-terminal tail of α- and β-tubulin begins with the addition of the first Glu of the chain to the branching Glu of the primary sequence by the enzymes TTLL4, 5, and 7. Chain elongation is performed by TTLL1, 6, 11, and 13. The reverse reaction is catalysed by deglutamylase enzymes. CCP1, 2, 3, 4 and 6 remove the linked Glu by peptide bonds from the polyglutamate chain, but only CCP5 is capable of hydrolysing the isopeptide bond of branched Glu. TTLL = TTL-like ligase; CCP = cytosolic carboxypeptidase.

The reverse reaction, deglutamylation, is carried out by the members of the cytosolic carboxypeptidases, where CCP5 specifically removes the branching point, and CCP1, CCP2, CCP3, CCP4 and CCP6 shorten the acidic side chain (Kimura et al., 2010; Rogowski et al., 2010; Tort et al., 2014). The deglutamylation process is not only restricted to tubulin, but as other substrates have also been described.

Glutamylation as a PTM is a fine regulator mechanism that is able to generate a wide range of functional signals based on different specific patterns. These patterns are defined by the density of modified tubulin heterodimers within a MT, the type of subunit (α or β) and the different isotypes, the length of the polyglutamate chains, and the specific site of the C-terminal tail where the modification is taking place (Janke et al., 2008). Thus, depending on the structure, cell type or tissue, MTs may present a different type of patterns. For instance, the cytoplasmatic MTs of the interphase cells have low glutamylation levels, while the transition zone of ciliary MTs is monoglutamylated and stable MTs (usually found in neurons, centrioles, axonemes and ciliary basal bodies) are highly polyglutamylated (Garnham & Roll-Mecak, 2012). In addition, it is also important to note that polyglutamylation levels can be locally and temporally changed, as they appear to be elevated in dynamic MTs of the mitotic spindle and the midbody during cell division (Regnard et al., 1999; Verhey & Gaertig, 2007). Regarding their general control, Bompard *et al.* identified cilia and spindle-associated protein (CSAP) as a master regulator of tubulin glutamylases (Bompard et al., 2018), which is thought to play a role in the regulation of MT stability and tubulin glutamylation in neuron biology (van der Laan et al., 2019).

Glutamylation has been reported to be essential for the motility of cilia and flagella, acting on their beating behaviour via the regulation of flagellar dynein motors (T. Kubo et al., 2010; Suryavanshi et al., 2010). Depletion or knockout (KO) of single TTLL enzymes can lead to ciliary defects, such as the *Ttll1*^{-/-} mouse that presents alterations in motile cilia of the trachea epithelium (Lan et al., 2020). However, this same depletion did not show obvious neuronal defects in mouse (Vogel et al., 2010), suggesting that the nonredundant regulatory function of glutamylase enzymes in cilia is not found in neurons. On the other hand, neurons seem to be more sensitive to alterations in deglutamylase activity, as the mutation of CCP1 in the *pcd* mouse is a well-stablished model for neurodegeneration (Mullen et al., 1976). In addition, experimental data suggest that MAPs and kinesins bind

preferentially to polyglutamylated tubulin (Bonnet et al., 2001). In this way, Sirajuddin *et al.* showed in 2014 that processivity of MTs undergone by kinesin-2 was significatively enhanced by polyglutamylation (Sirajuddin et al., 2014) while Lacroix *et al.* demonstrated how MT severing was induced by recruitment of katanin and spastin in polyglutamylated neurons (Lacroix et al., 2010). In addition, a recent study reported a decrease in the overall transport of mitochondria in CCP1 deficient neurons (Gilmore-Hall et al., 2019), suggesting that abnormally long Glu chains can block the accessibility of motor proteins or even structural MAPs as EB1, PRC1 and Tau protein (Bigman & Levy, 2020).

Besides tubulins, other proteins have been identified to undergo glutamylation modifications. For instance, nucleosome assembly protein 1-like 1 and 4 (NAP1L1 and NAP1L4) (Regnard et al., 2000), the high mobility group B family (HMGB), the TRAF-type zinc finger domain-containing protein 1 (TRAFD1) (Tanco et al., 2015), the DnaJ homolog subfamily C member 7 (DNAJC7) (C. Li et al., 2016), the cyclic GMP-AMP synthase (cGAS) (Xia et al., 2016), the X-linked retinitis pigmentosa GTPase regulator (RPGRORF15) (Rao et al., 2016), the interleukin-7 receptor subunit alpha (IL-7Rα) (Liu et al., 2017) and the ubiquitin carboxyl-terminal hydrolase (BAP1) (Xiong et al., 2020). In addition, other putative substrates for this modification have been reported with an enriched relation with chromatin remodelation processes, suggesting a role in the relation between the mitotic spindle and chromatin structure during mitosis (van Dijk et al., 2007).

1.3.3.3   The tubulin code in the nervous system

In a unique way compared with other cell types, neurons present a high number of PTMs in their MT cytoskeleton. These PTM accumulate in neurons as they mature (Mansfield & Gordon-Weeks, 1991), serving as an important object of study for neuronal differentiation. Apart from a differential distribution of tubulin PTMs, the nervous system also present differences in their tubulin isotype composition.

1.3.3.3.1   Tubulin isoforms in the nervous system

Neuronal microtubules present two predominant β-tubulin isoforms, the β2- and the β3-tubulin (Joshi & Cleveland, 1989), being the β3 isotype almost exclusive of neurons (Ferreira & Caceres, 1992) and testis (Mariani et al., 2015). The β3-tubulin is encoded in the TUBB3 gene, which is upregulated during regeneration of sensory nerves (Moskowitz & Oblinger,

1995). Indeed, it has been observed that loss of TUBB3 activity impairs neuronal proliferation and cannot be rescued by other tubulin isotypes (Saillour et al., 2014), showing its critical importance for neuronal development. The effects of depletion of TUBB3 show a similar phenotype of the one found in the αTAT1 (α-tubulin acetyl transferase) KO mice, showing how different elements of the tubulin code are interconnected to control MT functions (Morley et al., 2016).

1.3.3.3.2   PTMs of tubulin in the nervous system

PTMs are not uniformly distributed into the neuron MTs. In general terms, we can observe two different tubulin populations depending on their stability. This way we find acetylated MTs with a low tyrosination level in the centre of dendrites (long-living MTs), and tyrosinated MTs with a low acetylation level at their periphery (growing cone) (Tas et al., 2017). This determined pattern allows both the retrograde transport mediated by kinesin-1 at the centre of the dendrites (highly modified MTs) and the anterograde one driven by kinesin-3 at their periphery (low modified MT) (Figure 1.15).
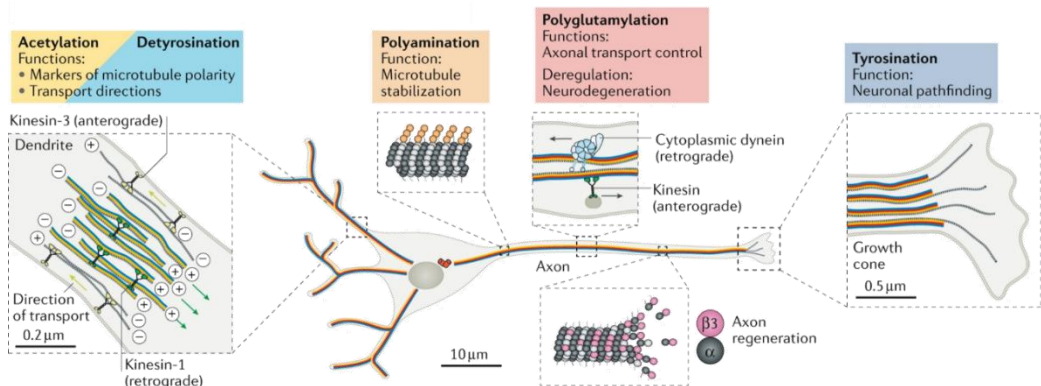
FIGURE 1.15. TUBULIN CODE IN NEURONS. Summary of involved tubulin modification occurring in neurons and their effect.

Different post-translational modifications are key factors in neuronal formation and maintenance. For instance, the tyrosination/detyrosination cycle is important in early neuronal development, as mice lacking tyrosinated MTs by depletion of the *Ttl* gene undergoes perinatal death caused by neurodevelopmental defects (Erck et al., 2005). In a similar way, mutations in the small vasohibin-binding protein (SVBP), a cofactor needed for vasohibins to remove the C-terminal tyrosine residue of tubulin, has been linked to microcephaly and neurodevelopmental affections in humans (Iqbal et al., 2019).

Regarding acetylation modifications in tubulin, mice lacking the gene encoding for the αTAT1 does not show a severe neurodegenerative phenotype, but present significant loss of touch perception (Morley et al., 2016). These findings highlight the role of acetylation in the dendritic refinement of sensory neurons. However, the direct implication in neurodegeneration in humans is still in discussion. It has been shown that the inhibition of the activity of the deacetylase HDAC6 causes neuronal death; nevertheless, HDAC6 is not an exclusive α-tubulin deacetylase, acting on proteins important for neuronal homeostasis (Dompierre et al., 2007; Kalinski et al., 2019).

On the other hand, polyglutamylation has been directly related with neurodegeneration having the *pcd* mouse as a well-stablished model (Mullen et al., 1976). The *pcd* mouse carries a mutation in the gene encoding for the deglutamylase CCP1 and causes the accumulation of hyperglutamylated tubulin in the cerebellum (Rogowski et al., 2010). It has been suggested that tubulin hyperglutamylation is the main cause of the neuronal degeneration, as the rapid progression of the disease is diminished by the deletion of TTLL1, the main polylgutamylase in neurons. Nevertheless, the increasing number of polyglutamylated substrates found for CCP1 in both the cytoplasm and the nucleus may show a different implication. The recent discovery of the childhood-onset neurodegeneration with cerebellar atrophy condition in humans (Shashi et al., 2018) has stablished the dysregulation of polyglutamylation as a cause of human neurodegeneration. To date, defects in axonal transport have been reported (Magiera et al., 2018), suggesting a role of polyglutamylation in binding and distribution of neuronal MAPs. In that way, molecules inhibiting tubulin-modifying enzymes could prove to be potential therapies for neurodegenerative disorders linked to perturbed microtubule polyglutamylation.

Lastly, phosphorylation has also been linked with neuronal perturbations, as changes in this modification by DYRK1A lead to defects in dendrite branching and excitability in *Drosophila melanogaster* (Ori-McKenney et al., 2016). Human DYRK1A has been linked to Down syndrome and autism-spectrum disorders (Guimerá et al., 1996; Willsey & State, 2015).

1.3.3.4   Microtubule interacting proteins

Microtubules are often associated to a complex set of interacting proteins to modulate part of their function and dynamics. These interacting proteins can recognise or be influenced by the previously generated PTM, which are seen as regulators of them (Nehlig et al., 2017). Microtubule interacting proteins are classified into three subfamilies: the microtubule-associated proteins (MAPs), the plus-end tracking proteins (+TIPs) and the motor proteins.

1.3.3.4.1   Microtubule-associated proteins

MAPs are key components for the regulation of MT dynamics, as polymerisation, depolymerisation and catastrophe rates may vary depending on the present MAPs. MAPs were first identified on brain tissue, were they play an important role, and were classified based on their molecular weight (MW). MAPs with a MW between 55-62 kDa are called τ (tau) proteins, which have been observed to promote nucleation and prevent disassembly (Mandelkow & Mandelkow, 1995), but also implicated in Alzheimer's disease (Bramblett et al., 1993). On the other hand, MAPs with 200-1000 kDa molecular weight are classified into MAP-1 to MAP-4 families. MAP-1 and MAP-2 are present in neurons, being the dendrites the only known location for MAP-2 proteins. In neurons, MAP-1b and MAP-2 bind to moderate polyglutamylated MTs (3 Glu), while MAP-1A binds to long polyglutamylated chains (6 Glu) (Bonnet et al., 2001). Other MAPs called katanin, spastin and fidgetin were later identified, with a destabilising activity. In this case, spastin and katanin prefer MTs with long polyglutamylated chains, generating new (+) and (-) ends after their rupture (Bailey et al., 2015; Valenstein & Roll-Mecak, 2016).

1.3.3.4.2   +TIPs

Plus-end tracking proteins are specific MAP which transitorily binds to the tip of growing microtubules modulating their dynamics and their interaction with other cellular structures. +TIPs have been observed to participate in the MT-chromosome interaction during mitosis (Galjart, 2010). The first identified +TIP was the cytoplasmatic linker protein 170 (CLIP170), which plays a role in MT depolymerisation rescue events.

1.3.3.4.3   Motor proteins

Motor proteins are involved in vesicle trafficking along MTs and cell division, using the hydrolysis of ATP as a source of energy to generate mechanical work. The majority of motor proteins are kinesins, which tend to move towards de (+) end of the MT, and dyneins, which moves to the (-) end. Both types of motor proteins are composed by two identical chains which make up two globular head domains. Kinesins are involved in the transport of vesicles, organelles, protein complexes and mRNAs towards the (+) end. Several PTMs modulate the mechanism of kinesins, as detyrosination impedes the binding between MTs and the depolymerising motor protein MCAK and KIF2A. Other modifications as deglutamylation of the MTs diminish the affinity between MTs and KIF17 and KIF1A, affecting the trafficking of synaptic vesicles and synaptic transmission (X. Wu et al., 2006).

1.3.4   Cilia and flagella

MTs or tubulin complexes are the major structural components of highly specialized organelles such as centrioles and axonemes, which are the backbones of cilia and flagella (Bornens, 2012; Satir & Christensen, 2007). The mature (mother) and daughter centrioles are located at the centre of the centrosome and are composed of nine triplets of microtubule "blades" grouped around a central cartwheel. The centrioles are important in attracting the proteins that make up the pericentriolar material, where MTs are formed. In most eukaryotes, the mature centriole also plays a role in the nucleation of cilia and flagella development (Gönczy & Hatzopoulos, 2019; Loncarek & Bettencourt-Dias, 2018). The intraflagellar transport system (IFT) is required for the creation and operation of the cilia or flagella, which has been conserved from protists to humans (Scholey, 2008).

1.3.4.1   Basal body and the axoneme

The mature centriole produces cilia, which are membrane-bound projections. The cilium contains a microtubular structure called the ciliary axoneme, which is embedded in the ciliary membrane in the cilium. The axoneme of mammalian multiciliated cells of the epithelia has a structural feature of 9 microtubular doublets surrounding a central pair of singlet MTs (9+2). The axoneme also has outer and inner dynein arms, which are the molecular motors that slide the doublet microtubules and thus generate movement. Interdoublet linkages and the radial spoke/central-pair interaction modify the helical beat

produced by the dynein arms, resulting in regulated bending and effective stroke (Lindemann & Lesich, 2010; Y. Okada et al., 2005).
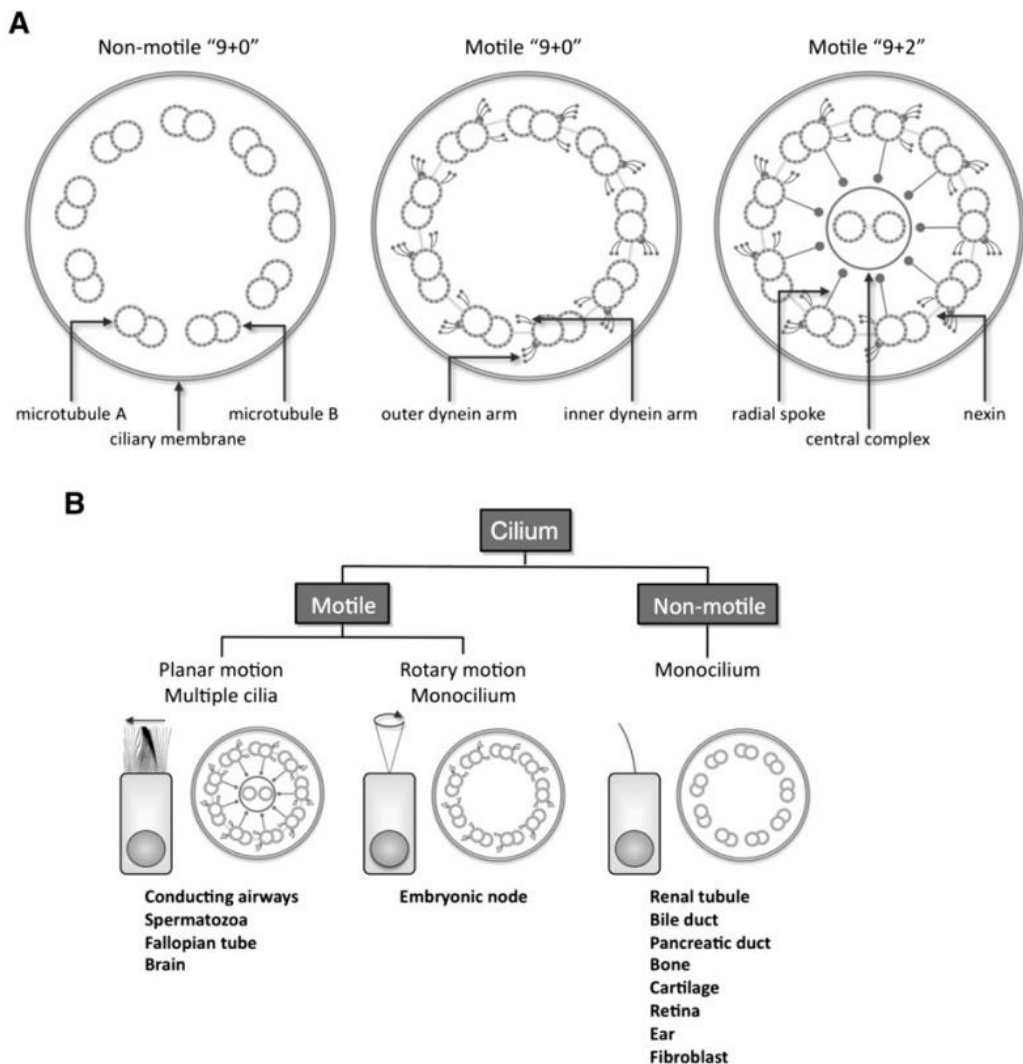
FIGURE 1.16. COMPONENTS AND CROSS-SECTIONAL STRUCTURE OF MOTILE AND PRIMARY CILIA. A, Schematic diagram showing the structural elements of motile ''9 + 2,'' motile ''9 + 0,'' and non-motile ''9 + 0'' ciliary axonemes. B, Classification and sites of different cilia, showing the coordinated synchronous motion of motile ''9 + 2'' cilia, the rotary motion of motile ''9 + 0'' nodal monocilium, and non-motile ''9 + 0'' primary monocilium (modified from Ferkol & Leigh, 2012.

The solitary, immotile primary cilium has a 9+0 structure without the distinctive dynein arms (Bettencourt-Dias et al., 2011; Satir & Christensen, 2007). During development, a unique type of motile monocilium with a 9+0 configuration was discovered in the embryonic node (Figure 1.16). During organ formation, the nodal cilia regulate the left-right body

asymmetry by generating a leftward flow in the extraembryonic fluid (Mirvis et al., 2018). Specific receptors and ion channels are found in the ciliary membranes of both motile and immotile cilia, which activate signalling pathways governing motility and/or linking mechanical and chemical inputs (ligands).

The cilia are rooted in a ciliary pocket, which is an invagination from the plasmatic membrane that contains clathrin-coated pits for endocytic activities and has intimate connections to the actin cytoskeleton (Long & Huang, 2020). Surprisingly, cilia have a close relationship with pathways activated by ligands as diverse as Sonic hedgehog, growth hormones, cytokines, and Ca^{2+}. During development and adulthood, intracellular transduction cascades regulate differentiation, migration, and cell expansion, and pathways operating in the cilium have an impact on the whole cell. While the relevance of motile cilia and flagella in biology has long been recognized (for example, in the respiratory epithelium, the female reproductive tract, and male sperm), primary cilia were once assumed to be a vestigial organelle. The relevance of primary cilia, especially severe clinical manifestations, is becoming increasingly clear (Satir & Christensen, 2007).

1.3.4.2   Primary cilia and ciliopathies

The primary cilium is a sensory organelle that takes mechanical and chemical signals from other cells and the environment and sends them to the nucleus in order to trigger a cellular response. Primary cilia have a structure similar to motile cilia, but they lack the central pair of microtubules in the axoneme and the dynein arms (thus their immobility). They are small and can be seen on mammalian epithelial cells including kidney tubules, bile and pancreatic ducts, as well as non-epithelial cells such chondrocytes (Poole et al., 1985), fibroblasts, and neurons (Lee & Gleeson, 2011). (Figure 1.17).

The production of primary cilia is tightly linked to the cell cycle in most cells. When fibroblasts in culture become confluent and reach G0, primary cilium begins to develop (Wheatley, 1971). As a result, the cell cycle and primary cilia are tightly regulated (Kim and Tsiokas, 2011), and some cilia and centrosome components, such as IFT88, are shared (Robert et al., 2007).
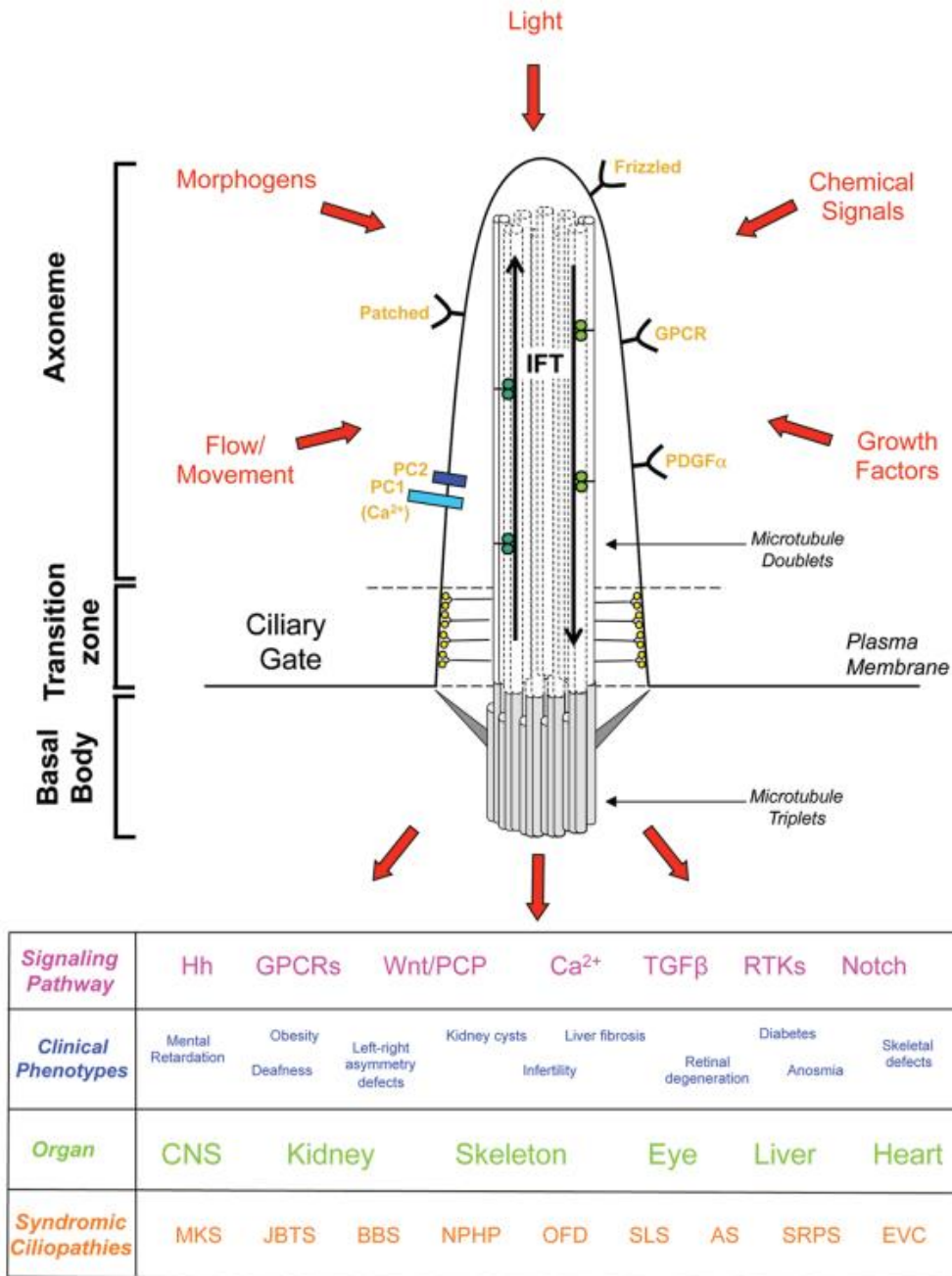
FIGURE 1.17. SCHEMATIC OVERVIEW OF THE PRIMARY CILIUM. A diagram of the primary cilium, showing the signalling pathways controlled by this organelle, as well as the clinical phenotypes, organ involvement, and syndromic ciliopathies linked to primary cilium signalling abnormalities. MKS stands for Meckel-Gruber Syndrome; JBTS stands for Joubert Syndrome; BBS stands for Bardet Biedl Syndrome; NPHP stands for nephronophthisis; OFD stands for Oral-Facial-Digital Syndrome; SLS stands for Senior-Lken Syndrome; AS stands for Alstrom Syndrome; SRPS stands for Short Rib-Polydactyly Syndrome; EVS stands for Ellis-van Creveld Syndrome. (Adapted from (Fry et al., 2014)

The transmission of signalling pathways involved in differentiation and development is a major role of primary cilia (Figure 1.17). (Pan et al., 2013). These signal pathways ensure homeostasis, or the maintenance of the differentiated tissue state or regulated division and differentiation, under normal conditions. However, improper ciliary signalling (caused by abnormal ciliogenesis, misplacement, or mutation of ciliary membrane components) causes inappropriate tissue growth, aberrant cell division, and a variety of human diseases (Satir & Christensen, 2007).

Primary cilia serve an important role in governing neuronal growth and altering many signal transduction pathways in the nervous system. Cerebellar malformation and oculomotor apraxia (lack of voluntary eye movement control) are examples of nervous system defects, as is mental retardation (Lee & Gleeson, 2011). Thus, primary cilium in development has implication in several neurological defects and other ciliopathies.

In pathological situations, the relationship between primary cilia and the cell cycle is also important. There is a clear link between primary cilia dysfunction and carcinogenic processes (Eguether & Hahne, 2018). Signal transduction pathways such as Sonic hedgehog (Shh) (Bangs & Anderson, 2017) and platelet derived growth factor receptor A are blocked by primary cilium malfunction (Pala et al., 2017). Shh plays a role in the left-right body axis, neural tube closure, and the patterning and production of the limbs, teeth, pancreas, lungs, and hair follicles during development. Normal embryogenesis, inflammation, and wound healing all require PDGFR. The loss of primary cilia has been documented in a variety of cancer types (Eguether & Hahne, 2018) and has been linked to increased cancer/tumour growth and a worse prognosis (Emoto et al., 2014).

Ciliopathies, conditions caused by defects in one or more of the many proteins important in ciliary function, share many features including renal disease, retinal dystrophy, and polydactyly (Badano et al., 2006). Retinitis pigmentosa, for example, is a primary cilia condition characterized by night blindness and progressive loss of peripheral vision due to rod photoreceptor cell death (Ramamurthy & Cayouette, 2009). The outer segment of the photoreceptor cells of the retina is a highly specialized primary cilium that is required for photosensation. The cilium's axoneme and disk membrane components are found in the outer segment. The optical pigments (opsins or rhodopsins) must be constantly delivered to

the disk membranes by IFT. Mutations that alter photoreceptor protein trafficking or ciliogenesis cause visual pigment mislocalisation or accumulation, which can lead to photoreceptor cell death and retinitis pigmentosa (Ramamurthy & Cayouette, 2009).

Other ciliopathies related with primary cilia dysfunction are related with the nervous system. Joubert syndrome (JS), for example, is marked by cerebellar hypoplasia and neurological symptoms like as ataxia, psychomotor delay, and oculomotor apraxia, as well as a pathognomonic 'molar tooth sign' on brain imaging. JS is commonly accompanied by a variety of multi-organ signs and symptoms, such as retinal dystrophy, nephronophthisis, liver fibrosis, and polydactyly, all of which are linked to ciliopathy illnesses such as Meckel-Gruber Syndrome, Bardet-Biedl syndrome, and nephronophthisis (Parisi, 2009). Although the link between ciliary abnormalities and specific symptoms has not been fully established, it is known that Shh signalling is required for both neural tube dorsal-ventral patterning and cerebellar granule cell proliferation in the case of JS (Doherty, 2009). Conditional deletion of ciliary genes (such as the JS-causative gene Rpgrip1l) or Shh pathway genes (such as Smo) led in faulty neuronal precursor development and significant hypotrophy of the dentate gyrus in animal models. Primary cilia also perform a directing function in the migration of postmitotic interneurons in the developing brain, according to a recent work using Arl13b conditional knock-out mice. These findings imply that ciliary malfunction and aberrant cortical neuronal growth may play a role in the cognitive impairments reported in JS. All the genes known to have pathogenic mutations that cause JS are found in the primary cilium, basal body, and centrosome, where they may play a role in their development, shape, and/or function.

Objectives

Chapter 2. Objectives

The research group of Professor Julia Lorenzo from the Institute of Biotechnology and Biomedicine of the Autonomous University of Barcelona has been studying metallocarboxypeptidases and their inhibitors structurally and functionally for many years. The group was involved in the discovery and first description of cytosolic carboxypeptidases, one of the most recent carboxypeptidase subfamilies. The overall goal of this thesis is to characterise the functional role of cytosolic carboxypeptidases 1 and 6 (CCP1 and CCP6) with special emphasis on their biomedical context. Extensive research was conducted for this goal, ranging from studies at the protein level to cellular models. The following specific objectives have been defined for each chapter:

Chapter 3. To characterize human CCP1, focusing on its nuclear function.

- To determine the subcellular localisation of cytosolic carboxypeptidase 1 (CCP1), with special emphasis on its variation along the cell cycle and its nuclear localisation.
- To assess the implications of CCP1 in general deglutamylation processes in the cell.
- To evaluate the functional role of CCP1 within the cell nucleus, focusing on the alterations previously found in the *pcd* mouse model.

Chapter 4. To identify the CCP1 and CCP6 interactome landscape.

- To apply the BioID interactomics approach on cytosolic carboxypeptidases 1 and 6 (CCP1 and CCP6) to identify new potential interactors and/or substrates in a cellular context.
- To gain insight into the functional role of CCP1 in the cellular nucleus via its novel potential interactors.
- To gain insight into the functional role of CCP6 in the centrosome via its novel potential interactors.

Chapter 5. To characterise the N-domain of cytosolic carboxypeptidases.

-   To obtain a mutant of the conserved F[E,D]SGNL motif located at the N-domain of human CCP6 (CCP6 G53R).

-   To optimize the recombinant expression and purification of human CCP6 and human CCP6 G53R mutant in the HEK293F mammalian cell system.

-   To evaluate the activity of the human CCP6 G53R compared to wild type CCP6 and the dead version of the enzyme displaying a punctual mutation at the catalytic Glu401 (CCP6 E401Q).

-   To assess the effect of the CCP6 G53R mutation on general protein stability.

-   To determine the intracellular localisation of CCP6 G53R compared with wild type CCP6 and CCP6 E401Q mutant.

-   To elucidate the implication of the N-domain in the CCP6-tubulin interaction.

CHAPTER 3

GENERAL CHARACTERISATION OF HUMAN CCP1

The cytosolic carboxypeptidase CCP1 is an enzyme that acts removing acidic C-terminal residues in the main or side chains of proteins. CCP1 is well-known as a microtubule deglutamylase, but it has been recently associated with other substrates both cytoplasmic and nuclear, according to its dual localisation. Among them, we found proteins involved in the reorganization of chromatin and protein transcription. These substrates and other potential ones could explain how its absence generates an ataxic phenotype by neurodegeneration including Purkinje neurons.

In this work, immunocytochemistry and confocal laser microscopy studies in human cells show that CCP1 presents a diffuse pattern in the cytoplasm, where it co-localises with paxillin, a protein expressed in focal adhesions, suggesting a role of CCP1 in the formation and/or maintenance of this structure for cell attachment. We have also found a strong CCP1 immunoreactivity in the form of small aggregates in the cell nucleus where it co-localises with fibrillarin in the dense fibrillar component of the nucleolus, but not in other structures such as histones or nuclear speckles. These results suggest that CCP1 could be involved in functions such as ribosome biogenesis, playing a role in the cell's response to stress.

Interestingly, immunocytochemistry also revealed that CCP1 in dividing cells associates peripherally to chromosomes during the different mitotic phases. Together, these results indicate that CCP1 could be involved in cell cycle control and cell survival.

Chapter 3. General characterisation of human CCP1

3.1 Introduction

Cytosolic carboxypeptidase 1 (CCP1) was discovered in 2000 during a search for overexpressed mRNAs during the axogenesis and reinnervation processes (Harris et al., 2000). Mouse RNA differential screening after sciatic nerve transection or crush injury showed the rapid induction of a 4-kb transcript named Nna1. The name 'NNA' was based on the assumption that the protein was predominantly expressed in the nucleus of neurons, and that the mRNA was induced by axotomy. Nna1 was predicted to be a zinc metallocarboxypeptidase containing a nuclear localisation and an ATP/GTP binding motif. Accordingly, the gene encoding CCP1 was named ATP/GTP binding protein 1 (AGTPBP1) although there is no empirical evidence of such binding (Harris et al., 2000).

All CCPs act as deglutamylating enzymes, controlling the length of the post-translational modification (PTM) known as polyglutamylation (Rogowski et al., 2010; Tort et al., 2014). Polyglutamylation is a modification that consists of the addition of polyglutamate side chains at specific sites on a target protein. It was initially discovered on the proteins that build microtubules (MTs), the α-tubulins and β-tubulins (Eddé et al., 1990), where is crucial for its proper behaviour (van Dijk et al., 2008). The length of the added side chains can vary from 1 to about 20 glutamyl units, which allows diverse signals to be encoded on a single modification site. The selectivity for α- or β-tubulin, as well as the presence of several modification sites within a single tubulin molecule, increases the complexity of the signals that polyglutamylation can generate on MTs. This is a highly regulated PTM and involves the action of both glutamylases (tubulin Tyr ligase-like proteins or TTLLs) and deglutamylases (CCPs). Understanding the impact of the information encoded by polyglutamylation on the

regulation of cellular function is therefore especially challenging. It is believed that polyglutamylation regulates cell functions such as the cell cycle and neuronal differentiation. Regarding to tubulin, polyglutamylation controls the association of motor associated proteins (MAPs) with microtubules (Sirajuddin et al., 2014). Otherwise, and knowing that there are many nuclear polyglutamylated proteins, it has been suggested that this modification could be involved in the regulation of the nucleus-cytoplasm protein transport (Baltanás, Casafont, Lafarga, et al., 2011; Baltanás et al., 2019).

Although polyglutamylation was discovered first in both α and β tubulin (Alexander et al., 1991), a few studies found a broader spectrum of proteins that could also be affected by this PTM and therefore be potential substrate of CCPs (van Dijk et al., 2008).

Mutant mice with loss of function in CCP1 presents cerebellar ataxia mediated by the neurodegeneration of the Purkinje cells (*pcd* mouse) (Fernandez-Gonzalez et al., 2002). The degeneration suffered by these cells is characterized by a change in the nuclear architecture, suggesting that CCP1 may have a role in chromatin remodelling (Chakrabarti et al., 2009). The *pcd* mutation induces the transcriptional repression of Purkinje cells, generating a deep reorganization of the nuclear chromatin architecture, leading to an accumulation of unrepaired DNA, with a consequent genic silencing and, finally, neuronal death (Baltanás, Casafont, Lafarga, et al., 2011).

CCP1 has 1,226 residues with a molecular weight of 138.448 Da, being the largest CCP of the human family. Like all CCPs, CCP1 has a catalytic carboxypeptidase-like domain and an adjacent conserved N-terminal domain (N-domain) (Figure 3.1).

It has been hypothesized that CCP1 could be required for cell survival because only the gene rescue of catalytic active CCP1 is able to reverse the ataxic phenotype in *pcd* mice, whereas other CCPs, as CCP4 and CCP6 had little or no activity, indicating that they are not functionally equivalent to CCP1 *in vivo* (H. Y. Wu et al., 2015). It should be noted that CCP1 is the only one of these three enzymes which is localised in the nucleus (Rodríguez de la Vega et al., 2013). Although the molecular processes by which the loss of function of CCP1 leads to neuronal degeneration and subsequent death of *pcd* mice remains unknown, different molecular mechanisms have been proposed: endoplasmic reticulum stress (Chakrabarti et al., 2009), decreased peptide replacement by the proteasome (Kyuhou et

al., 2006), mitochondrial dysfunction and altered proteolytic processing of interactor proteins with CCP1 (Gilmore-Hall et al., 2019), dysfunction of microtubule stability (Tanco et al., 2015) and a transcriptional silencing due to progressive accumulation of DNA damage (Baltanás, Casafont, Lafarga, et al., 2011; Baltanás, Casafont, Weruaga, et al., 2011; Baltanás et al., 2019; Valero et al., 2006).
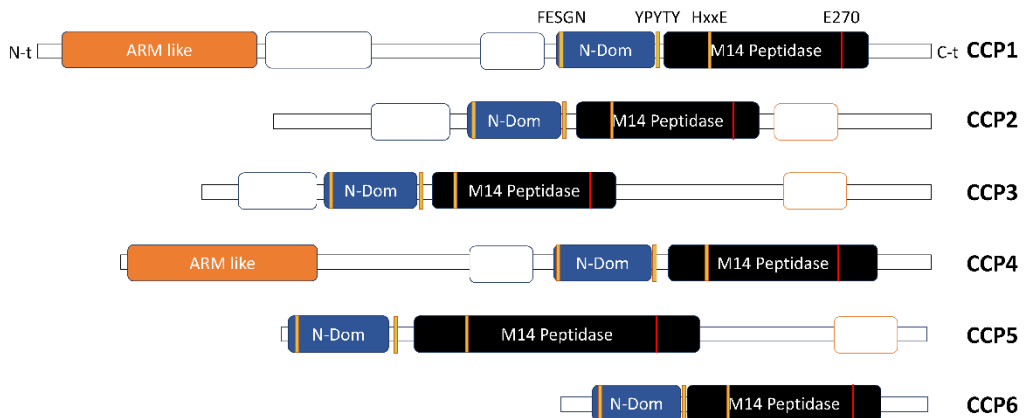
FIGURE 3.1. REPRESENTATION OF THE ARCHITECTURE OF HUMAN CCPS. The core domains of CCPs are the carboxypeptidase catalytic domain M14 Peptidase) and the characteristic conserved N-domain (N-Dom). ARM-like represents an armadillo-like domain and the other represented domains are poorly defined, displaying no homology with known domains.

Another open question about CCP1 is its possible nuclear function. Due to the presence of nuclear localisation sequences (NLS) and nuclear exportation sequences (NES) that directly binds CCP1 to the nuclear exportation receptor CRM1, it is allowed to localise both in the nucleus and in the cytoplasm (Thakar et al., 2013). Consistent with a nuclear role of CCP1 in the cell nucleus, it has been shown that the *pcd* mutation in mice induced the formation of DNA damage/repair foci of mitral cells in the olfactory bulb, being these DNA alterations associated with the inhibition of the transcription, heterochromatisation, nuclear segregation and the reorganization of nuclear speckles and Cajal bodies (Baltanás et al., 2019; Valero et al., 2006). In addition, recently in our group, we have developed and optimized C-terminal proteomic methods for proteases and their application has led us to identify seven potential new substrates for CCP1 in addition to tubulin (Tanco et al., 2015). These include proteins such as HMBGs 1, 2 and 3 (High Mobility Group Proteins) or NAP1 (nucleosome assembly protein-like 1), highly polyglutamylated proteins associated with chromatin remodelling (Regnard et al., 2000).

Despite the great knowledge of the CCP1 function in the cytoplasm, little is known about their interactions and effects on cell nucleus. Understanding the biological role of the CCPs may reveal new perspectives for understanding the maintenance of the neuron and the *pcd* phenotype, giving new perspectives to help in the ataxia treatment in humans.

Therefore, the first objective of this work is to assess the specific nuclear localisation of CCP1 with a particular emphasis on its differential role within the nucleus.

3.2   Material and methods

3.2.1   Cell culture

3.2.1.1   Cell lines and maintenance

Adherent HeLa (human cervix adenocarcinoma) cells were purchased from the American Type Culture Collection (ATCC), were cultured in Minimum Essential Medium Alpha (MEM-Alfa, Gibco) supplemented with 10% foetal bovine serum (FBS, Invitrogen) and maintained at 5% CO_2 at 37 °C. Adherent HEK293T (Human Embryonic Kidney, ATCC) were maintained in Dulbecco's Modified Eagle's Medium (DMEM, Gibco) supplemented with 10% FBS and incubated at 37 ºC with 10% CO_2. Adherent SH-SY5Y (human brain-derived from metastatic bone marrow, ATCC) cell line was cultured in Dulbecco's Modified Eagle's Medium and Ham's F-12 with 4500 mg/L glucose, GlutaMAX–I and pyruvate (DMEM:F-12, Gibco) supplemented with 10% FBS and maintained with 5% CO_2 at 37 ºC.

3.2.1.2   Mitotic cell arrest by nocodazole

Adherent HeLa cells were seeded into 100 mm dishes at 2×10^5 cells/mL in 10 mL of complete culture medium and incubated at 37 ºC in a humidified atmosphere with 10% CO_2 for 24 h. For mitotic cell arrest, nocodazole (Sigma) was added to the dishes at a final concentration of 0.5 µg/mL. Cells with nocodazole were incubated for 10 hours at the previously stated conditions. Next day, cells were released from nocodazole-mediated arrest in early M phase by shaking the plates and gently pipetting the medium. Medium containing detached cells was centrifuged at 1,400 rpm for 5 minutes and pelleted cells were washed twice with cold phosphate buffered saline (PBS). Cells were resuspended in 10 mL of complete medium and were re-plated in 24-well plates at 50,000 cells/well. Samples were collected every 1.5 h to obtain a profile of the cell cycle progression and prepared for subsequent immunocytochemistry assays.

3.2.1.3   CCP1 *in vitro knockout* in SH-SY5Y cells

3.2.1.3.1   *CRISPR/Cas9 KO plasmid transfection*

For knockout (KO) generation of CCP1 in the neuroblastoma cell line SH-SY5Y, three different guide sequences targeting exons 3, 4 and 8 of the human AGTPBP1 gene were used cloned the CRISPR/Cas9 KO Plasmid from Santa Cruz Biotechnology. Each plasmid encoded the Cas9 nuclease and a target-specific 20 nucleotide guide RNA. Cells were seeded on 6-

well tissue culture plates with standard growth medium and incubated at 37 ºC in a humidified atmosphere with 5% CO_2 for 24h.

Next day, cells at a 40-80% confluency were transfected with AGTPBP1 CRISPR/Cas9 KO Plasmid (Santa Cruz Biotechnology) using Lipofectamine 2000 (Invitrogen) according to the manufacturer's protocol. Briefly, 3 µg of DNA was diluted to a final volume of 150 µL of Opti-MEM (Gibco) medium and 15 µL of Lipofectamine 2000 Reagent was also diluted in 150 µL of Opti-MEM. Both solutions were combined, vortexed and let stand at room temperature for 5 minutes.

Prior to transfection, media was replaced with fresh antibiotic-free growth medium. 300 µL of the mixed solution were added to each well, with gentle mix by swirling the plate. Cells were then incubated for 24 hours under standard conditions. After incubation, successful transfection of CRISPR/Cas9 KO Plasmid was visually confirmed by detection of the green fluorescent protein (GFP) via fluorescent microscopy.

3.2.1.3.2   *Transfected cells selection by cell sorting*

Transfected cells were isolated by fluorescence activated cell sorting (BD FACSJazz), using low-intensity GFP-positive pass gating and seeded as single cells onto a 96-well plate with standard medium. CRISPR clones were cultivated for two weeks selecting clones with no discernible CCP1 protein expression by immunoblotting. Among total surviving clones screened, which exhibited identical phenotypes and no detectable CCP1 expression, one was selected for use in this study.

3.2.1.4   Neuron differentiation assay of wild-type and CCP1KO SH-SY5Y cells

3.2.1.4.1   *Differentiation induction by retinoic acid*

SH-SY5Y and SH-SY5Y CCP1KO cells were differentiated in a single-step protocol. Adherent cells were seeded into 100 mm dishes coated with 0.5 mg/ml collagen (Sigma) at 2×10^5 cells/ml in 10 ml of complete culture medium further supplemented with 10 µM all-trans retinoic acid (RA, Sigma) before adding the medium to the cells. Cells were incubated at 37 ºC in a humidified atmosphere with 10% CO_2 for 8 days.

3.2.2   Functional analysis

3.2.2.1   BrdU assay

Adherent HEK293T cells were seeded into 24-well plates at 5 x 10^4 cells/mL in 1 mL of complete culture medium and incubated at 37 ºC in a humidified atmosphere with 10% CO_2 for 24h. Next day, the culture media was replaced with 10 µM of 5-bromo-2'deoxyuridine (BrdU, Abcam) labelling solution by dilution of 10 mM BrdU stock solution in cell culture medium. Cells were then incubated for additional 24 h and the BrdU labeling solution was removed from the cells and washed twice in PBS for about 5 seconds per wash.

Cells were fixed and permeabilized according to previously described immunocytochemistry protocols. However, before proceeding with immunostaining, cells were incubated in 1 M HCl for 30 minutes at RT.

3.2.2.2   Inhibition by actinomycin D

Adherent WT and CCP1KO SH-SY5Y were seeded on 24-well at 5 x 10^4 cells/mL in 1 mL of standard medium. Cells were let to adhere for 24 h at 37 °C, 10% CO_2. Next day, cells from the first well were fixed as the first time point with 4% paraformaldehyde. Remaining wells were supplemented with 10 µl of 1 mg/mL Actinomycin D stock (Sigma) to obtain a final concentration of 10 µg/mL in 1 mL of culture media. Subsequent wells were fixed at 1, 2, 4, 6 and 8 h time points following Actinomycin D addition and were prepared for immunostaining assay.

3.2.3   Protein analysis

3.2.3.1   Subcellular fractionation

Cells were grown to confluence in 100 mm diameter dishes and were washed with ice-cold PBS, scraped from culture dishes on ice using a plastic cell scraper and collected in 1.5 mL micro-centrifuge tubes in 1 mL of ice-cold PBS. After spin centrifugation, the supernatant was removed from each sample and cell pellets were resuspended in 900 µL of ice-cold 0.1% NP40 (Sigma) in PBS and resuspended 5 times up and down with a p1000 micropipette. 300 µL of the lysate was removed as "whole cell lysate" and 100 µL of 4 × Laemmli sample buffer was added to it, then kept on ice until the sonication step. The remaining (600 µL) material was centrifuged for 10 sec in 1.5 mL micro-centrifuge tubes and 300 µL of the supernatant was removed as the "cytosolic fraction". 100 µL of 4 × Laemmli sample buffer was added to

this fraction and boiled for 1 min. After the remaining supernatant was removed, the pellet was resuspended in 1 mL of ice-cold 0.1% NP40 in PBS and centrifuged as above for 10 sec and the supernatant was discarded. The pellet (~20 μL) was resuspended with 180 μL of 1 × Laemmli sample buffer and designated as "nuclear fraction". Nuclear fractions and whole cell lysates that contained DNA were sonicated using microprobes (Misonix, NY, USA) at level 2, twice for 5 sec each, followed by boiling for 1 min.

3.2.3.2 Western blotting

For immunoblotting in selecting clones with no discernible CCP1 protein expression after CRISPR assay, equivalent amounts of each lysate or fraction were analysed by sodium dodecyl sulphate polyacrylamide gel electrophoresis (SDS-PAGE), and the separated proteins were electrophoretically transferred onto polyvinylidene difluoride (PVDF) membranes (Millipore). Non-specific binding sites on the PVDF membranes were blocked by incubation with 5% skim milk for 1 h. The PVDF filters were then incubated with anti-CCP1 antibody (dilution 1:1,000; Proteintech) overnight at 4 °C. After washing with PBS containing 0.05% Tween 20, the filters were incubated with goat anti-rabbit IgG-peroxidase (dilution 1:10,000; Bio-rad) for 1 h. After three rinses, immunoreactive bands were visualized with a chemiluminescence detection kit (Millipore) using the Molecular Imager VersaDoc (Bio-rad).

To assess the neural differentiation of WT and CCP1KO SH-SY5Y cells by RA, whole cell lysate, cytoplasmic and nuclear fractions, were loaded and electrophoresed using SDS-PAGE gels and transferred to PVDF membranes. Membranes were incubated with anti-CCP1 or anti-NAP1L4 antibodies. Anti-GAPDH and anti-lamin b were used as cytoplasmic and nuclear markers. The protocol described above was used to reveal the membranes.

3.2.4 Confocal microscopy

For CCP1 cellular distribution analysis, HeLa and HEK293T cells were fixed with 4% paraformaldehyde (Sigma) for 30 minutes at room temperature (RT). Cells were further permeabilized with PBS containing 0.5% Triton X-100 (Sigma) for 30 minutes. Cells were then blocked with 1% bovine serum albumin (BSA, Sigma) in PBS 0.05% Tween (Sigma) for 30 minutes and then incubated with 1/100 dilution of anti-CCP1 antibody (Proteintech) overnight at 4ºC. Cells were washed and incubated with Alexa anti-rabbit 488 (Molecular

Probes) for 1 hour at room temperature and nuclei were further counterstained with 4',6-diamidino-2-phenylindole (DAPI). Samples were then mounted with ProLong Gold (Life Technologies).

Double immunolabelling combining anti-CCP1 with anti-nucleolin (Santa Cruz Biotechnology), Fibrillarin, U2B, Pan-Histone, Paxillin, α-tubulin and GM-130 (Sigma) was done using the same protocol plus the respective antibodies in a step before to the anti-AGTPBP1 addition with 3 hours incubation at RT. For CCP1 cell cycle distribution, samples from the mitotic arrest were prepared according to the same immunostaining protocol, selecting the time points corresponding to the different mitotic phases. Immunofluorescence images were collected on an inverted confocal microscope (Leica SP5) with a 63X objective. Images were analysed using Imaris software (Bitplane).

3.3   Results and discussion

3.3.1   Human CCP1 localisation varies along the cell cycle

Taking into consideration that tubulin is a CCP1 substrate, both proteins are expected to associate along the cell cycle (Rodríguez de la Vega et al., 2013). Moreover, nuclear staining has been previously described for CCP1 in interphasic cells, suggesting participation in nuclear functions that might be related to chromatin remodelling, DNA repair processes and nucleolar maintenance (Baltanás, Casafont, Weruaga, et al., 2011; Rodríguez de la Vega et al., 2013; Valero et al., 2006). Thus, the intracellular localisation of endogenous CCP1 was analysed in HeLa cells using confocal fluorescence laser scanning microscopy. Immunocytochemical labelling of HeLa cells with an affinity-purified polyclonal antibody against the whole CCP1 protein showed CCP1-immunoreactivity predominantly in the cytoplasm (Figure 3.2, Interphase) as described previously (Rodríguez de la Vega et al., 2013). However, the staining also appeared more concentrated in perinuclear structures and was observed in the cell nucleus as small aggregates (Figure 3.2, Interphase).

In cells in proliferative phase, we observed that CCP1-immunoreactivity was particularly intense in the nucleus where chromatin condensation was observed by DAPI counterstaining (Figure 3.2), showing a higher association with DNA at all stages of mitosis (Figure 3.2). Thus, we focused on the localisation and distribution of CCP1 in mitotic cells by obtaining confocal immunocytochemistry images after mitotic arrest with nocodazole. Interestingly, we observed changes in the protein localisation along the different cell cycle phases and, despite not having a clearly marked pattern; CCP1 shows a spatial distribution that aligns with the chromosomes (Figure 3.2). It is believed that CCP1 could be involved in cell cycle control and neurodegeneration due to its deglutamylation action over microtubules (Sirajuddin et al., 2014). Although CCP1 has not been directly linked to any mitotic phase, the highly important implication in tubulin PTM points out a possible implication in the formation and function of the mitotic spindle. In addition, we observed that there is a difference in the general pattern distribution of CCP1 among HeLa cells in relation to its confluence state. Hence, we can distinguish two conditions when observing the localisation of our protein of interest: low confluence cells (~50%) and high confluence cells (~80-90%).

HEK293T mitosis cycle
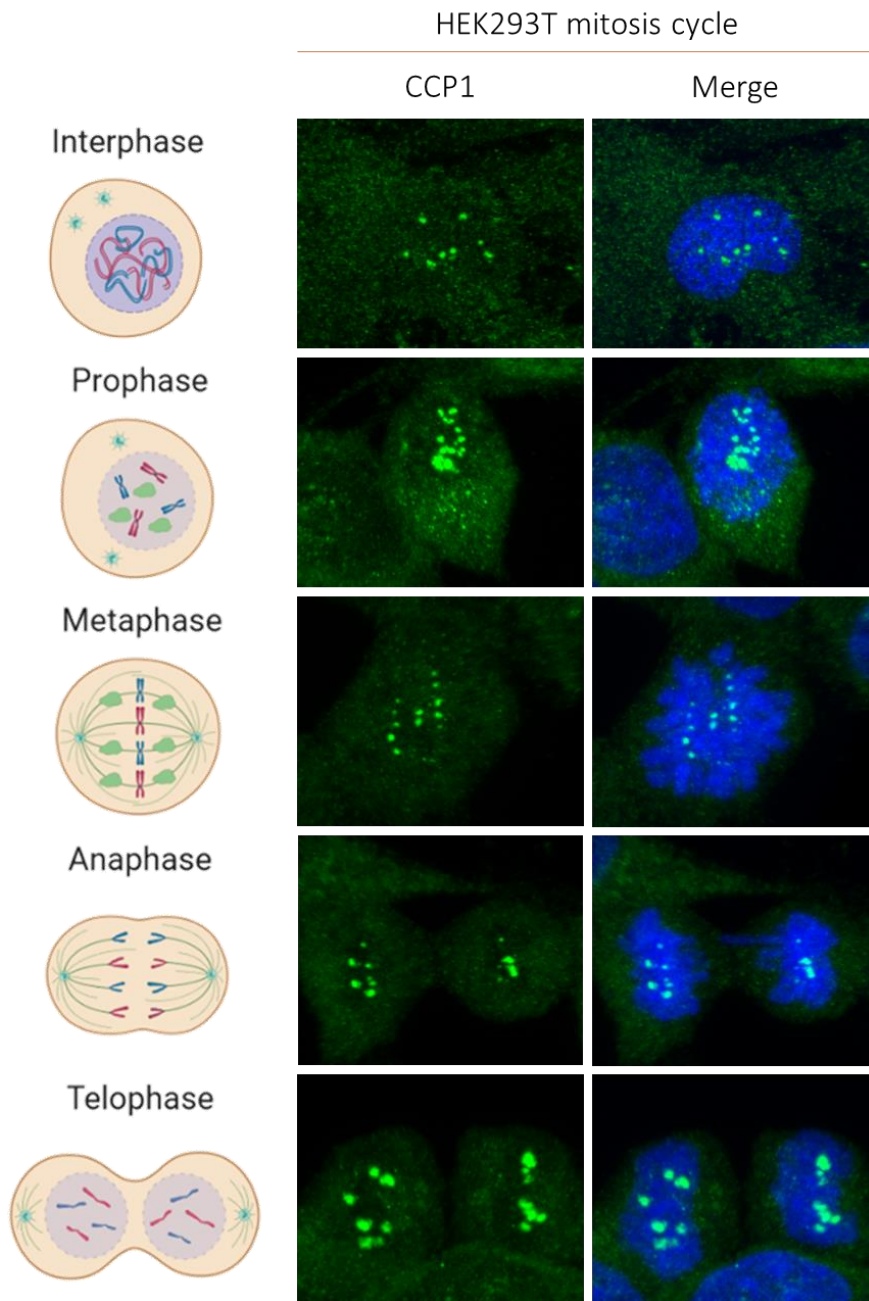
FIGURE 3.2. IMMUNOFLUORESCENCE ANALYSIS OF CCP1 DURING MITOSIS IN HELA CELLS. HeLa cells at different mitotic stages from interphase to telophase exhibiting DNA staining (DAPI, in blue), and CCP1 staining (in green). The images were acquired in an inverted confocal microscope (Leica TCS SP5) at room temperature and using an X63 objective and analysed with the Imaris software (Bitplane).

If we observed the general localisation pattern of CCP1 at low confluence, it is noticeable how the protein staining near the cytoplasm membrane resembles cell focal adhesions for cell attachment to the extracellular matrix (Figure 3.3). To confirm the CCP1 focal adhesion-like pattern in HeLa cells, we performed an immunostaining assay looking for co-localisation between CCP1 and paxillin, a protein that actively participates in the adhesion processes of the cell (Dong et al., 2016). The visual analysis confirmed that the patterns are alike, indicating a possible role of this cytosolic carboxypeptidase in cell attachment structures. The involvement of CCP1 in focal adhesions, however, is not constitutive, as is only seen in certain cells and occasions. The cell culture must be actively growing, and at relatively low cell confluences, suggesting that the carboxypeptidase is participating in the initial generation of the final structures. Since CCP1 has a well-studied role in cytoskeletal remodelling by microtubule deglutamylation (H. Y. Wu et al., 2015), it is expected that its function could be related to the junctions of microtubules with the adhesion complexes (Dong et al., 2016). However, no evidence of CCP1 function in cellular adhesion has been reported to date. The transient localisation of CCP1 in focal adhesions may have an implication in its role during ataxia generation in *pcd* mice, as the disease occurs a few weeks after mice are born, in a specific moment of neuronal development. We can speculate that loss of CCP1 localisation in these structures at the appropriate time in *pcd* mice could be involved in Purkinje cells neurodegeneration. Possibly, the absence of CCP1 in focal adhesions would impede the correct elongation of the dendrites of these cells, leading to their death.

Nevertheless, it is also worth mentioning how CCP1 staining in the cytoplasm in high confluence HeLa cell cultures near the nucleus resembles the Golgi apparatus (Figure 3.3). In order to confirm the presence of this carboxypeptidase in this subcellular compartment, we performed an immunostaining assay looking for co-localisation between CCP1 and GM-130, a common marker for Golgi in human cells. The visual analysis confirmed the overlapping of Golgi and CCP1 (Figure 3.3). As told before, the specific localisation of CCP1 in this area of the cell is directly related to the confluence of the cell culture and, therefore, with the time the cells have been growing. Thus, our protein tends to accumulate in the Golgi when the cell culture has been stabilized and there is no need for further duplication and growth. The Golgi apparatus is known to carry most of the PTMs affecting proteins, as

glycosylation or sulfation (Egea & Ríos, 2008). This specific localisation in the Golgi apparatus could favour the CCP1's deglutamylase activity over different cellular substrates, acting as a general modifying enzyme in this subcellular structure.
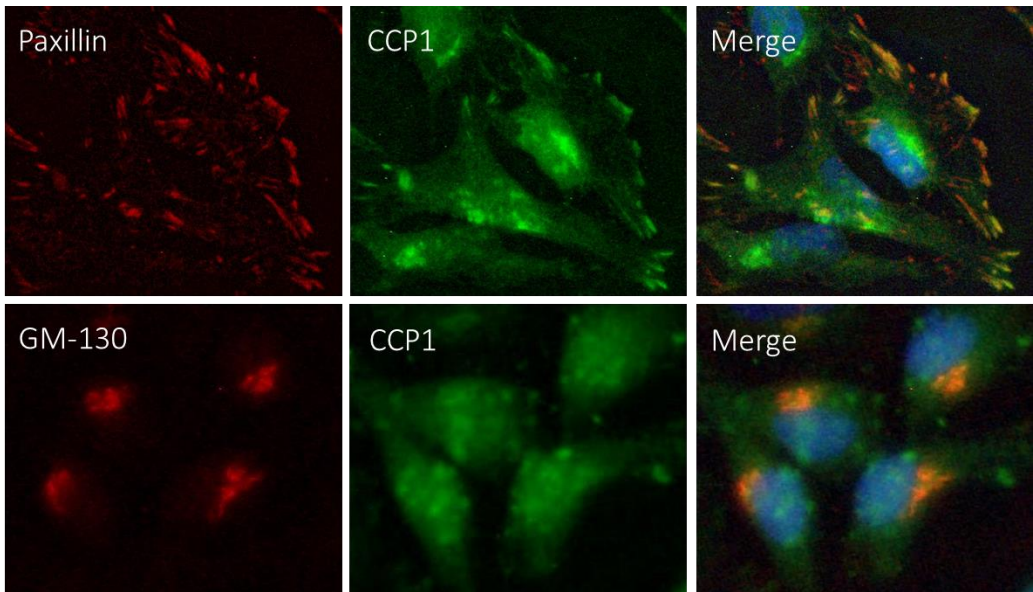
FIGURE 3.3. GENERAL DISTRIBUTION OF CCP1 AT DIFFERENT CYTOPLASMATIC LOCALISATIONS. Confocal micrographs of HeLa cells immunostained with anti CCP1 antibody (green), anti-paxillin antibody (Focal adhesions, red) and anti-GM130 (Golgi apparatus, red). The Z-projections of a stack of images were obtained with the Easy 3D tool (Imaris software, Bitplane).

3.3.2 CCP1 is involved in correct cell cycle progression and general polyglutamylation state

Following the CCP1 characterisation, we wanted to gain insight into the functional affection of loss of CCP1 in a cellular model. As previously mentioned, loss of function of CCP1 has been related to several cellular processes, being involved not only in microtubule remodelling, but also nuclear-related mechanisms. Hence, the generation of a cell line constitutively lacking CCP1 protein expression would let us investigate the effects of the protein at a cellular level, allowing us to further explore how CCP1 is involved in cell cycle progression. For this purpose, we established a CRISPR-Cas9-mediated knockout mutant for the CCP1 gene in HEK293T cells where clones with no CCP1 expression after CRISPR-Cas9 transfection were selected via immunoblotting against the full protein.

Tubulin is the main described CCP1 substrate for its deglutamylase activity, as it acts as a post-translational modifying enzyme (Rodríguez de la Vega et al., 2013; H. Y. Wu et al.,

2015). In cells, tubulin post-translational modifications constitute a powerful mechanism for the rapid and generally reversible regulation of the dynamics and functionality of cytoskeletal MTs. Most of the known PMTs take place in the C-terminal tail of tubulin, which corresponds to the interaction sites of the MAPs proteins, plus-end tracking proteins and molecular motors that are involved in the stability of MTs, intracellular trafficking and cell division, among other functions. The main MPTs associated with the C-terminal region of tubulin include deglutamylation / polyglutamylation, tyrosination / detyrosination, deglycylation / polyglycylation, and the generation of Δ2-tubulin and Δ3-tubulin (Garnham & Roll-Mecak, 2012; McKean et al., 2001).

The enzymes that catalyse the polyglutamylation, polyglycylation and tyrosination of tubulin belong to the tubulin tyrosine ligase-like family (Ikegami & Setou, 2009; Rogowski et al., 2009; van Dijk et al., 2007; Wloga et al., 2009), whereas the enzymes that catalyse the deglutamylation of poly-E side chains in the C-terminal region of tubulin and the generation of Δ2-tubulin and Δ3-tubulin are part of the M14D subfamily of metallocarboxypeptidases, the CCPs. To date, the CCP family, with six different members, is the only enzyme family described with deglutamylase activity.

Regarding the broad implications that CCP1's activity may have over MTs, we first focused on determining the changes in the PTMs generated in the C-terminal region of tubulin after CCP1 loss of action. For this purpose, we used the CCP1KO HEK293T cells, and compared them with wild type HEK293T cells. The soluble protein fractions of confluent cells were analysed by western blot with specific antibodies against tubulin PTMs that have been widely used in numerous studies and constitute one of the main tools to analyse this type of modifications (Magiera & Janke, 2013).

The glutamylation state in the C-terminal region of α- and β-tubulin was analysed using the GT335 antibody, which specifically recognizes the first branched Glu of the chain, and the anti-PolyE antibody, which detects long extensions of polyglutamate containing ≥3 Glu. Immunodetection with the two antibodies determined that CCP1 is directly involved in the general tubulin polyglutamylation state of cells, as polyglutamylated lateral chains (anti-PolyE) levels are increased in the knockout cells compared to the wild type control (Figure 3.4). Interestingly, GT335 levels were also increased in knockout cells despite CCP1 is not

involved in the removal of the first Glu from the chain at the branch point (Rogowski et al., 2010). The obtained results also reveal that there is not a significant change in the levels of Δ2-α-tubulin, suggesting that other members of the CCP subfamily are able to compensate CCP1's loss of activity in this case (Figure 3.4).

Most tissues present an overlapping expression of several CCPs, enabling redundant functions able to compensate a loss of function of one of them. However, recent studies support the growing evidence that not all CCPs have equivalent functions *in vivo* and that they act cooperatively or additively to activate signals in cellular MTs (Berezniuk et al., 2012, 2013; Kalinina et al., 2007; Rogowski et al., 2010; Tort et al., 2014; H. Y. Wu et al., 2017).
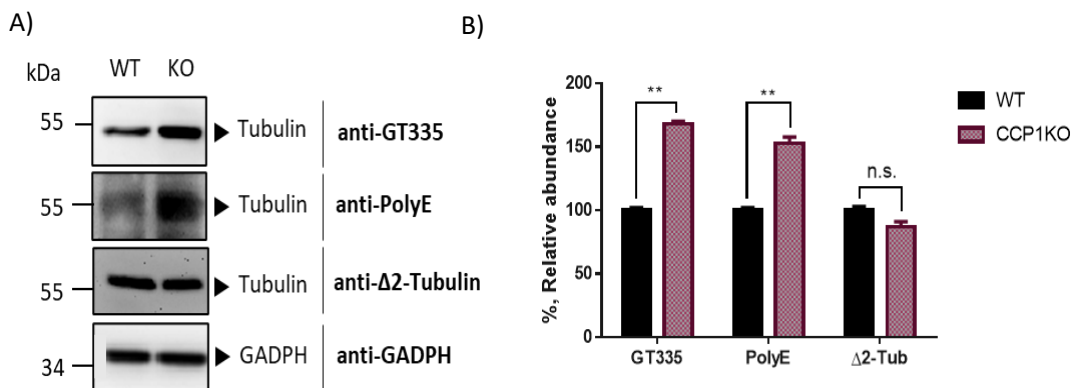
FIGURE 3.4. C-TERMINAL TUBULIN POST-TRANSLATIONAL MODIFICATIONS GENERATED BY CCP1. A) Western blot analysis from extracts of wild type (WT) and CCP1 knockout (CCP1KO) HEK293T cells for the specific immunodetection of Δ2-tubulin (anti-Δ2-tubulin), monoglutamylation (GT335) and polyglutamylation (anti-PolyE) in the C-terminal region of tubulin. Total tubulin levels were determined with α-tubulin antibody, whereas CCP1 expression was monitored with specific anti-CCP1 antibody. B) Analysis of the obtained data by densitometry comparison of the immunodetected bands.

With the present results, we can argue that loss of CCP1 activity is sufficient to alter general polyglutamylation levels in cellular microtubules as its action cannot be compensated by other CCPs in the cell. However, we did not observe significant changes in Δ-2 tubulin levels, suggesting a possible overlapping activity with other CCPs in different specific actions over the substrates. This substrate preference of CCP1 may constitute a mechanism of functional specialization that could be dependent on the cellular type or moment of the cell cycle.

Once the lack of CCP1 was determined to induce general changes in the post-translational state of microtubules, we next focused on its direct relationship with tubulin as a substrate and its location along the mitotic process, investigating how the mutated cells were affected by their cycle progression. Thus, to identify potential mitotic defects, we performed immunostaining experiments to label the mitotic spindles using an anti-α-tubulin antibody in the generated knockout HEK293T cells.

The identification of prometaphase defects was done using high-resolution confocal microscopy and led us to observe different mitotic affectations caused by the lack of CCP1 (Figure 3.5). The results showed prominent defects including monopolar and multipolar spindles with a significantly higher number of aberrant cells compared to wild type HEK293T cells (Figure 3.5). Most of the multipolar spindles exhibited a tripolar morphology, although multipolar cells with a higher number of spindle poles were also observed. It is noteworthy to mention that monopolar spindles were found to be more abundant than multipolar spindles in knockout cells (33 ± 3 % and 11 ± 3 %, respectively).

This data shows how CCP1 activity is directly related to mitotic spindle formation, promoting an abnormal formation when it is not present in cells. The formation of abnormal spindles is generally caused by defects in the maintenance of the mitotic spindle pole integrity. Specifically, multipolar spindles are usually the results of a centriole overduplication which in turn leads to a general loss of spindle pole integrity (Maiato & Logarinho, 2014). On the other hand, monopolar spindles can be formed as a result of defects leading to an inhibition of centrosome duplication, defects in motor-dependent forces, defects in microtubule dynamics or kinase-dependent defects (Tillement et al., 2009).

As seen in Figure 3.5, the CCP1 mutant shows both mitotic defects. At this point, we could assume that CCP1's action could be involved in a common step for the formation of the mitotic spindle, as the regulation of kinesin motor proteins. It has been observed that the *C. elegans* CCP1 orthologue CCPP-1 regulates the localisation and velocity of specific kinesin motors to maintain the structural integrity of microtubules in sensory cilia (O'Hagan et al., 2011). Hence, CCP1 would be acting in a similar way in mammalian cells, being an important protein for general spindle integrity in humans.
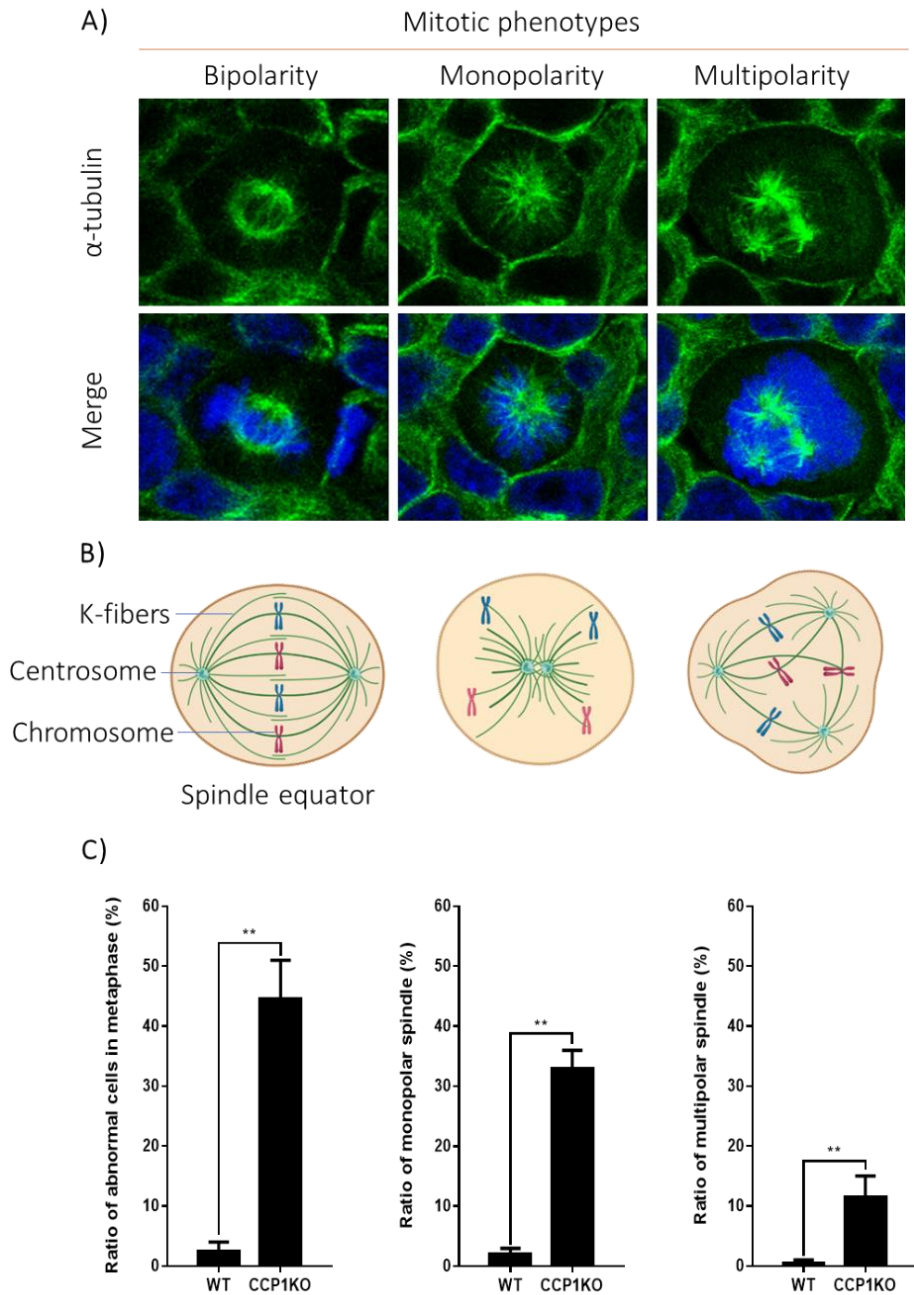
FIGURE 3.5. ANALYSIS OF THE MITOTIC DEFECTS CAUSED BY KNOCKING DOWN CCP1. A) Embryonic wild type and CCP1 knockout HEK293T cells were immunostained with DAPI (blue) to detect the nucleus and α-tubulin (green) to visualise the mitotic spindle (upper images). B) Schematic representation of wild type (left), monopolar (centre) and multipolar (right) mitotic spindles and chromosomes distribution in cells. C) The percentage of mitotic cells exhibiting multipolar spindles or lagging chromosomes for each condition. Error bars represent the mean ± S.E.M. from 3 independent experiments. ** = P ≤ 0.01. P-value derived from paired two-tailed t-test.

3.3.3 Human CCP1 is active in the dense fibrillar component of the nucleolus in the cell nuclei.

As mentioned before, CCP1 is not only involved in MT regulation by its deglutamylase action but has also been found to interact with other substrates (Tanco et al., 2015). Moreover, a nuclear function has been previously hypothesized for CCP1, suggesting a participation in nuclear functions that might be related to chromatin remodelling, DNA repair processes and nucleolar maintenance (Baltanás, Casafont, Lafarga, et al., 2011; Baltanás, Casafont, Weruaga, et al., 2011; Baltanás et al., 2019; Rodríguez de la Vega et al., 2013; Valero et al., 2006).

Hence, we focused on the specific nuclear localisation of CCP1 to identify the structures in which it could have a role. To determine the spatial relationship of nuclear foci of CCP1 to the different nuclear structures or nuclear compartments, we double-stained HeLa cells with CCP1 in combination with antibodies that recognize pan-histone as a chromatin marker; U2B as a marker of nuclear speckles of splicing factors; nucleolin as a marker of the nucleolus and fibrillarin as a marker of the dense fibrillar component (DFC) of the nucleolus to determine their co-localisation using confocal microscopy.

Regarding the findings in *pcd* mice that identified nucleolar disruption and nucleolin reorganisation in the Purkinje cells, we first examined the nucleolar markers fibrillarin and nucleolin. As shown in Figure 3.6, double staining between CCP1 and the nucleolar markers showed an evident co-localisation between both proteins in HeLa cells (Figure 3.6A) thus indicating that CCP1 is highly present in this nuclear structure. In a more detailed analysis carried by confocal microscopy and 3D reconstruction, we observed that CCP1 is localised inside the dense fibrillar component region (Figure 3.6) where the maturation of rRNA occurs (Sia et al., 2016). Interestingly, in a work realized in the research group using high-throughput proteomics screening on fibroblasts of WT and *pcd* mice that identifies proteins that were up-regulated or down-regulated by the presence or absence of CCP1 (unpublished results); we found fibrillarin as one of the downregulated ones when CCP1 was absent.
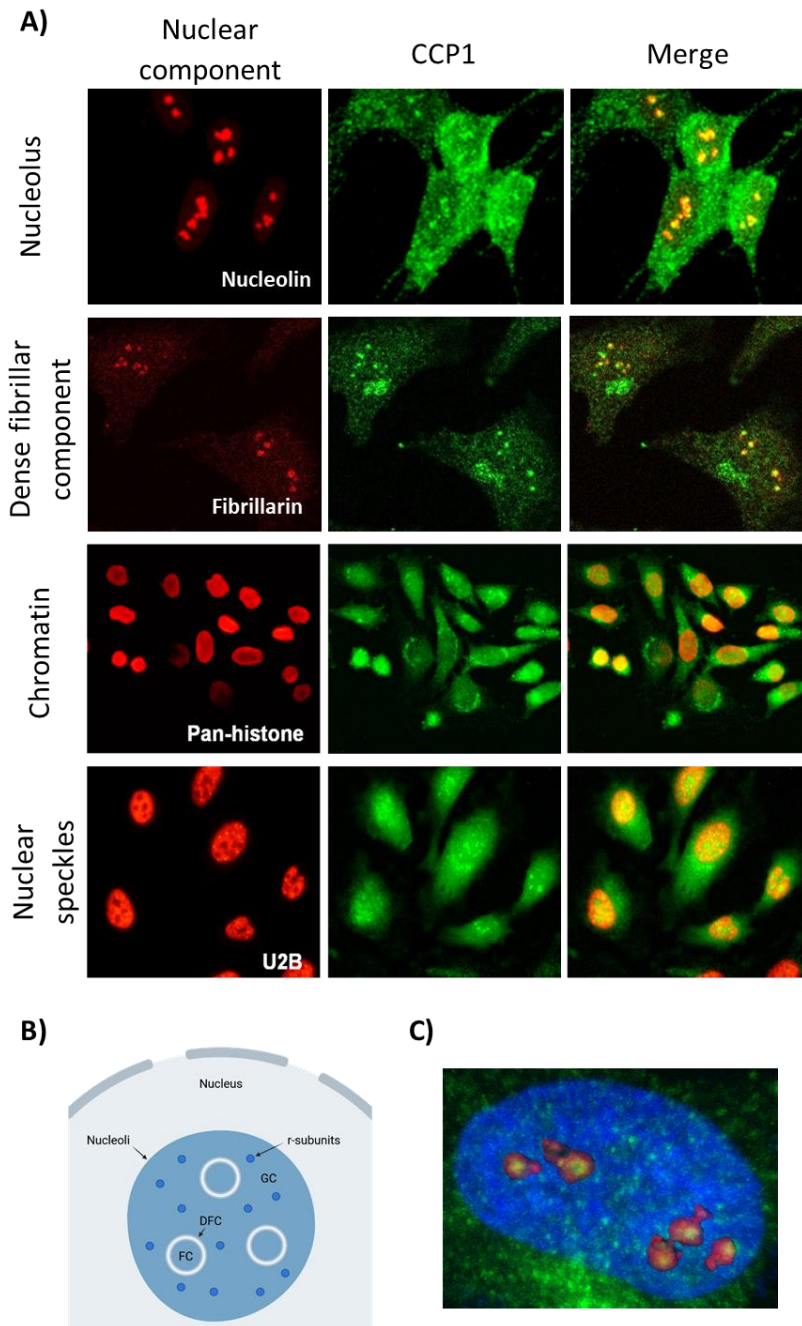
FIGURE 3.6. NUCLEOLAR LOCALISATION OF CCP1 IN HEK293T CELLS. A) Immunodetection by confocal microscopy of CCP1, nucleolin (nucleolus) and fibrillarin (DFC). Images were obtained on an inverted confocal microscope (Leica SP5) using a 63X objective and analysed with Imaris software (Bitplane). B) Schematic representation of the cell nucleolus identifying its principal components. GC = granular component, DFC = dense fibrillar component, FC = fibrillar component. C) 3D nucleus reconstruction of HEK293T cells stained with fibrillarin (red) and CCP1 (green)

Apart from the nucleolus, we also tested co-localisation with other two proteins, U2B and pan-histone, in order to test alternative nuclear localisations. However, not a clear co-localisation between CCP1 and U2B nor pan-histone has been found (Figure 3.6), showing that CCP1 may not be involved in pre-mRNA splicing.

Hence, we found that CCP1 function may be related to the nucleolus not only in Purkinje cells, but also in other tissues. At the microscopic level, the nucleolus has three morphologically distinct sub-compartments: the fibrillar centre (FC), the dense fibrillar component, where fibrillarin is localised, and the granular component (GC). In general, nucleolin could stain all the nucleolar structures. These parts are related to ribosome biogenesis by the recruitment of RNA polymerase I (RNA pol I) into the nucleolus for the initiation of rDNA transcription at the borders of the FC and DFC. At the same time, ribosomal proteins, made in the cytoplasm, are recruited into the DFC and GC to be assembled with the mature rRNAs to form the 40S and 60S ribosomal subunits (Sia et al., 2016).

Furthermore, nucleolar stress (disruption of the nucleolus) has been reported to cause neurodegeneration due to failure of ribosome biogenesis in diseases like Parkinson or Alzheimer, where the nucleolus has aberrant morphologies or sizes (Lessard et al., 2010). The generation of ataxic mice models by depletion of CCP1 due to neurodegeneration of Purkinje cells, and the observed localisation inside the DFC, suggest an important role in the whole nucleolar integrity. The absence of CCP1 in its nuclear localisation in the nucleolus may cause sufficient stress to prevent the correct development of the nucleolar processes, as the ribosome biogenesis, and neuronal growth in the brain areas where other CCPs cannot supplement its function.

3.3.4   CCP1 is directly involved in transcription processes

The aforementioned results show a link between CCP1 and the nucleolus *in vitro*, which is in concordance with a recent study on *pcd* mice characterisation where nucleolar stress is a key feature of the nucleolar Purkinje cell-phenotype (Baltanás et al., 2019). Nucleolar stress is associated with several neurodegenerative disorders, including Alzheimer's and Parkinson's diseases (Garcia-Esparcia et al., 2017; Haeusler et al., 2014; Hernández-Ortega et al., 2016; Hetman and Pietrzak, 2012; Parlato and Kreiner, 2013; Rieker et al., 2011; Tapia

et al., 2017). For instance, nucleolar stress induced by perturbation of rRNA synthesis after knocking out Tif1a, an RNA Pol I coactivator, leads to neurodegeneration in mice (Kreiner et al., 2013; Parlato et al., 2008). Moreover, reduction of rRNA synthesis and nucleolar size occurs during aging, which represents a major risk factor for neurodegenerative disorders (Mattson and Magnus, 2006). Nucleoli, and more precisely, the dense fibrillar component has been argued to be an important site for transcription, which is consistent with the high RNA production rate of this compartment (Casafont et al., 2006; Koberna et al., 2002). Thus, we first wanted to establish if there was a relationship between CCP1 and active transcription sites.

Transcription foci and the nuclear accumulation of newly synthesized RNA in cell nuclear domains were detected following the administration of 5-FU to cell culture medium. The nuclear incorporation of this halogenated nucleotide analogue into nascent RNA was visualized by immunocytochemistry with an anti-BrdU antibody (Boisvert et al., 2000). A short incubation of 30 minutes labelled predominantly the nucleolar RNA (Figure 3.7), concordant with the great concentration of active ribosomal genes within the nucleolus (Raška et al., 2004). Double labelling experiments for 5-FU incorporation and detection of CCP1 showed that both were co-localising into the nucleolus (Figure 3.7), thus indicating that CCP1 is present in active transcription sites *in vitro.*
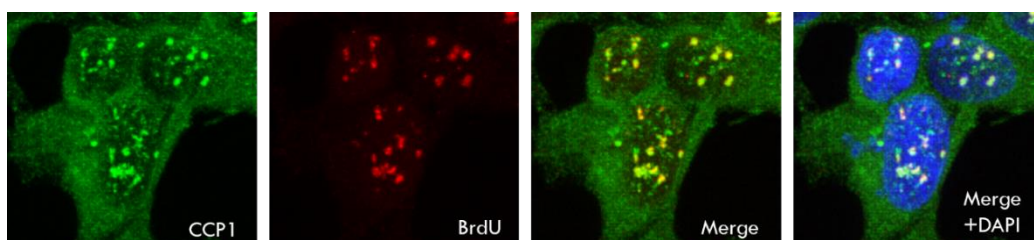
FIGURE 3.7. DOUBLE STAINING OF 5'FU INCORPORATION ASSAY AND CCP1 IN HEK293T CELLS. Human HEK293T cells were pulse-labelled with 5'fluorouridine (5'FU) for 10 min to label nascent RNA. Double immunofluorescence was performed with an anti-BrdU antibody to detect 5'FU and anti-CCP1, as indicated. Nuclei were visualised with DAPI (blue). Images were obtained on an inverted confocal microscope (Leica SP5) using a 63X objective and analysed with Imaris software (Bitplane).

Having established the nuclear co-localisation of nascent RNA and CCP1, we next investigate the nuclear dynamics of CCP1 incorporation in response to the inhibition of global transcription with actinomycin D (Act D). This antitumor antibiotic binds to DNA and

interferes with the progression of RNA polymerases (Sobell, 1985). Although Act D inhibits all kinds of cellular RNA synthesis, the nucleolar transcription of the ribosomal genes is particularly sensitive, even with very low doses of Act D treatment (Trask & Muller, 1988), resulting in a severe nucleolar dysfunction with segregation of the structural nucleolar components (Puvion-Dutilleul et al., 1992). In this context, we combined the administration of Act D treatment with the CCP1 and nucleolin staining to determine their affectation.
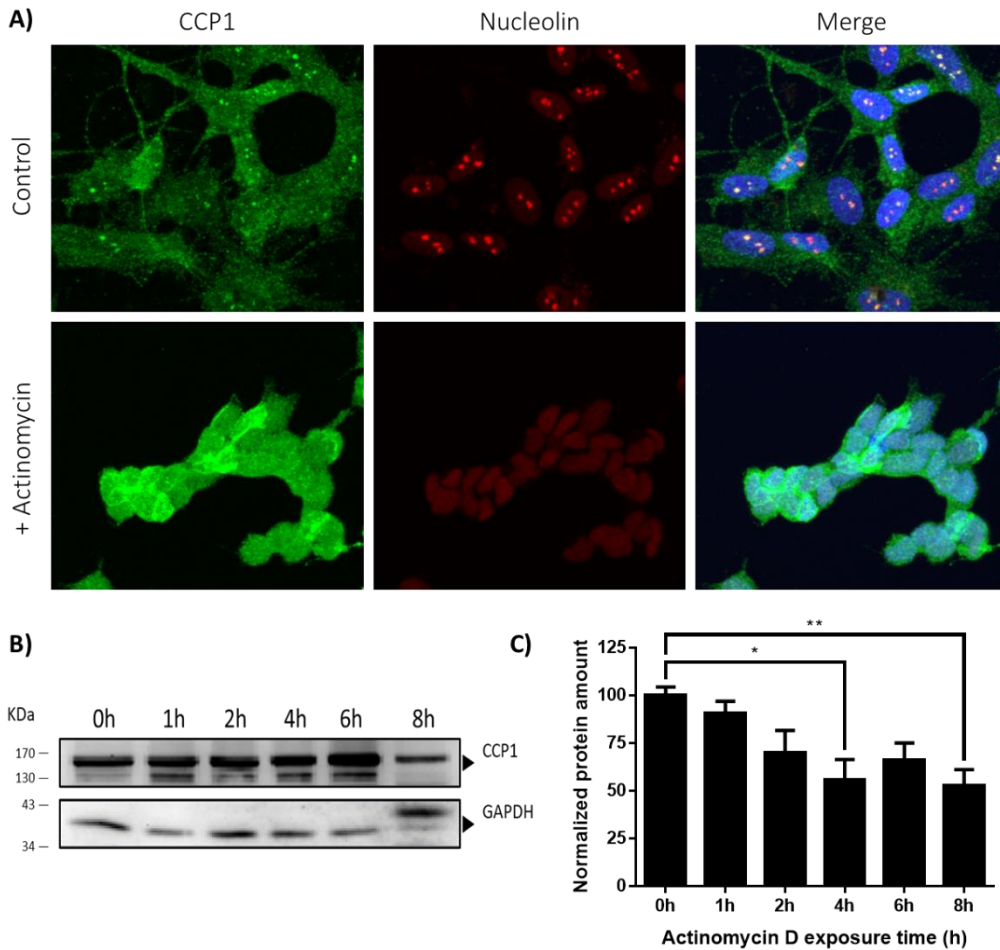
FIGURE 3.8. EFFECT OF TRANSCRIPTION INHIBITION OVER CCP1 LOCALISATION AND EXPRESSION. A) Immunofluorescence analysis of CCP1 in actinomycin D treated HEK293T cells. Cells were fixed after 4h treatment and double immunostained with anti-nucleolin and anti-CCP1 antibodies. Untreated cells were used as a control. Images were obtained on an inverted confocal microscope (Leica SP5) sing a 63X objective and analysed with Imaris software (Bitplane). (B) HEK293T cells were treated with 100 ng/mL of actinomycin D for the indicated time periods. Expression of CCP1 was monitored by western blot. (C) CCP1 ratios relative to GAPDH were determined by densitometry. Data are representative of three independent determinations. * = P ≤ 0.05, ** = P ≤ 0.01. P-value derived from multiple comparison one-way ANOVA test.

First results showed that the incubation of Act D for 4 h notably reduced the CCP1 signal in comparison with untreated control cells when assayed by immunoblotting of whole lysates (Figure 3.8). As can be seen, CCP1's presence in the cell nucleoli and its total expression is affected by RNA synthesis inhibition (Figure 3.8). These observations led us to elucidate that the presence of CCP1 into the DFC could depend on the presence of RNA in this nuclear compartment. To analyse the general CCP1 distribution in cells after Act D administration, we double stained HEK293T cells with anti-CCP1 and anti-nucleolin antibodies in the absence or presence of Act D. As expected, results showed a redistribution of nucleolar protein nucleolin from nucleoli to nucleoplasm after treatment with actinomycin D (Figure 3.8). More strikingly, CCP1 distribution also showed a relevant change in its cellular localisation. Regarding its characteristic nucleolar distribution, CCP1 was mainly dislocated from the nucleolus to the nucleoplasm (Figure 3.8). Moreover, the cytoplasmatic distribution of CCP1 was also affected, as the protein was primarily localised inside the nucleus (Figure 3.8). Our results showed the in-situ evidence that actinomycin D did induce dislocation of CCP1 in HEK293T cells, suggesting that the retention of CCP1 within nucleolus could be related to RNA synthesis.

3.4 Conclusions

In the present work, we focused on the general characterisation of CCP1, a member of the subfamily of cytosolic carboxypeptidases, focusing on its nuclear localisation. Since its discovery in 2000 during a search for overexpressed mRNAs involved in the axogenesis and reinnervation processes in mice, CCP1 has been linked to different neuropathologies in both humans and mice. Despite previous work has been done to characterize this protein and its relationship with the cytoskeleton, little information is known about its nuclear function and its importance in this cellular compartment. Apart from characterising the neuropathology of Purkinje cells obtained from the *pcd* mouse, CCP1 has not been directly related to any nuclear function. Accordingly, the conclusions of this chapter are:

1. In proliferative cells, CCP1 is mainly associated with condensed DNA, displaying a cell cycle-dependent subcellular distribution.

2. CCP1 changes its subcellular localisation depending on the cellular confluence state, locating in focal adhesions at low confluences and in the Golgi apparatus at higher confluences.

3. Loss of CCP1 activity influences the general polyglutamylation level of cells but does not affect the Δ2-tubulin generation.

4. CCP1 is related to spindle pole generation and/or maintenance, promoting abnormal mitosis when it is not present.

5. In the cellular nucleus, CCP1 is found in the dense fibrillar component of the cell nucleolus.

6. CCP1 is present at active transcription sites, where it colocalises with nascent RNA.

7. CCP1 is involved in transcription processes, and its nuclear/cytoplasmic shuttle is guided by the general transcription activity of the cell.

Characterising of the CCP1 and CCP6 interactome

The cytosolic carboxypeptidases 1 and 6 (CCP1 and CCP6) are metallocarboxypeptidases that catalyse the deglutamylation of the polyglutamate side chains generated as a post-translational modification in some proteins such as tubulins. While these two enzymes act as long-chain deglutamylases, they are not able to remove the branching point glutamate, a process catalysed by CCP5. They are implied in a wide spectrum of cell processes, such as spermatogenesis, antiviral activity, embryonic development and neurodegeneration. In fact, the lack of expression of CCP1 leads to selective and progressive degeneration of specific neuronal populations, including the Purkinje cells (PC) of mice cerebellum. In the present work, the role of CCP1 and CCP6 has been assessed by the BioID system, a proximity based labelling method for interactomics analysis. This method allowed us to screen for physiologically relevant protein interactions that occur in living cells in a high-throughput manner. Results for CCP1 linked the carboxypeptidase with the nucleosome assembly mechanism and RNA metabolism, giving an interesting approach to other less studied roles which can be key for the implication of this protein in processes like neurodegeneration. The results for CCP6 showed a great number of proteins associated with the centrosome and other related cellular structures such as centriolar satellites; indicating that it could be present in the pericentriolar material matrix (PCM). In addition, we identified proteins present in the microtubule organizing centre (MTOC) and the protein TTLL5 (associated with polyglutamylation), as putative interactors of CCP6. Further bioinformatics analysis revealed that CCP6 was presumably involved in processes including the centrosome organization, the cell projection organization and the microtubule-organizing centre, giving a broad overview of the implication of this enzyme in the cell cycle and in microtubule stabilisation.

Chapter 4. Characterising of the CCP1 and CCP6 interactome

4.1 Introduction

Disruption of the gene encoding for CCP1 in mice and humans has been reported to perturb neuronal maintenance, thus generating the Purkinje cell degeneration (*pcd*) model in mice, and the infantile-onset neurodegeneration in humans (Fernandez-Gonzalez et al., 2002; Shashi et al., 2018). Moreover, in mammals, mRNA expression of CCP1 is upregulated during axogenesis and reinnervation processes, suggesting a role of CCP1 in neuroregeneration (Harris et al., 2000). Different studies have been conducted to elucidate the role of CCP1 in neurodegeneration processes, pointing to different possible mechanisms such as endoplasmic reticulum stress (Kyuhou et al., 2006), decreased peptide turnover downstream from the proteasome (Berezniuk et al., 2010), mitochondrial dysfunction (Chakrabarti et al., 2009; Gilmore-Hall et al., 2019), dysfunction in microtubule stability (J. Li et al., 2010), transcriptional silencing due to the accumulation of DNA lesions (Baltanás, Casafont, Lafarga, et al., 2011; Baltanás, Casafont, Weruaga, et al., 2011) and induction of p53-dependent nucleolar stress (Baltanás et al., 2019). The whole picture of the involvement of CCP1 in the processes of neuronal degeneration and regeneration, still, remains elusive.

The role of CCP1 in its cytoplasmic localisation, mainly associated with the assembly and elongation of microtubules by its action as tubulin deglutamylase (T. Kubo et al., 2010; Rodríguez de la Vega et al., 2013; Suryavanshi et al., 2010), is a fundamental component for the understanding of CCP1's function. However, the cytoplasmatic role is not sufficient for explaining the nuclear affectations observed in the mouse models. It has been observed that CCP1 contains both a nuclear localisation signal and a nuclear export signal, allowing its continuous shuttling between the nucleus and the cytoplasm (Thakar et al., 2013). Nonetheless, the primary nuclear functional role of CCP1 remains mostly unknown.

On the other hand, CCP6 loss of function has been related to a great variety of cellular processes including the development of megakaryocytes (Ye et al., 2014), response to DNA virus infection (Xia et al., 2016), embryonic development (Ye et al., 2018) and oncogenic processes (C. Li et al., 2016). These findings exemplify the importance of this protein in the general control of cell fate. At the structural level, CCP6 is the shortest member of the CCPs, consisting only of the catalytic core and the characteristic N-domain that share all CCPs (Otero et al., 2012; Rodríguez de la Vega et al., 2013). Thus, the study of CCP6 is essential for the understanding of the roles and implications of CCPs during the cell cycle. As seen, numerous approaches have been conducted to identify the relation between the loss of function of CCPs and cellular processes or pathologies, however, there is still much to discover.

It is known that many proteins are found as part of multimolecular assemblies to perform their biological functions. These assemblies form a large network of molecular interactions, including interactions among molecules of the same type, for example, protein–protein interactions (PPIs). The vast array of molecular interactions in the cell is referred to as its interactome. The aim of this work, then, is to study the interactome landscape of CCP1 and CCP6 by means of an innovative proximity ligation interactomics approach, since the interactome of a cell is more diverse and can adapt more quickly to environmental cues than the transcriptome and proteome.

The proximity-dependent biotin identification (BioID) methodology is a unique method used to screen for physiologically relevant PPIs that occur in living cells (Roux et al., 2012). This methodology uses an *Escherichia coli* biotin protein ligase harbouring an R118G mutation, referred herein as BirA*, that is fused in frame to a protein of interest. The R118G BirA* mutant can still catalyse the formation of activated biotin (biotinyl-5'-AMP) but quickly dissociates from this intermediate (Kwon & Beckett, 2000). The BirA* tagged bait therefore, generates a cloud of activated biotin *in vivo*, which in turn can react with free primary amines, notably with the epsilon amine of lysine residues. As interaction partners and neighbours are marked by stable covalent modifications of their lysine side-chains, it is unnecessary to maintain protein complexes throughout the purification scheme. Harsh lysis conditions can thus be employed to effectively solubilize most cellular proteins. Subsequently, interaction partners of a BirA*-tagged bait can be effectively enriched by

performing a purification with streptavidin (which avidly binds to biotin) coupled to mass spectrometric analysis (Figure 4.1). To date, the BioID approach has been applied to baits located at the centrosome (Lambert et al., 2015), the nuclear envelope (D. I. Kim et al., 2016), and the Golgi apparatus (Chan et al., 2019) among others.
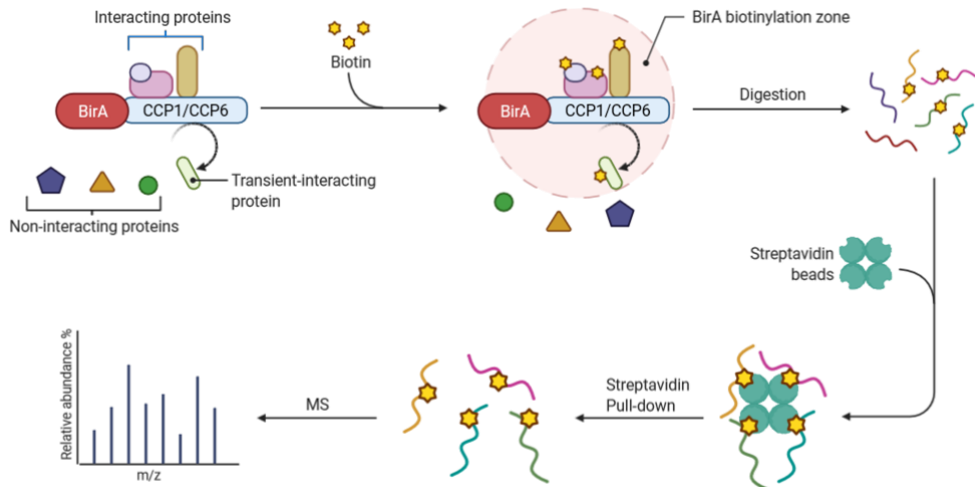
FIGURE 4.1. SCHEME OF THE BIOID METHODOLOGY. The protein of interest is fused with a promiscuous form of the bacterial biotin ligase BirA (BirA*) and expressed in cells. BirA* converts exogenously added free biotin to highly reactive but labile biotinyl-5'-AMP (yellow) which is released from the enzyme's active site allowing it to react with primary amines on proximal proteins, irrespective of whether they interact directly (pink and dark yellow) or indirectly (pale green) via additional protein–protein interactions with the fusion protein (labeling radius ~10 nm). Distal proteins (purple, orange and dark green) are not labeled. Following biotin labeling, cells are lysed, and proteins extracted under relatively harsh conditions. Biotinylated proteins are then purified using streptavidin (nonbiotinylated proteins are discarded) and identified by MS.

Using this methodology herein, we describe the human CCP1 and CCP6 interactome. We also developed methods to identify the implication of CCP1 over neuron cell progression focusing on its nuclear function as well as identifying the relation between CCP6 and its related ciliopathies. Our results suggest that CCP1 could control histone deposition by its deglutamylating activity over nucleosome assembly proteins. We also propose that CCP6 has a relevant function in the generation and maintenance of the cilia and the kinetochore, but further work will be necessary to know the whole implications of all the detected interactors.

4.2   Methods and materials

4.2.1   Cell lines and cell culture

Adherent HEK293T (ATCC), Flp-In T-REX 293 cells (HEK293T cells containing a single stably integrated FRT site at a transcriptionally active genomic locus, Thermo Fisher Scientific), and SH-SY5Y (ATCC) cell lines were cultured in DMEM and DMEM:F-12 (Gibco) supplemented with 10% heat-inactivated FBS. Cells were incubated at 37 °C in a humidified atmosphere with 10% and 5% CO_2 respectively.

4.2.1.1   Differentiation induction by retinoic acid

SH-SY5Y and SH-SY5Y CCP1KO cells were differentiated in a single-step protocol. Adherent cells were seeded into 100 mm dishes coated with 0.5 mg/ml collagen (Sigma) at 2×10^5 cells/ml in 10 ml of complete culture medium further supplemented with 10 µM all-trans retinoic acid (Sigma) before adding the medium to the cells. Cells were incubated at 37 °C in a humidified atmosphere with 10% CO_2 for 8 days.

4.2.1.2   Cell migration assay

To study the functional effect of CCP1 after DNA damage, we performed an *in vitro* scratch assay as it is a simple method to study cell growth and migration. By creating an artificial gap on a confluent cell monolayer (i.e., a "scratch") the cells of the edge will migrate to close the gap until cell-cell contacts are established anew (Liang et al., 2007). This method can be used to mimic cell migration in wound healing *in vivo*.

Sub-confluent SH-SY5Y and SH-SY5Y CCP1KO cells were plated into 6-well plates (Corning Inc) and cultured until confluence was reached. Confluent cells were washed twice with PBS and then incubated in the presence or absence of doxorubicin (0.2 µg/ml) for 24 h. After treatment, the cells were washed, and a one-centimetre scratch was performed in each well with a 200 µl tip (Star Lab). Afterwards, cell debris was washed out with complete medium. Plates were then incubated for 96 hours at 37°C with a periodical visual examination.

4.2.2   Interactomic studies

4.2.2.1   Molecular cloning and generation of stable cell lines

All plasmids used in this study were constructed by PCR and restriction enzyme digestion. BioID scaffold plasmids constructed for inducible expression (pcDNA5_FRT-TO_FLAGBirA-

[MCS]) were obtained from Addgene. CCP1 and CCP6 ORFs were obtained from previously generated plasmids in our laboratory. Both constructs had 5×glycine-alanine linkers added between BioID and the ORFs to provide flexibility between the modules. All constructs were sequence verified and protein expression was assessed by western blotting with an anti-FLAG antibody (Sigma-Aldrich) Flp-In™ T-REx™293 cells (purchased from Thermo Fisher Scientific, catalogue number: R78007), which constitutively express the Tet repressor, were used to generate the stable cell lines. Stable cell lines were generated by transfection with Lipofectamine 2000 (Thermo Fisher Scientific) and a combination of the appropriate pcDNA5 construct and pOG44, which expresses a Flippase. After recovery from transfection, cells were grown in DMEM containing 10% FBS, and 50 μg/mL Hygromycin B. Colonies were isolated, expanded, and screened for expression of the fusion proteins by Western Blotting with an anti-FLAG antibody (A8592, Sigma-Aldrich). All DNA transfections were carried out using polyethylenimine (PEI), linear, 25 kDa (PolySciences, Warrington, PA, USA). Briefly, DNA was mixed with PEI in a ratio of 1:3 and incubated in the presence of serum-free medium for 15 minutes at room temperature. Cells, at a 40-50% confluency, were exposed to the transfection complex at 1.4 ug DNA per ml medium concentration.

4.2.2.2   BioID

To initiate the BioID experiment, low passage cells were plated at 1×10^7 cells/plate in 15 cm dishes as four replicates, with each replicate consisting of 6 × 15 cm plates. After 6 h of plating, tetracycline was added to the media at a final concentration of 1 μg/ml. After 24 h, biotin was added to the media to a final concentration of 50 μM, and the cells were incubated for an additional 24 hr. After decanting the media, cells were collected from each plate by pipetting with ice-cold PBS. Cells were centrifuged at 1400 rpm for 5 min and the PBS was decanted. Cells were washed once more with ice-cold PBS before proceeding to cell lysis. Cells were resuspended and lysed in 9 mL stringency buffer (100 mM Tris-HCl, pH 7.5; 150 mM NaCl, 2% (w/v) SDS, 8 M urea, and protease inhibitors (Complete Protease Inhibitor Cocktail, Roche; Switzerland)) by gentle rocking for 5–10 min at 4°C. The cell lysate was sonicated to reduce viscosity (4 sonication cycles consisting of 3 groups of 25 seconds bursts, 40% intensity amplitude, 0.5/0.5 cycles). The sonicated lysates were combined with 500 μL streptavidin-conjugated agarose beads (Novagen, Germany) and incubated overnight at 4 °C with gentle rocking. Bead/lysate mixtures were collected by centrifugation

at 500 g for 5 minutes. The beads were then washed 4 times with 1 mL stringency buffer. Washed beads were then changed to 1 mL high salt buffer (100 mM Tris pH 7.5; 1 M NaCl) for 30 minutes at room temperature with gentle agitation and washed once with 1 mL ultrapure water. Typically, 50 µL of the bead suspension in 1 mL ultrapure water were analysed by SDS-PAGE after protein elution in elution buffer (2% (w/v) SDS, 3 mM biotin, 8M urea in PBS) and 10 minutes heating at 96 °C. Beads were separated from the elution solution by centrifugation. The rest of the washed beads ultrapure water were used for on bead trypsin digestion.

4.2.2.3   Mass spectrometry

4.2.2.3.1   Sample preparation

Sample preparation was performed at the Universidade Nova de Lisboa under guidance of Dr. Hugo Santos. In brief, beads were washed three times with 1 ml of 50 mM ammonium bicarbonate pH 8.0 (ABC buffer) and pelleted by centrifugation at 600 g for 2 minutes. Washed beads were re-suspended in 600 µL ABC buffer, and 1 µg trypsin was added to each peptide mixture. On bead trypsin digestion was incubated overnight at 37 °C with gentle agitation. Next day, additional 0.5 µg of trypsin were added to each sample (in 10 µL 50 mM ABC) and samples were incubated for an additional 2 hours at 37 °C. Trypsinised beads were then pelleted (600 g, 2 min) and the trypsin-digested proteins supernatant was transferred to a low-binding 1.5 mL tube. Beads were then rinsed 2 times with 300 µL of mass spec-grade H_2O. Rinses were combined with the original supernatant. The pooled fractions were acidified with 10% formic acid (to get a final concentration of 0.2% of formic acid), centrifuged at 16,100 g for 20 minutes, and the supernatant was transferred to a new low-binding 1.5 mL tubs and dried in a speed-vac. Samples were resuspended in 25 µl of 2% acetonitrile, 2 mM TCEP buffer (Tris [2-Carboxylethyl]-Phosphine Hydrochloride) and centrifuged at 16,100 g for 15 minutes and used for analysis.

4.2.2.3.2   Data acquisition

Each trypsin-digested sample was analyzed independently by reverse-phase liquid chromatography MS/MS (EASY-nLC + UHR-QTOF IMPACT HD, Bruker). Operational management and data analysis was performed by Dr. Hugo Santos. In brief, label-free quantification was carried out using MaxQuant software V1.6.0.16. All raw files were

processed in a single run with default parameters. Database searches are performed using the Andromeda search engine with the UniProt-SwissProt Human Uniprot Proteome database (release 2020_3) as a reference and a contaminants database of common contaminants. Data processing was performed using Perseus (version 1.5.0.31). Protein group LFQ intensities were log 2-transformed to reduce the effect of outliers. To overcome the obstacle of missing LFQ values, missing values were imputed before fitting the models. Log ratios were calculated as the difference in average log2 LFQ intensity values between the two digestion methods tested (two-tailed, Student's t-test). A protein was considered statistically significant if its fold-change was ≥1.5 and FDR ≤ 0.01.

4.2.3 Protein analysis

4.2.3.1 Subcellular fractionation

Cells were grown as monolayers in 100 mm diameter dishes and were washed in ice-cold PBS, scraped from culture dishes on ice using a plastic cell scraper and collected in 1.5 ml micro-centrifuge tubes in 1 mL of ice-cold PBS. After spin centrifugation, the supernatant was removed from each sample and cell pellets were resuspended in 900 µL of ice-cold 0.1% NP40 (Sigma) in PBS and triturated 5 times using a p1000 micropipette. 300 µL of the lysate was removed as "whole cell lysate" and 100 µL of 4 × Laemmli sample buffer was added to it, then kept on ice until the sonication step. The remaining (600 µL) material was centrifuged for 10 sec in 1.5 ml micro-centrifuge tubes and 300 µl of the supernatant was removed as the "cytosolic fraction". 100 µL of 4 × Laemmli sample buffer was added to this fraction and boiled for 1 min. After the remaining supernatant was removed, the pellet was resuspended in 1 ml of ice-cold 0.1% NP40 in PBS and centrifuged as above for 10 sec and the supernatant was discarded. The pellet (~20 µL) was resuspended with 180 µL of 1 × Laemmli sample buffer and designated as "nuclear fraction". Nuclear fractions and whole cell lysates that contained DNA were sonicated using microprobes (Misonix, NY, USA) at level 2, twice for 5 sec each, followed by boiling for 1 min.

4.2.3.2 Co-immunoprecipitation

Wild-type HEK293T and SH-SY5Y cells were used to confirm the interaction between CCP1 and their potential interactors at endogenous conditions. Cells were seeded at 2×10^6 cells/dish in 100 mm dishes and collected after 24 hours. Harvested cells were lysed at 4 °C

for 1 hour with NP40 lysis buffer (0.1% NP40 in PBS) supplemented with protease inhibitors without EDTA (Complete Protease Inhibitor Cocktail EDTA-free, Roche; Switzerland) and centrifuged at 12,000 rpm for 10 min. Protein G magnetic particles (Dynabeads® Protein G, Thermo Fisher Scientific) were first conjugated with the appropriate antibody (1 µg of antibody in 1.5 mg of magnetic particles) and rotated for 10 minutes at room temperature. The previously obtained supernatant containing the antigen was added (1 mL) to the magnetic beads and rotated for 30 minutes at 4 °C. Magnetic bead-Ab-Ag complex was washed 3 times using NP40 lysis buffer and samples were eluted with 1X SDS loading buffer and boiled for 5 minutes. The samples were subjected to western blot. Western blotting analysis and antibodies

Lysates and eluates were run on 4–12% polyacrylamide gels and transferred to PVDF (Immobilon-P, EMD Millipore; Billerica, MA) for 1.5 hr at 100 V constant current. Blots were blocked for 30 min with PBST 5% dry milk (w/v) and immunoblotted with appropriate antibodies. All antibodies were diluted in PBST 2% milk (w/v). Primary antibodies were incubated overnight at 4°C, while secondary antibodies were incubated for 1 h at room temperature. Antibodies used were mouse monoclonal anti-FLAG (Sigma, 1:5000 dilution), rabbit polyclonal anti-AGTPBP1 (Proteintech 1:500 dilution), rabbit polyclonal anti-NAP1L4 (Proteintech, 1:1000 dilution), rabbit polyclonal anti-GT335 (Adipogen 1:5000 dilution), mouse anti-GAPDH (Sigma 1:1000), mouse anti-H3 (Sigma, 1:1000), goat anti-rabbit HRP (BioRad, 1:5000 dilution) and goat anti-mouse HRP (BioRad, 1:5000 dilution). Western blots were visualized with Luminata Forte (Merck Millipore) and a VersaDoc imaging system (Bio-Rad Laboratories; Hercules, CA). Image intensity histograms were adjusted, and images were analysed with ImageLab software (Bio-Rad) to make figures.

4.2.4   Confocal microscopy

4.2.4.1   Proximity ligation assay (PLA)

To latter confirm the localisation of the found PPIs, we performed a Duolink® Proximity Ligation Assay (PLA) which allows *in situ* detection of protein interactions that can be readily detected and localised in unmodified cells and tissues. Briefly, 4% paraformaldehyde fixed cells samples were blocked with Duolink® Blocking Solution for 60 minutes at 37 °C. Blocked samples were then incubated with specific primary antibodies to the proteins to be detected

overnight at 4 °C with gentle agitation. Secondary antibodies conjugated with oligonucleotides (PLUS and MINUS probes) were added to the reaction and incubated for 1 hour at 37 °C. Ligation solution, consisting of two oligonucleotides and ligase, was added, and incubated for 30 minutes at 37 °C. In this assay, the oligonucleotides hybridize to the two PLA probes and join to a closed loop if they are in close proximity. Amplification solution, consisting of nucleotides and fluorescently labelled oligonucleotides, was added together with polymerase, and incubated for 100 minutes at 37 °C. The oligonucleotide arm of one of the PLA probes acts as a primer for "rolling-circle amplification" using the ligated circle as a template, and this generates a concatemeric product. Fluorescently labelled oligonucleotides hybridize to the amplified product. The PL signal was visible as a distinct fluorescent spot and was analysed by confocal microscopy (Duolink, Sigma-Aldrich). Control experiments included routine immunofluorescence staining of proteins of interest under identical experimental conditions.

4.2.4.2   Image acquisition

Cells were fixed with 4% paraformaldehyde for 30 minutes at room temperature. Cells were further permeabilized with PBS containing 0.5% Triton X-100 for 30 minutes, blocked with 1% BSA in PBS 0.05% Tween for 30 minutes and then incubated with the appropriated primary antibodies overnight at 4 °C. For detection of the BioID constructs, 1/100 dilution of anti-CCP1 antibody and 1/1000 dilution of anti-FLAG antibody were used. For the analysis of CCP1 constructs, the anti-HA antibody was used at 1/1000 dilution, while NAP1L4 and IPO7 antibodies were used at 1/200 dilution. Anti-PCM1 and anti-Agbl4 were used at 1/500 dilution for CCP6 analysis. Cells were then washed and incubated with Alexa anti-rabbit 488 and Alexa anti-mouse 555 for 1 hour at room temperature and nuclei were further counterstained with DAPI.

4.3   Results and discussion

4.3.1   Validation of the BioID constructs

Traditional affinity purifications are good at detecting specific and direct connections, but they fall short when it comes to discovering transient and/or weak interactions, such as those that may occur between CCPs and their substrates. Furthermore, the interacting spectrum may be large, allowing only high abundant interactions partners to be recognized. As a result, the adoption of a system termed BioID (Roux et al., 2012), which is represented in Figure 4.1, is particularly ideal for charting the very transient interactions occurring between CCPs and their substrates. Despite being less specific than traditional affinity purification, the technique has been shown to capture both transitory and stable interactions. For instance, the BioID methodology has been used for interaction mapping of several cellular complexes as the centrosome, the mitochondria, and the histones H2B and H3 (Gupta et al., 2015; Lambert et al., 2015; Rhee et al., 2013), among others.

In our study, to globally identify the human CCP1 and CCP6 interactome, we applied the BioID system. The broad application to different CCPs, the capacity to detect transitory interactions *in vivo* and its inhibitor independence (Coyaud et al., 2015) are benefits over earlier proteome-wide techniques as immunoprecipitation assays. Thus, a HEK293T-based Flp-In T-REx system was employed to fuse the promiscuous biotin ligase BirA to CCP1 and CCP6 (proteins of interest, POI), generating stable and inducible (Tet-ON) cell lines. Due to the presence of the carboxypeptidase catalytic domain at the C-terminal end of CCPs, the BirA* protein was fused to their N-terminal end to rule out potential protein function interferences. Each construct also includes a FLAG tag, which allows for the analysis of the fusion proteins' expression and subcellular localisation using immunoblotting and fluorescence microscopy. For a successful interaction characterisation, we also performed the BioID methodology on parental Flp-In T-REX 293 cells (WT) as well as on cell lines stably expressing BirA*-FLAG tag fused to the green fluorescent protein (GFP), to thoroughly investigate the background proteins identified by the approach.

To determine the proper functioning of the constructs, we began by biochemically characterizing our BirA*-POI BioID constructs that were stably expressed in Flp-In T-REX 293.

First, the expression of the CCP1-BirA construct and biotinylation in the associated cell line was validated by immunoblotting to confirm its proper function. For this, construct overexpression was induced by tetracycline, followed by the addition of free biotin for the effective labelling of interacting proteins. As seen in Figure 4.2A, the construct is expressed upon tetracycline induction, with a band size corresponding to the expected molecular weight of the BirA*-CCP1 FLAG-tagged construct. We also detected a strong biotinylated pattern by streptavidin labelling on western blot compared with the parental control without the BirA* enzyme (Figure 4.2A), thus showing the presence of biotinylase activity in the stably generated cells.

After the correct expression of our POIs was determined, we characterised the correct localisation of the expressed fusion BirA-POI compared with the endogenous protein by means of fluorescence microscopy. As observed in Figure 4.2B, FLAG-stained cells showed the previously described CCP1 localisation pattern, with CCP1-immunoreactivity predominantly in the cytoplasm, in perinuclear structures and in the cellular nucleus forming small aggregates. This pattern was also confirmed after CCP1 immunostaining (Figure 4.2B).
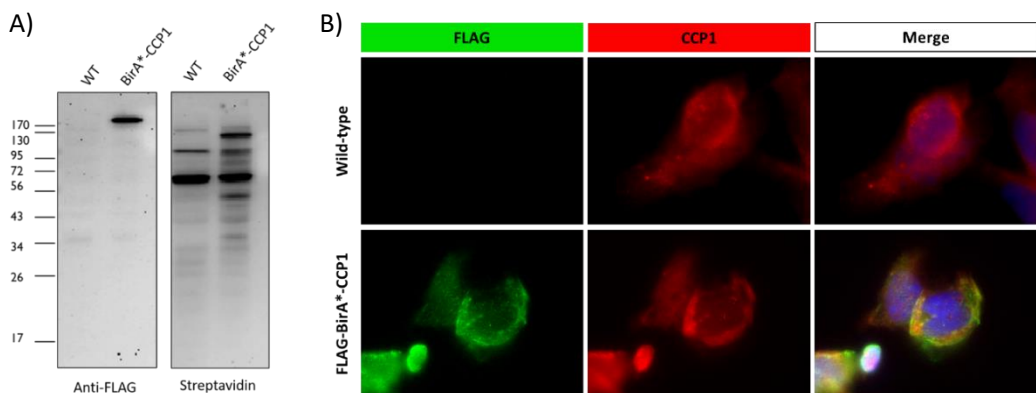
FIGURE 4.2. BIRA*-CCP1 CONSTRUCT VALIDATION. (A) Immunoblotting assay showing the correct expression of the BirA*-CCP1 construct expression (anti-FLAG) and its functionality as a promiscuous biotin ligase (streptavidin) in comparison with wild type cells. (B) Immunocytochemistry of the BirA*-CCP1 construct and endogenous CCP1 showing their intracellular localisation.

After completing the first analysis of the stable cell lines mentioned above, we performed affinity purification (AP) of proteins biotinylated by BirA*-fused CCPs.

Tetracycline was used to induce stable cell lines to express the BirA*-POI fusion proteins in the cell for 24 hours. In cell culture, none of the cell lines displayed an obvious growth deficiency or any other morphologic characteristic. After tetracycline induction, 50 μM of biotin was added to the cell culture medium to supply the biotin ligase with its substrate for another 24 h.

To explore the CCP1 and CCP6 interactomes, we identified the biotinylated proteins by mass spectrometry using a label-free quantitative proteomics approach to calculate the enrichment of each identified protein relative to BirA*-GFP control after streptavidin AP pulldown. To capture low abundant proteins with high confidence, all BioID experiments with tagged CCP1 or CCP6 enzymes were performed in quadruplicate (independent isolations from different passage cells). 'Hits' were proteins with greater than 3-fold enrichment and p-values greater than 0.05 relative to the control. These parameters led to an initial relative abundance list that was dominated by the metabolic enzymes pyruvate carboxylase (PC), propionyl-CoA carboxylase (PCCA), acetyl-CoA carboxylase 1 (ACACA) and methylcrotonoyl-CoA carboxylase (MCCC1) that either possess biotin carboxylase activity or are known to be endogenously biotinylated. The obtained data then, needed to be filtered to reduce false positive results. The identified false positive candidates correspond to highly abundant in cells, proteins that interact unspecifically with the agarose affinity matrix and naturally biotinylated proteins. To accomplish this true interactor filtering we used the CRAPome database, which was established to identify known contaminants for affinity purification-mass spectrometry data (Mellacheruvu et al., 2013).

4.3.2   Identification of the CCP1 interactome

We first characterised the interactome of CCP1 protein, which is known to have a role in cytoskeletal structures maintenance in its cytoplasmic localisation by its action over tubulin (Rodríguez de la Vega et al., 2013) whereas its nuclear functional role is mostly unknown. Recent studies had related loss of function of CCP1 with nucleolar stress and dysfunction of pre-rRNA processing and mRNA translation (Baltanás et al., 2019) as well as dysregulation in mitochondrial fusion and motility (Gilmore-Hall et al., 2019).

The data validation described above allowed us to categorize the identified proteins based on their enrichment versus an appropriate set of controls. Specifically, BirA*-CCP1

APs was compared to reference background samples allowed us to identify a total of 52 candidates after the filtering process (Table 4.2, Figure 4.3). Promisingly, a large number of interactors or substrates were related to CCP1's nuclear putative role. These results indicate that BioID is able to provide a wide view of the CCP1 interactome and can be useful for its functional characterisation.
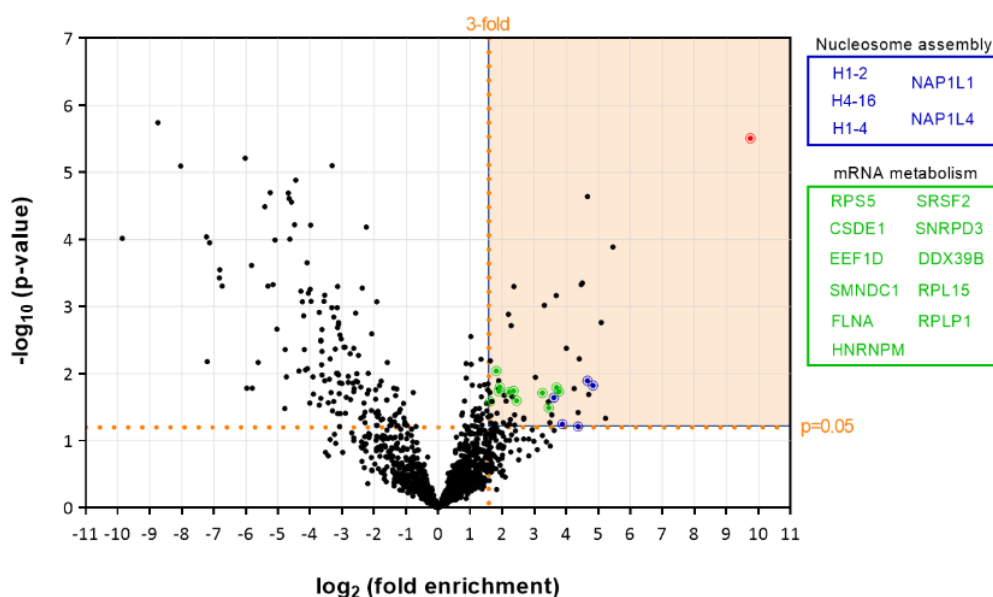
FIGURE 4.3. BioID METHODOLOGY FOR CCP1 IN HEK293T CELLS. Volcano plot showing the statistical significance versus the fold enrichment of proteins identified in BioID-CCP1 experiments relative to WT and GFP control experiments. A quadrant (dashed orange line) bounded by a p-value of 0.05 and 3-fold enrichment contained CCP1 (red), as well as candidate interactors related to nucleosome assembly (dark blue) and mRNA metabolism (green).

In the CCP1 and control proxeomes we identified contained a total of 1513 proteins. In order to characterize the composition of this set of proteins, we performed Gene Ontology (GO) analysis by ranking the data according to the enrichment p-value. Significant GO terms are summarised in Table 4.1, showing the protein enrichment compared with the background, and the -$\log_{10}$ (p-value) and the false discovery rate (FDR) of the analysed data. The differentially enriched GO terms are shown in the category 'Process' for the CCP1 interacting proxeome. This analysis of the CCP1 hits enriched in the found dataset were consistent with the previously mentioned studies on its nuclear role (Baltanás et al., 2019) as significant enrichment GO terms for the CCP1 interactome were led by nucleosome assembly activity (GO:0006334), cytoplasmic translation (GO:0002181) and RNA metabolic

process (GO:0016070) (Table 4.1). Proteins included in the nucleosome assembly category were histones H1.2, H1.4 and H4 and nucleosome assembly proteins NAP1L1 and NAP1L4. Interestingly, NAP1L1 and NAP1L4 had been described as polyglutamylated proteins by TTLL4 in mice (van Dijk et al., 2007) and had been related to embryonic cell proliferation and differentiation in the developing brain (Qiao et al., 2018). These characteristics make NAP proteins promising candidates to elucidate the nuclear role of CCP1 in the nucleus in relation to neuron degeneration.

TABLE 4.1. ENRICHED GO TERMS FOR THE CCP1 INTERACTING PROTEOME. Data was analysed with the Panther Classification System, using the GO biological process complete data set with Fisher's exact test and False Discovery Rate (FDR) correction. Analysis results are hierarchically sorted. Sorting is done only by the most specific subclass first, with its parent terms indented directly below it.

GO biological process	Fold Enrichment	-log$_{10}$ (p- value	FDR
Nucleosome assembly	17.89	4.95	1.72E-02
Cellular protein-containing complex assembly	4.63	4.27	3.83E-02
Cellular process	1.32	5.14	1.40E-02
Cellular component biogenesis	2.77	4.63	2.15E-02
Chromatin assembly	13.48	4.39	3.19E-02
Chromatin assembly or disassembly	11.73	4.11	4.84E-02
Nucleosome organization	12.90	4.30	3.72E-02
Chromatin remodelling	8.78	4.16	4.68E-02
Cytoplasmic translation	14.81	4.58	2.30E-02
Translation	7.90	5.08	1.43E-02
Gene expression	3.26	5.36	1.13E-02
Cellular macromolecule biosynthetic process	3.43	4.11	4.68E-02
Peptide biosynthetic process	7.45	4.90	1.77E-02
Peptide metabolic process	6.27	4.87	1.72E-02
Nitrogen compound metabolic process	2.94	7.10	1.24E-03
Cellular metabolic process	1.80	4.48	2.68E-02
Amide biosynthetic process	5.78	4.13	4.76E-02
Cellular nitrogen compound biosynthetic process	4.20	5.77	1.30E-02
Cellular biosynthetic process	3.15	5.75	9.24E-03
Biosynthetic process	2.99	5.39	1.28E-02
Organic substance biosynthetic process	3.07	5.57	1.04E-02
RNA metabolic process	3.61	4.64	2.22E-02
Nucleobase-containing compound metabolic process	2.92	5.24	1.28E-02
Organic cyclic compound metabolic process	2.60	4.72	2.12E-02
Heterocycle metabolic process	2.75	4.85	1.68E-02
Aromatic compound metabolic process	2.69	4.70	2.07E-02
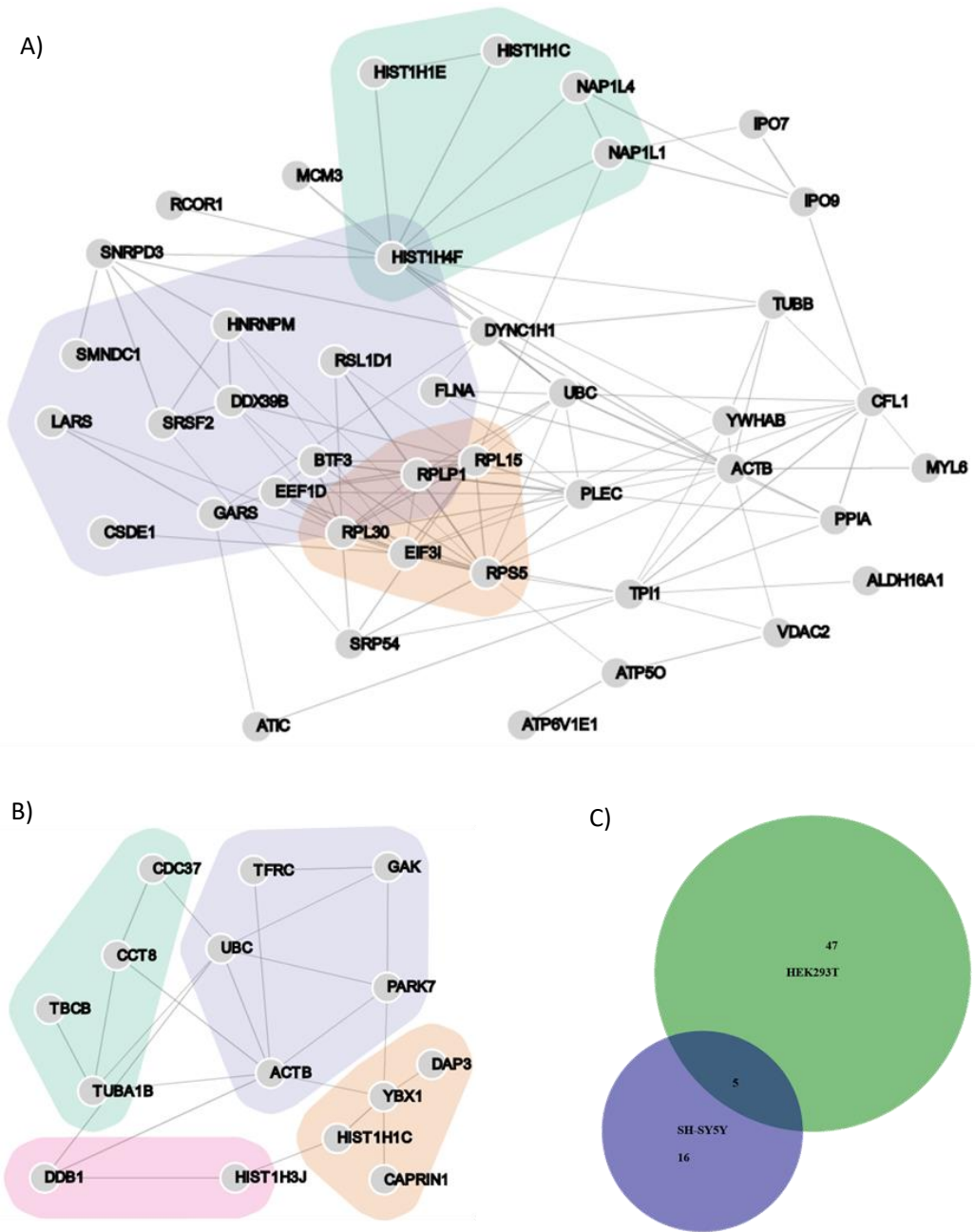
FIGURE 4.4. NETWORK ANALYSIS OF THE ENRICHED PROTEINS IN THE BIOID EXPERIMENT. Interaction data was retrieved from the STRING database and plotted with the NORMA software for enriched GO terms. (A) Data from HEK293T cells, were nucleosome assembly (green), cytoplasmic translation (blue) and RNA metabolism (orange) proteins are highlighted. (B) Data from SH-SY5Y cells. (C) Venn diagram showing common proteins for both datasets.

Next, we inquired whether any protein complexes or functionally related protein groups are related to CCP1. As a result, we mapped the identified proteins to the entire STRING network (https://string-db.org/, August 2021), which contains 9606 interactions of varying types. Only above medium confidence interactions with a STRING interaction score greater than 0.4 were taken into account. Figure 4.4 shows an overview of networks retrieved from the obtained filtered data for CCP1. Specific complexes, such as nucleosome assembly and RNA metabolism are found in the extracted network. These identified complexes have functions in the nucleus, which is consistent with the previous data about CCP1 implications. This data implies that CCP1, although being an important tubulin modifying enzyme, is involved in important nuclear processes not assessed before.

As disruption of the CCP1 gene has been shown to disrupt neuronal maintenance, resulting in the *pcd* mouse model and causing infantile-onset neurodegeneration in humans (Fernandez-Gonzalez et al., 2002; Shashi et al., 2018), we wanted to further characterise the CCP1 interactome, paying special attention in its role in the nervous system. Because human Purkinje cell neurons, the cells most afflicted by CCP1's loss of function, are difficult to collect and maintain as primary cells, we conducted our research using long-term neuronal cell lines, specifically the neuroblastoma SH-SY5Y lineage. Thus, we generated a new BioID experiment using the SH-SY5Y neuroblastoma cell line using the same parameters as described before.

The obtained results in this neuronal cell line are summarized in the Table 4.3. Compared with the analysis on HEK293T cells, this new BioID approach showed no significant functional enrichment due to the low number of significant proteins after the filtering process. Nevertheless, we found proteins related to nucleosome assembly and RNA metabolism, indicating a similar function for CCP1 in both HEK293T and SH-SY5Y cells. More precisely, a comparison between the two BioID datasets showed five common candidate interactors that are predicted to be important for the CCP1 functional role (Figure 4.4). These interactors are the importin IPO7, the nucleosome assembly protein NAP1L4, the polyubiquitin UBC, the actin ACTB and the histone H1.2.

TABLE 4.2. PROTEINS IDENTIFIED IN BioID METHODOLOGY FOR CCP1 IN HEK293T CELLS. Results showed are thresholded by a p-value of 0.05 and 3-fold enrichment. The list reports the bait protein (CCP1, light red), as well as candidate interactors. Proteins related to nucleosome assembly (light blue) and mRNA metabolism (light green) are highlighted.

Nº	Protein	Gene	log2 (Fold)	-log (p-value)	Function
0	Cytosolic carboxypeptidase 1	AGTPBP1	9.7435	5.5098	Metallocarboxypeptidase that catalyses the deglutamylation of polyglutamate side chains generated by post-translational polyglutamylation. Also removes gene-encoded polyglutamates from the carboxy-terminus.
1	Cofilin-1	CFL1	5.4594	3.8869	Binds to F-actin and exhibits pH-sensitive F-actin depolymerizing activity. Required for the centralization of the mitotic spindle and symmetric division of zygotes. Required for neural tube morphogenesis and neural crest cell migration.
2	PRA1 family protein 3	ARL6IP5	5.2305	1.3351	Regulates intracellular concentrations of taurine and glutamate. Negatively modulates SLC1A1/EAAC1 glutamate transport activity.
3	Importin-7	IPO7	5.0929	2.7629	Functions in nuclear protein import serving itself as receptor for nuclear localization signals and to promote translocation of import substrates through the nuclear pore complex. Mediates the nuclear import of ribosomal proteins and histones.
4	Histone H1.4	H1-4	4.8292	1.8202	Binds to linker DNA between nucleosomes forming the macromolecular structure known as the chromatin fibre. Acts also as a regulator of individual gene transcription through chromatin remodelling, nucleosome spacing and DNA methylation.
5	Thioredoxin-like protein 1	TXNL1	4.6953	1.6895	Active thioredoxin with a redox potential of about -250 mV.
6	Nucleosome assembly protein 1-like 1	NAP1L1	4.6670	1.8907	Histone chaperone, imports H2A-H2B assembly nucleosomes. Participates in chromatin remodelling for DNA repair. Plays a role in embryonic neurogenesis regulation. Regulates neurogenesis by promoting H3K4 methylation.
7	60S ribosomal protein L30	RPL30	4.6642	4.6399	Component of the ribosome, a large ribonucleoprotein complex responsible for the synthesis of proteins in the cell.
8	Myosin light polypeptide 6	MYL6	4.4992	3.3528	Regulatory light chain of myosin. Does not bind calcium.
9	Voltage-dependent anion-selective channel protein 2	VDAC2	4.4713	3.3273	Forms a channel through the mitochondrial outer membrane that allows diffusion of small hydrophilic molecules. Binds ceramide, promoting the mitochondrial outer membrane permeabilization (MOMP) apoptotic pathway.
10	Tubulin beta chain	TUBB	4.4047	2.2198	One of the major constituents of microtubules.
11	Transcription factor BTF3	BTF3	4.3731	1.4208	Prevents inappropriate targeting of non-secretory polypeptides to the endoplasmic reticulum. BTF3 is also a general transcription factor that can form a stable complex with RNA polymerase II. Required for the initiation of transcription.
12	Nucleosome assembly protein 1-like 4	NAP1L4	4.3670	1.2097	Acts as histone chaperone in nucleosome assembly.
13	Retinol-binding protein 1	RBP1	4.2502	1.7735	Cytoplasmic retinol-binding protein.
14	Triosephosphate isomerase	TPI1	4.0011	2.3796	Catalyses the interconversion between dihydroxyacetone phosphate (DHAP) and D-glyceraldehyde-3-phosphate (G3P) in glycolysis and gluconeogenesis. Produces methylglyoxal that modifies and can alter proteins, DNA and lipids.
15	Histone H4	H4C1	3.8820	1.3478	Core component of nucleosome.

#	Protein	Gene	Value 1	Value 2	Description
16	Small nuclear ribonucleoprotein SmD3	SNRPD3	3.7738	1.7319	Plays role in pre-mRNA splicing by spliceosomal snRNP assembly and as component of the spliceosomal U1, U2, U4 and U5 small nuclear ribonucleoproteins (snRNPs). As part of the U7 snRNP it is involved in histone pre-mRNA 3'-end processing
17	Cold shock domain-containing protein E1	CSDE1	3.6934	1.7923	RNA-binding protein involved in translationally coupled mRNA turnover. Implicated with other RNA-binding proteins in the cytoplasmic deadenylation/translational and decay interplay of the FOS mRNA.
18	Leucine-tRNA ligase, cytoplasmic	LARS	3.6850	3.1673	Catalyses the specific attachment of an amino acid to its cognate tRNA. Exhibits a post-transfer editing activity to hydrolyse mischarged tRNAs.
19	Histone H1.2	H1-2	3.6169	1.6441	Binds to linker DNA between nucleosomes forming the macromolecular structure known as the chromatin fibre. Acts also as a regulator of individual gene transcription through chromatin remodelling, nucleosome spacing and DNA methylation.
20	Actin, cytoplasmic 1	ACTB	3.4936	1.3710	Polymerizes to produce filaments that form cross-linked networks in the cytoplasm of cells. G- and F-actin also localize in the nucleus, regulating gene transcription and motility and repair of damaged DNA
21	60S acidic ribosomal protein P1	RPLP1	3.4583	1.4901	Plays an important role in the elongation step of protein synthesis.
22	14-3-3 protein beta	YWHAB	3.4424	1.5793	Adapter protein implicated in the regulation of signalling pathways. Negative regulator of osteogenesis. Involved in blockage of neuronal apoptosis. Negative regulator of signalling cascades that mediate activation of MAP kinases via AKAP13.
23	Surfeit locus protein 4	SURF4	3.3136	3.0209	May play a role in the maintenance of the architecture of the endoplasmic reticulum-Golgi intermediate compartment and of the Golgi.
24	Heterogeneous nuclear ribonucleoprotein M	HNRNPM	3.2525	1.7112	Pre-mRNA binding protein in vivo, binds avidly to poly(G) and poly(U) RNA homopolymers in vitro. Involved in splicing.
25	DNA replication licensing factor MCM3	MCM3	3.0387	1.9440	Acts as component of the MCM2-7 complex (MCM complex) which is the putative replicative helicase essential for 'once per cell cycle' DNA replication initiation and elongation in eukaryotic cells. Required for DNA replication and cell proliferation.
26	Vacuolar protein sorting-associated protein 35	VPS35	2.6763	1.3196	Acts as component of the retromer cargo-selective complex (CSC). Prevent missorting of selected transmembrane cargo proteins into the lysosomal degradation pathway.
27	Bifunctional purine biosynthesis protein PURH	ATIC	2.6753	1.3398	Bifunctional enzyme that catalyses the last two steps of purine biosynthesis.
28	Filamin-A	FLNA	2.4506	1.5976	Promotes branching of actin filaments and links actin filaments to membrane glycoproteins. Allows neuroblast migration from the ventricular zone into the cortical plate. Involved in ciliogenesis. Required for growth cone collapse in axons.
29	Catenin delta 1	CTNND1	2.3929	1.3832	Key regulator of cell-cell adhesion of both C-, E- and N-cadherins, being critical for their surface stability. Regulates gene transcription through several transcription factors, the activity of Rho family GTPases and downstream cytoskeletal dynamics.
30	Plectin	PLEC	2.3841	1.2349	Interlinks intermediate filaments with microtubules and microfilaments and anchors intermediate filaments to desmosomes or hemidesmosomes. Binds muscle proteins to membrane complexes. May be involved in filaments dynamics regulation.
31	Elongation factor 1-delta	EEF1D	2.3662	3.2973	Stimulates the exchange of GDP bound to EF-1-alpha to GTP for transfer of aminoacyl-tRNAs to the ribosome. Regulates induction of heat-shock-responsive genes through heat shock transcription factors and direct DNA-binding.
32	Secernin-1	SCRN1	2.3568	1.7423	Regulates exocytosis in mast cells. Increases both the extent of secretion and the sensitivity of mast cells to stimulation with calcium.

#	Protein	Gene	Value 1	Value 2	Description
33	Peptidyl-prolyl cis-trans isomerase	PPIA	2.3217	1.6515	Catalyses the cis-trans isomerization of proline imidic peptide bonds in oligopeptides.
34	Polyubiquitin-C	UBC	2.2811	2.7160	Polyubiquitin chains, when attached, have different functions depending on the residue of the ubiquitin that is linked. When polyubiquitin is free, it also has distinct roles, such as in activation of protein kinases, and in signalling pathways.
35	Glycine--tRNA ligase	GARS	2.2533	1.3151	Catalyses the ATP-dependent ligation of glycine to the 3'-end of its cognate tRNA, via the formation of an aminoacyl-adenylate intermediate (Gly-AMP).
36	40S ribosomal protein S5	RPS5	2.2130	1.7227	Component of the ribosome, a large ribonucleoprotein complex responsible for the synthesis of proteins in the cell.
37	Ribosomal L1 domain-containing protein 1	RSL1D1	2.1543	1.2224	Regulates cellular senescence through inhibition of PTEN translation. Acts as a pro-apoptotic regulator in response to DNA damage.
38	Cytoplasmic dynein 1 heavy chain 1	DYNC1H1	2.0561	1.6798	Cytoplasmic dynein 1 acts as a motor for the intracellular retrograde motility of vesicles and organelles along microtubules. Plays a role in mitotic spindle assembly and metaphase plate congression.
39	REST corepressor 1	RCOR1	2.0301	1.2671	Component of the BHC complex, represses transcription of neuron-specific genes in non-neuronal cells. Acts by modifying histones, thereby acting as a chromatin modifier. Plays a central role in demethylation of histone H3.
40	60S ribosomal protein L15	RPL15	1.9234	1.8004	Component of the ribosome, a large ribonucleoprotein complex responsible for the synthesis of proteins in the cell.
41	Spliceosome RNA helicase DDX39B	DDX39B	1.8998	1.7339	Involved in nuclear export of spliced and unspliced mRNA. Assembling component of the TREX complex which couples mRNA transcription, processing, and nuclear export, and specifically associates with spliced mRNA and not with unspliced pre-mRNA.
42	NADH-cytochrome b5 reductase 3	CYB5R3	1.8921	1.8918	Desaturation and elongation of fatty acids, cholesterol biosynthesis, drug metabolism, and, in erythrocyte, methaemoglobin reduction.
43	Eukaryotic translation initiation factor 3 subunit I	EIF3I	1.8866	1.7744	Component of the eukaryotic translation initiation factor 3 (eIF-3) complex. The eIF-3 complex specifically targets and initiates translation of a subset of mRNAs involved in cell proliferation, including cell cycling, differentiation and apoptosis.
44	Importin-9	IPO9	1.8434	1.4068	Functions in nuclear protein import using NLS and promotes translocation through the nuclear pore complex. Mediates the nuclear import of ribosomal proteins and histones, shielding exposed basic domains. Mediates the nuclear import of actin
45	Serine/arginine-rich splicing factor 2	SRSF2	1.8204	2.0394	Necessary for the splicing of pre-mRNA. It is required for formation of the ATP-dependent splicing complex and interacts with spliceosomal components during spliceosome assembly. It also is required for interactions of snRNPs with pre-mRNA.
46	Guanine nucleotide-binding protein G(o) subunit alpha	GNAO1	1.7958	1.3491	Guanine nucleotide-binding proteins (G proteins) are involved as modulators or transducers in various transmembrane signalling systems. The G(o) protein function is not clear. Stimulated by RGS14.
47	Aldehyde dehydrogenase family 16 member A1	ALDH16A1	1.7589	1.3257	Oxidoreductase activity, acting on the aldehyde or oxo group of donors, NAD or NADP as acceptor.
48	Signal recognition particle 54 kDa protein	SRP54	1.6866	1.5829	Binds to the signal sequence of presecretory protein when they emerge from the ribosomes and transfers them to TRAM. Plays a role in proliferation and differentiation of granulocytic cells, neutrophils migration capacity and pancreas development
49	V-type proton ATPase subunit E 1	ATP6V1E1	1.6434	1.3711	Subunit of the V1 complex of vacuolar(H+)-ATPase (V-ATPase), a multisubunit enzyme composed of a peripheral complex (V1) that hydrolyses ATP and a membrane integral complex (V0) that translocate protons.

Nº	Protein	Gene	$\log_2$ (Fold)	-log (p-value)	Function
50	Neurosecretory protein VGF	VGF	1.6357	2.1913	Secreted polyprotein that is proteolytically processed in a cell-type-specific manner. VGF and peptides derived from its processing play roles in neurogenesis and neuroplasticity associated with learning, memory, depression and chronic pain.
51	Survival of motor neuron-related-splicing factor 30	SMNDC1	1.6227	1.5818	Necessary for spliceosome assembly. Overexpression causes apoptosis.
52	ATP synthase subunit O	ATP5O	1.6136	1.7197	Mitochondrial membrane ATP synthase (F_1F_0 ATP synthase or Complex V) produces ATP from ADP in the presence of a proton gradient across the membrane which is generated by electron transport complexes of the respiratory chain.

TABLE 4.3. PROTEINS IDENTIFIED IN BioID METHODOLOGY FOR CCP1 IN SH-SY5Y CELLS. Results showed are thresholded by a p-value of 0.05 and 3-fold enrichment. The list reports the bait protein (CCP1, light red), as well as candidate interactors. Proteins identified in both HEK293T and SH-SY5Y cells are highlighted (light yellow).

Nº	Protein	Gene	$\log_2$ (Fold)	-log (p-value)	Function
0	Cytosolic carboxypeptidase 1	AGTPBP1	9.6396	2.7543	Metallocarboxypeptidase that catalyses the deglutamylation of polyglutamate side chains generated by post-translational polyglutamylation. Also removes gene-encoded polyglutamates from the carboxy-terminus.
1	Nucleosome assembly protein 1-like 4	NAP1L4	9.6780	4.7929	Acts as histone chaperone in nucleosome assembly.
3	T-complex protein 1 subunit theta	CCT8	9.2475	3.2352	Component of the chaperonin-containing T-complex (TRiC). The TRiC complex regulates telomere maintenance. May play a role in the assembly of BBSome, involved in ciliogenesis. The TRiC complex plays a role in the folding of actin and tubulin.
4	Importin-7	IPO7	8.3028	4.1215	Functions in nuclear protein import serving itself as receptor for nuclear localization signals and to promote translocation of import substrates through the nuclear pore complex. Mediates the nuclear import of ribosomal proteins and histones.
5	Polyubiquitin-C	UBC	6.2392	2.1538	Polyubiquitin chains, when attached, have different functions depending on the residue of the ubiquitin that is linked. When polyubiquitin is free, it also has distinct roles, such as in activation of protein kinases, and in signalling pathways.
6	Histone H3	H3C1	6.1442	1.3480	Core component of nucleosome, limiting DNA accessibility to the cellular machineries. Plays a role in transcription regulation, DNA repair, DNA replication and chromosomal stability.
7	Actin, cytoplasmic 1	ACTB	6.1346	1.6635	Polymerizes to produce filaments that form cross-linked networks in the cytoplasm of cells. G- and F-actin also localize in the nucleus, regulating gene transcription and motility and repair of damaged DNA
8	Histone H1.2	H1-2	4.6213	1.3954	Binds to linker DNA between nucleosomes forming the macromolecular structure known as the chromatin fibre. Acts also as a regulator of individual gene transcription through chromatin remodelling, nucleosome spacing and DNA methylation.
9	Tubulin alpha-1B chain	TUBA1B	4.0671	1.7322	One of the major constituents of microtubules.
10	Fibrillin-1	FBN1	3.1205	2.0265	Structural component of the 10-12 nm diameter microfibrils of the extracellular matrix, which conveys both structural and regulatory properties to load-bearing connective tissues.
11	Transferrin receptor protein 1	TFRC	2.7737	1.5313	Receptor for cellular uptake of iron into specialized endosomes. Endosomal acidification leads to iron release. Transferrin receptor is necessary for development of erythrocytes and the nervous system.

	Name			Description
12	Nuclease-sensitive element-binding protein 1	YBX1	2.4029	1.9664	DNA- and RNA-binding protein involved in various processes, such as translational repression, RNA stabilization, mRNA splicing, DNA repair and transcription regulation.
13	DNA damage-binding protein 1	DDB1	2.2669	1.3152	Involved in DNA repair and protein ubiquitination, as part of the UV-DDB complex and DCX complexes, respectively. Recognizes UV-induced DNA damage and recruit proteins of the nucleotide excision repair pathway to initiate DNA repair.
14	UDP-glucose:glycoprotein glucosyltransferase1	UGGT1	2.1548	1.3428	Recognizes glycoproteins with minor folding defects. Reglucosylates the misfolded part of the protein, thus providing quality control for protein folding. Reglucosylated proteins are recognized for recycling and refolding or degradation.
15	28S ribosomal protein S29	DAP3	2.0946	1.7534	Involved in mediating interferon-gamma-induced cell death.
16	Cyclin-G-associated kinase	GAK	2.0214	1.3135	Associates with cyclin G and CDK5. Seems to act as an auxilin homolog that is involved in the uncoating of clathrin-coated vesicles by Hsc70 in non-neuronal cells. Expression oscillates slightly during the cell cycle, peaking at G1.
17	Serine/threonine-protein phosphatase	PPP3CA	1.9877	1.5295	Calcium-dependent, calmodulin-stimulated protein phosphatase which plays an essential role in the transduction of intracellular Ca2+-mediated signals.
18	Hsp90 co-chaperone Cdc37	CDC37	1.8757	1.7150	Co-chaperone that binds to numerous kinases and promotes their interaction with the Hsp90 complex, resulting in stabilization and promotion of their activity.
19	Tubulin-folding cofactor B	TBCB	1.6942	1.3107	Binds to alpha-tubulin folding intermediates to properly fold the heterodimer. Involved in regulation of tubulin heterodimer dissociation. May function as a negative regulator of axonal growth.
20	Parkinson disease protein 7	PARK7	1.6862	1.3305	Multifunctional protein. Plays a role in cell protection against oxidative stress. It is involved in neuroprotective mechanisms, male fertility as well as cell growth and transformation. Binds to mRNAs. Required for correct mitochondrial morphology.
21	MICOS complex subunit MIC13	MICOS13	1.6709	1.4010	Component of the MICOS complex, a large protein complex of the mitochondrial inner membrane that plays crucial roles in the maintenance of crista junctions, inner membrane architecture, and formation of contact sites to the outer membrane.
22	Caprin-1	CAPRIN1	1.6516	1.7876	May regulate the transport and translation of mRNAs of proteins involved in synaptic plasticity in neurons and cell proliferation and migration in multiple cell types. In neuronal cells, directly binds to several mRNAs.

Regarding the five common candidate interactors, analysis of the data shows that these proteins share a nuclear role and, except the importin IPO7, are related with protein-DNA complex assembly, the previous step to nucleosome assembly. This data is consistent with the *pcd* mouse derived knowledge, where nuclear architecture has a significant impact on Purkinje cell degeneration (Baltanás, Casafont, Lafarga, et al., 2011). In this work, Baltanás et al. showed that the phosphorylation of H2AX, a DNA damage signal, and trimethylation of the histone H4K20, a repressive mark, were epigenetic signatures of chromatin in degenerating PCs. These histone changes are linked to chromatin reconfiguration on a broad scale, telomere clustering, and heterochromatin-induced gene silencing, all of which are important contributors in PC degeneration. All in all, the presented data suggests that CCP1 might have an important role in nucleosome assembly in neuronal cells leading to a correct DNA architecture, pointing to NAP proteins as interesting substrates for its activity.

4.3.3   Analysis of the CCP1-NAP1L4 interaction

Following the CCP1 interactome characterisation, we focused on the nucleosome assembly related proteins, as they are thought to be important to understand the nuclear role of CCP1. Specifically, we wanted to gain insight into neuronal related processes, thus choosing the SH-SY5Y interaction list for a starting. As observed in Table 4.2, NAP1L4 is the first nucleosome assembly-related protein found, which is also the protein with the highest enrichment compared to control cells. Hence, we initially characterised the CCP1-NAP1L4 physical interaction *in vitro.*

To explore the interaction between CCP1 and NAP1L4, we first assessed the endogenous localisation of NAP1L4 within undifferentiated SH-SY5Y cells in relation to overexpressed CCP1 (HA-tagged protein). To this end, we double-stained adherent SH-SY5Y cells after paraformaldehyde fixation with specific anti-NAP1L4 and anti-HA antibodies for high-resolution confocal microscopy. At first glance, NAP1L4 (red) does not show an apparent co-localisation with CCP1 (green), as it shows a diffuse cytosolic pattern with low to no presence in the nucleus (Figure 4.5A). This pattern is supported in the literature, where NAP1L4 was shown to be present in the cytoplasm and excluded from the nucleus during G0/G1 phase and then relocates to the nucleus by time cells are in the S phase (Rodriguez et al., 1997).

Considering that NAP1L4 nuclear localisation is limited only to the S phase, which could lead to an underrepresentation of the CCP1-NAP1L4 in non-dividing cells, we then performed an immunoprecipitation (IP) assay for SH-SY5Y cells to investigate the protein-protein physical association after CCP1 enrichment. For this assay, we lysed proliferating cells and captured CCP1 using a specific CCP1 antibody. Immunoprecipitation results showed a clear NAP1L4 detection among immunoprecipitants of endogenous CCP1 (Figure 4.5B), showing that CCP1 interacts with NAP1L4. As observed, NAP1L4 immunodetection shows a characteristic pattern, with a main band corresponding to the full-length protein (52 KDa) and other three bands with lower molecular weight that might correlate with processed or truncated forms of NAP1L4 (Figure 4.5B). This pattern is observed both in the whole cell lysate and in the IP elute.

Once the CCP1-NAP1L4 interaction was determined, we next wanted to define if NAP1L4 was a substrate for CCP1's deglutamylation activity or just an interactor partner. Murine NAP1L4 has been described to be polyglutamylated by TTLL4 (van Dijk et al., 2007), suggesting a similar role for the human orthologue. The presence of polyglutamate side chains in mice makes human NAP1L4 a promising candidate protein for being a substrate of CCPs by similarity. For this purpose, we compared the deglutamylating activity of CCP1 over NAP1L4 in wild type SH-SH5Y cells and CCP1 knockout SH-SY5Y cells. To examine whether CCP1 was active over human NAP1L4, we immunoprecipitated NAP1L4 in SH-SY5Y cells expressing CCP1 and SH-SY5Y CCP1KO cells and the eluate was subjected to immunoblot analysis with anti-polyglutamylation (PolyE) antibody that recognise chains of 3 or more glutamates. Results show a clear polyglutamylated band corresponding to the full-length protein only in SH-SY5Y CCP1KO cells, whereas it was diminished in cells expressing CCP1 (Figure 4.5C). These results show that human NAP1L4 is polyglutamylated, and CCP1 is capable to act over modified NAP1L4 reducing its general polyglutamate level. This indicates that NAP1L4 is a substrate and not only an interactor partner of CCP1 (Figure 4.5D). These findings may indicate that CCP1 could act as chromatin organiser via modification of nucleosome assembly proteins, offering a possible mechanism to the nuclear impairments found in the *pcd* mouse model.
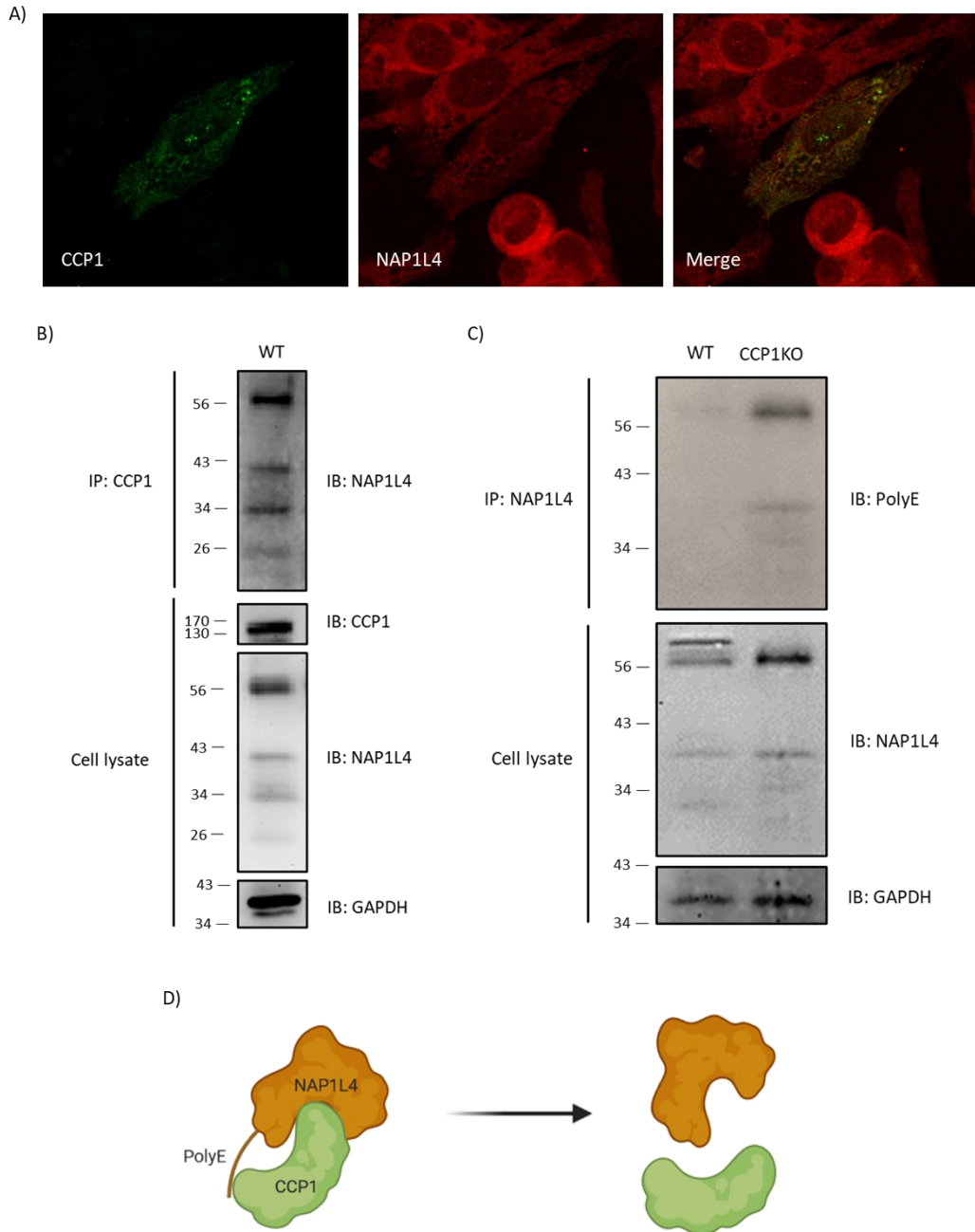
FIGURE 4.5. CHARACTERISATION OF THE CCP1-NAP1L4 INTERACTION. (A) Immunocytochemistry of overexpressed CCP1 (green) and endogenous NAP1L4 (red) showing their intracellular localisation. Images were obtained on an inverted confocal microscope (Leica SP5) sing a 63X objective and analysed with Imaris software (Bitplane). **(B)** Immunoprecipitation assay where endogenous CCP1 was captured with its specific antibody using protein G-coupled magnetic Dynabeads and NAP1L4 was immunoblotted with its specific antibody. C) Immunoprecipitation assay capturing NAP1L4 with its specific antibody and immunoblotted with polyE antibody. **(D)** Schematic representation of the interaction and enzymatic activity of CCP1 over NAP1L4.

Regarding to the NAP1L4 interactome, some of their interactions with other proteins have been described. For instance, a previous work assessing the interaction properties of NAP1L4 and the diacylglycerol kinase ζ (DGKζ) determined that nuclear localisation signal was essential for DGKζ's binding capacity (M. Okada et al., 2011). Similar to DGKζ, CCP1 contains a NLS near to its N-terminal as well as nuclear export sequence (NES) at the end of its carboxypeptidase domain. CCP1's NLS has not been well characterised, whilst NES was found to allow CCP1's binding to the nuclear export receptor CRM1 for its consequent translocation from the nucleus to the cytoplasm (Thakar et al., 2013). Due to these similarities, we wondered whether the binding region between CCP1 and NAP1L4 could be specifically mapped to these regions.

To this aim, we generated substitution mutants for both the NLS and the NES regions of full-length CCP1 by site-directed mutagenesis QuickChange kit. In terms of sequences, classical NLSs can be divided into two categories: monopartite basic amino acid stretches (PKKKRK) or bipartite (two short sequences with a spacer) basic amino acid stretches (KRPAATKKAGQAKKKKLDK) (Görlich & Kutay, 1999; Hodel et al., 2001). On the other hand, classical NESs are composed of a leucine-rich region of about 10 amino acid length (Kanwal et al., 2002). Hence, the NLS region of CCP1 was identified as [1007]KRLPLVYCDYHGHSRKKNV[1025] were lysines 1007, 1022 and 1023 could be crucial amino acids for this localisation function. For the NES region, the identified amino acids on CCP1 were [79]DLQTTLNILSILVEL[94] where leucines 80, 84, 87, 90 and 94 form the leucine-rich sequence. Both sequences were muted by changing key residues to alanine using the QuickChange site-directed mutagenesis kit (Agilent, USA) to obtain specific mutations that alter their function. The generated mutations were analysed by BLAST sequencing analysis (https://blast.ncbi.nlm.nih.gov/Blast.cgi) confirming the changes in the lysins 1007 and 1022 to alanine (K1007A and K1022A) for the NLS mutant and changes in the leucines 80 and 84 to an alanine (L80A and L84A) for the NES mutant. The generated mutants were tested by immunocytochemistry to assess how the sequence mutations affected the cellular localisation after CCP1 overexpression. Results showed a clear distinct localisation of the transfected mutants between the nucleus and the cytosol (Figure 4.6A), indicating that the target signals were modified and are affecting CCP1's cellular localisation.
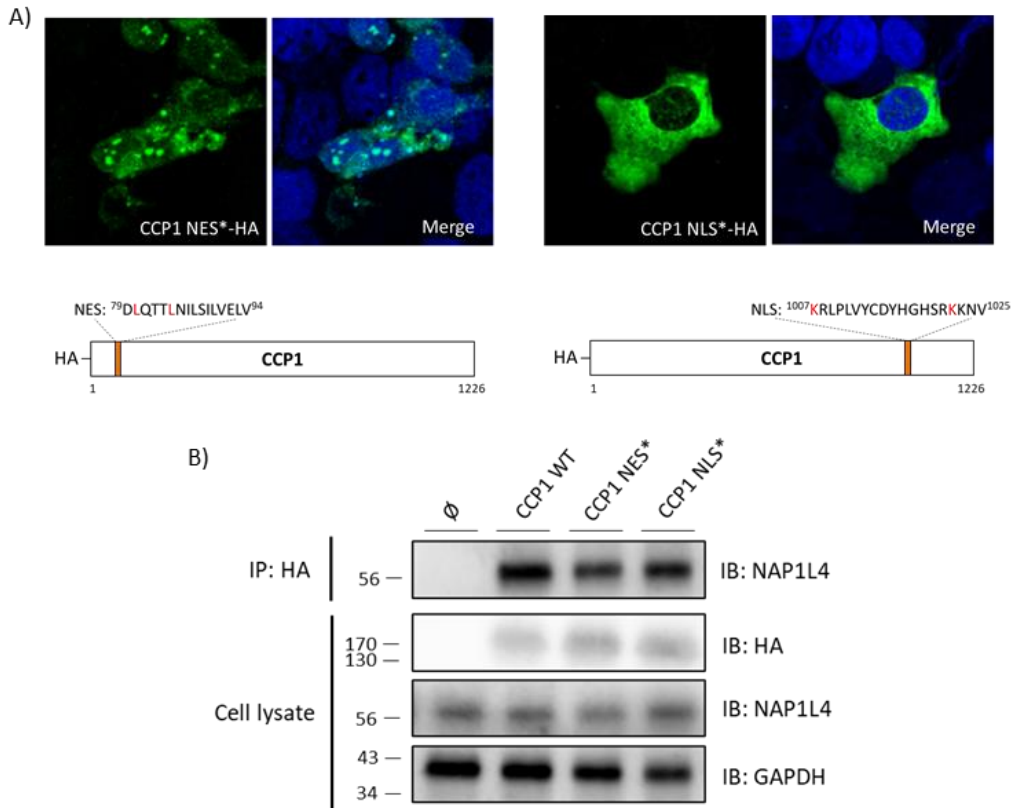
FIGURE 4.6. BINDING REGION CHARACTERISATION BETWEEN CCP1 AND NAP1L4. (A) Immunocytochemistry of NES mutant CCP1 (green, left) and NLS mutant CCP1 (green, right), showing their intracellular localisation. Images were obtained on an inverted confocal microscope (Leica SP5) using a 63X objective and analysed with Imaris software (Bitplane). (B) Immunoprecipitation assay where overexpressed CCP1 mutants were captured with HA-tag specific antibody using protein G-coupled magnetic Dynabeads and NAP1L4 was immunoblotted with its specific antibody.

Once the region mutants were successfully determined, we performed different IP assays in cells after overexpression of full-length CCP1 and the two generated mutants. Thus, after successfully determining the mutant generation, cells were co-transfected with deletion mutants for the NES and NLS signals of CCP1 to establish whether our protein had the same mechanism of action as DGKζ. Immunoprecipitation assays revealed that NAP1L4 was able to associate with the two mutated forms of CCP1 the same way that wild type protein, suggesting that the localisation sequences are not directly involved in the interaction between NAP1L4 and CCP1 (Figure 4.6B).

4.3.4   Nuclear role of CCP1

Although the molecular pathways through which the loss of CCP1 function leads to neuronal degeneration and death in *pcd* mice remain undefined, different cellular mechanisms have been proposed: endoplasmic reticulum stress (Kyuhou et al., 2006), decreased peptide turnover downstream from the proteasome (Berezniuk & Fricker, 2010), mitochondrial dysfunction and altered proteolytic processing of CCP1-interacting proteins (Chakrabarti et al., 2010; Gilmore-Hall et al., 2019), a dysfunction of microtubule stability (J. Li et al., 2010), and a progressive transcriptional silencing due to the accumulation of DNA lesions (Baltanás, Casafont, Lafarga, et al., 2011; Baltanás, Casafont, Weruaga, et al., 2011; Baltanás et al., 2019; Valero et al., 2006). Accordingly, several studies suggest the nuclear role of CCP1 as the cause for neuron degeneration.

The proximity biotinylation experiments conducted in this work show different nuclear partners for CCP1, especially related to chromatin remodelling and transcription processes. Among these interactors, we identified nucleosome assembly-like proteins, which present a nuclear role that has been related to embryonic neural progenitor cell proliferation and differentiation (Qiao et al., 2018). NAP1L4, which has been defined as a substrate for CCP1, is then a promising candidate for defining the CCP1 function that leads to neuronal degeneration and death in *pcd* mice.

To specifically study the effect of CCP1 over NAP1L4 during neuron differentiation, we used SH-SY5Y neuroblastoma cells. The immortalized and proliferative cell line SH-SY5Y is one of the most used cell lines in neuroscience research. However, undifferentiated SH-SY5Y cells share few properties with mature neurons. For our study on the nuclear role of CCP1, we differentiated wild type and CCP1KO SH-SY5Y cells in a two-step protocol using all-trans retinoic acid (Korecka et al., 2013) and used them to assess the effects of CCP1 depletion compared with not differentiated cells. The differentiation process was followed-up by morphological characterisation (Figure 4.7).

This characterisation showed how WT undifferentiated SH-SY5Y cells formed cell clumps within 3 days from plating (Figure 4.7, Day 0). At 3 days differentiation, clumps unwounded, and cells spread out neurites (Figure 4.7, Day 3). At the end of differentiation (Figure 4.7, Day 8), cells were evenly distributed and interconnected via a network of branched neurites.

For CCP1KO cells, we did not find significant differences with WT cells during the differentiation process, as both cell lines were able to reach a similar differential stage at day 8 with a similar progression over time.
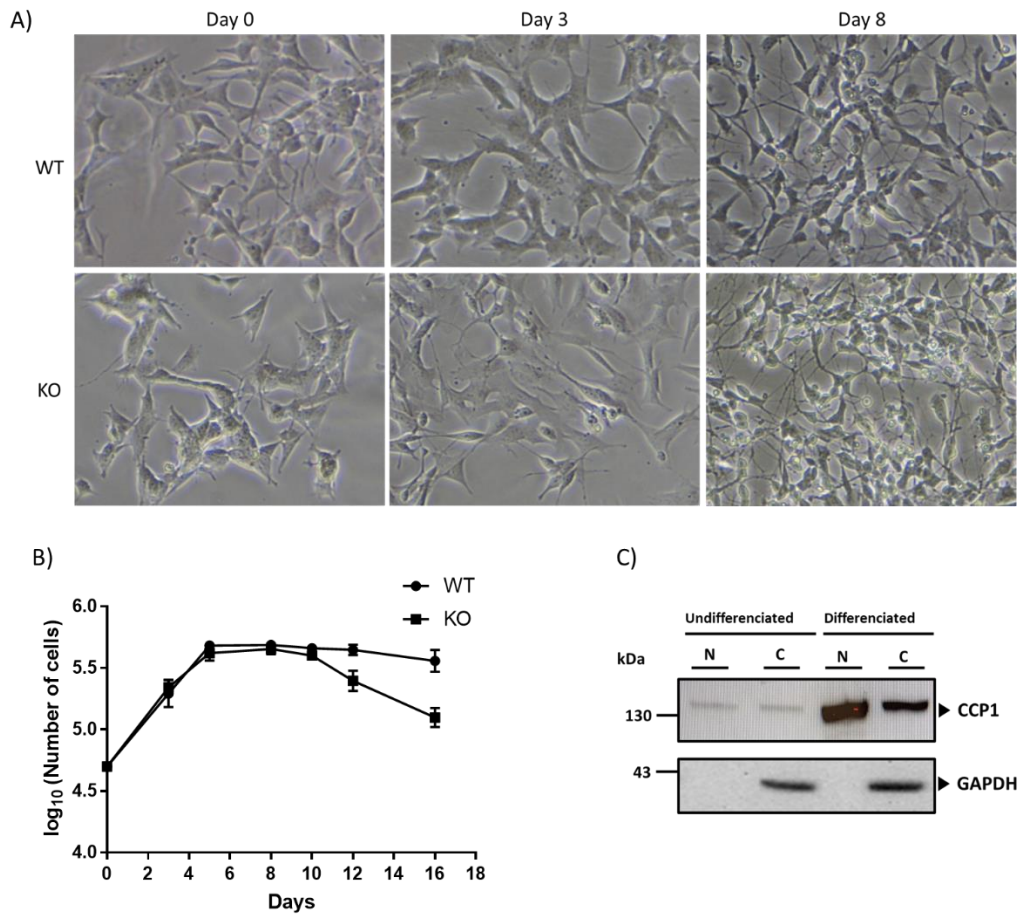
FIGURE 4.7. MORPHOLOGIC CHANGES AND CELL GROWTH CURVE OF SH-SY5Y DIFFERENTIATION. (A) phase contrast images of differentiated WT and CCP1KO SH-SY5Y cells chronically exposed to 20 µM retinoic acid for 8 days. (B) Growth curve of WT and CCP1KO Sh-SY5Y cells during retinoic acid-induced differentiation. Induction was performed on day 0 at a cell density of 50,000 cells/ml and cell number was evaluated for 16 days. Each point represents the mean ± SEM of triplicate experiments. (C) CCP1 expression level in undifferentiated (day 0) and differentiated (day 8) WT SH-SY5Y. Cell lysates were fractionated into nucleus (N) and cytoplasm (C), and CCP1 was immunoblotted by its specific antibody.

Interestingly, cultures presented a different growing behaviour long term after differentiation. Thus, we performed a growth curve for both cultures to assess the differences induced by loss of CCP1. The obtained growth curves showed an identical cell proliferation rate until day 10 after RA induction, after this point of time, cell viability was

reduced in CCP1KO cultures compared to the WT (Figure 4.7B). These results reinforce the importance of CCP1 in neuron maintenance, although it might no be directly involved in differentiation processes.

Next, we focused on how neuron differentiation was affecting CCP1. Hence, we investigated how the CCP1 expression levels changed after the differentiation process by paying closer attention to its subcellular localisation. Results show how CCP1 is overexpressed compared to undifferentiated SH-SY5Y and is mainly localised in the cell nucleus (Figure 4.7C).

SH-SY5Y differentiation assays have shown how CCP1 activity is an important factor for neuronal maintenance. The fact that CCP1 undergoes a significant expression increase when the culture is stably differentiated with special mention to the cellular nucleus and that its loss is directly involved in cell culture maintenance at this stage reinforces the importance of its nuclear role in neuronal degeneration.

4.3.5   Depletion of CCP1 affects NAP1L4 nuclear localisation in differentiated neurons

After assessing the behavourial changes ocurring during SH-SY5Y neuron differentiation regarding CCP1 loss and expression, we focused on how these differences were affecting the previous identified interactor. Hence, we examined whether the knockout of CCP1 would change the NAP1L4 expression levels in undifferentiated and differentiated SH-SY5Y cells. For this experiment, we assessed the relative NAP1L4 expression in four different conditions which include the neuronal differentiation state and the presence or not of CCP1.

As shown in Figure 4.8A, undifferentiated cells showed no significant change in total NAP1L4 expression level between WT and CCP1KO conditions, indicating that our POI is not affecting NAP1L4 expression in this condition. Interestingly, when assessing differentiated cells, the total expression level of NAP1L4 was 2-fold reduced in CCP1KO cells compared to the WT control (Figure 4.8A). These results show how CCP1 and NAP1L4 are directly related during the neuronal differentiation process, but not during normal proliferation state, reinforcing CCP1's involvement into chromatin reorganisation via NAP regulation.
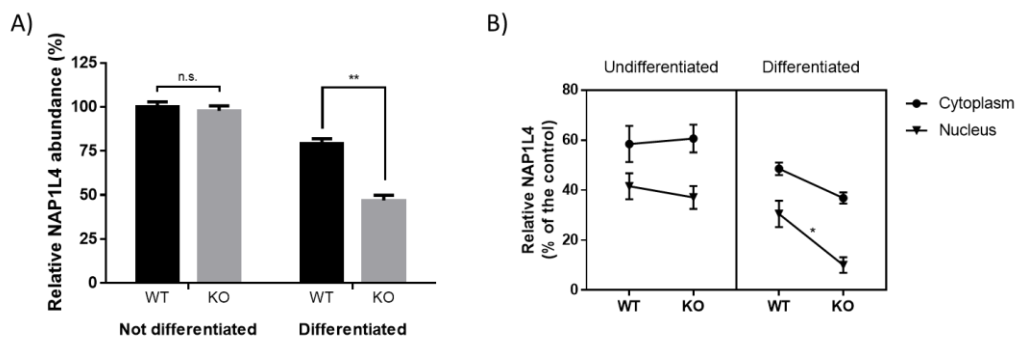
FIGURE 4.8. EFFECT OF CCP1KO OVER NAP1L4 IN THE DIFFERENTIATION PROCESS. (A) Immunoblotting assay of NAP1L4 in undifferentiated (day 0) and differentiated (day 8) WT and CCP1KO SH-SY5Y cells. (B) Immunoblotting assay of NAP1L4 after subcellular fractionation of the cytoplasm and the nucleus in undifferentiated and differentiated WT and CCP1KO cells.

Focusing on NAP1L4 nuclear localisation, we performed a subcellular fractionation of the cellular lysate of WT and CCP1KO SH-SY5Y cells and immunoblotted for assessing the NAP1L4 levels in each fraction at day 0 and 8 of differentiation. In these experiments we found that not only the total protein expression level was diminished in the CCP1KO after differentiation (Figure 4.8A), but also had a more noticeable presence in the cytosolic fraction compared to the nuclear one (Figure 4.8B). This change was only observed in the differentiated CCP1KO condition, whereas the other examined conditions showed no significant changes in its location. The collected data indicates that changes in NAP1L4 levels during differentiation in CCP1KO cells are mainly due to its loss of nuclear localisation, suggesting that CCP1 could play a key role over NAP1L4 nuclear function or shuttling during the neuron differentiation process.

Changes in NAP1L4 location during differentiation are presumed to be important for essential DNA-related cell processes as replication, DNA repair or transcription due to its role as histone chaperone (Rodriguez et al., 1997). These kinds of chaperones associate with histones upon their synthesis, escort them into the nucleus, and modulate their specific association with DNA, being also involved in histone storage preventing non-specific DNA aggregation (Avvakumov et al., 2011). Hence, lower presence into the nucleus could be sufficient for inducing changes in general DNA architecture in differentiating neurons, which could in turn modify its behaviour causing the observed neurodegenerative phenotype by loss of function of CCP1.

4.3.6 CCP1 might regulate nucleosome assembly processes by deglutamylation activity

Regarding the previously observed changes in expression level and location of NAP1L4, we wanted to gain insight into the impact of CCP1 loss of function over nucleosome assembly activity. It is known that glutamylation of NAP1 in *Xenopus laevis* modules histone dynamics and chromosome condensation, as it increases the deposition rate of the histone H1M when Nap1 is highly glutamylated (Miller & Heald, 2015). These findings indicate that human histone deposition by NAP proteins could be also modulated by their glutamylation levels, being CCP1 one of the main candidates to perform their specific deglutamylation.

Thus, we first assessed how histone H3 expression levels were affected by CCP1 loss of function in differentiated WT and CCP1KO SH-SY5Y cells at endogenous levels immunoblotting whole cell lysates of RA-induced cells. First results showed how histone H3 was 3-fold overexpressed in CCP1KO cells compared to the wild type control (Figure 4.9A and B). These observations point out that CCP1's activity is indeed affecting histone regulation, acting as an indirect DNA modulator.

To form nucleosomes, NAP1-like proteins bind and deposit the H3/H4 histones to DNA prior to the H2A/H2B deposition (Tachiwana et al., 2008). It is also known that yeast Nap1 bind histones H3 and H4 in a tetrameric conformation, directly depositing them into the nucleosome (Bowman et al., 2011). Observing the previous information and the fact that the *pcd* model mouse lacks CCP1 activity and presents a large-scale chromatin reorganisation due to histone modifications (Baltanás, Casafont, Lafarga, et al., 2011) we investigated whether the loss of deglutamylating activity or interaction between CCP1 and NAP1L4 could lead to a defective interaction between NAP1L4 and the core histones.

For this purpose, we immunoprecipitated NAP1L4 at endogenous levels in differentiated SH-SY5Y cells both WT and CCP1KO to assess the binding capacity with the core histone H3 in vivo. Results showed no apparent loss of interaction between these proteins when CCP1 is not present, indicating that his function is not required for the correct interaction between NAP1L4 and histone H3 (Figure 4.9C). During the performance of this experiment, we also noticed a change in the observed molecular weight of the detected histone H3 in immunoprecipitated fraction compared to the whole cell lysate. IP samples showed H3

detected at 56 KDa, whereas individual H3 weight is 17 KDa. This change in weight could be indicating that in the same way as yeast Nap1, human NAP1L4 is binding the H3/H4 tetramer (H3 = 17 KDa, H4 = 11 KDa; (17 x 2) + (11 x 2) = 56 KDa).
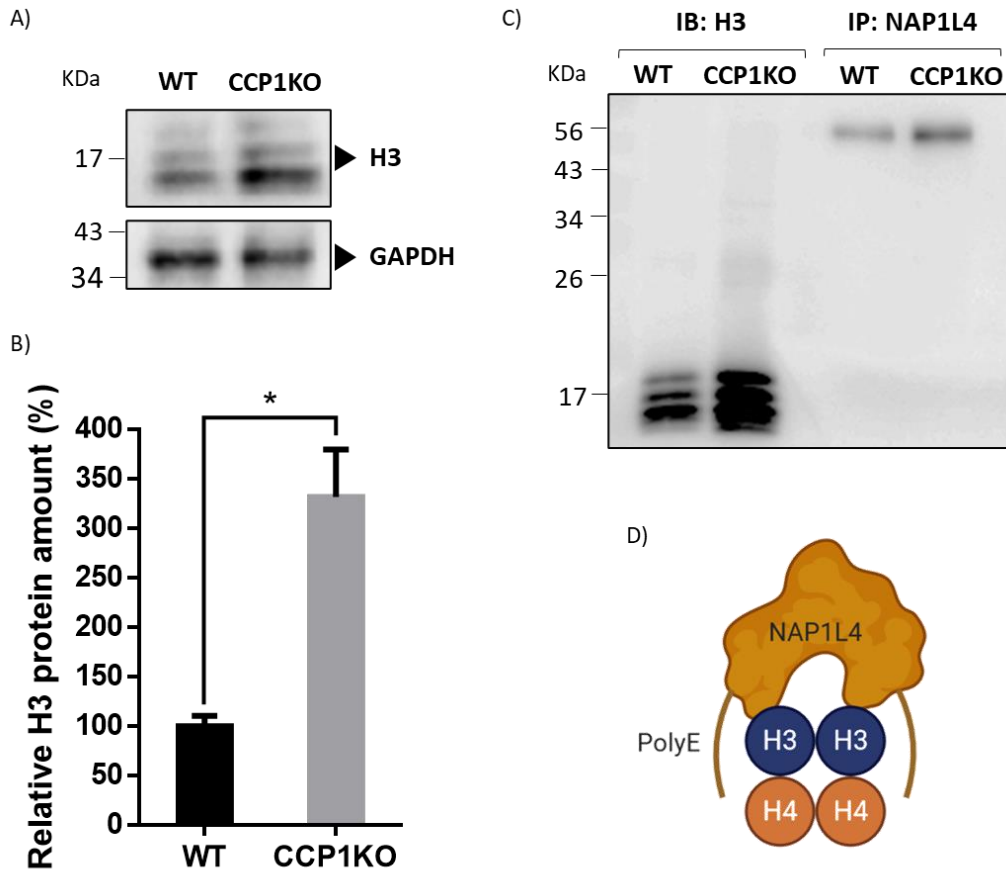
FIGURE 4.9. EFFECT OF CCP1 LOSS OF FUNCTION OVER HISTONE H3 EXPRESSION. (A) Western blot analysis from extracts of WT and CCP1KO SH-SY5Y cells for the specific immunodetection of H3 histone. GAPDH was used as a control. (B) Relative quantification of the data obtained in (A) for WT H3. Data is representative of two independent replicates. (C) Immunoprecipitation assay where endogenous NAP1L4 was captured with its specific antibody using protein G-coupled magnetic Dynabeads and H3 was immunoblotted with its specific antibody. Total cell lysate was used as a control in IB:H3. (D) Schematic representation of the NAP1L4 – H3/H4 tetramer interaction.

The gathered data could be consistent with the role of glutamylation as a modulator PTM of histone deposition. For instance, another histone PTM (i.e., acetylation/deacetylation is known to affect nucleosome assembly and disassembly through changes in the net charge carried by specific histone regions (Verdone et al., 2005). In our case, polyglutamylation would also cause alterations in negatively charged residues which could be comparable to

those seen in acetylation. Polyglutamylation's unique structure, with the side chain extending away from the core polypeptide, may allow for substantial stability of connections with positively charged partners. In addition, frog NAP1 was found to harbour polyE chains in both its C- and N-terminal (Miller & Heald, 2015). The presence of two negatively charged polyE chains could be essential for the correct stability of the NAP – histone interaction, as they could stabilise the histone's positive surface necessary for DNA interaction (Figure 4.9D). Hence, CCP1 could regulate DNA–protein interactions by shortening the length of these acidic tails.

4.3.7   CCP1 participates in DNA repair after doxorubicin-induced damage

It has been previously reported that Purkinje cell degeneration induced by CCP1 loss of function involves the progressive accumulation of nuclear DNA damage (Baltanás, Casafont, Weruaga, et al., 2011), leading to irreversibly compromising global gene transcription when DNA damage accumulated in chromosome territories (Baltanás, Casafont, Lafarga, et al., 2011). Recently, it has been demonstrated that mutations in the CCP1 gene induce p53-dependent nucleolar stress response in PCs which led to chromosome instability and accumulation of DNA damage (Baltanás et al., 2019). Moreover, it has been reported that NAP1L4 regulate cell fate by controlling the expression of p53-responsive prearrest and pro-apoptotic genes (Tanaka et al., 2019), having a role in DNA damage response, as overexpression of NAP1L4 protects cells from doxorubicin-induced (DOX) cell death (M. Okada et al., 2011). Moreover, the knockdown of NAP1L1, a paralogue of NAP1L4, decreases neural progenitor cell proliferation, inducing premature neuronal differentiation during cortical development (Qiao et al., 2018). All in all, these findings indicate that the CCP1-NAP1L4 interaction may play a role in DNA damage response, being essential for DNA repair and cell proliferation before neuronal differentiation processes.

To determine the functional effect of CCP1 in protection after DOX-induced DNA damage in undifferentiated neuronal cells, we performed an *in vitro* scratch assay. This assay was undergone on wild-type and CCP1KO SH-SY5Y cells treated or not with DOX. Briefly, by creating an artificial gap on a confluent cell monolayer, a "scratch", the cells of the edge would migrate to close the gap until cell-cell contacts are established anew. When treated with DOX, cells would only close the gap if they were capable to overtake the produced damage.
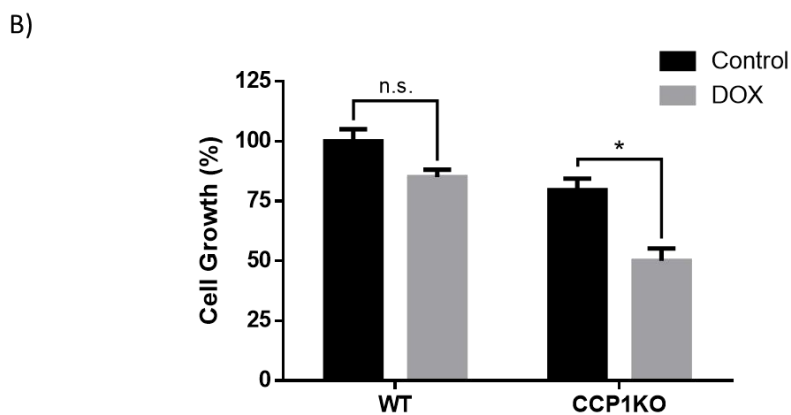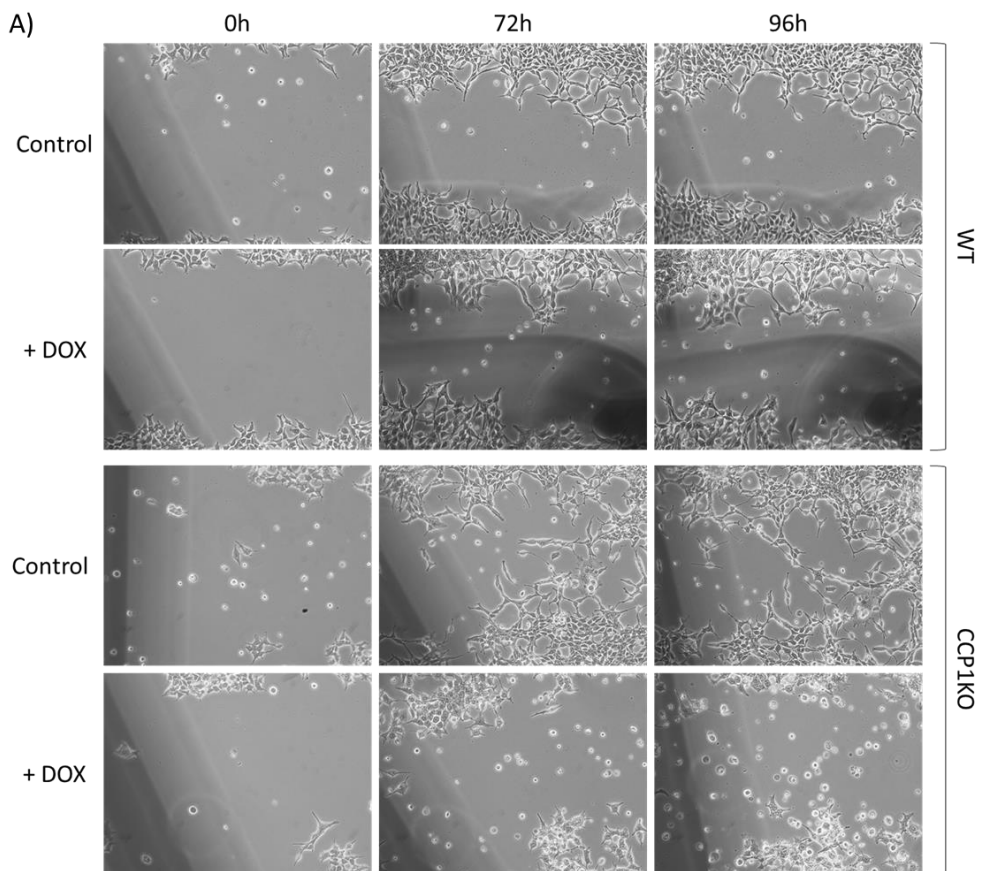
FIGURE 4.10. WOUND HEALING ASSAY OF SH-SY5Y IN PRESENCE OF DOXORUBICIN. (A) Confluent WT and CCP1KO SH-SY5Y cells treated or not with DOX and a scratch was performed. Cell migration was monitored by optical microscopy for 96 hours. (B) Cell growth was measured as the comparison of the area occupied by cells between 0 and 96 h in the different conditions.

As shown in Figure 4.10A, WT SH-SY5Y cells treated with DOX are capable to recover similar growth levels compared with not treated control cells, indicating they have enough mechanisms to repair the induced damage. Similarly, not treated CCP1KO cells present a migrating capacity comparable with WT cells (Figure 4.10A). On the contrary, knockout of CCP1 had a negative effect on cell migrating capacity after doxorubicin-induced DNA damage without notably affecting cell viability (Figure 4.10B), indicating they have lost essential mechanisms for DNA repair.

Thus, the gathered data suggest that CCP1 has a protective effect against doxorubicin-induced DNA damage, allowing a correct cell proliferation in undifferentiated neurons after DNA repair mechanisms. These effects are in coherence with the DNA damage accumulation found in the *pcd* mice, reinforcing the nuclear role of CCP1 in its neurodegenerative involvement.

4.3.8 IPO7 as a shuttle for CCP1 nuclear internalisation

As previously said, CCP1 is known to encode sequences for both NLS and NES localisation regions, allowing it to localise both in the nucleus and in the cytoplasm. So far, CCP1's NLS has not been well characterised, whilst NES has been found to allow CCP1's binding to the nuclear export receptor CRM1 for its consequent translocation from the nucleus to the cytoplasm (Thakar et al., 2013). The performed interactomics analysis by proximity biotinylation assessing the CCP1 interactome landscape, indicated that importins IPO7 and IPO9 could be interactors or substrates for CCP1, thus being candidates for CCP1's translocation to the nucleus (Figure 4.3, Table 4.2). These proteins have been described as nuclear importing proteins either by acting as autonomous nuclear transport receptors or as adapter-like proteins in association with the importin-beta subunit KPNB1 (Jäkel et al., 1999; Jäkel & Görlich, 1998). Acting autonomously, they are thought to serve themselves as receptor for NLSs and to promote translocation of import substrates through the nuclear pore complex by an energy-requiring, Ran-dependent mechanism. In association with KPNB1, they mediate the nuclear import of H1 histone, and their Ran-binding site is not required but synergizes with that of KPNB1 in importin/substrate complex dissociation. *In vitro*, these importins mediate the nuclear import of H2A, H2B, H3 and H4 histones (Taylor et al., 2018).

Regarding their function as receptor for NLS, we first analysed if IPO7 served as an importin for the localisation of CCP1 into the nucleus. To investigate this function, we first validated the CCP1-IPO7 interaction by performing a proximity ligation assay which allows *in situ* detection of protein interactions that can be readily detected and localised in unmodified cells and tissues. Briefly, our two POIs were targeted by primary antibodies from different species. Corresponding secondary antibodies with DNA probes were added, being able to hybridise if they are in proximity. The *in situ* amplification of the DNA probes using fluorescent nucleotides led to visualization of the interaction as a *red dot* with a high-resolution microscope (Figure 4.11A).

As seen in Figure 4.11B, PLA results showed a positive interaction between our two proteins, with both cytoplasmic and nuclear localisation of the complex. These results confirm the data obtained in the proteomics assay, revealing the importing IPO7 as a physical interactor of CCP1. This discovery could be useful for the identification of the nuclear localisation mechanism which allows CCP1 to shuttle to this structure when needed. Regarding the here reported importance of its nuclear role, understanding how the complete translocation of CCP1 works can be helpful for assessing its role in neurodegeneration.

Having assessed their interaction, we next proceeded to evaluate the effect of IPO7 over CCP1 by silencing the IPO7 gene using a siRNA-mediated knocking down strategy. For this experiment, HEK293T cells were transfected with specific IPO7 siRNA for 48 hours prior to cell fixation and immunocytochemistry analysis by confocal microscopy. As a result, we expected a change in CCP1 location, with a loss of its nuclear presence, if IPO7 was responsible for its nuclear internalisation.

The observed results, indeed, showed a significant change in its location. Even though CCP1 was not completely depleted from the nucleus, it presented a greater perinuclear accumulation. Having a closer look at its nuclear localisation after the knocking down of IPO7, it is observed that there is a general loss of the characteristic nucleolar accumulation, acquiring a diffuse nuclear pattern (Figure 4.11C). The results here exposed indicate that IPO7 is involved in CCP1 correct localisation pointing out IPO7 as a the responsible for its nuclear localisation, which could be mediated by its NLS recognition.
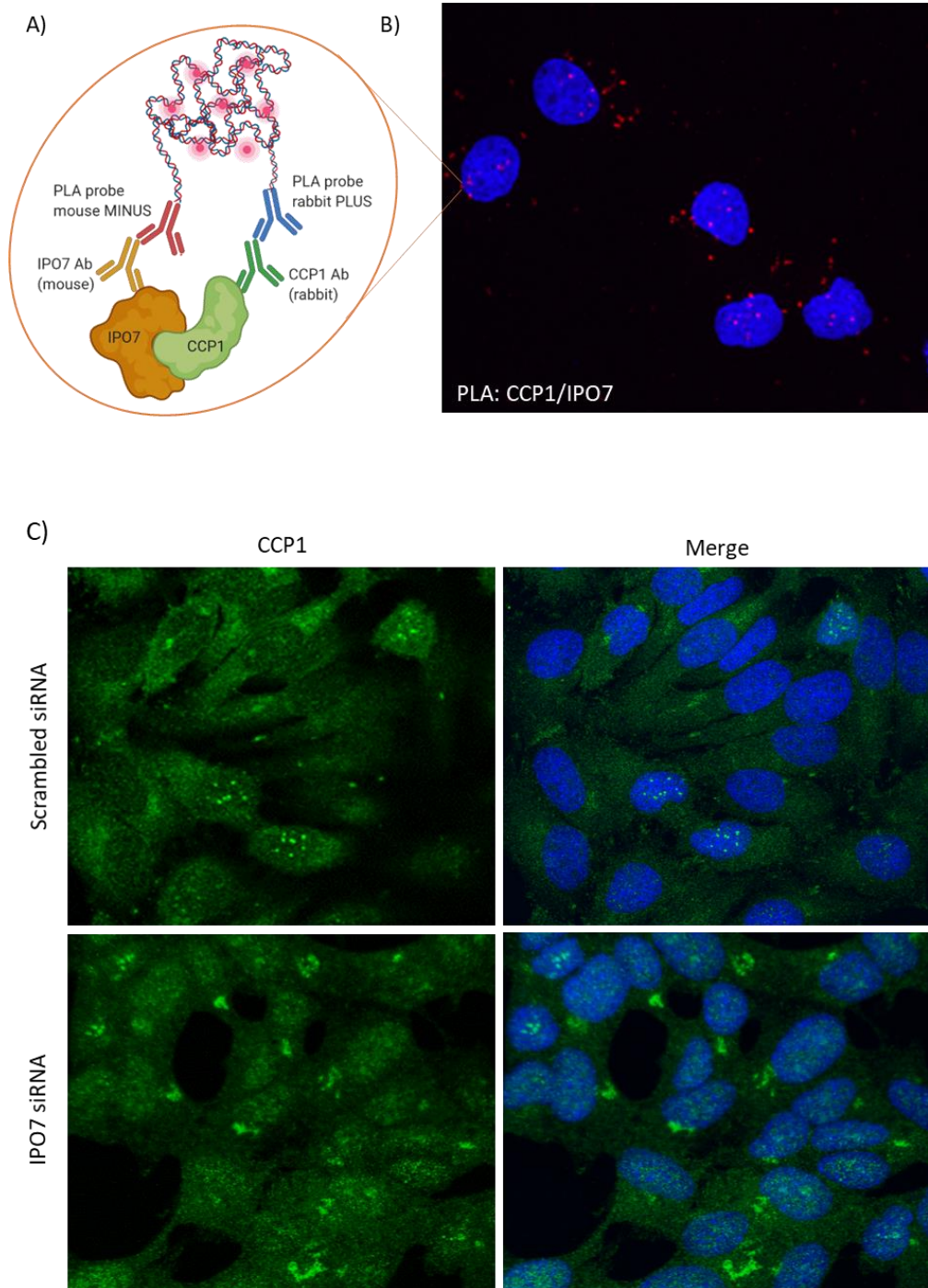
FIGURE 4.11. ASSESSMENT OF THE CCP1-IPO7 INTERACTION. (A) Scheme of PLA technique used to assess the CCP1-IPO7 interaction. (B) Representative PLA signal of CCP1-IPO7 complex in HEK293T cells. The interaction is represented by fluorescent rolling circle products (red). Nuclei were stained with DAPI (blue). (C) Images of WT and transfected with IPO7 siRNA HEK293T cells. CCP1 (green) was stained with its specific antibody and nuclei (blue) were stained using DAPI.

4.3.9   Identification of the CCP6 interactome

After characterising the CCP1 interactome, we focused on the analysis of CCP6. This member of the CCP subfamily is known to be localised in the Golgi complex, as well as in the centrioles at interphase and diving cells (Rodríguez de la Vega et al., 2013). The function of CCP6 has been related to the assembly of the cilia basal bodies and flagellar motility (Rodríguez de la Vega et al., 2013; Ye et al., 2014), as well as other cellular processes as megakaryopoiesis (Ye et al., 2014), viral defence (Xia et al., 2016) or embryonic development (Ye et al., 2018). The ability of CCP6 to trim proteins other than tubulins suggests that it could be involved in other cellular processes yet unexplored. Hence, the BioID interactomics approach was used to identify potential functional partners of CCP6. Our CCP6 BioID dataset identified a total of 41 candidates after the filtering process (Figure 4.12, Table 4.5). Promisingly, a large number of interactors or substrates were related with the centrosome, the centriole, cilium biogenesis and ciliopathies. These results indicate that BioID is able to provide a wide view of the CCP6 interactome and can be useful for its functional characterisation.
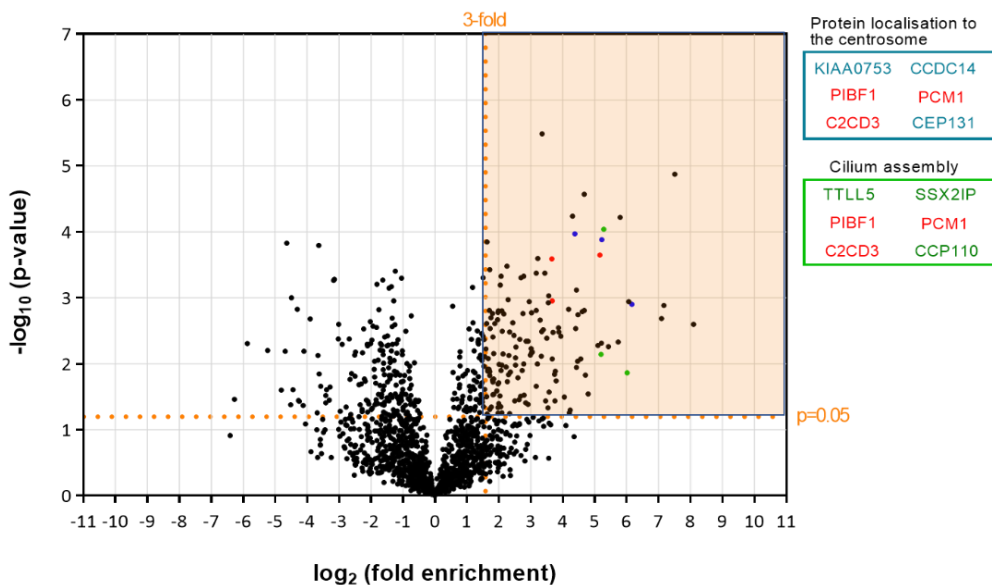
FIGURE 4.12. BIOID VOLCANO PLOT OF THE CCP6 ANALYSIS IN HEK293T CELLS. A volcano plot showing the statistical significance versus the fold enrichment of proteins identified in BioID-CCP6 experiments relative to control experiments. A quadrant (dashed orange line) bounded by a p-value of 0.05 and 3-fold enrichment contained CCP6 (red), as well as candidate interactors related to localisation to the centrosome (dark blue) and cilium assembly (green).

Analysis of the CCP6 hits enriched in the found dataset were consistent with the previously mentioned studies on the centriolar and cilia-related roles (Rodríguez de la Vega et al., 2013) as significant enrichment GO terms were led by cilium assembly (GO:0035735 and GO:1905515) and centrosome/centriole related processes (GO: 0071539 and GO:0007099). We also found snoRNA localisation (GO:0048254) as enriched (Table 4.4).

TABLE 4.4. GENE ONTOLOGY ANALYSIS OF THE CCP6 INTERACTOMIC LANDSCAPE. Data was analysed with the Panther Classification System, using the GO biological process complete data set with Fisher's exact test and FDR correction. Analysis results are hierarchically sorted.

GO biological process complete	Fold Enrichment	$-\log_{10}$ (p- value)	FDR
Intraciliary transport involved in cilium assembly	> 100	6.03	5.85E-04
Cilium assembly	14.61	7.98	1.16E-05
Cilium organization	14.59	8.85	2.46E-06
Plasma membrane bounded cell projection assembly	11.35	7.06	7.92E-05
Organelle assembly	9.97	11.03	2.43E-08
Organelle organization	2.77	4.97	5.61E-03
Cellular component assembly	3.70	6.09	5.24E-04
Cellular component biogenesis	3.56	6.23	3.98E-04
Plasma membrane cell projection organization	4.59	4.33	2.13E-02
Cell projection assembly	10.90	6.92	9.90E-05
Cell projection organization	4.82	4.95	5.70E-03
Intraciliary transport	36.78	4.03	3.88E-02
Cellular localisation	3.90	6.83	1.16E-04
Microtubule-based transport	13.18	4.38	1.98E-02
Microtubule-based movement	8.26	4.06	3.76E-02
Microtubule-based process	10.26	11.99	3.17E-09
snoRNA localisation	> 100	4.07	3.79E-02
Macromolecule localisation	3.40	5.22	3.24E-03
Protein localisation to centrosome	> 100	17.19	1.02E-13
Protein localisation to microtubule organizing centre	> 100	17.05	6.99E-14
Protein localisation to microtubule cytoskeleton	> 100	15.51	1.61E-12
Protein localisation to cytoskeleton	> 100	15.16	2.69E-12
Protein localisation to organelle	9.19	8.38	5.44E-06
Cellular protein localisation	4.63	5.65	1.34E-03
Cellular macromolecule localisation	4.60	5.62	1.40E-03
Protein localisation	3.61	4.84	7.13E-03
Centriole replication	> 100	8.59	3.70E-06
Cell cycle process	6.73	6.33	3.31E-04
Cell cycle	4.88	5.45	1.99E-03
Centriole assembly	84.54	8.14	8.79E-06
Non-membrane-bounded organelle assembly	12.95	6.74	1.38E-04
Microtubule organizing centre organization	33.65	8.66	3.44E-06
Microtubule cytoskeleton organization	12.24	10.59	5.82E-08
Cytoskeleton organization	5.87	7.35	4.38E-05
Centrosome duplication	70.05	7.77	1.79E-05
Centrosome cycle	39.01	9.08	1.63E-06
Non-motile cilium assembly	47.15	6.97	9.23E-05
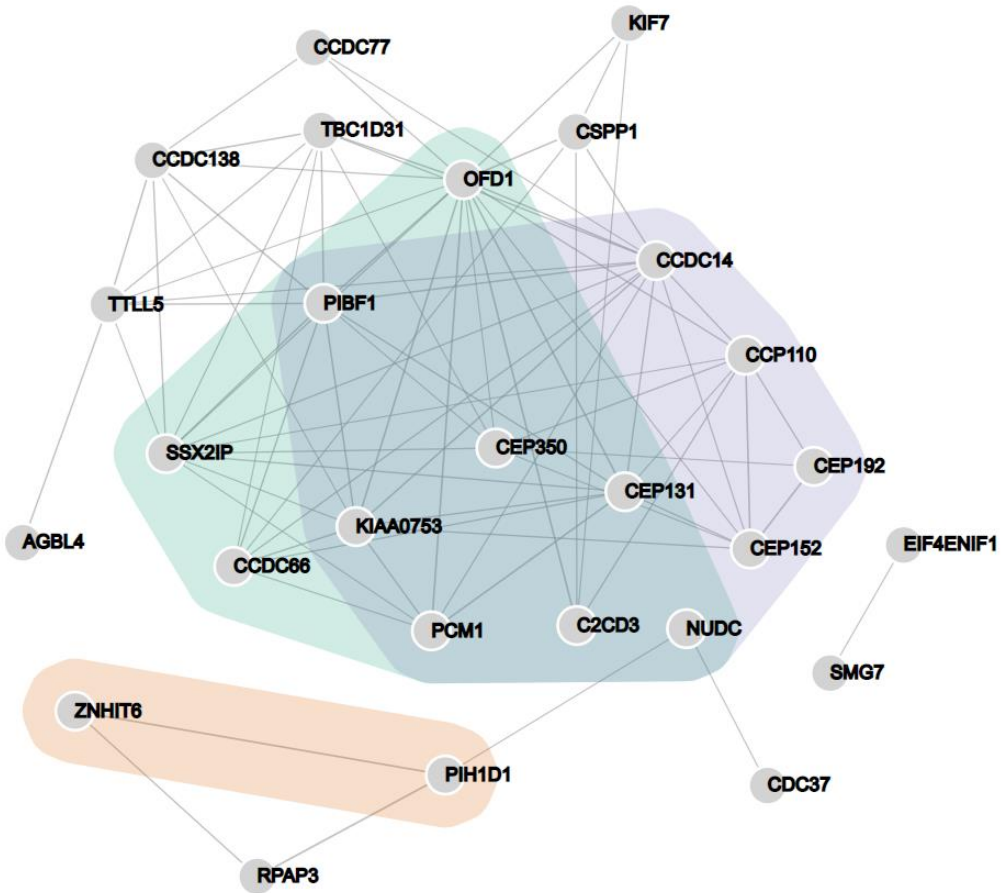
FIGURE 4.13. NETWORK ANALYSIS OF THE ENRICHED PROTEINS IN THE BIOID EXPERIMENT. Interaction data were retrieved from the STRING database and plotted with the NORMA software for enriched GO terms. Data from HEK293T cells, were cilium assembly (green), localisation to the centrosome (purple) and snoRNA localisation (orange) proteins are highlighted.

Among the identified clusters, proteins directly related to cilium assembly were NUDCD3, PIBF1, CEP131, PCM1, C2CD3, CEP350, CCDC66, SSX2IP, and OFD1 (Figure 4.13, green) whereas proteins related to localisation to the centrosome were PIBF1, CEP131, KIAA0753, NUDCD3, CEP350, CEP192, C2CD3, PCM1, and CCDC14 (Figure 4.13, purple). In both enriched processes, we found PCM1, which is one of the most characterised components of the centrosome assembly. PCM1 is known to be required to anchor microtubules to the centrosome and is involved in the biogenesis of the cilia (Dammermann & Merdes, 2002; Hames et al., 2005; Srsen et al., 2006). Another well-characterised component of the centriolar material found in both datasets is the protein PIBF1 (also known as CEP90). In fact, PCM1 in association with PIBF1 are predicted to be involved in

primary cilia formation and maintenance of the mitotic spindle (K. Kim et al., 2012; K. Kim & Rhee, 2011).

Polyglutamylation has a role in cilia/flagella motility modulation as well as flagella beating behaviour control. Previous functional and localisation studies have shown that TTLLs and CCPs are necessary in cilia and basal bodies, confirming this involvement. *In vivo*, the relevance of polyglutamylation in cilia can be deduced in part from the abnormalities seen in TTLL or CCP knockout mice, which are similar to phenotypes seen in ciliopathies in some circumstances. For instance, disruption in glutamylation levels produced by TTLL1 absence causes respiratory cilia and sperm motility failure; similarly, male infertility is also seen in the CCP1 knockout *pcd* mouse. As a result, both hyperpolyglutamylation and hypopolyglutamylation are potential cause of ciliopathies. The presented results reinforce the involvement of CCP6 in controlling ciliary structure and maintenance. Interestingly, four of the found interactors (PIBF1, CSPP1, OFD-1 and KIF7) were related to a single pathology, the Joubert syndrome (JS). This ciliopathy is marked by cerebellar hypoplasia and neurological symptoms like ataxia, psychomotor delay, and oculomotor apraxia. JS is commonly accompanied by a variety of multi-organ signs and symptoms, such as retinal dystrophy, nephronophthisis, liver fibrosis, and polydactyly, all of which are linked to ciliopathy illnesses such as Meckel-Gruber Syndrome, Bardet-Biedl syndrome, and nephronophthisis (Parisi, 2009). This data reinforces the relation of CCPs with neuronal disorders, widely exemplified in the *pcd* mouse model.

On the other hand, regarding the enrichment analysis, it is also important to note that two identified proteins were involved in snoRNA localisation (PIH1D1 and ZNHIT6), a very specialised cellular process. In relation to RNA processing, we also found the protein EIF4E, which is related to transcription initiation. As previously mentioned, RNA processing was also found in the CCP1 interactome landscape, pointing CCPs as crucial enzymes for RNA-related processes. These results reinforce the importance of CCP6 in the regulation of key cellular processes, as it could have different potential specialised roles depending on the tissue or cell line where it is being expressed.

TABLE 4.5. PROTEINS IDENTIFIED IN BioID METHODOLOGY FOR CCP6. Results showed are thresholded by a p-value of 0.05 and 3-fold enrichment. The list reports the bait protein (CCP6, light red), as well as candidate interactors. Proteins related to cilia and centrosome (light green) and RNA metabolism (light blue) are highlighted.

Nº	Protein	Gene	$\log_2$ (Fold)	-log (p-value)	Function
0	Cytosolic carboxypeptidase 6	AGBL4	7.0889	2.6883	Metallocarboxypeptidase that catalyses the deglutamylation of polyglutamate side chains generated by post-translational polyglutamylation. Also removes gene-encoded polyglutamates from the carboxy-terminus.
1	Centrosome and spindle pole-associated protein 1	CSPP1	8.0967	2.6013	May play a role in cell-cycle-dependent microtubule organization.
2	Protein FAM217B	FAM217B	7.5067	4.8713	-
3	Coiled-coil domain-containing protein 77	CCDC77	7.1701	2.8829	-
4	Protein moonraker	KIAA0753	6.1700	2.8994	Involved in centriole duplication. Positively regulates CEP63 centrosomal localization. Required for WDR62 centrosomal localization and promotes the centrosomal localization of CDK2
5	DDRGK domain-containing protein 1	DDRGK1	6.0664	2.9455	Substrate adapter for ufmylation, the covalent attachment of the ubiquitin-like modifier UFM1 to substrate proteins, which plays a key role in reticulophagy
6	Afadin- and alpha-actinin-binding protein	SSX2IP	6.0236	1.8657	Acts as a centrosome maturation factor by maintaining the integrity of the pericentriolar material and proper microtubule nucleation at mitotic spindle poles. Belongs to an adhesion system, which plays a role in cell-cell adherens junctions
7	Oral-facial-digital syndrome 1 protein	OFD1	5.8035	4.2177	Component of the centrioles controlling mother and daughter centrioles length. Involved in the biogenesis of the cilium, a centriole-associated function. Plays an important role in development by regulating Wnt signalling.
8	Coiled-coil domain-containing protein 66	CCDC66	5.7373	2.3312	Microtubule-binding protein required for ciliogenesis. May function in ciliogenesis by mediating the transport of proteins to the cilium, but also through the organization of the centriolar satellites. Plays a role in retina morphogenesis and homeostasis
9	Olfactory marker protein	OMP	5.4371	2.2599	May act as a modulator of the olfactory signal-transduction cascade.
10	Centriolar coiled-coil protein of 110 kDa	CCP110	5.2816	4.0412	Necessary for centrosome duplication at different stages of procentriole formation. Acts as a key negative regulator of ciliogenesis. Also involved in promoting ciliogenesis. Required for correct spindle formation.
11	Centrosomal protein of 131 kDa	CEP131	5.2232	3.8840	Component of centriolar satellites contributing to the building of a complex and dynamic network required to regulate cilia/flagellum formation.
12	Serine/threonine-protein kinase RIO1	RIOK1	5.2088	2.3117	Involved in the final steps of cytoplasmic maturation of the 40S ribosomal subunit. Involved in processing of 18S-E pre-rRNA to the mature 18S rRNA. Required for the recycling of NOB1 and PNO1 from the late 40S precursor.
13	Tubulin polyglutamylase TTLL5	TTLL5	5.2017	2.1430	Polyglutamylase which preferentially modifies α-tubulin. Involved in the side-chain initiation step of the polyglutamylation reaction rather than in the elongation step
14	Pericentriolar material 1 protein	PCM1	5.1612	3.6499	Required for centrosome assembly and function. Required to anchor microtubules to the centrosome. Involved in the biogenesis of cilia.

#	Protein	Gene			Description
15	G kinase-anchoring protein 1	GKAP1	5.1048	2.2797	Regulates insulin-dependent IRS1 tyrosine phosphorylation in adipocytes by modulating the availability of IRS1 to IR tyrosine kinase. Its association with IRS1 is required for insulin-induced translocation of SLC2A4 to the cell membrane.
16	Kinesin-like protein KIF7	KIF7	4.8002	1.5427	Essential for hedgehog signalling regulation. Involved in the regulation of microtubular dynamics. Required for localization of GLI3 to cilia in response to Shh. Involved in the regulation of epidermal differentiation and chondrocyte development.
17	Pleckstrin homology domain-containing family G member 1	PLEKHG1	4.7152	1.8304	-
18	FERM, RhoGEF and pleckstrin domain-containing protein 2	FARP2	4.6790	2.8104	Functions as guanine nucleotide exchange factor that activates RAC1. Plays a role in the response to class 3 semaphorins and remodelling of the actin cytoskeleton. Plays a role in osteoclast differentiation. Regulates integrin signalling and cell adhesion.
19	Eukaryotic translation initiation factor 4E transporter	EIF4ENIF1	4.6770	4.5684	EIF4E-binding protein that regulates translation and stability of mRNAs in processing bodies (P-bodies). Component of a multiprotein complex that sequesters and represses translation of proneurogenic factors during neurogenesis.
20	Claspin	CLSPN	4.6113	2.7889	Required for checkpoint mediated cell cycle arrest in response to inhibition of DNA replication or to DNA damage induced by both ionizing and UV irradiation. May have a role as a sensor which monitors the integrity of DNA replication forks.
21	Protein FAM193A	FAM193A	4.5589	2.0744	-
22	Centrosomal protein of 192 kDa	CEP192	4.4823	2.7447	Required for mitotic centrosome maturation and bipolar spindle assembly. Appears to be a major regulator of pericentriolar material (PCM) recruitment, centrosome maturation, and centriole duplication.
23	NudC domain-containing protein 3	NUDCD3	4.4661	2.0397	-
24	PIH1 domain-containing protein 1	PIH1D1	4.4293	1.9445	Involved in the assembly of C/D box small nucleolar ribonucleoprotein (snoRNP) particles.
25	M-phase phosphoprotein 9	MPHOSPH9	4.4282	3.1154	-
26	TBC1 domain family member 31	TBC1D31	4.4037	2.5331	-
27	Coiled-coil domain-containing protein 14	CCDC14	4.3815	3.9687	Negatively regulates centriole duplication. Negatively regulates CEP63 and CDK2 centrosomal localization.
28	Thioredoxin-like protein 1	TXNL1	4.3127	4.2356	Active thioredoxin with a redox potential of about -250 mV.
29	Coiled-coil domain-containing protein 138	CCDC138	4.1831	2.8253	-
30	RNA polymerase II-associated protein 3	RPAP3	3.9434	2.4173	Forms an interface between the RNA polymerase II enzyme and chaperone/scaffolding protein, suggesting that it is required to connect RNA polymerase II to regulators of protein complex formation.
31	Striatin-3	STRN3	3.8758	2.4805	Binds calmodulin in a calcium dependent manner. May function as scaffolding or signalling protein.

32	Protein SDE2 homolog	SDE2	3.8652	2.5481	Involved in both DNA replication and cell cycle control. necessary to counteract damage due to ultraviolet light induced replication stress.
33	Centrosome-associated protein 350	CEP350	3.7002	2.4754	Plays an essential role in centriole growth by stabilizing a procentriolar seed composed of at least, SASS6 and CENPJ. Required for anchoring microtubules to the centrosomes and for the integrity of the microtubule network.
34	C2 domain-containing protein 3	C2CD3	3.6697	2.9573	Component of the centrioles that acts as a positive regulator of centriole elongation. Promotes assembly of centriolar distal appendage. Required for primary cilium formation. Required for sonic hedgehog signalling and for processing of GLI3.
35	Progesterone-induced-blocking factor 1	PIBF1	3.6573	3.5883	Pericentriolar protein required to maintain mitotic spindle pole integrity. Via association with PCM1 may be involved in primary cilia formation. Together with CEP63 promotes centriole duplication.
36	Hsp90 co-chaperone Cdc37	CDC37	3.5604	3.0312	Co-chaperone that binds to numerous kinases and promotes their interaction with the Hsp90 complex, resulting in stabilization and promotion of their activity. Inhibits HSP90AA1 ATPase activity
37	Phosphorylated adapter RNA export protein	PHAX	3.5492	2.9254	A phosphoprotein adapter involved in the XPO1-mediated U snRNA export from the nucleus. Plays also a role in the biogenesis of U3 snoRNA. Involved in the U3 snoRNA transport from nucleoplasm to Cajal bodies. Binds also to telomerase RNA.
38	Centrosomal protein of 152 kDa	CEP152	3.4380	3.3764	Necessary for centrosome duplication. Also plays a key role in deuterosome-mediated centriole amplification in multiciliated that can generate more than 100 centrioles.
39	Nuclear migration protein nudC	NUDC	3.3546	5.4836	Plays a role in neurogenesis and neuronal migration. Necessary for correct formation of mitotic spindles and chromosome separation during mitosis. Necessary for cytokinesis and cell proliferation.
40	Box C/D snoRNA protein 1	ZNHIT6	3.2151	3.5987	Required for box C/D snoRNAs accumulation involved in snoRNA processing, snoRNA transport to the nucleolus and ribosome biogenesis.
41	Protein SMG7	SMG7	3.1703	3.3735	Plays a role in nonsense-mediated mRNA decay. Together with SMG5 is thought to provide a link to the mRNA degradation machinery involving exonucleolytic pathways, and to serve as an adapter for UPF1 to protein phosphatase 2A.

4.3.10 CCP6 binds to PCM1

Following the CCP6 interactome characterisation, we focused on the pericentriolar matrix proteins, as they are thought to be important for understanding the implications of CCP6 in the centrosome and cilia. Specifically, we wanted to gain insight into cilium assembly and protein localisation to the centrosome, thus choosing the PCM1 protein as a starting point. Hence, we initially characterised the CCP6-PCM1 physical interaction *in vitro.*

To explore this interaction, we first assessed the localisation of PCM1 within HEK293T cells in relation to CCP6. To this end, we double-stained adherent cells after paraformaldehyde fixation with specific antibodies for high resolution confocal microscopy. At first glance, PCM1 (red) presents co-localisation with CCP6 (green), as it shows a clear centriolar pattern (Figure 4.14A). This pattern is supported in the literature, where it was shown to be required to anchor microtubules to the centrosome (Gupta et al., 2015).

To further investigate the endogenous interaction between CCP6 and PCM1 inside HEK293T cells, we then performed a PLA assay assessing both the presence and location of CCP6-PCM1 interaction. As seen in Figure 4.14B, PLA results showed a positive interaction between the two proteins, with a cytoplasmic localisation of the complex in a structure that could resemble the centriole. These results confirm the data obtained in the proteomics assay, revealing the pericentriolar matrix protein PCM1 as a physical interactor of CCP6. PCM1-CCP6 co-localisation, however, seems to not be only restricted to the cellular centriole, as we observed less intense positive localisations at different cell locations.

The presence of alternative interacting locations apart from the centrosome could be due to the recruiting capacity of PCM1 (A. Kubo et al., 1999). The PCM1 protein has been implicated in centrosomal trafficking in a variety of studies, as it is not concentrated only at the centrosome. This fact raises the notion that PCM1 could function as a transporter or assembly factory for other centrosomal proteins (Dammermann & Merdes, 2002). This way, the different cellular localisations of the complex apart from the centrosome could imply that PCM1 functions as a recruiter for CCP6 to the pericentriolar matrix. This relation could be useful for the identification of the centriolar localisation mechanism which allows CCP6 to shuttle to this structure when needed. Understanding how the complete translocation of CCP6 works can be helpful for assessing CCP6 role in ciliopathies.
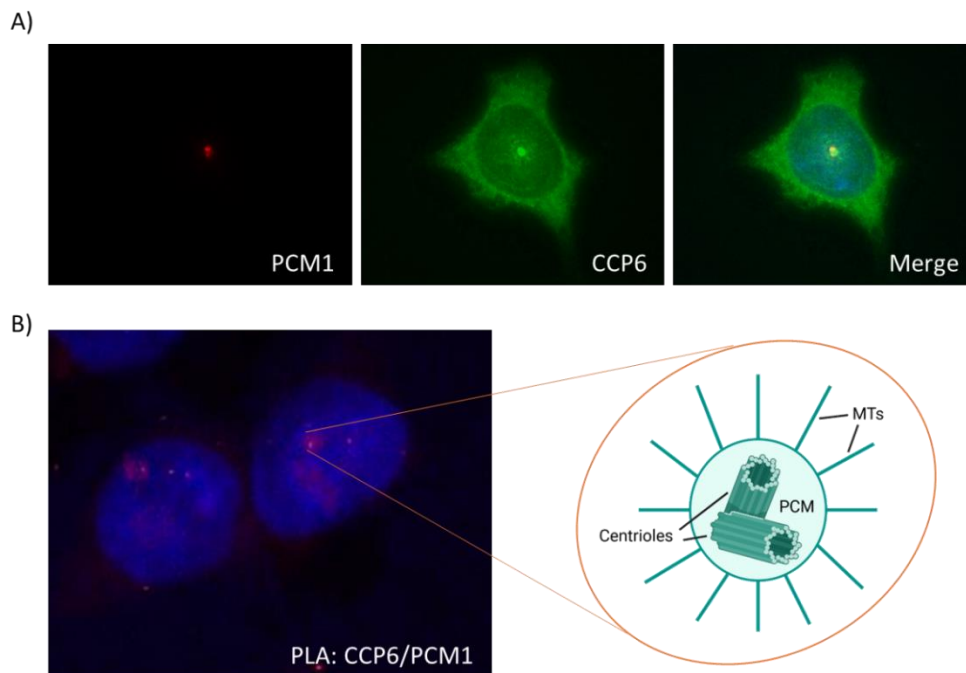
FIGURE 4.14. CHARACTERISATION OF THE CCP6-PCM1 INTERACTION. (A) Immunocytochemistry of endogenous CCP6 (green) and PCM1 (red) showing their intracellular localisation. Images were obtained on an inverted confocal microscope (Leica SP5) using a 63X objective and analysed with Imaris software (Bitplane). **(B)** Representative PLA signal of CCP6-PCM1 complex in HEK293T cells. The interaction is represented by fluorescent rolling circle products (red dots). Nuclei were stained with DAPI (blue).

4.3.11 Relation between CCP6 and the Joubert syndrome

To further characterise the link between CCP6 and Joubert syndrome, we investigated whether this was associated with CCP6 localisation in the cilia or was directly related to CCP6 function. Thus, we studied the four JS-related proteins enriched in the BioID dataset. Regarding their individual localisation, the detected interactors are located in different regions of the centrosome and the axoneme. Whereas CSPP1 and PIBF1 proteins are found only in the centrosome or the centriolar matrix (Frikstad et al., 2019; Lachmann et al., 2004), OFD-1 has a dual localisation in both the centriole and the basal body (Giorgio et al., 2007; Singla et al., 2010) and KIF7 is found in the axoneme distal tip (Endoh-Yamagami et al., 2009). These changes in location are not sufficient to discriminate a direct role of CCP6, as they are related along the cell cycle and axoneme formation. Next, we focused on the deglutamylating activity of CCP6 and its relation with the Joubert syndrome. First, we found that tubulin glutamylation occurring in the ciliary axoneme has been suggested to be

important for ciliary function (Yang et al., 2021). In addition, we also found that axoneme polyglutamylation and its regulation are marginally required for cilia stability but essential for cilia signalling (K. He et al., 2018). Interestingly, this regulation was done by another JS-related protein, the ARL13B, which imports the glutamylases TTLL5 and TTLL6 to the cilia (Figure 4.15). As shown in Table 4.5, TTLL5 was also found as a candidate interactor for CCP6, suggesting a possible relation between CCP6 activity and cilia signalling. A recent study also demonstrated that dysfunction in the ARM9/TOGARAM1 protein module, one of the causes of JS, altered the axonemal polyglutamylation state, further affecting ciliary stability (Latour et al., 2020). Strikingly, this same study also found one of our interactor candidates, the CCDC66 protein, to be interacting with the ARM9/TOGARAM1 protein module.

FIGURE 4.15. SCHEMATIC MODEL OF POLYGLUTAMYLATION REGULATION AND FUNCTION IN THE CONTEXT OF CILIA. In cilia, axoneme polyglutamylation is controlled by the balanced enzymatic activities between TTLLs and CCPs. Polyglutamylated axoneme anchors sensory receptor polycystins to the ciliary surface, which could interact with the glutamylated chain. Additionally, axoneme polyglutamylation is required for proper translocation of Shh signaling GLI3 to the ciliary tip. Figure adapted from (K. He et al., 2018)

All this data suggests that CCP6, indeed, may play a crucial role in the development of the Joubert syndrome by means of tubulin polyglutamylation regulation in the cilia. Thus, suggesting a potential therapeutic strategy by targeting polyglutamylation machinery to promote ciliary targeting of signalling machinery and correct signalling defects in ciliopathies.

4.4   Conclusions

The purpose of this study was to globally identify the human CCP1 and CCP6 interactome by applying the BioID system, a novel interactomic methodology based on proximity-dependent biotin identification. Since their discovery, CCP1 and CCP6 have been studied and characterised, reveling their relationship with several cellular processes. Despite previous work has been done to characterise these proteins in their cellular context, little is known about their interactome landscape. Consequently, the main conclusions of this chapter are:

1. BioID-based constructs for CCP1 and CCP6 were developed to study the interactome landscape of CCPs.

2. BioID methodology was able to identify 52 putative CCP1 protein interactors in a cellular context.

3. Analysis of the CCP1 interactome identified the nucleosome assembly and RNA-related metabolic processes as important biological processes where it coul be related.

4. NAP1L4 was identified as a novel CCP1 interacting protein. CCP1 is able to deglutamylate NAP1L4, thus affecting its regulation.

5. CCP1-NAP1L4 interaction is not mediated by the NLS or NES sequences of CCP1.

6. CCP1 does not appear to be involved in SH-SY5Y neuron differentiation but is necessary for their long-term maintenance.

7. CCP1 is overexpressed after SH-SY5Y neuron differentiation, with a special increment in the cellular nucleus.

8. Glutamylation levels of NAP1L4 remain unchanged in undifferentiated cells, whereas they are increased in CCP1KO-differentiated SH-SY5Y cells. Furthermore, polyglutamylated NAP1L4 was mainly localised in the nucleus of differentiated WT cells, whereas CCP1KO cells did not show differences from undifferentiated cells.

9. Undifferentiated WT SH-SY5Y cells did not show any significant change in total NAP1L4 expression level between WT and KO cells, while differentiated CCP1KO cells showed a significant reduction of NAP1L4 expression level compared to WT differentiated cells.

10. Loss of CCP1 glutamylating activity does not interfere with NAP1L4-Histone H3 interaction.

11. Knockout of CCP1 had a negative effect on cell migrating capacity after doxorubicin-induced DNA damage without affecting cell viability.

12. IPO7 knockdown induces changes in CCP1 subcellular localisation, which is depleted from nucleoli.

13. The BioID methodology was able to identify 41 putative CCP6 protein interactors in a cellular context.

14. The bioinformatics analysis of the BioID data revealed that CCP6 is presumably involved in processes including the centrosome, MTOC and the cell projection organization.

15. CCP6 binds to PCM1 in the pericentriolar matrix.

16. The association between CCP6 and centrosomes is probably the link with ciliopathies, as the Joubert syndrome.

.

Characterising the N-domain of cytosolic carboxypeptidases

The cytosolic carboxypeptidases (CCPs) are metallocarboxypeptidases that catalyse the deglutamylation of the polyglutamate side chains generated as a post-translational modification in some proteins such as tubulins. They are involved in a wide spectra of cell processes, as spermatogenesis, antiviral activity, embryonic development, and neurodegeneration. All members of this subfamily have two highly conserved domains between species: the catalytic carboxypeptidase C-terminal domain and the N-domain. This last one, exclusive of this subfamily, shows three conserved motifs and a folding that has not been previously described in any protein. Nevertheless, it has been impossible to assign a function to N-domain or to any of its motifs.

The goal of the present study is to determine the specific function or functions of the N-domain. For this purpose, we recreated on human CCP6 a naturally found mutation on motif I of the N-domain of the CCPP-1 homologue of *Caenorhabditis elegans*. This mutation led to a partial loss of protein´s catalytic function, depriving cells of cilia-based signal transduction that resulted in neuronal deficiencies in *C. elegans*. Biochemical and proteomic analyses were performed using this mutant and compared with wild type and catalytically dead versions of human CCP6. The results showed that this domain was involved in the catalytic activity of human CCPs, impairing their deglutamylating activity on cellular substrates such as tubulin, but not on small synthetic substrates. Protein stability assays determined that this was not due to a misfolding of the protein. However, subsequent analysis of the mutant´s ability to bind to its substrate showed that it did not bind to tubulin.

The silico studies based on models carried out to determine how the mutation could affect the general conformation indicated that this mutation caused a lower exposure of motif I and it had less conformational flexibility to recognize tubulin and the rest of its specific substrates. These observations suggest that the loss of catalytic function in the mutant protein could be due to a lack of binding to the substrate and not an actual lack of catalytic activity. Highlighting a possible role of the N-domain in the specific enzyme-substrate recognition of CCPs and being an essential domain for the correct *in vivo* catalytic activity.

Chapter 5. Characterising the N-domain of cytosolic carboxypeptidases

5.1 Introduction

Metallocarboxypeptidases are zinc-dependent enzymes that catalyse the sequential hydrolysis of C terminal amino acids from peptides and proteins (Arolas et al., 2007). According to the MEROPS database, the most numerous families of MCPs corresponds to the proteases of the M14 family (Rawlings et al., 2014). In 2007, a new subfamily of MCPs of the M14 family was identified, named M14D or cytosolic carboxypeptidases (Kalinina et al., 2007; Rodriguez de la Vega et al., 2007). Unlike the other subfamilies, CCPs are intracellular, present both in the cytosol and in other cell compartments (Guinand et al., 1979; Kalinina et al., 2007; Rodriguez de la Vega et al., 2007).

The number of genes coding for CCPs is variable, from a single gene in proteobacteria to 32 genes in the hairy protozoan *Paramecium tetraurelia* (Rodríguez de la Vega et al., 2013). The human and mouse genomes encode for 6 CCPs called CCP1-CCP6 (hereinafter hCCPs or mCCPs) according to the order in which they were discovered (Kalinina et al., 2007; Rodriguez de la Vega et al., 2007; Rodríguez de la Vega et al., 2013).

Currently, the structural and functional information regarding these enzymes remains very limited, especially for human CCPs. As far as we know, human CCPs correspond to large

multi-domain proteins with great structural heterogeneity. It is not known whether CCPs in higher eukaryotes are monomeric or multimeric proteins, as the CCP homolog from *Pseudomonas aeruginosa* was crystalized and structurally solved as a monomer (Otero et al., 2012) while the bacterial CCP homolog from *Burkholderia cenocepacia* was solved as a tetramer (Rimsa et al., 2014). Their molecular weight varies from 55 to 138 kDa in humans, and they are synthesized in their active form not containing disulphide bonds in their structure.

CCPs have in common an N-domain with a β-sandwich fold exclusive to this subfamily, juxtaposed to the catalytic carboxypeptidase domain, the latter with a conserved α/β hydrolase fold in all members of the M14 family of the MCPs (Otero et al., 2012; Rimsa et al., 2014). CCPs are distinguished by their structural heterogeneity and by the presence of additional N-terminal and C-terminal domains and extensions (Rodriguez de la Vega et al., 2007). CCP1 is the one that contains more additional domains and extensions, while CCP6 represents the minimum expression of the CCPs, formed only by the two domains characteristic of this subfamily (Figure 5.1).

Although mammalian CCPs' structure has not yet been elucidated in a high-resolution format, structural modelling based on bacterial CCPs structures can give relevant structural information (Otero et al., 2012; Rimsa et al., 2014). The active centre of CCPs contains all those residues necessary for the functionality of the enzyme, including the amino acids conserved in the M14 peptidases involved in the coordination of the zinc ion, catalysis and binding to the substrate (S. Wu et al., 2010). The binding of the substrate to the active centre allows the catalytic process that leads to the excision of the C-terminal peptide bond to be carried out. The residues of the substrate that recognize the active centre promote the rearrangement of the lateral chain of one of the residues of union to the substrate. This rearrangement allows the fixation of the free carboxyl group of the C-terminal residue of the substrate, necessary to begin the catalysis (Avilés et al., 1993). Although the residues of the active centre are clearly defined, the catalytic mechanism of the M14s remains unclear. Numerous kinetic and crystallographic experiments support anhydrous and water-driven as the two most likely catalytic mechanisms, although the latter is currently the most widely supported (Avilés et al., 1993).
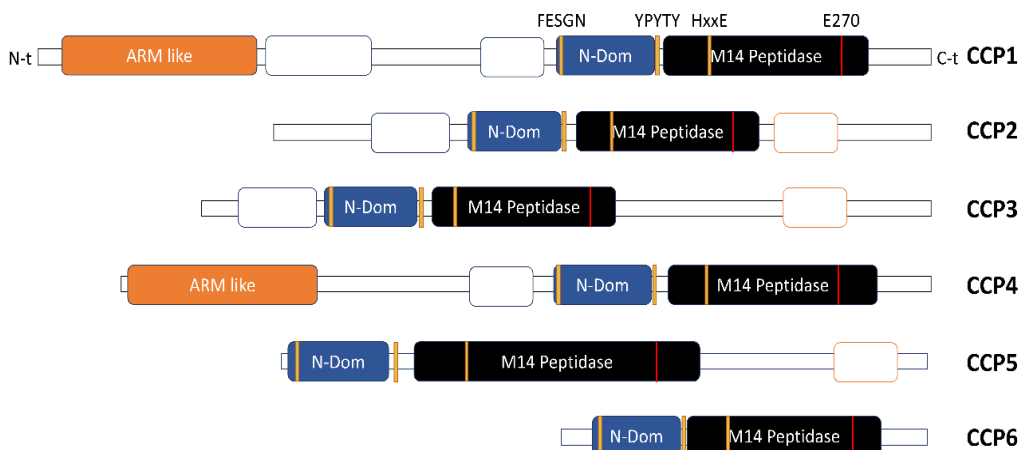
FIGURE 5.1. SCHEMATIC REPRESENTATION OF THE DOMAIN STRUCTURES OF M14D subfamily members identified in humans. All members of the M14 subfamily of metallocarboxypeptidases contain a carboxypeptidase M14 catalytic domain (Peptidase M14, shown in black) and an N-domain (N-Dom, shown in blue). Furthermore, all members have additional extensions or domains at the N- and/or C- sides of the N-Dom+M14-catalytic domain set such as the armadillo (ARM) like domain (orange), and other less characterized (shown in white).

In addition to the carboxypeptidase domain, all CCPs contain a domain of ~120 residues that has sequence similarity between individual CCPs, but not with metallocarboxypeptidases of the M14A or M14B subfamilies. This ~120 residue domain is known as the 'N-domain' (Otero et al., 2012). Based on the structures of the bacterial CCPs (Otero et al., 2012; Rimsa et al., 2014), the N-domain of the mammalian CCPs is predicted to fold as a β-sandwich consisting of 9 β-strands, containing three highly conserved motifs that seem to be important for its correct folding or substrate recognition. Motif I (F[E,D]SGNL) is the closest one to the N-terminal end, located in the loop between the chains β1 and β3. Motif II (W[F,Y][Y,H,N][F,Y]) is located 60 residues away from motif I as part of the β4-chain and contributes significantly to the formation of the hydrophobic nucleus together to other aromatic residues. Motif III ([F,Y]P[F,Y][S,T]Y) is located at the C-terminal end of the N-domain and represents the end of this domain before the catalytic CP domain (Figure 5.1) (Otero et al., 2012; Rimsa et al., 2014). These conserved motifs seem to contribute to the formation of the hydrophobic nucleus (Rimsa et al., 2014). The orientation of the N-domain with respect to the catalytic domain partially blocks the entrance to the active centre, leaving a small open channel accessible to the solvent (Otero et al., 2012).

In contrast to their structural heterogeneity, mammalian CCPs exhibit a common O-type substrate specificity, with a clear preference for the hydrolysis of peptide bonds of acidic C-terminal residues (Garcia-Guerrero et al., 2018). At the molecular level, CCPs are defined as enzymes with deglutamylase activity (Rogowski et al., 2010; Tort et al., 2014). They catalyse the cleavage of the genetically encoded Glu at the C-terminal end of previously detyrosinated α-tubulin (generating Δ2- and Δ3-α-tubulin), and the swallowing of the side chain of Glu generated post-translationally in the C-terminal region of the α and β subunits of tubulin (Aillaud et al., 2016; Rogowski et al., 2010; H. Y. Wu et al., 2015) (Figure 5.2). Although all CCPs catalyse essentially the same reactions, they have been shown to differ in their preferences for poly-E lateral chain length and kinetic properties (H. Y. Wu et al., 2015). Modulation of the levels of polyglutamylation in the subunits α and β of tubulin by the CCPs allows the regulation of the functions and the structures of MTs: mitotic spindle, neuronal axons, centrioles, basal bodies, and axonemes of cilia and flagella (Janke et al., 2008; Janke & Bulinski, 2011; Rogowski et al., 2010). Several pathologies of unknown cause have been genetically mapped to CCPs-associated regions and are related to dysregulation of MTs and their associated structures (Baird & Bennett, 2013). In addition to modifying tubulin, CCPs are also capable of acting on other endogenous substrates such as MLCK1 and telokin proteins (Rogowski et al., 2010; Tort et al., 2014).

Most functional studies have been performed using mice CCPs (Kalinina et al., 2007; Rogowski et al., 2010; Tort et al., 2014; H. Y. Wu et al., 2015), while the study of human CCPs is an emerging field due to the direct implication between their loss of function and human pathologies. Mutations responsible for the loss of function of human CCPs are related to a wide range of pathologies and abnormal cellular function (Branham et al., 2016; W. P. He & Wang, 2019; Karakaya et al., 2019; Kastner et al., 2015; C. Li et al., 2016; Meyer, 2014; Patel et al., 2016; Peterfi et al., 2020; Shashi et al., 2018; L. L. Wang et al., 2018; Xia et al., 2016; Zhang et al., 2014). Interestingly, recent studies in humans have linked the loss of hCCP1 function to childhood onset neurodegeneration disorders that primarily affect the cerebellum, motor neurons, and peripheral nerves (Karakaya et al., 2019; Shashi et al., 2018). In these studies, rare and harmful biallelic variants have been found in the gene coding for hCCP1 and the absence of functional hCCP1 has been confirmed along with the deregulation of tubulin polyglutamylation (Karakaya et al., 2019; Shashi et al., 2018; Sheffer

et al., 2019). All the reported mutations in CCP1 have appeared both in the coding sequence for the catalytic carboxypeptidase domain and the N-domain, the necessary domains for the correct function of the CCPs. The mutations located in the coding sequence for the CP catalytic domain modify the amino acids and the coordination between them, preventing the catalytic process. However, the cause of the absence of catalytically active CCPs in the mutations located in the coding sequence for the N-domain is unknown.
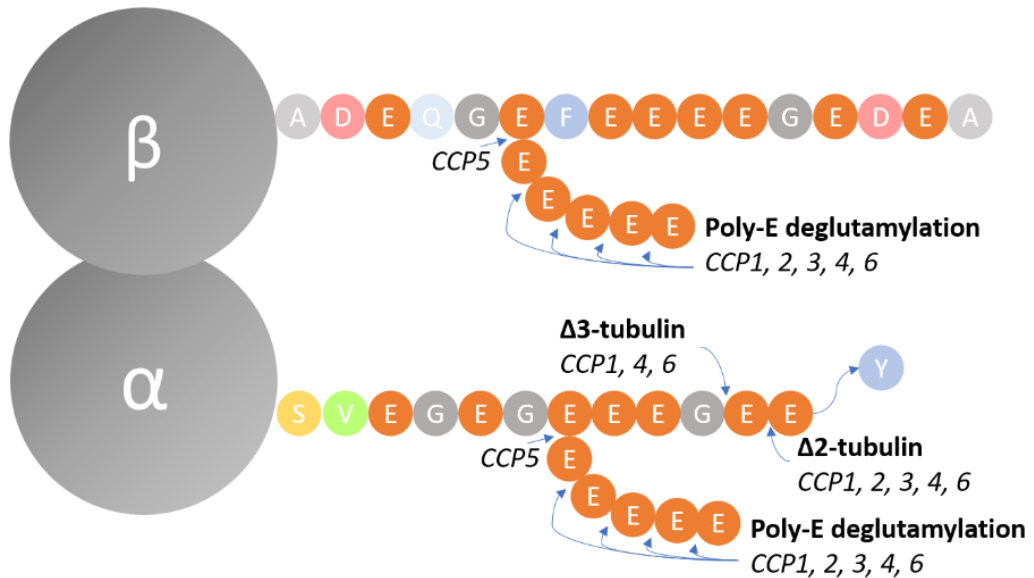
FIGURE 5.2. SCHEMATIC REPRESENTATION OF THE POST-TRANSLATIONAL MODIFICATIONS CATALYSED BY THE METALLOCARBOXYPEPTIDASES OF THE M14D SUBFAMILY. CCPs are tubulin deglutamylases with different substrate specificities that catalyse the elimination of post-translationally generated Glu side chains in the C-terminal tail of the α- and β-tubulin subunits, and the Glu genetically encoded at the C-terminal end of the detyrosinated α-tubulin, generating Δ2- and Δ3-tubulin. CCP5 is the only enzyme capable of removing the first Glu from the branch point of the poly-E side chain. The Tyr cleaved by vasohibin proteins at the C-terminal end of the α-tubulin is represented as a lilac circle. Amino acids are indicated in a single letter code and coloured according to their biochemical properties. The C-terminal sequence of α- and β-tubulin corresponds to the isotypes αIa and βIIb, respectively.

Nevertheless, studies in *Caenorhabditis elegans* proposed that neurodegeneration caused by the loss of CCPs in mammals could be linked to the incorrect functioning of the cilia. These studies showed that G596R substitution in the conserved F[E,D]SGNL motif of the N-domain of the CCP homolog CCPP-1 causes the accumulation of the motor protein kinesin KLP-6, depriving the cell of cilia-based signal transduction (O'Hagan et al., 2011).

Despite performing homology studies of sequences between species and executing methods of recognition of folds, it has been impossible to assign a function to the N-domain. Some studies suggest that it could act as an assistance domain to the folding of the adjacent catalytic CP domain, analogous to the N-terminal pro-segment and the TTL domain of the subfamily M14A and M14B, respectively (Alonso-del-Rivero et al., 2012; Otero et al., 2012; Rodríguez de la Vega et al., 2013). Alternatively, it has been suggested that the N-domain could act as a regulatory domain, limiting access to the active centre, or as a binding domain to other proteins, analogously to the N-terminal extensions of the M14C subfamily (Kemmler et al., 1971).

The present research study is focused on determining the specific function of the N-domain of CCPs. Human CCP6 constitutes the model CCP for the study of this subfamily of human MCPs thanks to its reduced size and structural simplicity with respect to the other members of the M14D subfamily. Therefore, a mutation in a conserved motif of its N-domain and its subsequent functional characterization would unveil its function and importance. Specifically, the change from glycine to arginine in the motif I (F[E,D]SGNL) of the N-domain, which causes a malfunction in the CCPP-1 orthologue (O'Hagan et al., 2011), could be a candidate substitution to achieve the objective of this study at the cellular level. As a starting point, we studied the recombinant production of hCCP6 and hCCP6 G53R in a mammalian expression system to obtain enough protein in its soluble, stable, and active conformation that would allow us to carry out biochemical and functional characterization studies. In parallel, we carried out functional studies of hCCP6 aimed at characterizing its activity over known substrates *in vitro* to compare it with the mutant protein. Using different experimental approaches, we analysed the capacity of the mutant hCCP6 to generate post-translational modifications in the C-t region of tubulin, its enzymatic activity respect telokins and its behaviour with synthetic peptides. Moreover, we undergone specific studies determining the binding capacity of hCCP6 and its mutant with tubulin, paying close attention on the interaction between these two proteins. The knowledge of the function of the N-domain could be relevant not only for understanding the mechanism of action of CCPs and their clinical role in the pathologies in which they are involved. It could also be important for the knowledge of new protein domains since the uniqueness of the N-domain could serve to discover the singularity of other domains.

5.2   Methods and materials

5.2.1   Cell lines and cell culture

HeLa human cervix carcinoma cells, HEK293T and HEK293F human embryonic kidney cells were cultured in Minimum Essential Medium α (MEM α), Dulbecco's modified Eagle's medium (DMEM) and FreeStyle 293 Expression Medium respectively. MEM α and DMEM were supplemented with 10% heat-inactivated foetal bovine serum. Cells were incubated at 37 °C in a humidified atmosphere with 5%, 10% and 8% CO_2 respectively.

5.2.1.1   Plasmids and transfection

Full length hCCP6 and catalytically dead hCCP6 E401Q mutant (point mutant E401Q, equivalent to E270Q in the canonical bCPA sequence) were cloned into a pTriEX-6 vector (Merck Millipore) as previously described (Tanco et al., 2015).

F[E,D]SGNL hCCP6 G53R mutant (point mutant G53R) was obtained by site-directed mutagenesis on the hCCP6 vector using the QuickChange Site-Directed Mutagenesis Kit (Stratagene) following manufacturer's procedure. Briefly, primers (Table 5.1) containing the desired point mutation were extended during temperature cycling (parameters described in Table 5.2) by Phusion DNA polymerase (Thermo Scientific). Incorporation of the primers generated a mutated plasmid containing staggered nicks. Following temperature cycling, the product was treated with DpnI endonuclease (target sequence: 5′-Gm6ATC-3′) to digest the methylated parental DNA template and to select the mutation-containing synthesized DNA. The mutant was obtained by the changing from guanine to cytosine at position 157 of the hCCP6 cDNA sequence.

The nicked vector DNA containing the desired mutation was ligated and transformed into supercompetent *Escherichia coli* XL1-Blue cells. The ligation procedure was carried out incubating the obtained vector with the T4 ligase (Roche) for 1 hour at room temperature. Midi-preparations of plasmid DNA for transfection into mammalian cells were obtained from 50 ml of transfected XL1-Blue bacterial culture grown over-night in LB with antibiotic, using the Plasmid Midi-Kit (GeneJET Plasmid Miniprep kit, Thermo Scientific). DNA concentration and purity were assessed using the Nanodrop spectrophotometer (Thermo Scientific). Purified clones were evaluated by full sequencing analysis (Macrogen). The

sequential identity of the protein was verified using the BLAST tool (https://blast.ncbi.nlm.nih.gov/Blast.cgi). Quality, quantity, and size of the vectors were determined by agarose gel electrophoresis at each stage of the procedure.

TABLE 5.1. MUTAGENIC PRIMERS FOR HCCP6. POINT MUTATION IS SHOWED IN RED.

Gene	Vector	Primers Fw/Rev
hCCP6 G53R	pTriEx-6	Fw: CCACCCGGCCCAGGTTACGACTTTC Rev: CTTTGATGCTTGCTTTGAAAGTCGTAACC

TABLE 5.2. CYCLING PARAMETERS FOR THE QUIKCHANGE SITE-DIRECTED MUTAGENESIS METHOD.

Segment	Cycles	Temperature	Time
1	1	98 ºC	30 seconds
2	16	98 ºC	30 seconds
		55 ºC	1 minute
		72 ºC	1 minute/kb of plasmid length

5.2.1.2 Recombinant production

Recombinant plasmids pTriEx-6 cloned with the cDNA coding for hCCP6 (Uniprot: Q5VU57), the catalytically inactive mutant hCCP6 E401Q, and the F[E,D]SGNL motif mutant hCCP6 G53R were used for protein production. Recombinant proteins contain the Strep-tag® II tag (Schmidt & Skerra, 2007) and the hemagglutinin (HA) epitope at their N-terminal end, allowing the purification and immunodetection of the recombinant protein. hCCP6, hCCP6 E401Q and hCCP6 G53R were produced intracellularly by transient transfection of HEK293F mammalian cells grown in suspension. Briefly, 1 mg of DNA of each construct were mixed with polyethyleneimine (PEI) (linear 25 kDa, Polysciences Inc.) at a ratio of 1:3 DNA:PEI (w/w) in 100 ml of fresh FreeStyle 293 Expression Medium (Gibco, Thermo Scientific) and incubated for 20 minutes at room temperature. DNA-PEI complexes were then added to 1 l culture at a cell density of $1 \cdot 10^6$ cells/ml and incubated on a rotary shaker (135 rpm) at 37°C, 8% CO_2 and 80% humidity for 72 hours. Each culture pellet containing recombinant hCCP6, hCCP6 E401Q and hCCP6 G53R was recovered by centrifugation at 300xg for 15 minutes. The collected pellet was washed twice with phosphate buffered saline, pH 7.4, (PBS, Life Technologies) and resuspended in 100 ml (the volume

corresponding to one tenth of the initial volume of the culture) lysis buffer (100 mM (tris (hydroxymethyl) aminomethane (Tris-HCl, Sigma-Aldrich), pH 8, 150 mM sodium chloride (NaCl, Sigma-Aldrich), 0.1% (w/v) Nonidet-P40 (NP-40, Sigma-Aldrich), and 1:1000 (v/v) of EDTA-free protease inhibitors cocktail (EMD Millipore)).Lysed cells were then incubated for 30 minutes on ice and further lysed using 3 freezing/thawing cycles in liquid nitrogen and 37ºC water bath. Finally, the cell extracts were centrifuged at 16,000xg for 15 min at 4ºC for the clarification of the cell extracts. Protein concentration of the soluble fractions was determined by the Bradford method (Bradford, 1976) using bovine serum albumin (BSA, Sigma) as protein standard.

The eluted fractions containing different hCCP6 variants were pooled and loaded into a 5 ml Strep-Tactin® MacroPrep® column (IBA GmbH) previously equilibrated in 100 mM Tris-HCl, pH 7.5, 150 mM NaCl (Buffer W). After washing with 5 column volumes of Buffer W, bound proteins were eluted with 3CV of 100 mM Tris-HCl, pH 7.5, 150 mM NaCl 2.5 mM desthiobiotin (Buffer E) in 0.5 mL fractions. Eluted fractions containing our protein of interest was concentrated using a centrifugal filter (Amicon Ultra-15 Centricon filter device 30-kDa, Millipore). The purity of the hCCP6 variants was determined by SDS-PAGE.

5.2.2   Enzymatic activity assays

5.2.2.1   Tubulin and telokin deglutamylation activity

Analysis of the tubulin and telokin deglutamylation activity of the recombinant hCCP6, hCCP6 E401Q and hCCP6 G53R was performed by western blot quantification after protein overexpression. Samples were incubated in 6X Laemmli sample buffer (450 mM β-mercaptoethanol, 10% SDS, 400 mM Tris-HCl pH 6.8) for 5 minutes at 96°C. Next, 30 μg of total protein from the soluble fractions were loaded into an SDS-PAGE minigel with the help of a Mini-Protean (Bio-Rad) vertical electrophoresis module. The gels used contained a 10% polyacrylamide separating gel in 125 mM Tris-HCl buffer, pH 6.8, and 0.1% SDS. The migration buffer in which the electrophoresis was performed corresponded to the Tris-Gly buffer, and the protein marker used was the EZ-RUN Prestained Rec Protein Ladder (Fisher Scientific).

After electrophoresis, the gel proteins were transferred to a polyvinylidene fluoride membrane (PVDF, Immobilon-P, EMD Millipore). The transfer was made at 4 ºC in Tris-Gly

buffer, pH 8.3, with 10% methanol, and with the help of a Mini Trans-Blot wet transfer module (Bio-Rad). The membranes were then blocked for 1 hour at room temperature with a 5% skimmed milk solution in PBS-T buffer (PBS, pH 7.4, and 0.05% of Tween-20 detergent, Sigma). After washing the membranes with PBS-T buffer, they were incubated over-night at 4ºC with the following primary antibodies prepared in a 2% skimmed milk solution in PBS-T buffer: anti-HA (1:5000, Bio-Rad), anti-Δ2-tubulin (1:1000, Millipore EMD), anti-PolyE (1:1000, Sigma), anti-GFP (1:2000, Sigma) and anti-GAPDH (1:5000, Bio-Rad). Anti-HA and anti-GFP were used to verify that recombinant proteins were successfully transfected. Anti-GAPDH was used as a housekeeping protein and anti-Δ2-tubulin and anti-PolyE as products of hCCP6 activity. Finally, the membranes were washed with PBS-T and incubated for 1 hour at room temperature with a PBS-T solution containing the secondary anti-Mouse-IgG antibody (1:2000, Bio-Rad) and anti-Rabbit-IgG (1:2000, Bio-Rad), both produced in goat and conjugated to horseradish peroxidase (HRP). The immunoreactivity of the protein bands was visualized by chemiluminescence using the substrate Luminata Forte Western HRP substrate (EMD Millipore) and with the help of the VersaDoc detection systems (Bio-Rad).

5.2.2.2   Enzymatic activity for synthetic peptides

In order to further analyse the catalytic activity of hCCP6 G53R, the activity of the recombinant proteins hCCP6, hCCP6 E401Q and hCCP6 G53R purified from HEK293F cells after overexpression was determined by an enzymatic assay on synthetic substrates.

For enzymatic activity, the substrate Biotin-5E (five consecutive glutamic acid residues on a biotin scaffold, synthesized by the Peptide Synthesis Facility of the Universitat Pompeu Fabra, Spain) were used as substrates to assess the influence of the F[E,D]SGNL motif mutation on hCCP6 activity, while the CCP inhibitor 2-PMPA was used as negative control. Briefly, 100 µl reaction mixture containing 1 µg of purified hCCP6, hCCP6 G53R or hCCP6 E401Q, and 100 µM biotin-5E in 25 mM HEPES-K buffer (pH 7.4) was incubated at 37 °C for 4h. Enzymatic activities were determined using the colorimetric method described previously (Doi et al., 1981) Method C), which detects the release of free glutamate residues in a direct relationship scale.

5.2.2.3   Protein stability analysis

In order to analyse the protein stability of hCCP6 G53R, the recombinant proteins hCCP6 WT, hCCP6 E401Q and hCCP6 G53R were transfected into HEK293T cells. After 24 hours of expression, 20 µM of proteasome inhibitor MG132 (Calbiochem) was added to the corresponding cultures for 24 hours incubation. The effect of this inhibitor was analysed by western blot and untreated cultures were also analysed as controls. The primary antibodies used for the detection of these proteins were anti-HA (1:5000, Bio-Rad), anti-β-catenin (1:5000, Bio-Rad), as positive control, and anti-GAPDH (1:5000, Bio-Rad), as housekeeping protein. The secondary anti-Mouse-IgG antibody (1:2000, Bio-Rad) was used for all cases.

5.2.2.4   Tubulin binding capacity

To assay the tubulin binding capacity of hCCP6 and its variants, the microtubule framework was isolated from HeLa control cells and HeLa cells overexpressing hCCP6, hCCP6 E401Q or hCCP6 G53R. This procedure was based on the Fourest-Lieuvin method (Fourest-Lieuvin, 2006) that consists of extracting MTs from the insoluble cellular fraction, which are then subjected to depolymerization and polymerization steps to obtain human tubulin (HTub) with its microtubule-associated proteins. Briefly. ~$2 \cdot 10^9$ HeLa cells were trypsinised at 37 ºC after PBS washing and collected by centrifugation. Cell pellets were resuspended in 40 ml PEM (100 mM Pipes, pH 6.7, 1 mM EGTA, and 1 mM MgCl2) at 37 °C and centrifuged at 320 xg for 5 minutes. The cell pellet was then lysed in 40 ml microtubule preservation buffer at 37 ºC (MPB, 80 mM Pipes, pH 6.7, 1 mM EGTA, 1 mM MgCl2, 0.5% Triton X-100, 10% glycerol, 1 µM pepstatin, and 400 µM PMSF). Lysed cells were centrifuged at 320 g for 3 min at 37 °C and the supernatant was carefully discarded. The pellet was sheared in 2 ml MPB at 4 °C, by gently pipetting it through a 1 ml pipet tip. After 15 min ice incubation, the pellet was sheared thoroughly once again, and ultracentrifuged at 200,000xg for 10 min at 4 °C. The supernatant was supplemented with 5 mM MgCl2, 1 mM GTP, and 5% DMSO (final concentrations). The solution was then incubated for 30 min at 35 °C to allow microtubule polymerisation. The polymerised sample was laid on a cushion of PEM/60 % glycerol/400µM PMSF at 35 °C, and ultracentrifuged at 200,000xg for 20 min at 35 °C. The microtubule pellet was washed carefully, without resuspension, with 1 ml of warm PEM50 (50 mM Pipes, pH 6.7, 1mM EGTA, 1 mM MgCl2, 1 µM pepstatine, and 400 µM PMSF). Cold PEM50 (600 µl) was then added on the pellet, which was depolymerised on ice for 15 minutes before

resuspension. The resulting tubulin suspension was cleared by ultracentrifugation at 200,000xg for 10 minutes at 4 °C. The concentrations of Pipes and GTP were then raised to 100 and 1 mM, respectively, before storage at -80 °C. The concentration and purity of HTub was evaluated by SDS–PAGE, comparing with known concentrations of porcine brain tubulin (Cytoskeleton). Relative quantities of tubulins on a gel were evaluated using the Quantity one software (Bio-Rad).

Western blot analysis of the samples from the different steps of tubulin purification was carried out. The primary antibodies used were anti-HA (1:5000, Bio-Rad), anti-α-tubulin (1:3000, Sigma-Aldrich) and anti-GAPDH (1:5000, Bio-Rad), all produced in mouse. The secondary antibody used was anti-Mouse-IgG (1:2000, Bio-Rad).

5.2.3   Confocal microscopy

For hCCP6, hCCP6 E401Q and hCCP6 G53R cellular distribution analysis, HeLa and HEK293T cells were fixed with 4% paraformaldehyde (Sigma) for 30 minutes at room temperature. Cells were further permeabilized with PBS containing 0.5% Triton X-100 (Sigma) for 30 minutes. Cells were then blocked with 1% BSA (Sigma) in PBS 0.05% Tween (Sigma) for 30 minutes and then incubated with 1/100 dilution of anti-HA antibody (Sigma) for the detection of the three recombinant hCCP6 forms overnight at 4ºC. Cells were then washed and incubated with Alexa anti-mouse 488 (Molecular Probes) for 1 hour at room temperature. Nuclei was further counterstained with 4',6-diamidino-2-phenylindole (DAPI). Samples were mounted with ProLong Gold (Life Technologies), cured and stored at 4ºC until observation.

Double immunolabelling combining anti-HA with anti-γtubulin (Abcam) for centriole staining and anti-GM130 (Santa Cruz Biotechnology) for Golgi staining was done using the same protocol plus the respective antibodies in a step before to the anti-HA addition with 3 hours incubation at RT. Alexa anti-rabbit 555 was used as secondary antibody. Immunofluorescence images were collected on an inverted confocal microscope (Leica SP5) with a 63X objective. Images were analysed using Imaris software (Bitplane).

5.3   Results

5.3.1   Site-directed mutagenesis

Based on previous studies in *C. elegans*, where the G596R substitution in the conserved F[E,D]SGNL motif of the N-domain of the CCP homolog CCPP-1 was related with an abnormal behaviour of the protein (O'Hagan et al., 2011). In order to assess the functional characterisation of the conserved N-domain of human CCPs, we generated the same single mutation of this motif in human CCP6, consisting in the substitution of the glycine 53 to an arginine (G53R). Thus, QuickChange site-directed mutagenesis performed on the previously generated in the group pTriEX-6 hCCP6 plasmid to obtain the hCCP6 G53R mutant.
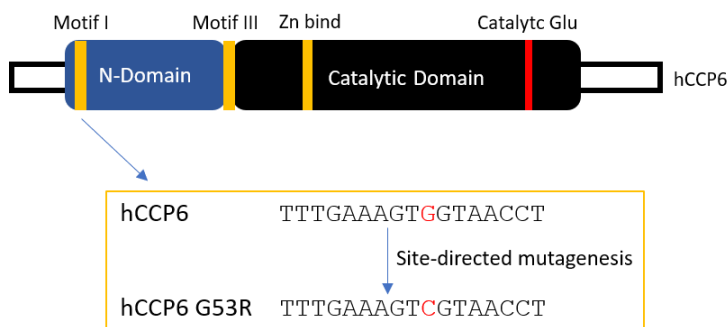
FIGURE 5.3. GENERATION OF MUTANT HCCP6 G53R. Serial Cloner alignment between the hCCP6 WT and hCCP6 G53R sequence showed a change from guanine to cytosine at position 157. This substitution results in the translation to arginine instead of glycine at position 53 of the hCCP6 protein sequence.

Sequencing analysis showed the correct substitution from guanine to cytosine in the position 157 of canonical hCCP6 (Figure 5.3). This mutation was analysed by BLAST sequencing analysis (https://blast.ncbi.nlm.nih.gov/Blast.cgi) and led to a mutation in the glycine 53 to an arginine (G53R) in the motif I of the N-terminal domain of hCCP6.

5.3.2   hCCP6 and hCCP6 G53R expression and purification in a mammalian cell system

Once the plasmid encoding for the mutant CCP6 G53R was obtained, we focused in the obtention of purified recombinant protein of both CCP6 wild type and (CCP6 WT) and CCP6 G53R to perform enzymatic and stability analysis. Purified human and/or mouse CCPs had been previously obtained from different expression systems ranging from insect Sf9 cells to mammalian HEK 293F cells using His6 and Strep tags to further purification (Aillaud et al.,

2016; Rogowski et al., 2010; Tort et al., 2014; H. Y. Wu et al., 2015). Best results were obtained in the mammalian cell line HEK293F, which can provide the appropriate expression context for obtaining recombinant eukaryotic proteins that cannot be efficiently produced in any other expression system. This system facilitates chaperones, cofactors, binding proteins, and catalytic enzymes of PTMs, necessary for the correct folding, stability and functionality of the protein of interest (Francis & Page, 2010). In this work, to obtain the CCP6 variants, we transfected a construct with the hCCP6 cDNA inserted into the expression vector pTriEx-6 in cultures of mammalian HEK293F cells grown in suspension, and overexpressed the protein for 72 h. At the same time, we transfected cultures with a second construct that included the hCCP6 G53R gene, which encodes for a mutation in the conserved F[E,D]SGNL motif. Both constructs incorporated the Strep-tag® II and the HA tags into the protein sequence at its N-terminal end to facilitate purification and immunodetection of the recombinant protein. To assess the functional analysis of CCP6 WT and CCP6 G53R, the soluble protein fraction of the cell extracts was analysed by SDS-PAGE electrophoresis followed by Coomassie blue G-250 staining (Figure 5.4), and by western blotting for the specific immunodetection of the protein of interest with the anti-HA antibody (Figure 5.4).
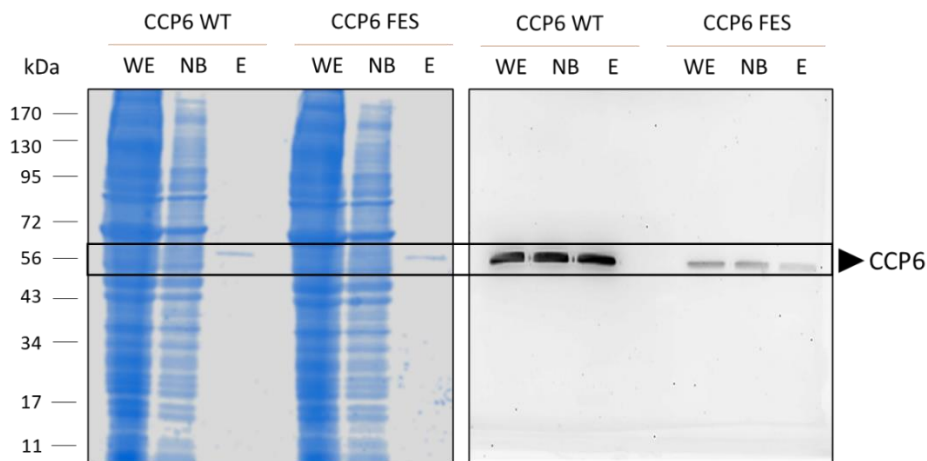
FIGURE 5.4. ANALYSIS OF HUMAN CCP6 EXPRESSION IN MAMMALIAN HEK293 F CELLS. (A) SDS-PAGE electrophoresis and (B) western blot for qualitative evaluation of the yield and quality of the wild-type recombinant hCCP6 and the F[E,D]SGNL mutant hCCP6 G53R produced. in HEK293 F cells after 72h of post-transfection expression. In each lane we loaded 30 μg of total protein for the soluble fractions of the wild type hCCP6 (WT) and the mutant hCCP6 G53R (FES). The SDS-PAGE gel was stained with Coomassie blue G-250 and immunodetection of recombinant hCCP6 was performed with the anti-HA antibody.

The results obtained in the western blotting revealed the presence of a single protein band with the expected size (~58 kDa) in the soluble fraction of the cellular homogenates corresponding to the recombinant hCCP6 (WT) and hCCP6 G53R (FES). Next, we purified the hCCP6 present in the soluble fraction by means of anti-Strep-tag® II affinity chromatography. As shown in the gel of Figure 4, the eluted hCCP6 and hCCP6 G53R was obtained partially pure. Additional purification steps like size exclusion chromatography or ion exchange columns were previously tried in our group. Nevertheless, we were not able to increase the purity of the protein due to its instability once enriched. Elution in Strep-tag affinity procedures then, resulted in substantial enrichment, although with poor stability of the purified protein. This way, enzymatic characterization needed to be carried out on fresh batches of the purified enzyme.

These results show that the mammalian cell-based expression system HEK293 F is appropriate to produce small amounts of recombinant hCCP6 and hCCP6 G53R, useful for biochemical and functional assays. In this case, the recombinant protein could be purified from the soluble fraction by a single purification step and the resulting semi-purified protein was useful for enzyme activity assays. Even though the protein is produced in its soluble form and is relatively stable and active, the low performance of the system is insufficient to carry out conventional structural studies.

5.3.3   F[E,D]SGNL mutation affects hCCP6 subcellular localisation

As previously mentioned, CCP6 is a known deglutamylase of microtubules which is capable to cleave glutamate residues from its lateral chain as well as generate Δ2-tubulin, a form of α-tubulin resulting of the excision of a glutamic residue from its main chain after detyrosination (Aillaud et al., 2016). Apart from tubulin, hCCP6 has also been reported to hydrolyse genetically encoded Glu in the primary C-terminal sequence of telokin protein (Rogowski et al., 2010; Tort et al., 2014). Polyglutamylated tubulin is widely present in cultured cells and CCP6's loss of function is predicted to increase its glutamylation rate to detectable levels by specific immunoblotting (Rodriguez de la Vega et al., 2007). It has been previously reported that a single aminoacidic mutation in the conserved catalytic site E401 (corresponding to the E270 in the canonical bCPA sequence) directly affects hCCP6 catalytic function being unable to hydrolyse acidic residues (Tanco et al., 2015; H. Y. Wu et al., 2012). Moreover, it has also been reported that a single mutation encoding a G596R amino acid

substitution in the conserved F[E,D]SGNL motif of the CCPP-1, a homologue of the CCPs in *C. elegans*, affected to its catalytic function despite not being directly involved in the active site nor any key amino acid residues that function in catalysis and/or the binding of zinc and substrates (O'Hagan et al., 2011). Since mutations in the F[E,D]SGNL conserved motif could be involved in cellular localisation, we opted to perform immunolabeling of the expressed hCCP6, hCCP6 E401Q and hCCP6 G53R proteins in HEK293T cell cultures to verify the presence of the mutant proteins at their correct localisation (Figure 5.5).
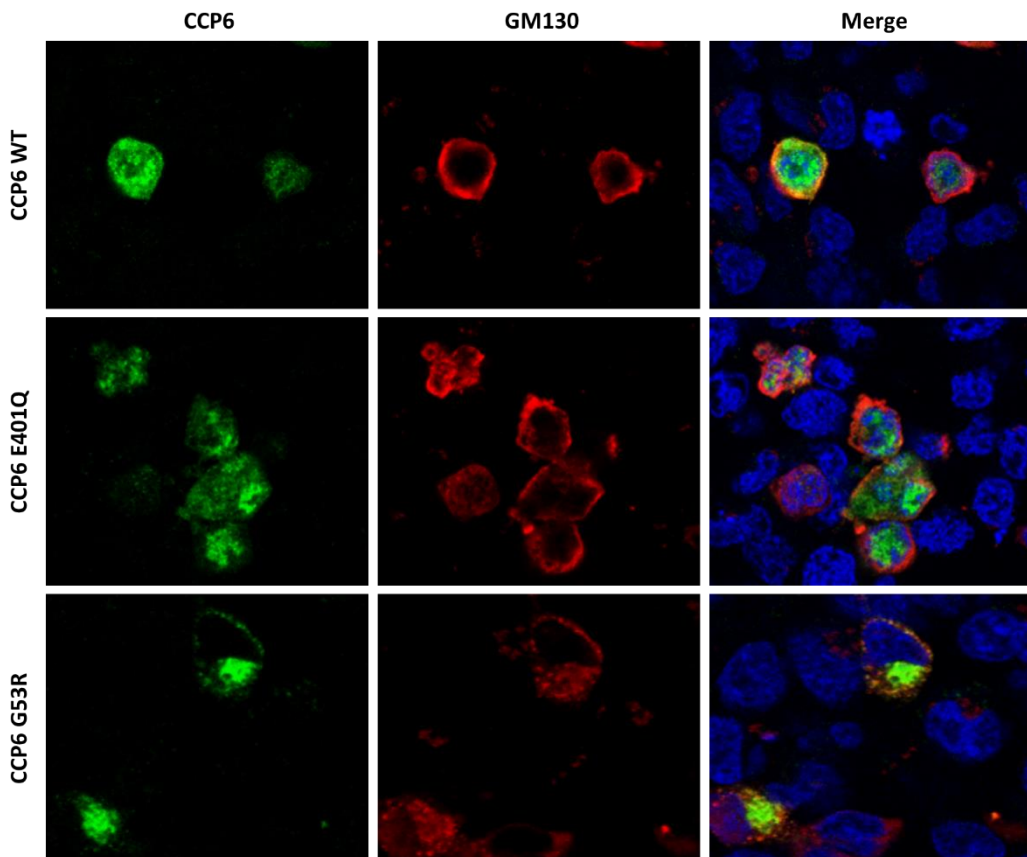
FIGURE 5.5. STUDY OF THE SUBCELLULAR LOCALISATION OF HCCP6 AND ITS MUTANTS BY IMMUNOCYTOCHEMISTRY. After fixing mammalian HEK293T cells that overexpressed wild type hCCP6, hCCP6 E401Q mutant and hCCP6 G53R mutant for 48 h, we immunodetected the presence of the proteins with the anti-HA antibody. As hCCP6 presents a particular and known location in cells, specific antibody against GM-130 was used to stain the Golgi apparatus. The images were acquired in an inverted confocal microscope (Leica TCS SP5) at room temperature and using an X63 objective and analysed with the Imaris software (Bitplane).

Regarding to the general hCCP6 subcellular localisation, although it presents a ubiquitous cytoplasmic presence, CCP6 has been previously found to be highly localised in the Golgi apparatus and centrioles of interphase cells. In mitotic cells, the CCP6 signal is stronger in centrioles and colocalises with γ-tubulin (centrosomes and spindle poles bodies). Moreover, CCP6 is detected in the basal bodies of ciliated cells (Rodríguez de la Vega et al., 2013).

The presence of hCCP6 in the Golgi apparatus could be related with the relation of this organelle with the microtubules. In most animal cells, the Golgi apparatus is shaped as a ribbon and closely associated with the centrosome. Microtubule-dependent molecular motors are also essential for Golgi organization, particularly the minus-end directed motor, cytoplasmic dynein (de Forges et al., 2012). Moreover, the Golgi apparatus has been recently defined as a new microtubule organisation centre (Zhu & Kaverina, 2013). Previous studies in our group identified proteins involved in the transport of vesicles through the Golgi network as CCP6 interactors (Otero, 2014).

In line with available data, we observed the HA-signal for WT hCCP6 expression to be coherent with its general cytoplasmic localisation whilst also enriched at the Golgi apparatus (Figure 5.5). Interestingly, the mutant protein hCCP6 G53R showed distinct general distribution, as it was not observed uniformly along the cytoplasm but formed protein accumulation in a specific perinuclear region (Figure 5.5). Further analysis of this specific localisation showed that CCP6 G53R was being mainly accumulated into the Golgi apparatus, where it co-localised with the general Golgi marker GM-130 (Figure 5.5). Transfection with catalytically dead hCCP6 E401Q protein showed results comparable to the WT construct, showing no evident accumulation nor mislocalisation of the protein. The empty vector which encodes for the HA epitope was used as a negative control.

The obtained results suggest that the mutation in the F[E,D]SGNL motif let to a mislocalisation of hCCP6, which could have been impaired in its cytoskeletal activity or interaction, thus losing its general cytoplasmic localisation. This lack of interaction could be the reason for the Golgi accumulation. Hence, loss of function or interaction against tubulin and other known substrates could be consequence of the G53R mutation.

5.3.4 The F[E,D]SGNL motif is essential for tubulin and telokin deglutamylation by CCP6 in humans.

To determine whether the conserved domain F[E,D]SGNL is essential for human CCP6's enzymatic function, we analysed the general glutamylation state of tubulin and the presence of Δ2-tubulin after hCCP6 and its mutant overexpression in cultured cells. Immunoblotting detection with the polyclonal polyglutamylation (PolyE) antibody that recognise chains of 3 or more glutamates was used to determine the CCP6 activity as a deglutamylase of lateral chains, while a specific anti-Δ2-tubulin antibody was used for assessing CCP6 activity on the main chain on deTyr-α-tubulin. Catalytically dead hCCP6 E401Q was used as a negative control.
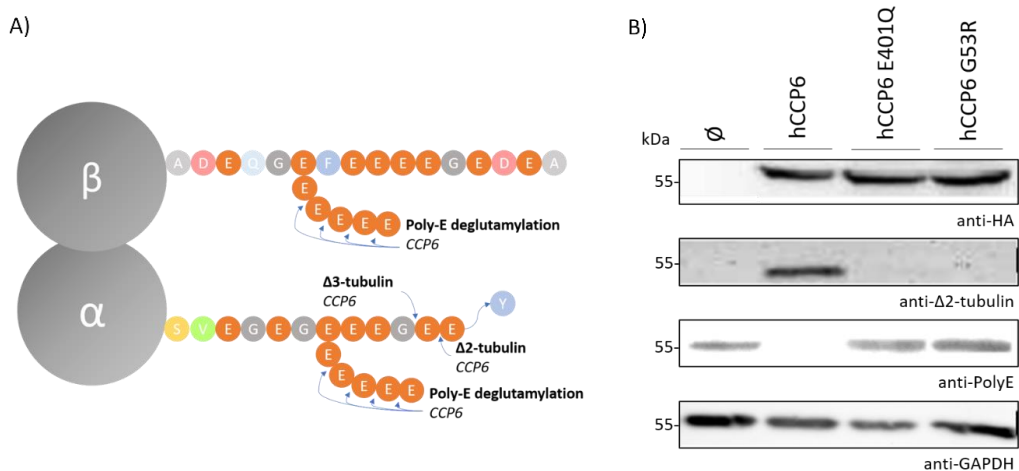
FIGURE 5.6. ANALYSIS OF THE CATALYTIC ACTIVITY OF CCP6 G53R. (A) CCP6-directed catalysis for the formation of Δ2-tubulin from the excision of α-tubulin's c-terminal glutamic acid (B) Specific immunodetection of Δ2-tubulin levels (anti- Δ2-tubulin) and poly-glumatamte chains (PolyE) by western blot of HEK 293F cells that overexpressed hCCP6 WT, hCCP6 E401Q and hCCP6 G53R. The synthesis of recombinant hCCP6 was verified with anti-HA antibody. Negative control of protein expression of recombinant hCCP6 corresponds to cultures of untransfected HEK 293F cells (∅).

The results on cultured HEK293T cells show that tubulin polyglutamylation was undetectable by Poly-E staining after hCCP6 overexpression, whereas a positive staining of Poly-E immunoblotting was detectable after hCCP6 E401Q and hCCP6 G53R overexpression with similar results to untransfected cells (Figure 5.6B). Moreover, Δ2-α-tubulin is only detectable in hCCP6 expressing cells, while mutation in the F[E,D]SGNL motif and the catalytic domain led to undetectable Δ2-tubulin levels. These observations indicates that

CCP6 G53R is not capable of trimming polyglutamylated tubulin nor generate Δ2-α-tubulin, being inactive in its cellular context.
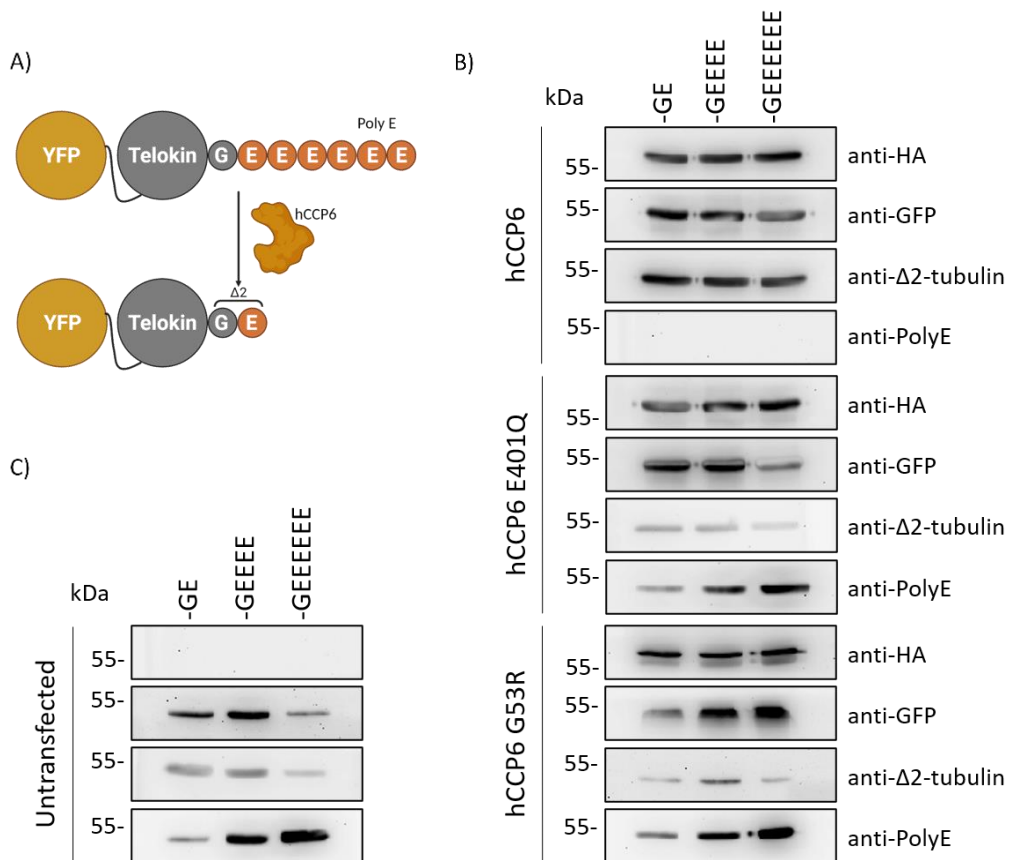
FIGURE 5.7. SUBSTRATE SPECIFICITY OF HCCP6 AND ITS MUTATED VARIANTS. A) Schematic representation of the experimental setup. PolyE antibody recognizes telokin constructs with three or more consecutive C-terminal glutamate residues, while anti-Δ2-tubulin antibody detects specifically the C-terminal –GE epitope. C-terminal degradation is detected by generation of the Δ2-tubulin epitope on telokin (Rogowski et al., 2010). B) Immunoblot analysis of HEK293T extracts after co-expression of different HA-hCCP6 variants and YFP-telokin variants. This immunoblot shows how the polyE and anti-Δ2-tubulin antibodies detect the different telokin variants in absence of CCP activity. The activity of mutated hCCP6 E401Q and hCCP6 G53R is tested with telokin variants with different numbers of consecutive glutamate residues to test processivity. (C) Immunoblot of control cells.

To further characterize if hCCP6 and hCCP6 G53R can remove subsequent glutamate residues from other substrates apart from tubulin, C-terminally engineered versions of telokin were used. Telokin is a short version of MLCK, which is one of the few known substrates of CCP6 (Rogowski et al., 2010). Wild-type and F[E,D]SGNL mutant versions of

hCCP6 were co-expressed in HEK 293T cells together with different C-terminal variants of YFP-telokin. The deglutamylation (removal from long glutamate chains) was monitored using the poly-E antibody in immunoblot analysis (Shang et al., 2002), and the final deglutamylation product (carrying only one glutamate) was detected with the anti-Δ2-tubulin antibody (Figure 5.7).

Result show that only wild-type hCCP6 was able to trim long (7-Glu) and shorter polyglutamate chains from the C-terminus of engineered telokin, as shown by decreased poly-E signals and increased of Δ2-tubulin immunoreactivity (Figure 5.7). On the other hand, hCCP6 G53R and hCCP6 E401Q were unable to trim the telokin substrates.

These results show that the F[E,D]SGNL conserved domain of hCCP6 is essential for its catalytic function as tubulin and telokin deglutamylase in cell culture. Similar results were previously reported in *C. elegans*, where the *my22* lesion affecting the F[E,D]SGNL domain was shown to increase tubulin polyglutamylation levels in sensory cillia, leading to defective behaviour response (O'Hagan et al., 2011).

However, the loss of function of hCCP6 G53R could be dependant of the cellular environment or the substrate specificity. To confirm the general loss of catalytic activity of the F[E,D]SGNL mutated CCP, both hCCP6 and hCCP6 G53R proteins were also assayed using synthetic CCP substrates resembling the polyglutamylated C-terminus of tubulin in a biotin scaffold. This small substrate assayed using standard enzymatic methods avoided any other factor that could be involved in its activity as cellular localisation or substrate recognition (H. Y. Wu et al., 2015). For this study, we used the synthetic substrate Biotin-EEEEE, as hCCP6 had been observed to metabolize synthetic substrates with ≥4 consecutive Glu preferring >5 consecutive Glu chains (H. Y. Wu et al., 2015). As controls for this assay, we prepared two additional reactions containing the substrate without the enzyme to determine any unspecific Glu release and the substrate with semi-purified hCCP6 and the known CCP inhibitor 2-PMPA (2-(phosphonomethyl)pentanedioic acid) (R. Wang et al., 2020) to corroborate that the observed activity is specific for hCCP6. The activity of the enzyme was measured by quantifying the released glutamate residues by the ninhydrin-CdCl2 method ((Doi et al., 1981) method C).

The obtained results showed similar results in hCCP6 and hCCP6 G53R activity on the biotin-EEEEE synthetic substrate compared to the controls, which indicates that the hCCP6 produced in mammalian cells HEK293F is active and the mutation in the F[E,D]SGNL domain does not completely affect its catalytic activity on synthetic substrates. Since this activity was not observed in the hCCP6 incubated with its inhibitor or in the negative control (C-) without enzyme, we can assure that the hydrolysis of the glutamate residues of the substrates is specifically due to the proteolytic activity of hCCP6 and hCCP6 G53R (Figure 5.8).
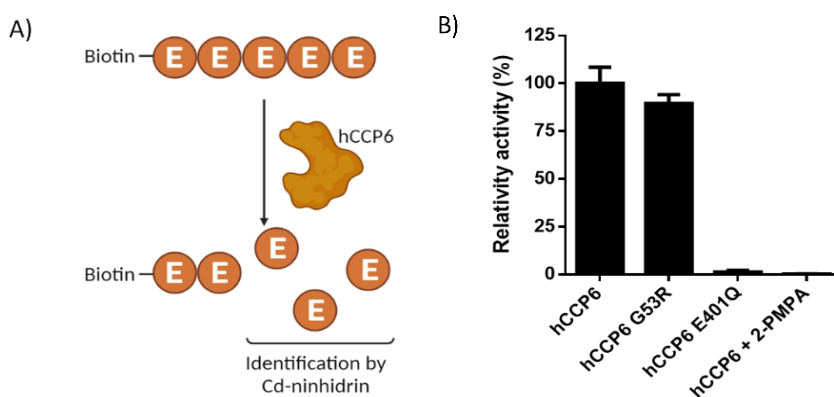
FIGURE 5.8. GLUTAMYLASE ACTIVITY OF HCCP6, HCCP6 E401Q AND HCCP6 G53R AGAINST SYNTHETIC SUBSTRATES. A) Schematic representation of the experimental setup. (B) 3 µg of each purified protein were used in this assay with the synthetic peptide biotin-5E. Relative activity was quantified after 4-hour incubation of the enzyme and the synthetic peptide using the substrate alone as negative control. Activity on wild-type hCCP6 was taken as the positive control, while hCCP6 E401Q, hCCP6 G53R and hCCP6 in the presence of the specific 2-PMPA CCP inhibitor results were compared to it. The colorimetric Cd-ninhydrin method was used to assay the glutamic release after hCCP6 deglutamylase activity (Doi et al., 1981).

The assayed enzymatic methods reveal that mutations in the conserved F[E,D]SGNL motif does affect the enzymatic activity of hCCP6 *in vitro*, making it uncapable of hydrolysing C-terminal glutamic residues of known substrates when assayed in cultured cells. Nevertheless, the catalytic activity of hCCP6 G53R found against synthetic peptides on a biotin scaffold, which is comparable to wild-type hCCP6, suggests that the region responsible for catalysis and the binding of zinc is not affected and there are other involved processes affected by the F[E,D]SGNL motif.

5.3.5 The F[E,D]SGNL motif does not affect protein stability

It had been proposed that the conserved motifs of CCPs could be involved in protein stability and be necessary for their correct expression and folding (Otero et al., 2012; Rodríguez de la Vega et al., 2013). Therefore, to determine whether the folding of hCCP6 G53R was correct, HEK293T cells overexpressing the different recombinant variants of hCCP6s were treated with MG132. MG132 inhibits the proteasome, responsible for degrading abnormal proteins, short-lived proteins, ER-associated proteins, and unfolded proteins (Coux et al., 2020). The presence or absence of hCCP6 was analysed by western blot.

Immunodetection of hCCP6, hCCP6 E401Q and hCCP6 G53R was carried out by anti-HA antibody, allowing simultaneous verification of transfection of recombinant hCCP6s and effect of the proteasome inhibition. Negative controls of expression of recombinants hCCP6s corresponded to cultures of untransfected HEK293T cells. As a positive control of MG132 inhibitor function, β-catenin levels were analysed using anti-β-catenin antibody, as it is a short-lived protein (Figure 5.9) (Cervello et al., 2004; Hwang et al., 2005).
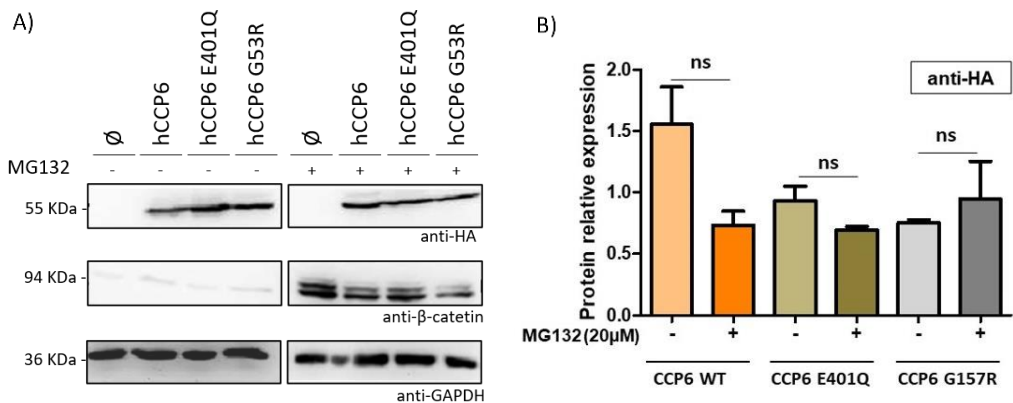
FIGURE 5.9. ANALYSIS OF PROTEIN STABILITY OF CCP6 G53R. (A) Specific immunodetection of hCCP6 levels (anti-HA) by western blot of MG132-treated and untreated HEK 293T cells that overexpressed hCCP6 WT, hCCP6 E401Q or hCCP6 G53R. As a positive control of the correct functioning of MG132, β-catenin expression levels (anti-β-catenin) were immunodetected. Negative control of protein expression of recombinant hCCP6 corresponds to cultures of untransfected HEK 293T cells (Ø). (B) Comparison of hCCP6s expression levels between MG132-treated and untreated cells. The statistical procedure used to determine the differences between hCCP6s, and β-catenin expression levels was the nonparametric Mann-Whitney test (N=4).

Levels of different recombinant hCCP6 in MG132-treated and untreated HEK 293T cells were equivalent (Figure 5.9). Statistical analysis showed no significant differences in the level of expression of hCCP6, hCCP6 E401Q and hCCP6 G53R synthesized in MG132-treated and untreated cells (Figure 5.9). These results suggest that G53R mutation in the N-domain did not destabilize the hCCP6 protein. As opposed to recombinant CCP6s levels, β-catenin expression levels were higher in MG132-treated cells than in untreated cells (Figure 5.9). Statistical analysis showed significant differences (p-value< 0.05) in the level of expression of β-catenin in MG132-treated and untreated cells (not shown), which could imply that the MG132 inhibitor works correctly.

These results suggest that mutation in the F[E,D]SGNL motif is not significatively affecting the folding of hCCP6. Expression levels of hCCP6 G53R are comparable to hCCP6, and neither of them were increased after proteasome inhibition. Observing these results, it seems that protein stability is not involved in *in vitro* loss of function mediated by F[E,D]SGNL mutation.

5.3.6   hCCP6 G53R does not bind tubulin in cultured cells

To further study the association of hCCP6 with MTs and the role of the F[E,D]SGNL motif in this association, we partially purified tubulin from HeLa control cells and HeLa cells overexpressing hCCP6, hCCP6 E401Q and hCCP6 G53R (Figure 5.10). This partial purification is based on the Fourest-Lieuvin method (Fourest-Lieuvin, 2006) that consist of extracting MTs from the insoluble cellular fraction (Ext I), which are then subjected to depolymerization and polymerization steps to obtain human tubulin (Htub) with MAPs (Figure 5.10A).

Results showed that recombinant hCCP6 and hCCP6 E401Q are present in the MT fractions along the purification process, as well as in the final semi-purified tubulin fraction named HTub (Figure 5.10B). However, hCCP6 G53R was not detected in the final semi-purified tubulin fraction Htub (Figure 5.10B) suggesting that is not able to bind to tubulin.

In order to verify that tubulin was present in Htub fraction, α-tubulin levels were analysed in this fraction. Specific immunodetection of α-tubulin of the Htub fraction showed an expression of α-tubulin in both untransfected HeLa cells and HeLa cells overexpressing recombinants hCCP6s (Figure 5.10C), indicating that tubulin is present in Htub fraction.
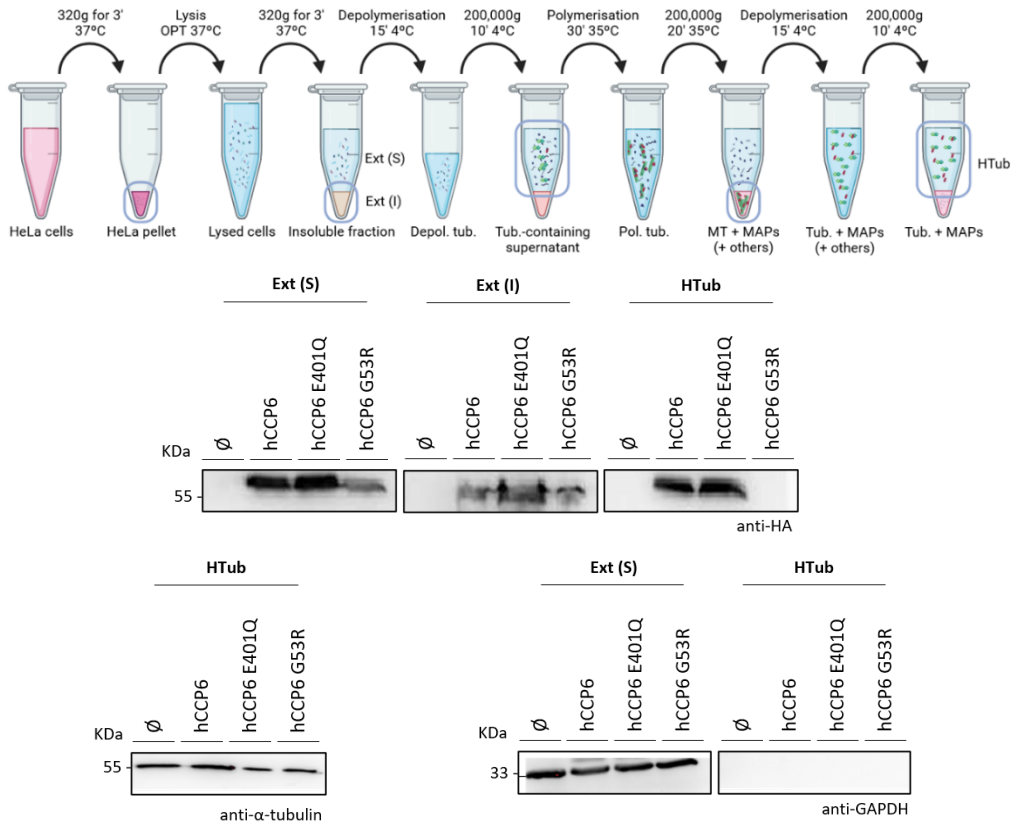
FIGURE 5.10. ANALYSIS OF THE TUBULIN BINDING CAPACITY. (A) Scheme of tubulin purification from untransfected HEK293T cells (Ø) and HEK293T cells overexpressing hCCP6 WT, hCCP6 E401Q and hCCP6 G53R for 72h, based on the Fourest-Lieuvin method. (B) Western blot analysis of samples from different steps of tubulin purification. The samples analysed were: Ext (S), initial soluble extract; Ext (I), initial insoluble extract containing MTs; and Htub, final soluble extract containing Htub with MAPs. Recombinant hCCP6 variants were detected with anti-Ha antibody. (C) Western blot analysis of Htub fractions showing the presence or absence of α-tubulin (anti-α-tubulin). (D) Western blot analysis of Ext (S) and Htub fractions showing the presence of GAPDH (anti-GAPDH).

Immunodetection of hCCP6, hCCP6 E401Q and hCCP6 G53R was carried out by anti-HA antibody. Negative control of expression of recombinants hCCP6s corresponded to cultures of untransfected HeLa cells. As a positive control of the binding of CCP6 to tubulin, levels of wild type hCCP6 were analysed.

Although many proteins might indirectly co-purify with MTs (through a protein that binds to them) at the first steps, those indirectly bound proteins should decrease after the *in vitro* depolymerization and repolymerization steps (Fourest-Lieuvin, 2006). In order to determine that there was a decrease in unspecific tubulin binding proteins along the copurification

steps, GAPDH levels were assayed by immunodetection in Ext (S) and Htub fractions, detectable levels of GAPDH were present only in Ext (S) fraction (Figure 5.10D).

Therefore, hCCP6 G53R is not directly associated to MTS, not following tubulin through successive *in vitro* depolymerization/polymerization cycles. This result suggests that this mutation in the N-terminal domain could prevent the specific binding of the hCCP6 to the substrate thus preventing its catalytic activity. It is noteworthy to point that the catalytically dead form of hCCP6 is found to bind to MTs, yet not having activity over them, whereas the mutation in the F[E,D]SGNL motif appears to interfere only with the binding process.

5.4 Conclusions

In the present study we focused on the functional characterisation of one of the conserved motifs present in the N-domain of CCPs, an exclusive domain of this carboxypeptidase subfamily. With about 150 residues, this domain contains three conserved motifs in eukaryotic and bacterial CCPs. Despite previous work has been done to characterize these proteins and their relationship with pathologies in which they are involved; little information has been obtained about the specific function and/or importance of the conserved N-domain, while most of the work has been done focusing on the catalytic core. Therefore, other than performing homology studies of sequences between species and carry out methods of fold recognition, it had been impossible to assign a function to the N-domain or to any of its motifs. Consequently, the main conclusions of this chapter are:

1. A mutant in the conserved F[E,D]SGNL motif of the human CCP6 N-domain was obtained based on a natural variant that occurs in *C. elegans*. The generated mutant was verified by sequencing analysis and the G53R substitution was confirmed.

2. Human recombinant CCP6 WT and CCP6 G53R were correctly produced in their soluble form using HEK293F cells as a mammalian expression system. Sufficient stable protein was obtained for subsequent functional analyses.

3. The CCP6 G53R mutant prevents the correct tubulin and telokin deglutamylation activity *in vitro* not being capable of trimming polyglutamylated chains nor generating Δ2-α-tubulin.

4. The catalytic activity of the CCP6 G53R mutant was not affected when tested against biotin-scaffolded synthetic substrates, where it showed a deglutamylating activity comparable to wild type CCP6.

5. Loss of catalytic activity is not related with impairments on protein stability, as CCP6 G53R is not affected by proteasome inhibition.

6. The F[E,D]SGNL motif integrity is necessary for the *in vitro* tubulin binding capacity of CCP6.

7. The G53R mutation affects the cellular localisation of hCCP6, accumulating in the Golgi apparatus rather than in the centrosomes.

GENERAL DISCUSSION

Chapter 6. General discussion

Proteases are presumed to regulate almost all biological function, since they represent a considerable percentage of the genome. However, little is known about the *in vivo* biological functions of many proteases (Bond, 2019). This is especially true for cytosolic carboxypeptidases, which have suggested functions and implications, but are often unknown in terms of their true biological activities and involvement in complex cellular processes. The present thesis work reports on the general functional characterisation of CCP1 and CCP6, two deglutamylating enzymes members of the M14D subfamily of metallocarboxypeptidases which has been related to relevant cellular processes. Therefore, our research has focused specifically on determining the functional role of CCPs from a biomedical point of view, trying to arise new insights into their implication in health and disease.

For this purpose, we used a variety of approaches, including *in vitro* cell biology, proteomic studies, and enzymatic characterisation. Among these approaches, it is important to highlight the application of the BioID methodology, a recently developed interactomics strategy that allows the identification of transient and weak natural interactors in a cellular context (Roux et al., 2012). The identification of the interactome landscape of CCP1 and CCP6, combined with data obtained from other techniques, had provided a new understanding of the field.

The present work has been divided into three chapters, each with a different approach to answer the main objective and give insight into the functional role of cytosolic carboxypeptidases. Overall, the gathered information from the different chapters has

provided different approaches to understanding these enzymes and their relationship with their cellular environment. In the following pages, we will attempt to discuss how the present thesis work provides evidence, but also new perspectives for the future in the field of cytosolic carboxypeptidases.

How are cells affected by the loss of CCP activity?

Loss of CCP activity has been linked to several diseases, ranging from infantile-onset neurodegeneration (Shashi et al., 2018) to late-onset Fuchs corneal dystrophy (Riazuddin et al., 2013) depending on the enzyme affected. Previous work has been carried out to evaluate how the loss of CCP activity is involved, mainly focused on *pcd* mouse derived cells, describing the cellular changes that occur compared to healthy mice. However, more work had to be done to fully characterise their effect on non-degenerating cells. Hence, our work used cultured cell lines and their modification to achieve this goal.

In Chapter 3, we set out the general characterisation of human CCP1, focusing first on how cells are affected by its loss of activity. CCP1 is the largest member of the CCP subfamily, being the one with the largest number of predicted domains (Rodríguez de la Vega et al., 2013). Elucidation of the specific functional functions of organelles has long been a significant contributing factor to the study of CCPs. For instance, initial analysis on CCP1 behaviour was mainly directed at its role as a cytoskeletal modifying enzyme through its tubulin deglutamylase activity. Therefore, the first studies on the effect of CCP1 loss of function causing the *pcd* mouse model pointed to defects in axonal growth and transport (Landis & Mullen, 1978). Later studies allowed the nuclear characterisation of degenerating Purkinje cells, showing a clear misregulation that affects critical cellular processes (Baltanás, Casafont, Lafarga, et al., 2011; Baltanás et al., 2019). In this chapter, we have determined the general considerations of CCP1 regarding its functional role using gene knockout in specific cell lines, describing the subcellular localisation of CCP1 focusing on its implications in general deglutamylation processes and its specific nuclear functional role.

First of all, the assignation of specific subcellular localisation of CCP1 and the observation of its change over time, have allowed us to infer that CCP1 could be involved in cell cycle control due to its deglutamylation action on microtubules. Although CCP1 has not been directly related to any mitotic phase, the results presented point out a possible implication

in the formation and function of the mitotic spindle since CCP1 has a characteristic spatial distribution throughout the cell cycle. Furthermore, our studies have shown that CCP1 knockout cells show mitotic defects including monopolar and multipolar spindles with significantly higher numbers of aberrant cells compared to wild type cells. These knockout studies have also shown that solely CCP1 activity is enough to alter polyglutamylation levels in cellular microtubules as its action cannot be compensated by other CCPs activity. However, other specific tubulin modifications as Δ2-tubulin generation were not altered in these conditions. This substrate preference of CCP1 may constitute a mechanism of functional specialization that could be dependent on the cell type or moment of the cell cycle. The gathered information about CCP1 in its cytoplasmic distribution and general activity has shown that CCP1 is necessary for the correct development of a bipolar mitotic spindle, an action that could be mediated by its deglutamylating activity on microtubules. The role of CCPs as microtubule PTM regulators is especially interesting when looking at the microtubule organising centres (MTOC). The centrosome is the main MTOC in most animal cells, whose number is strictly controlled by the production of bipolar spindles and proper chromosomal segregation during mitosis (Gönczy & Hatzopoulos, 2019). Indeed, centrosome amplification can lead to serious problems such as multipolar spindle formation, chromosome missegregation, and genomic instability, all of which are hallmarks of CCP1 loss of function.

Having said that, in Chapter 5 in order to gain a more detailed view of into the influence of CCP6 loss of function by the mutation in the conserved N-domain *in vitro*, we also performed a subcellular location assay. For this assay, cultured cells were transfected with the different forms of CCP6 and immunolabeled with specific location markers of the immunocytochemical assay. As previously described (Rodríguez de la Vega et al., 2013), wild-type CCP6 was located mainly in the centrioles and the Golgi apparatus, where it co-localised with γ-tubulin and the GM130 marker respectively. However, the mutation in the N-domain of CCP6 changed the overall distribution of the protein. In this case, mutated CCP6 was not found in the centrioles bound to γ-tubulin but was principally localised in the Golgi apparatus. These results also suggest an involvement of CCP6 in MTOC regulation, since this same mutation in *Caenorhabditis elegans* is sufficient to produce defects in ciliary maintenance (O'Hagan et al., 2011), a process which is initiated by the correct formation of

the pericentriolar matrix (Bettencourt-Dias et al., 2011). All in all, the results presented suggest that MTOC activity could be regulated by CCPs, which is crucial for healthy cell development.

In this work, we have also shown that there is a distinct distribution pattern of CCP1 among cultured cells in relation to its confluence state. In this sense, CCP1 is present in focal adhesions in cells at low confluency, suggesting that one of its functions could be related to the regulation of the junctions of microtubules with adhesion complexes (Dong et al., 2016). In fact, the relationship of CCP1 and focal adhesions may have a significant implication in its role during ataxia generation in *pcd* mice, since the disease develops a few weeks after birth, during a critical period of neuronal development. It has been proposed that changes in the adhesivity of individual neural growth cones drive precise axonal targeting and the formation of specific synaptic contacts in the nervous system (Sperry, 1963). Therefore, the presence of CCP1 in this structure may be important for neurite outgrowth and it is realistic to expect a higher colocalisation of CCP1 in these structures during the neurodegeneration of Purkinje cells in *pcd* mice in future investigations.

Related to the previous statement, cell cultures of WT and CCP1KO SH-SY5Y cells were tested for *in vitro* neuronal differentiation. Results showed that both cultures were able to reach a similar differential stage with a similar progression over time. However, the cultures presented a different behaviour in the long term after differentiation since cell viability was reduced in CCP1 KO cultures. These results indicate that CCP1 might be involved in neuronal maintenance but not in differentiation.

As can be seen, our characterisation of CCP loss of function in the cytoplasm, which included the study of CCP1 and CCP6, has led to similar conclusions. The results reported in this thesis, in addition to the previous data on their involvement in cell processes and disease, seem to point out that CCPs are critical for the proper functioning of the MTOC components, which make these proteins critical not for the initiation, but for the maintenance of their dependent generated structures, such as cilia and axons.

How is CCP1 related to nuclear defects observed in the *pcd* mice model?

As previously mentioned, loss of CCP1 function generates the *pcd* mouse model, which is characterised by rapid Purkinje cell degeneration leading to cerebellar ataxia (Harris et al., 2000). The characterisation of neuronal tissue from this mouse model has provided interesting information on the pathological processes that are occurring in the disease. These data show different nuclear alterations that added to the aforementioned microtubule defects, generate the final neurodegeneration process. In this work, we attempt to unveil how CCP1 is related to nuclear affectations, since it is the only member of CCPs capable of being localised in the cell nucleus.

Therefore, focusing on its nuclear localisation, we have shown in chapter 3 that CCP1 is localised inside the dense fibrillar component of the nucleolus, especially at the active transcriptional sites. Furthermore, the presence of CCP1 in this organelle has been related to its participation in transcription, since it has been observed that RNA synthesis is necessary for its nucleolar localisation. Regarding the findings in the *pcd* mice that identified nucleolar disruption and nucleolin reorganisation in the Purkinje cells as hallmarks of neuronal degeneration (Baltanás, Casafont, Weruaga, et al., 2011), we can argue that CCP1 has an important role in the whole nucleolar integrity in cells and plays a key role in neurodegeneration. The absence of CCP1 at its nuclear localisation in the nucleolus, thus, can cause sufficient nucleolar stress to prevent the proper development of processes such as the ribosome biogenesis that is known to lead to neurodegeneration (Kreiner et al., 2013).

After the general characterisation of CCP1 undergone during the first part of this work, we wanted to know other cellular processes in which it could be related. Thus, in the first part of chapter 4 we set out to identify the human CCP1 interactome landscape from a biomedical point of view. Proteins rarely act alone in cellular processes of health and disease. For instance, a diseased state is usually associated with an increase in the number of signalling proteins, metabolic factors, and gene expression. Thus, unveiling the protein-protein interactions can reveal how they are involved in different processes, providing clues or help in determining their involvement in disease. The interactome has been widely used to elucidate the functions of previously unknown proteins, as proteins that interact with

each other often participate in similar or the same biological processes. Hence, finding the interacting partners of an unknown protein or metabolite can provide insight into its function. In this chapter, the interactome landscape of CCP1 was generated from *in vitro* human cells, identifying new potential interactors and substrates that have allowed us to better understand their functional role in the nucleus.

In this way, we carried out the BioID interactomics methodology on CCP1, which has led us to identify a total of 52 new substrates or interactomic partner candidates. Promisingly, a large number of interactors or substrates have been associated with its nuclear role. In fact, the GO terms for the CCP1 interactome were driven by nucleosome assembly activity, cytoplasmic translation, and RNA metabolic process. These data are coherent with CCP1's localisation into the nucleolus and its relationship with transcription, since RNA metabolic processes are necessary for the proper transcription initiation (Chen et al., 2016). In addition to RNA-related processes, the interactomics data led us to hypothesized that CCP1 may play a key role in nucleosome assembly, resulting in proper DNA architecture, being nucleosome assembly proteins (NAP) potential substrates for its activity. These results support previous findings from *pcd* mice, which showed that nuclear architecture has a considerable impact on Purkinje cell degeneration (Baltanás, Casafont, Lafarga, et al., 2011).

Our first characterisation in NAP was carried out with the NAP1L4 protein, which showed higher enrichment levels in both HEK293T and SH-SY5Y cells. It is important to note that murine NAP1L4 has been reported to be polyglutamylated by TTLL4 (van Dijk et al., 2007), suggesting a similar role for the human orthologue pointing to it as a candidate substrate for CCP1 deglutamylating activity. In our work, we have demonstrated that CCP1 and NAP1L4 physically interact *in vitro,* where NAP1L4 is a glutamylated protein being a substrate and not just an interactor partner of CCP1.

At this point, we wanted to go further into the study of the interaction between CCP1 and NAP1L4. Therefore, we first examined whether the knockout of CCP1 was affecting NAP1L4 expression levels in SH-SY5Y neuronal cells, with a special focus on the differentiation process. These experiments showed that the total protein expression level of NAP1L4 decreased in CCP1KO SH-SY5Y cells after differentiation. Subsequent experiments looking for the subcellular distribution of this protein under the conditions

mentioned above revealed that NAP1L4 was maintained in the cytoplasm but had a less noticeable presence in the nuclear fraction. Interestingly, when evaluating the glutamylation status of NAP1L4 in its specific subcellular localisation, we observed that glutamylated NAP1L4 is mainly localised in the nucleus of differentiated WT cells, while the differentiated CCP1KO cells did not show differences with undifferentiated cells.

The nucleosome assembly process carried out by NAP1L4 is mainly mediated by the nuclear import of histones, with proven activity on the deposition of H2A-H2B dimers as well as H3-H4 tetramers (Rodriguez et al., 1997, 2004). Histone acetylation/deacetylation is known to affect nucleosome assembly and disassembly since the large number of lysines involved in this regulation allows significant changes in the net charge carried by specific histone regions (Verdone et al., 2005). Polyglutamylation causes alterations in negatively charged residues that are comparable to those seen in acetylation. As a result, it is possible that the two changes work together to control the binding of NAP to histones. Polyglutamylation's unique structure, with the side chain extending away from the main polypeptide chain, may allow for substantial stability of connections with positively charged partners.

All these results show how the loss of CCP1 is affecting the overall behaviour of NAP1L4, suggesting that CCP1 would regulate (the avidity of) protein–protein and DNA–protein interactions by shortening the length of these acidic tails. In fact, this is consistent with the postulated functions of PTMs that alter the tubulin's C terminus, motor protein modulation, and MAPs binding to tubulin's C-terminal region (Janke & Bulinski, 2011). Similarly, Rusconi et al. hypothesized that the observed variability of telokin's C-terminus regulates the protein's interaction with other proteins (Rusconi et al., 1997). These findings, in relation to the nuclear impairments found in the *pcd* mouse model, may indicate that CCP1 could act as a chromatin organiser by modifying nucleosome assembly proteins.

Following the nuclear characterisation of CCP1, we wanted to know how CCP1 is related to DNA healing processes after external damage, since degeneration of Purkinje cells caused by CCP1 loss of function has previously been linked to the gradual build-up of nuclear DNA damage (Baltanás, Casafont, Lafarga, et al., 2011). Other studies have identified that NAP1L4 has a role in DNA damage response by modulating the expression of p53-responsive

prearrest and proapoptotic genes (Tanaka et al., 2019). Overexpression of this gene protects cells against doxorubicin-induced cell death. Knowing this, we hypothesised that CCP1 depletion in neuronal cells would impair the healing process.

In our work, we observed that knockout of CCP1 had a negative effect on cell migration capacity after doxorubicin-induced DNA damage without affecting cell viability. This data indicates that CCP1 is involved in DNA damage response, allowing a correct cell proliferation in undifferentiated neurons after DNA repair mechanisms.

In response to the question presented in this section, several contributions to the field have been provided. First, we have shown that CCP1 could be involved in nucleolar integrity, the presence of CCP1 in the nucleolus has been related to its participation in transcription which could lead to nucleolar stress when it is absent. In addition, the direct interaction between CCP1 and NAP1L4 affects the latter behaviour, which in turn could be regulated by its deglutamylating activity. This regulation on nucleosome assembly processes could be the cause of the inappropriate organization of chromatin and the impairment of DNA repair activity found in the nuclear phenotype of the *pcd* mouse. At this point, it is important to note that neurodegeneration induced by CCP1's loss of function seems to be a multi-mechanistic process, in which both nuclear and cytoplasmic defects act together to generate the ataxic phenotype observed.

What is the relationship between CCP6 and human ciliopathies?

Polyglutamylation is involved in the regulation of cilia/flagella movement as well as the control of flagella beating behaviour (Grau et al., 2013; Suryavanshi et al., 2010). Consisting with this role, TTLLs and CCPs are necessary for cilia and basal bodies, according to functional and localisation studies (O'Hagan et al., 2011; van Dijk et al., 2007). *In vivo*, the relevance of polyglutamylation in cilia can be inferred in part from the abnormalities seen in TTLL or CCP knockout mice, which are similar to the phenotypes seen in ciliopathies under certain circumstances.

In order to gain insight into the relation between CCPs and ciliopathies, we used the data obtained from the BioID methodology applied to CCP6 in chapter 4. This enzyme is localised in the Golgi complex, as well as in the centrioles in the interphase and diving cells, structures

closely related to cilia and flagella (Bettencourt-Dias et al., 2011). The BioID interactomics led us to identify 41 potential functional partners of CCP6. Among them, a large number were associated with centrosome, centriole, cilia biogenesis and ciliopathies with enriched GO terms led by protein localisation to the centrosome and cilium assembly.

A more detailed analysis of the data showed that Joubert syndrome (JS) pathology was overrepresented in the interactome landscape of CCP6, with 4 related genes. Consequently, we studied the four JS-related proteins enriched in the BioID dataset and found that they are located in different regions of the centrosome and axoneme. For instance, CSPP1 and PIBF1 are found in the centriole (Frikstad et al., 2019; Lachmann et al., 2004), OFD-1 in the basal body (Giorgio et al., 2007) and KIF7 in the axoneme distal tip (Endoh-Yamagami et al., 2009). Our subsequent investigations focused on whether the relationship was only due to its localisation in the cilia or whether it was directly related to CCP6 enzymatic function.

Tubulin glutamylation occurring in the ciliary axoneme has been suggested to be important for ciliary function (Yang et al., 2021) and its regulation is minimally necessary for cilia stability but essential for signalling. Interestingly, the reported regulation was done by another JS related protein, the ARL13B, which imports the glutamylases TTLL5 and TTLL6 into the cilia. Following this thread, we observed that TTLL5 was also found as a candidate interactor for CCP6, suggesting a possible relation between CCP6 activity and cilia signalling. Polyglutamylation has also been found on other JS-related proteins such as the ARM9/TOGARAM1 protein module (Latour et al., 2020), indicating that this PTM is highly related to this ciliopathy.

Additional discussion on CCP6 activity is conducted in chapter 5, which also points to the regulation of ciliopathies through deglutamylation activity. Due to the defects observed in *C. elegans,* we analysed the ability of mutated CCP6 to bind to tubulin. Analysis of the proteins found in the microtubule-associated fraction after tubulin purification in cultured cells showed that the mutated CCP6 was not able to bind tubulin. Moreover, subcellular localisation of the mutant protein was also modified, not being found in the centrosome. This loss of tubulin binding could be the reason for the phenotype observed in *C. elegans,* which is characterised by a progressive defect in ciliary maintenance. These results are in concordance with the relationship between CCP6 and ciliopathies.

Consequently, we can hypothesise that CCP6 may play a crucial role in the development of the Joubert syndrome by regulating tubulin polyglutamylation in cilia. This information suggests a potential therapeutic strategy by targeting this machinery to correct signalling defects in ciliopathies.

Which is the biological function of the N-domain of cytosolic carboxypeptidases?

In chapter 5, we aimed for the characterisation of the conserved N-domain of cytosolic carboxypeptidases, focusing on CCP6 as the minimal CCP expression unit. In this context, it is important to note that all CCPs contain a region of ~120 residues, known as the 'N-domain', which has sequence similarity between individual CCPs but not with other known peptidase. This characteristic domain is conserved throughout the evolutionary line, being present in all identified CCPs. It is reasonable to assume that this domain has specific characteristics that make it necessary for the correct functionality of CCPs. Although extensive work has been done to describe the conserved catalytic domain involved in their distinctive deglutamylase activity, little is known about the N-domain and its implication in CCP activity. At present, the only information reported regarding the N-domain has been obtained from the *my22* lesion of *C. elegans* which affects the N-domain in a single point mutation and is capable of inducing loss of enzymatic activity without affecting the catalytic site. In this chapter, we evaluated the effects of this point mutation on the enzymatic activity while assessing its implications in protein stability, subcellular localisation, and substrate specificity.

Based on previous studies in *C. elegans*, where the G596R substitution in the conserved F[E,D]SGNL motif of the N-domain of the CCP homolog CCPP-1 was associated with abnormal behaviour of the protein (O'Hagan et al., 2011), we generated the same single mutation of this motif in human CCP6, consisting in the substitution of the glycine 53 for an arginine (G53R). As CCP6 is defined as the minimal functional expression of human CCPs, only containing the N-domain and the carboxypeptidase domain characteristics of this subfamily, mutations in this specific protein gave us information without any other domain implication.

For a detailed characterisation of the significance of this conserved domain, the recombinant proteins CCP6 WT and CCP6 E401Q, a catalytically inactive mutant previously

obtained in our laboratory, were used as a comparison. Specifically, the CCP6 E401Q mutant was used to evaluate the contribution of the C-terminal carboxypeptidase domain to the activity, while the hCCP6 G53R mutant was intended to correctly evaluate the effects observed in the inactivation belonging exclusively to the N-domain.

We first evaluated the effect on catalytic activity. In this way, different approaches were used. First, we analysed their capacity to hydrolyse C-terminal glutamic residues of tubulin *in vitro* through the generation of Δ2-tubulin and the reduction of polyglutamate side-chains levels. In this case, neither of these actions were detected in cells expressing CCP6 G53R nor CCP6 E401Q, demonstrating that these mutants were not catalytically active against their major substrates in cells. After determining this loss of activity, we wondered if this phenomenon could be related to an alteration in the subcellular location. The subcellular localisation experiments performed indicate that the conserved F[E,D]SGNL motif of the N-domain of CCPs directly affects its distribution in cells. Regarding the previous results mentioned in the relationship between CCP6 and ciliopathies, it is plausible to determine that the inability of hCCP6 G53R to bind correctly the microtubules generates an accumulation in the Golgi apparatus, which is closely related to the MTOC (Zhu & Kaverina, 2013). Thus, unable to interact with its main substrate, hCCP6 G53R remains in the closest and most related subcellular location, a place where the wild-type form is also present but at lower levels.

Following these *in vitro* experiments, we analysed the activity of our proteins of study against another known CCP6 substrate, telokins with different polyglutamate ends (Rogowski et al., 2010; Tort et al., 2014). After co-transfection of the different CCP6 variants and telokins, we observed the same behaviour as previously described in tubulin. Interestingly, when activity was measured using the small synthetic substrate Biotin-Glu-Glu-Glu-Glu-Glu-OH, ideal for studying the recombinant deglutamylase activity on this non-specific substrate (H. Y. Wu et al., 2012, 2015), we observed activity in both wild-type and F[E,D]SGNL mutated CCP6 but not in the catalytically dead mutant.

The results of the evaluation of the catalytic activity of hCCP6 G53R in comparison with wild-type and the catalytically dead forms suggest that the N-domain is essential for the proper functioning of CCPs at cellular level. The fact that this mutated form was active

against small synthetic peptides suggests that this domain could be involved in specific substrate recognition. These findings are consistent with previous studies in which mutations located in the N-domain were associated with reduced function in *C. elegans*. In these studies, significant deficiencies were found, but the overall phenotype was not as severe as the catalytically dead mutant (O'Hagan et al., 2011).

At this point, we discussed whether the generated mutation was able to destabilize the protein. The results obtained using specific proteasome inhibition suggests that CCP6 G53R is stable and that motif I of the enzyme would not be involved in its correct stability. Therefore, the loss of catalytic function of CCP6 G53R in cells could not be attributed to enzyme instability due to a mutation in the N-domain. Since the CCP6 G53R mutant appears to be stable, we proceeded to analyse its ability to bind to tubulin, one of its most studied substrates (Kimura et al., 2010; Rogowski et al., 2010).

Analysis of the proteins found in the microtubule-associated fraction after tubulin purification in cultured cells showed that, unlike CCP6 and CCP6 E401Q, CCP6 G53R was not directly associated with tubulin. At this point, we found that both CCP6 G53R and CCP6 E401Q mutants are not catalytically active against tubulin but differ in their ability to bind to the substrate. More interestingly, when the purified versions of CCP6 were tested against purified tubulin, we observed the same results as the *in vitro* characterisation, indicating that CCP6 is not capable of deglutamylate tubulin neither in cell nor in its purified form

This result, added to the findings on small synthetic substrates and telokins, suggests that the loss of catalytic function in CCP6 G53R is caused by a lack of specific substrate binding and not by a real lack of catalytic activity as occurs in the case of the mutant CCP6 E401Q. Taking into account of all these results, it could be argued that the motif I of the N-terminal domain of the CCPs is involved in the specific enzyme-substrate recognition. This would be consistent with previous studies suggesting that the N-domain could act as a regulatory domain, limiting access to the active centre by specific recognition (Rodríguez de la Vega et al., 2013). However, the issue is much more complex, for two reasons: first, because other studies should be carried out including mutations in the rest of residues of this motif I and, second, because given the existence of two other conserved motifs in the N-terminal domain, the same study should be repeated for these two motifs. The complete

knowledge of the nature of this matter is still very distant, but the results obtained seem to be a correct approximation to this it, both theoretically and clinically.

Future perspectives

In conclusion, the results presented in this thesis work highlight the clinical importance of CCPs in health and disease, providing new data that attempt to unveil new aspects of CCP1 and CCP6 functionality. It is noteworthy to mention the application of the BioID methodology, which has allowed us dive into the interactome landscape of the studied CCPs. Thanks to the application of this strategy, we have been able to find new interacting partners and substrates of CCP1 and CCP6, while relating these enzymes with novel cellular processes as the nucleosome assembly and novel related ciliopathies as the Joubert syndrome.

At this stage, the work developed in this thesis opens the door to explore different strategies that can be applied in the fields of neuropathies and ciliopathies. First of all, it would be interesting to further explore how CCPs are related to cell cycle progression, with a special focus on the MTOC regulation. Having a better understanding of MT dynamics and control can contribute to the microtubule-related processes field. In addition, it would be very interesting to keep working on the relationship between CCP1 and the cell nucleus. The presented results relating CCP1 with transcription processes as well as DNA nucleation may contribute to the general understanding of cellular processes that lead to neurodegeneration. Finally, mechanisms for CCP regulation should be considered. Different CCPs have been found to have distinct localisations in the cell, implying that their regulation may be dependent on their location (Rodríguez de la Vega et al., 2013). Furthermore, as the N-domain has shown, CCPs contains a domain that may influence its substrate binding capacity. Additional regulatory mechanisms for CCPs can be proposed, including changes in expression level, proteolysis, and phosphorylation. More research is needed to fully understand the activity of these enzymes and their regulatory mechanisms.

REFERENCES

REFERENCES

Aillaud, C., Bosc, C., Saoudi, Y., Denariera, E., Peris, L., Sago, L., Taulet, N., Cieren, A., Tort, O., Magiera, M. M., Janke, C., Redeker, V., Andrieux, A., & Moutin, M. J. (2016). Evidence for new C-terminally truncated variants of α-and β-tubulins. *Molecular Biology of the Cell*, *27*(4), 640–653. https://doi.org/10.1091/mbc.E15-03-0137

Alberts, B., Alexander, J., Lewis, J., Morgan, D., Raff, M., Roberts, K., & Walter, P. (2014). The Cytoskeleton. In *Molecular Biology of the Cell* (6th ed., pp. 889–962). Garland Science Taylor & Francis Group.

Alexander, J. E., Hunt, D. F., Lee, M. K., Shabanowitz, J., Michel, H., Berlin, S. C., MacDonald, T. L., Sundberg, R. J., Rebhun, L. I., & Frankfurter, A. (1991). Characterization of posttranslational modifications in neuron-specific class III beta-tubulin by mass spectrometry. *Proceedings of the National Academy of Sciences of the United States of America*, *88*(11), 4685. https://doi.org/10.1073/PNAS.88.11.4685

Alonso-del-Rivero, M., Trejo, S. A., Reytor, M. L., Rodriguez-De-La-Vega, M., Delfin, J., Diaz, J., González-González, Y., Canals, F., Chavez, M. A., & Aviles, F. X. (2012). Tri-domain bifunctional inhibitor of metallocarboxypeptidases A and serine proteases isolated from marine annelid Sabellastarte magnifica. *Journal of Biological Chemistry*, *287*(19), 15427–15438. https://doi.org/10.1074/jbc.M111.337261

Arce, C. A., Rodriguez, J. A., Barra, H. S., & Caputto, R. (1975). Incorporation of l-Tyrosine, l-Phenylalanine and l-3,4-Dihydroxyphenylalanine as Single Units into Rat Brain Tubulin. *European Journal of Biochemistry*, *59*(1), 145–149. https://doi.org/10.1111/j.1432-1033.1975.tb02435.x

Arolas, J., Vendrell, J., Aviles, F., & Fricker, L. (2007). Metallocarboxypeptidases: Emerging Drug Targets in Biomedicine. *Current Pharmaceutical Design*, *13*(4), 349–366. https://doi.org/10.2174/138161207780162980

Audebert, S., Desbruyeres, E., Gruszczynski, C., Koulakoff, A., Gros, F., Denoulet, P., & Edde, B. (1993). Reversible polyglutamylation of α- and β-tubulin and microtubule dynamics in mouse brain neurons. *Molecular Biology of the Cell*, *4*(6), 615–626. https://doi.org/10.1091/mbc.4.6.615

Avilés, F. X., Vendrell, J., Guasch, A., Coll, M., & Huber, R. (1993). Advances in metallo-procarboxypeptidases: Emerging details on the inhibition mechanism and on the activation process. In *European Journal of Biochemistry* (Vol. 211, Issue 3, pp. 381–389). Eur J Biochem. https://doi.org/10.1111/j.1432-1033.1993.tb17561.x

Avvakumov, N., Nourani, A., & Côté, J. (2011). Histone Chaperones: Modulators of Chromatin Marks. *Molecular Cell*, *41*(5), 502–514. https://doi.org/10.1016/j.molcel.2011.02.013

Badano, J. L., Mitsuma, N., Beales, P. L., & Katsanis, N. (2006). The ciliopathies: An emerging class of human genetic disorders. In *Annual Review of Genomics and Human Genetics*

References

(Vol. 7, pp. 125–148). Annu Rev Genomics Hum Genet. https://doi.org/10.1146/annurev.genom.7.080505.115610

Bailey, M. E., Sackett, D. L., & Ross, J. L. (2015). Katanin Severing and Binding Microtubules Are Inhibited by Tubulin Carboxy Tails. *Biophysical Journal*, *109*(12), 2546–2561. https://doi.org/10.1016/j.bpj.2015.11.011

Baird, F., & Bennett, C. (2013). Microtubule Defects and Neurodegeneration. *Journal of Genetic Syndromes & Gene Therapy*, *04*(11). https://doi.org/10.4172/2157-7412.1000203

Baltanás, F. C., Berciano, M. T., Tapia, O., Narcis, J. O., Lafarga, V., Díaz, D., Weruaga, E., Santos, E., & Lafarga, M. (2019). Nucleolin reorganization and nucleolar stress in Purkinje cells of mutant PCD mice. *Neurobiology of Disease*, *127*, 312–322. https://doi.org/10.1016/j.nbd.2019.03.017

Baltanás, F. C., Casafont, I., Lafarga, V., Weruaga, E., Alonso, J. R., Berciano, M. T., & Lafarga, M. (2011). Purkinje cell degeneration in pcd mice reveals large scale chromatin reorganization and gene silencing linked to defective DNA repair. *The Journal of Biological Chemistry*, *286*(32), 28287–28302. https://doi.org/10.1074/jbc.M111.246041

Baltanás, F. C., Casafont, I., Weruaga, E., Alonso, J. R., Berciano, M. T., & Lafarga, M. (2011). Nucleolar disruption and cajal body disassembly are nuclear hallmarks of DNA damage-induced neurodegeneration in purkinje cells. *Brain Pathology (Zurich, Switzerland)*, *21*(4), 374–388. https://doi.org/10.1111/j.1750-3639.2010.00461.x

Bangs, F., & Anderson, K. v. (2017). Primary cilia and Mammalian Hedgehog signaling. *Cold Spring Harbor Perspectives in Biology*, *9*(5). https://doi.org/10.1101/cshperspect.a028175

Barrett, A. (2000). Proteases. *Current Protocols in Protein Science*, *21*(1), 21.1.1-21.1.12. https://doi.org/10.1002/0471140864.ps2101s21

Berezniuk, I., & Fricker, L. D. (2010). A defect in cytosolic carboxypeptidase 1 (Nna1) causes autophagy in Purkinje cell degeneration mouse brain. *Autophagy*, *6*(4), 558–559. https://doi.org/10.4161/auto.6.4.11813

Berezniuk, I., Lyons, P. J., Sironi, J. J., Xiao, H., Setou, M., Angeletti, R. H., Ikegami, K., & Fricker, L. D. (2013). Cytosolic carboxypeptidase 5 removes α- And γ-linked glutamates from tubulin. *Journal of Biological Chemistry*, *288*(42), 30445–30453. https://doi.org/10.1074/jbc.M113.497917

Berezniuk, I., Sironi, J., Callaway, M. B., Castro, L. M., Hirata, I. Y., Ferro, E. S., & Fricker, L. D. (2010). CCP1/Nna1 functions in protein turnover in mouse brain: Implications for cell death in Purkinje cell degeneration mice . *The FASEB Journal*, *24*(6), 1813–1823. https://doi.org/10.1096/fj.09-147942

Berezniuk, I., Vu, H. T., Lyons, P. J., Sironi, J. J., Xiao, H., Burd, B., Setou, M., Angeletti, R. H., Ikegami, K., & Fricker, L. D. (2012). Cytosolic carboxypeptidase 1 is involved in processing α- and β-tubulin. *Journal of Biological Chemistry*, *287*(9), 6503–6517. https://doi.org/10.1074/jbc.M111.309138

Bettencourt-Dias, M., Hildebrandt, F., Pellman, D., Woods, G., & Godinho, S. A. (2011). Centrosomes and cilia in human disease. In *Trends in Genetics* (Vol. 27, Issue 8, pp. 307–315). Trends Genet. https://doi.org/10.1016/j.tig.2011.05.004

Bigman, L. S., & Levy, Y. (2020). Tubulin tails and their modifications regulate protein diffusion on microtubules. *Proceedings of the National Academy of Sciences of the United States of America*, *117*(16), 8876–8883. https://doi.org/10.1073/pnas.1914772117

Bobinnec, Y., Khodjakov, A., Mir, L. M., Rieder, C. L., Eddé, B., & Bornens, M. (1998). Centriole disassembly in vivo and its effect on centrosome structure and function in vertebrate cells. *Journal of Cell Biology*, *143*(6), 1575–1589. https://doi.org/10.1083/jcb.143.6.1575

Bodakuntla, S., Jijumon, A. S., Villablanca, C., Gonzalez-Billault, C., & Janke, C. (2019). Microtubule-Associated Proteins: Structuring the Cytoskeleton. In *Trends in Cell Biology* (Vol. 29, Issue 10, pp. 804–819). Elsevier Ltd. https://doi.org/10.1016/j.tcb.2019.07.004

Boisvert, F.-M., Hendzel, M. J., & Bazett-Jones, D. P. (2000). Promyelocytic Leukemia (Pml) Nuclear Bodies Are Protein Structures That Do Not Accumulate RNA. *Journal of Cell Biology*, *148*(2), 283–292. https://doi.org/10.1083/JCB.148.2.283

Bompard, G., van Dijk, J., Cau, J., Lannay, Y., Marcellin, G., Lawera, A., van der Laan, S., & Rogowski, K. (2018). CSAP Acts as a Regulator of TTLL-Mediated Microtubule Glutamylation. *Cell Reports*, *25*(10), 2866-2877.e5. https://doi.org/10.1016/j.celrep.2018.10.095

Bond, J. S. (2019). Proteases: History, discovery, and roles in health and disease. *Journal of Biological Chemistry*, *294*(5), 1643–1651. https://doi.org/10.1074/jbc.TM118.004156

Bonnet, C., Boucher, D., Lazereg, S., Pedrotti, B., Islam, K., Denoulet, P., & Larcher, J. C. (2001). Differential Binding Regulation of Microtubule-associated Proteins MAP1A, MAP1B, and MAP2 by Tubulin Polyglutamylation. *Journal of Biological Chemistry*, *276*(16), 12839–12848. https://doi.org/10.1074/jbc.M011380200

Bornens, M. (2012). The centrosome in cells and organisms. In *Science* (Vol. 335, Issue 6067, pp. 422–426). American Association for the Advancement of Science. https://doi.org/10.1126/science.1209037

Boucher, D., Larcher, J. C., Gros, F., & Denoulet, P. (1994). Polyglutamylation of Tubulin as a Progressive Regulator of in Vitro Interactions between the Microtubule-Associated

References

Protein Tau and Tubulin. *Biochemistry*, *33*(41), 12471–12477. https://doi.org/10.1021/bi00207a014

Bowman, A., Ward, R., Wiechens, N., Singh, V., El-Mkami, H., Norman, D. G., & Owen-Hughes, T. (2011). The Histone Chaperones Nap1 and Vps75 Bind Histones H3 and H4 in a Tetrameric Conformation. *Molecular Cell*, *41*(4), 398–408. https://doi.org/10.1016/j.molcel.2011.01.025

Bradford, M. (1976). A Rapid and Sensitive Method for the Quantitation of Microgram Quantities of Protein Utilizing the Principle of Protein-Dye Binding. *Analytical Biochemistry*, *72*(1–2), 248–254. https://doi.org/10.1006/abio.1976.9999

Bramblett, G. T., Goedert, M., Jakes, R., Merrick, S. E., Trojanowski, J. Q., & Lee, V. M. Y. (1993). Abnormal tau phosphorylation at Ser396 in alzheimer's disease recapitulates development and contributes to reduced microtubule binding. *Neuron*, *10*(6), 1089–1099. https://doi.org/10.1016/0896-6273(93)90057-X

Branham, K., Matsui, H., Biswas, P., Guru, A. A., Hicks, M., Suk, J. J., Li, H., Jakubosky, D., Long, T., Telenti, A., Nariai, N., Heckenlively, J. R., Frazer, K. A., Sieving, P. A., & Ayyagari, R. (2016). Establishing the involvement of the novel gene AGBL5 in retinitis pigmentosa by whole genome sequencing. *Physiological Genomics*, *48*(12), 922–927. https://doi.org/10.1152/physiolgenomics.00101.2016

Caldecott, K. W. (2004). DNA single-strand breaks and neurodegeneration. In *DNA Repair* (Vol. 3, Issues 8–9, pp. 875–882). DNA Repair (Amst). https://doi.org/10.1016/j.dnarep.2004.04.011

Casafont, I., Navascués, J., Pena, E., Lafarga, M., & Berciano, M. T. (2006). Nuclear organization and dynamics of transcription sites in rat sensory ganglia neurons detected by incorporation of 5'-fluorouridine into nascent RNA. *Neuroscience*, *140*(2), 453–462. https://doi.org/10.1016/J.NEUROSCIENCE.2006.02.030

Cederquist, G., Luchniak, A., Tischfield, M., Peeva, M., Song, Y., Menezes, M., Chan, W.-M., Andrews, C., Chew, S., Jamieson, R., Gomes, L., Flaherty, M., Grant, P., Gupta, M., & Engle, E. (2012). An inherited TUBB2B mutation alters a kinesin-binding site and causes polymicrogyria, CFEOM and axon dysinnervation. *Human Molecular Genetics*, *21*(26), 5484–5499. https://academic.oup.com/hmg/article/21/26/5484/559404

Cervello, M., Giannitrapani, L., La Rosa, M., Notarbartolo, M., Labbozzetta, M., Poma, P., Montalto, G., & D'Alessandro, N. (2004). Induction of apoptosis by the proteasome inhibitor MG132 in human HCC cells: Possible correlation with specific caspase-dependent cleavage of beta-catenin and inhibition of beta-catenin-mediated transactivation. *International Journal of Molecular Medicine*, *13*(5), 741–748. https://doi.org/10.3892/ijmm.13.5.741

Chakrabarti, L., Eng, J., Ivanov, N., Garden, G. A., & La Spada, A. R. (2009). Autophagy activation and enhanced mitophagy characterize the Purkinje cells of pcd mice prior to neuronal death. *Molecular Brain*, *2*, 24. https://doi.org/10.1186/1756-6606-2-24

Chakrabarti, L., Zahra, R., Jackson, S. M., Kazemi-Esfarjani, P., Sopher, B. L., Mason, A. G., Toneff, T., Ryu, S., Shaffer, S., Kansy, J. W., Eng, J., Merrihew, G., MacCoss, M. J., Murphy, A., Goodlett, D. R., Hook, V., Bennett, C. L., Pallanck, L. J., & La Spada, A. R. (2010). Mitochondrial Dysfunction in NnaD Mutant Flies and Purkinje Cell Degeneration Mice Reveals a Role for Nna Proteins in Neuronal Bioenergetics. *Neuron*, *66*(6), 835–847. https://doi.org/10.1016/j.neuron.2010.05.024

Chakraborti, S., Natarajan, K., Curiel, J., Janke, C., & Liu, J. (2016). The emerging role of the tubulin code: From the tubulin molecule to neuronal function and disease. In *Cytoskeleton* (Vol. 73, Issue 10, pp. 521–550). John Wiley and Sons Inc. https://doi.org/10.1002/cm.21290

Chan, C. J., Le, R., Burns, K., Ahmed, K., Coyaud, E., Laurent, E. M. N., Raught, B., & Melançon, P. (2019). BioID performed on golgi enriched fractions identify C10orf76 as a GBF1 binding protein essential for golgi maintenance and secretion. *Molecular and Cellular Proteomics*, *18*(11), 2285–2297. https://doi.org/10.1074/mcp.RA119.001645

Chen, Y., Pai, A. A., Herudek, J., Lubas, M., Meola, N., Järvelin, A. I., Andersson, R., Pelechano, V., Steinmetz, L. M., Jensen, T. H., & Sandelin, A. (2016). Principles for RNA metabolism and alternative transcription initiation within closely spaced promoters. *Nature Genetics 2016 48:9*, *48*(9), 984–994. https://doi.org/10.1038/ng.3616

Christianson, D. W., & Lipscomb, W. N. (1986). X-ray crystallographic investigation of substrate binding to carboxypeptidase A at subzero temperature. *Proceedings of the National Academy of Sciences of the United States of America*, *83*(20), 7568–7572. https://doi.org/10.1073/pnas.83.20.7568

Coux, O., Zieba, B. A., & Meiners, S. (2020). The proteasome system in health and disease. In *Advances in Experimental Medicine and Biology* (Vol. 1233, pp. 55–100). Springer. https://doi.org/10.1007/978-3-030-38266-7_3

Coyaud, E., Mis, M., Laurent, E. M. N., Dunham, W. H., Couzens, A. L., Robitaille, M., Gingras, A.-C., Angers, S., & Raught, B. (2015). BioID-based Identification of Skp Cullin F-box (SCF)β-TrCP1/2 E3 Ligase Substrates. *Molecular & Cellular Proteomics : MCP*, *14*(7), 1781–1795. https://doi.org/10.1074/mcp.M114.045658

Cremer, T., & Cremer, C. (2001). Chromosome territories, nuclear architecture and gene regulation in mammalian cells. In *Nature Reviews Genetics* (Vol. 2, Issue 4, pp. 292–301). Nat Rev Genet. https://doi.org/10.1038/35066075

Dammermann, A., & Merdes, A. (2002). Assembly of centrosomal proteins and microtubule organization depends on PCM-1. *Journal of Cell Biology*, *159*(2), 255–266. https://doi.org/10.1083/jcb.200204023

de Forges, H., Bouissou, A., & Perez, F. (2012). Interplay between microtubule dynamics and intracellular organization. *The International Journal of Biochemistry & Cell Biology*, *44*(2), 266–274. https://doi.org/10.1016/J.BIOCEL.2011.11.009

References

Declerck, P. J. (2011). Thrombin activatable fibrinolysis inhibitor. In *Hamostaseologie* (Vol. 31, Issue 3, pp. 165–173). Hamostaseologie. https://doi.org/10.5482/ha-1155

Denoulet, P., Eddé, B., & Gros, F. (1986). Differential expression of several neurospecific β-tubulin mRNAs in the mouse brain during development. *Gene*, *50*(1–3), 289–297. https://doi.org/10.1016/0378-1119(86)90333-1

Desai, A., & Mitchison, T. J. (1997). Microtubule polymerization dynamics. *Annual Review of Cell and Developmental Biology*, *13*(1), 83–117. https://doi.org/10.1146/annurev.cellbio.13.1.83

Doherty, D. (2009). Joubert Syndrome: Insights Into Brain Development, Cilium Biology, and Complex Disease. In *Seminars in Pediatric Neurology* (Vol. 16, Issue 3, pp. 143–154). Semin Pediatr Neurol. https://doi.org/10.1016/j.spen.2009.06.002

Doi, E., Shibata, D., & Matoba, T. (1981). Modified colorimetric ninhydrin methods for peptidase assay. *Analytical Biochemistry*, *118*(1), 173–184. https://doi.org/10.1016/0003-2697(81)90175-5

Dollery, C. M., & Libby, P. (2006). Atherosclerosis and proteinase activation. In *Cardiovascular Research* (Vol. 69, Issue 3, pp. 625–635). https://doi.org/10.1016/j.cardiores.2005.11.003

Dompierre, J. P., Godin, J. D., Charrin, B. C., Cordelières, F. P., King, S. J., Humbert, S., & Saudou, F. (2007). Histone deacetylase 6 inhibition compensates for the transport deficit in Huntington's disease by increasing tubulin acetylation. *Journal of Neuroscience*, *27*(13), 3571–3583. https://doi.org/10.1523/JNEUROSCI.0037-07.2007

Dong, J. M., Tay, F. P. L., Swa, H. L. F., Gunaratne, J., Leung, T., Burke, B., & Manser, E. (2016). Proximity biotinylation provides insight into the molecular composition of focal adhesions at the nanometer scale. *Science Signaling*, *9*(432). https://doi.org/10.1126/scisignal.aaf3572

Eddé, B., Rossier, J., le Caer, J. P., Desbruyères, E., Gros, F., & Denoulet, P. (1990). Posttranslational glutamylation of alpha-tubulin. *Science (New York, N.Y.)*, *247*(4938), 83–85. http://www.ncbi.nlm.nih.gov/pubmed/1967194

Egea, G., & Ríos, R. M. (2008). *The role of the cytoskeleton in the structure and function of the Golgi apparatus* (pp. 270–300). https://doi.org/10.1007/978-3-211-76310-0_17

Eguether, T., & Hahne, M. (2018). Mixed signals from the cell's antennae: primary cilia in cancer. *EMBO Reports*, *19*(11). https://doi.org/10.15252/embr.201846589

Emoto, K., Masugi, Y., Yamazaki, K., Effendi, K., Tsujikawa, H., Tanabe, M., Kitagawa, Y., & Sakamoto, M. (2014). Presence of primary cilia in cancer cells correlates with prognosis of pancreatic ductal adenocarcinoma. *Human Pathology*, *45*(4), 817–825. https://doi.org/10.1016/J.HUMPATH.2013.11.017

Endoh-Yamagami, S., Evangelista, M., Wilson, D., Wen, X., Theunissen, J. W., Phamluong, K., Davis, M., Scales, S. J., Solloway, M. J., de Sauvage, F. J., & Peterson, A. S. (2009). The Mammalian Cos2 Homolog Kif7 Plays an Essential Role in Modulating Hh Signal Transduction during Development. *Current Biology*, *19*(15), 1320–1326. https://doi.org/10.1016/j.cub.2009.06.046

Erck, C., Peris, L., Andrieux, A., Meissirel, C., Gruber, A. D., Vernet, M., Schweitzer, A., Saoudi, Y., Pointu, H., Bosc, C., Salin, P. A., Job, D., & Wehland, J. (2005). A vital role of tubulin-tyrosine-ligase for neuronal organization. *Proceedings of the National Academy of Sciences of the United States of America*, *102*(22), 7853–7858. https://doi.org/10.1073/pnas.0409626102

Ferkol, T. W., & Leigh, M. W. (2012). Ciliopathies: The central role of cilia in a spectrum of pediatric disorders. *Journal of Pediatrics*, *160*(3), 366–371. https://doi.org/10.1016/j.jpeds.2011.11.024

Fernández, D., Pallarès, I., Vendrell, J., & Avilés, F. X. (2010). Progress in metallocarboxypeptidases and their small molecular weight inhibitors. In *Biochimie* (Vol. 92, Issue 11, pp. 1484–1500). Biochimie. https://doi.org/10.1016/j.biochi.2010.05.002

Fernandez-Gonzalez, A., La Spada, A. R., Treadaway, J., Higdon, J. C., Harris, B. S., Sidman, R. L., Morgan, J. I., & Zuo, J. (2002). Purkinje cell degeneration (pcd) phenotypes caused by mutations in the axotomy-induced gene, Nna1. *Science (New York, N.Y.)*, *295*(5561), 1904–1906. https://doi.org/10.1126/science.1068912

Ferreira, A., & Caceres, A. (1992). Expression of the Class III β-tubulin isotype in developing neurons in culture. *Journal of Neuroscience Research*, *32*(4), 516–529. https://doi.org/10.1002/jnr.490320407

Flexner, C., Bate, G., & Kirkpatrick, P. (2005). Tipranavir. In *Nature Reviews Drug Discovery* (Vol. 4, Issue 12, pp. 955–956). https://doi.org/10.1038/nrd1907

Fouquet, J. -P, Kann, M. -L, Edde, B., Wolff, A., Desbruyeres, E., & Denoulet, P. (1994). Differential distribution of glutamylated tubulin during spermatogenesis in mammalian testis. *Cell Motility and the Cytoskeleton*, *27*(1), 49–58. https://doi.org/10.1002/cm.970270106

Fourest-Lieuvin, A. (2006). Purification of tubulin from limited volumes of cultured cells. *Protein Expression and Purification*, *45*(1), 183–190. https://doi.org/10.1016/j.pep.2005.05.011

Francis, D. M., & Page, R. (2010). Strategies to optimize protein expression in E. coli. In *Current Protocols in Protein Science* (Vol. 61, Issue SUPPL. 61, pp. 5.24.1-5.24.29). John Wiley & Sons, Ltd. https://doi.org/10.1002/0471140864.ps0524s61

Francisconi, S., Codenotti, M., Ferrari-Toninelli, G., Uberti, D., & Memo, M. (2005). Preservation of DNA integrity and neuronal degeneration. *Brain Research. Brain*

Research Reviews, *48*(2), 347–351. https://doi.org/10.1016/J.BRAINRESREV.2004.12.023

Freije, J. M. P., Balbín, M., Pendás, A. M., Sánchez, L. M., Puente, X. S., & López-Otín, C. (2003). Matrix metalloproteinases and tumor progression. *Advances in Experimental Medicine and Biology*, *532*, 91–107. https://doi.org/10.1007/978-1-4615-0081-0_9

Frikstad, K. A. M., Molinari, E., Thoresen, M., Ramsbottom, S. A., Hughes, F., Letteboer, S. J. F., Gilani, S., Schink, K. O., Stokke, T., Geimer, S., Pedersen, L. B., Giles, R. H., Akhmanova, A., Roepman, R., Sayer, J. A., & Patzke, S. (2019). A CEP104-CSPP1 Complex Is Required for Formation of Primary Cilia Competent in Hedgehog Signaling. *Cell Reports*, *28*(7), 1907-1922.e6. https://doi.org/10.1016/j.celrep.2019.07.025

Fry, A. M., Leaper, M. J., & Bayliss, R. (2014). The primary cilium: Guardian of organ development and homeostasis. In *Organogenesis* (Vol. 10, Issue 1, pp. 62–68). Organogenesis. https://doi.org/10.4161/org.28910

Galjart, N. (2010). Plus-end-tracking proteins and their interactions at microtubule ends. In *Current Biology* (Vol. 20, Issue 12). Cell Press. https://doi.org/10.1016/j.cub.2010.05.022

García Guerrero, M. del C. (2017). Caracterización estructural y funcional de dos metalo-carboxipeptidasas de la familia M14 con especificidad de sustrato tipo acídico: carboxipeptidasa citosólica 6 y carboxipeptidasa O humanas. In *Diposit Digital de Documents*. https://ddd.uab.cat/pub/tesis/2017/hdl_10803_458537/mdcgg1de1.pdf

Garcia-Guerrero, M. C., Garcia-Pardo, J., Berenguer, E., Fernandez-Alvarez, R., Barfi, G. B., Lyons, P. J., Avilés, F. X., Huber, R., Lorenzo, J., & Reverter, D. (2018). Crystal structure and mechanism of human carboxypeptidase O: Insights into its specific activity for acidic residues. *Proceedings of the National Academy of Sciences of the United States of America*, *115*(17), E3932–E3939. https://doi.org/10.1073/pnas.1803685115

Garnham, C. P., & Roll-Mecak, A. (2012). The chemical complexity of cellular microtubules: Tubulin post-translational modification enzymes and their roles in tuning microtubule functions. In *Cytoskeleton* (Vol. 69, Issue 7, pp. 442–463). Cytoskeleton (Hoboken). https://doi.org/10.1002/cm.21027

Ghosh-Roy, A., Goncharov, A., Jin, Y., & Chisholm, A. D. (2012). Kinesin-13 and Tubulin Posttranslational Modifications Regulate Microtubule Growth in Axon Regeneration. *Developmental Cell*, *23*(4), 716–728. https://doi.org/10.1016/j.devcel.2012.08.010

Gilmore-Hall, S., Kuo, J., Ward, J. M., Zahra, R., Morrison, R. S., Perkins, G., & La Spada, A. R. (2019). CCP1 promotes mitochondrial fusion and motility to prevent Purkinje cell neuron loss in pcd mice. *Journal of Cell Biology*, *218*(1), 206–219. https://doi.org/10.1083/jcb.201709028

Giordano, T., Gadadhar, S., Bodakuntla, S., Straub, J., Leboucher, S., Martinez, G., Chemlali, W., Bosc, C., Andrieux, A., Bieche, I., Arnoult, C., Geimer, S., & Janke, C. (2019). Loss of

the deglutamylase CCP5 perturbs multiple steps of spermatogenesis and leads to male infertility. *Journal of Cell Science*, *132*(3), jcs226951. https://doi.org/10.1242/jcs.226951

Giorgio, G., Alfieri, M., Prattichizzo, C., Zullo, A., Cairo, S., & Franco, B. (2007). Functional characterization of the OFD1 protein reveals a nuclear localization and physical interaction with subunits of a chromatin remodeling complex. *Molecular Biology of the Cell*, *18*(11), 4397–4404. https://doi.org/10.1091/mbc.E07-03-0198

Gönczy, P., & Hatzopoulos, G. N. (2019). Centriole assembly at a glance. *Journal of Cell Science*, *132*(4), 228833. https://doi.org/10.1242/JCS.228833

Görlich, D., & Kutay, U. (1999). Transport between the cell nucleus and the cytoplasm. In *Annual Review of Cell and Developmental Biology* (Vol. 15, pp. 607–660). Annu Rev Cell Dev Biol. https://doi.org/10.1146/annurev.cellbio.15.1.607

Grau, M. B., Curto, G. G., Rocha, C., Magiera, M. M., Sousa, P. M., Giordano, T., Spassky, N., & Janke, C. (2013). Tubulin glycylases and glutamylases have distinct functions in stabilization and motility of ependymal cilia. *Journal of Cell Biology*, *202*(3), 441–451. https://doi.org/10.1083/jcb.201305041

Groves, M. R., & Barford, D. (1999). Topological characteristics of helical repeat proteins. *Current Opinion in Structural Biology*, *9*(3), 383–389. https://doi.org/10.1016/S0959-440X(99)80052-9

Guimerá, J., Casas, C., Pucharcòs, C., Solans, A., Domènech, A., Planas, A. M., Ashley, J., Lovett, M., Estivill, X., & Pritchard, M. A. (1996). A human homologue of Drosophila minibrain (MNB) is expressed in the neuronal regions affected in Down syndrome and maps to the critical region. *Human Molecular Genetics*, *5*(9), 1305–1310. https://doi.org/10.1093/hmg/5.9.1305

Guinand, M., Vacheron, M. J., Michel, G., & Tipper, D. J. (1979). Location of peptidoglycan lytic enzymes in Bacillus sphaericus. *Journal of Bacteriology*, *138*(1), 126.

Gupta, G. D., Coyaud, É., Gonçalves, J., Mojarad, B. A., Liu, Y., Wu, Q., Gheiratmand, L., Comartin, D., Tkach, J. M., Cheung, S. W. T. T., Bashkurov, M., Hasegan, M., Knight, J. D. R., Lin, Z. Y., Schueler, M., Hildebrandt, F., Moffat, J., Gingras, A. C., Raught, B., & Pelletier, L. (2015). A Dynamic Protein Interaction Landscape of the Human Centrosome-Cilium Interface. *Cell*, *163*(6), 1484–1499. https://doi.org/10.1016/j.cell.2015.10.065

Hallak, M. E., Rodriguez, J. A., Barra, H. S., & Caputto, R. (1977). Release of tyrosine from tyrosinated tubulin. Some common factors that affect this process and the assembly of tubulin. *FEBS Letters*, *73*(2), 147–150. https://doi.org/10.1016/0014-5793(77)80968-X

Hames, R. S., Crookes, R. E., Straatman, K. R., Merdes, A., Hayes, M. J., Faragher, A. J., & Fry, A. M. (2005). Dynamic recruitment of Nek2 kinase to the centrosome involves

microtubules, PCM-1, and localized proteasomal degradation. *Molecular Biology of the Cell*, *16*(4), 1711–1724. https://doi.org/10.1091/mbc.E04-08-0688

Harris, A., Morgan, J. I., Pecot, M., Soumare, A., Osborne, A., & Soares, H. D. (2000). Regenerating motor neurons express Nna1, a novel ATP/GTP-binding protein related to zinc carboxypeptidases. *Molecular and Cellular Neurosciences*, *16*(5), 578–596. https://doi.org/10.1006/mcne.2000.0900

He, K., Ma, X., Xu, T., Li, Y., Hodge, A., Zhang, Q., Torline, J., Huang, Y., Zhao, J., Ling, K., & Hu, J. (2018). Axoneme polyglutamylation regulated by Joubert syndrome protein ARL13B controls ciliary targeting of signaling molecules. *Nature Communications*, *9*(1), 3310. https://doi.org/10.1038/s41467-018-05867-1

He, W. P., & Wang, L. L. (2019). High expression of AGBL2 is a novel prognostic factor of adverse outcome in patients with ovarian carcinoma. *Oncology Letters*, *18*(5), 4900–4906. https://doi.org/10.3892/ol.2019.10829

Hodel, M. R., Corbett, A. H., & Hodel, A. E. (2001). Dissection of a nuclear localization signal. *Journal of Biological Chemistry*, *276*(2), 1317–1325. https://doi.org/10.1074/jbc.M008522200

Hwang, S. G., Yu, S. S., Ryu, J. H., Jeon, H. B., Yoo, Y. J., Eom, S. H., & Chun, J. S. (2005). Regulation of β-catenin signaling and maintenance of chondrocyte differentiation by ubiquitin-independent proteasomal degradation of α-catenin. *Journal of Biological Chemistry*, *280*(13), 12758–12765. https://doi.org/10.1074/jbc.M413367200

Ikegami, K., & Setou, M. (2009). TTLL10 can perform tubulin glycylation when co-expressed with TTLL8. *FEBS Letters*, *583*(12), 1957–1963. https://doi.org/10.1016/j.febslet.2009.05.003

Iqbal, Z., Tawamie, H., Ba, W., Reis, A., Halak, B. al, Sticht, H., Uebe, S., Kasri, N. N., Riazuddin, S., van Bokhoven, H., & Abou Jamra, R. (2019). Loss of function of SVBP leads to autosomal recessive intellectual disability, microcephaly, ataxia, and hypotonia. *Genetics in Medicine*, *21*(8), 1790–1796. https://doi.org/10.1038/s41436-018-0415-8

Ishikawa, T. (2012). Structural biology of cytoplasmic and axonemal dyneins. In *Journal of Structural Biology* (Vol. 179, Issue 2, pp. 229–234). Academic Press. https://doi.org/10.1016/j.jsb.2012.05.016

Jäkel, S., Albig, W., Kutay, U., Bischoff, F. R., Schwamborn, K., Doenecke, D., & Görlich, D. (1999). The importin β/importin 7 heterodimer is a functional nuclear import receptor for histone H1. *EMBO Journal*, *18*(9), 2411–2423. https://doi.org/10.1093/emboj/18.9.2411

Jäkel, S., & Görlich, D. (1998). Importin β, transportin, RanBP5 and RanBP7 mediate nuclear import of ribosomal proteins in mammalian cells. *EMBO Journal*, *17*(15), 4491–4502. https://doi.org/10.1093/emboj/17.15.4491

Janke, C., & Bulinski, J. C. (2011). Post-translational regulation of the microtubule cytoskeleton: Mechanisms and functions. In *Nature Reviews Molecular Cell Biology* (Vol. 12, Issue 12, pp. 773–786). Nat Rev Mol Cell Biol. https://doi.org/10.1038/nrm3227

Janke, C., & Kneussel, M. (2010). Tubulin post-translational modifications: Encoding functions on the neuronal microtubule cytoskeleton. In *Trends in Neurosciences* (Vol. 33, Issue 8, pp. 362–372). Trends Neurosci. https://doi.org/10.1016/j.tins.2010.05.001

Janke, C., & Magiera, M. M. (2020). The tubulin code and its role in controlling microtubule properties and functions. *Nature Reviews Molecular Cell Biology*, *21*, 307–326. https://doi.org/10.1038/s41580-020-0214-3

Janke, C., Rogowski, K., & van Dijk, J. (2008). Polyglutamylation: A fine-regulator of protein function? "Protein Modifications: Beyond the Usual Suspects" Review Series. In *EMBO Reports* (Vol. 9, Issue 7, pp. 636–641). EMBO Rep. https://doi.org/10.1038/embor.2008.114

Janke, C., Rogowski, K., Wloga, D., Regnard Catherine, Kajava Andrey, Strub, J.-M., Temurak, N., van Dijk, J., Boucher, D., van Dorsselaer, A., Suryvanshi, S., Gaertig, J., & Eddé, B. (2005). Tubulin Polyglutamylase Enzymes Are Members of the TTL Domain Protein Family. *Science*, *5729*(308), 1758–1762. https://pubmed.ncbi.nlm.nih.gov/15890843/?from_term=Tubulin+Polyglutamylase+Enzymes+Are+Members+of+the+TTL+Domain+Protein+Family&from_pos=1

Joshi, H. C., & Cleveland, D. W. (1989). Differential utilization of β-tubulin isotypes in differentiating neurites. *Journal of Cell Biology*, *109*(2), 663–673. https://doi.org/10.1083/jcb.109.2.663

Kalinina, E., Biswas, R., Berezniuk, I., Hermoso, A., Avilés, F. X., & Fricker, L. D. (2007). A novel subfamily of mouse cytosolic carboxypeptidases. *The FASEB Journal*, *21*(3), 836–850. https://doi.org/10.1096/fj.06-7329com

Kalinski, A. L., Kar, A. N., Craver, J., Tosolini, A. P., Sleigh, J. N., Lee, S. J., Hawthorne, A., Brito-Vargas, P., Miller-Randolph, S., Passino, R., Shi, L., Wong, V. S. C., Picci, C., Smith, D. S., Willis, D. E., Havton, L. A., Schiavo, G., Giger, R. J., Langley, B., & Twiss, J. L. (2019). Deacetylation of Miro1 by HDAC6 blocks mitochondrial transport and mediates axon growth inhibition. *Journal of Cell Biology*, *218*(6), 1871–1890. https://doi.org/10.1083/jcb.201702187

Kanwal, C., Li, H., & Lim, C. S. (2002). Model system to study classical nuclear export signals. *AAPS PharmSci*, *4*(3). https://doi.org/10.1208/ps040318

Karakaya, M., Paketci, C., Altmueller, J., Thiele, H., Hoelker, I., Yis, U., & Wirth, B. (2019). Biallelic variant in AGTPBP1 causes infantile lower motor neuron degeneration and cerebellar atrophy. *American Journal of Medical Genetics, Part A*, *179*(8), 1580–1584. https://doi.org/10.1002/ajmg.a.61198

References

Kastner, S., Thiemann, I. J., Dekomien, G., Petrasch-Parwez, E., Schreiber, S., Akkad, D. A., Gerding, W. M., Hoffjan, S., Güneş, S., Güneş, S., Bagci, H., & Epplen, J. T. (2015). Exome sequencing reveals AGBL5 as novel candidate gene and additional variants for retinitis pigmentosa in five Turkish families. *Investigative Ophthalmology and Visual Science*, *56*(13), 8045–8053. https://doi.org/10.1167/iovs.15-17473

Kelliher, M. T., Saunders, H. A., & Wildonger, J. (2019). Microtubule control of functional architecture in neurons. *Current Opinion in Neurobiology*, *57*, 39–45. https://doi.org/10.1016/j.conb.2019.01.003

Kemmler, W., Peterson, J. D., & Steiner, D. F. (1971). Studies on the conversion of proinsulin to insulin. I. Conversion in vitro with trypsin and carboxypeptidase B. *Journal of Biological Chemistry*, *246*(22), 6786–6791. https://doi.org/10.1016/S0021-9258(19)45914-0

Khan, S. U., Khan, M. Z., Asad, Z. U. A., Valavoor, S., Khan, M. U., Khan, M. S., Krupica, T., Alkhouli, M., & Kaluski, E. (2020). Efficacy and safety of low dose rivaroxaban in patients with coronary heart disease: a systematic review and meta-analysis. *Journal of Thrombosis and Thrombolysis*. https://doi.org/10.1007/s11239-020-02114-7

Kilshtain-Vardi, A., Glick, M., Greenblatt, H. M., Goldblum, A., & Shoham, G. (2003). Refined structure of bovine carboxypeptidase A at 1.25 Å, resolution. *Acta Crystallographica - Section D Biological Crystallography*, *59*(2), 323–333. https://doi.org/10.1107/S0907444902015706

Kim, D. I., Jensen, S. C., & Roux, K. J. (2016). Identifying protein-protein associations at the nuclear envelope with bioid. In *Methods in Molecular Biology* (Vol. 1411, pp. 133–146). Methods Mol Biol. https://doi.org/10.1007/978-1-4939-3530-7_8

Kim, J., Lee, J. E., Heynen-Genel, S., Suyama, E., Ono, K., Lee, K., Ideker, T., Aza-Blanc, P., & Gleeson, J. G. (2010). Functional genomic screen for modulators of ciliogenesis and cilium length. *Nature*, *464*(7291), 1048–1051. https://doi.org/10.1038/nature08895

Kim, K., Lee, K., & Rhee, K. (2012). CEP90 Is Required for the Assembly and Centrosomal Accumulation of Centriolar Satellites, Which Is Essential for Primary Cilia Formation. *PLoS ONE*, *7*(10). https://doi.org/10.1371/journal.pone.0048196

Kim, K., & Rhee, K. (2011). The pericentriolar satellite protein CEP90 is crucial for integrity of the mitotic spindle pole. *Journal of Cell Science*, *124*(3), 338–347. https://doi.org/10.1242/jcs.078329

Kimura, Y., Kurabe, N., Ikegami, K., Tsutsumi, K., Konishi, Y., Kaplan, O. I., Kunitomo, H., Iino, Y., Blacque, O. E., & Setou, M. (2010). Identification of tubulin deglutamylase among Caenorhabditis elegans and mammalian cytosolic carboxypeptidases (CCPs). *Journal of Biological Chemistry*, *285*(30), 22936–22941. https://doi.org/10.1074/jbc.C110.128280

King, J. v., Liang, W. G., Scherpelz, K. P., Schilling, A. B., Meredith, S. C., & Tang, W. J. (2014). Molecular basis of substrate recognition and degradation by human presequence protease. *Structure*, *22*(7), 996–1007. https://doi.org/10.1016/j.str.2014.05.003

Koberna, K., Malínský, J., Pliss, A., Mašata, M., Večeřová, J., Fialová, M., Bednár, J., & Raška, I. (2002). Ribosomal genes in focus new transcripts label the dense fibrillar components and form clusters indicative of "Christmas trees" in situ. *Journal of Cell Biology*, *157*(5), 743–748. https://doi.org/10.1083/JCB.200202007

Korecka, J. A., van Kesteren, R. E., Blaas, E., Spitzer, S. O., Kamstra, J. H., Smit, A. B., Swaab, D. F., Verhaagen, J., & Bossers, K. (2013). Phenotypic Characterization of Retinoic Acid Differentiated SH-SY5Y Cells by Transcriptional Profiling. *PLoS ONE*, *8*(5), e63862. https://doi.org/10.1371/journal.pone.0063862

Kreiner, G., Bierhoff, H., Armentano, M., Rodriguez-Parkitna, J., Sowodniok, K., Naranjo, J. R., Bonfanti, L., Liss, B., Schütz, G., Grummt, I., & Parlato, R. (2013). A neuroprotective phase precedes striatal degeneration upon nucleolar stress. *Cell Death and Differentiation*, *20*(11), 1455–1464. https://doi.org/10.1038/cdd.2013.66

Kubo, A., Sasaki, H., Yuba-Kubo, A., Tsukita, S., & Shiina, N. (1999). Centriolar satellites: molecular characterization, ATP-dependent movement toward centrioles and possible involvement in ciliogenesis. *The Journal of Cell Biology*, *147*(5), 969–979. https://doi.org/10.1083/JCB.147.5.969

Kubo, T., Yanagisawa, H. aki, Yagi, T., Hirono, M., & Kamiya, R. (2010). Tubulin Polyglutamylation Regulates Axonemal Motility by Modulating Activities of Inner-Arm Dyneins. *Current Biology*, *20*(5), 441–445. https://doi.org/10.1016/j.cub.2009.12.058

Kwon, K., & Beckett, D. (2000). Function of a conserved sequence motif in biotin holoenzyme synthetases. *Protein Science*, *9*(8), 1530–1539. https://doi.org/10.1110/PS.9.8.1530

Kyuhou, S., Kato, N., & Gemba, H. (2006). Emergence of endoplasmic reticulum stress and activated microglia in Purkinje cell degeneration mice. *Neuroscience Letters*, *396*(2), 91–96. https://doi.org/10.1016/j.neulet.2005.11.023

Lachmann, M., Gelbmann, D., Kálmán, E., Polgár, B., Buschle, M., von Gabain, A., Szekeres-Barthó, J., & Nagy, E. (2004). PIBF (progesterone induced blocking factor) is overexpressed in highly proliferating cells and associated with the centrosome. *International Journal of Cancer*, *112*(1), 51–60. https://doi.org/10.1002/ijc.20326

Lacroix, B., van Dijk, J., Gold, N. D., Guizetti, J., Aldrian-Herrada, G., Rogowski, K., Gerlich, D. W., & Janke, C. (2010). Tubulin polyglutamylation stimulates spastin-mediated microtubule severing. *Journal of Cell Biology*, *189*(6), 945–954. https://doi.org/10.1083/jcb.201001024

Lafanechère, L., & Job, D. (2000). The third tubulin pool. *Neurochemical Research*, *25*(1), 11–18. https://doi.org/10.1023/A:1007575012904

References

Lambert, J. P., Tucholska, M., Go, C., Knight, J. D. R., & Gingras, A. C. (2015). Proximity biotinylation and affinity purification are complementary approaches for the interactome mapping of chromatin-associated protein complexes. *Journal of Proteomics*, *118*, 81–94. https://doi.org/10.1016/j.jprot.2014.09.011

Lan, H., Suzuki, H., Nagatake, T., Hosomi, K., Ikegami, K., Setou, M., & Kunisawa, J. (2020). Impaired mucociliary motility enhances antigen-specific nasal IgA immune responses to a cholera toxin-based nasal vaccine. *International Immunology*. https://doi.org/10.1093/intimm/dxaa029

Landis, S. C., & Mullen, R. J. (1978). The development and degeneration of Purkinje cells in pcd mutant mice. *The Journal of Comparative Neurology*, *177*(1), 125–143. https://doi.org/10.1002/cne.901770109

Latour, B. L., van de Weghe, J. C., Rusterholz, T. D. S., Letteboer, S. J. F., Gomez, A., Shaheen, R., Gesemann, M., Karamzade, A., Asadollahi, M., Barroso-Gil, M., Chitre, M., Grout, M. E., van Reeuwijk, J., van Beersum, S. E. C., Miller, C. v., Dempsey, J. C., Morsy, H., Bamshad, M. J., Nickerson, D. A., … Doherty, D. (2020). Dysfunction of the ciliary ARMC9/TOGARAM1 protein module causes Joubert syndrome. *Journal of Clinical Investigation*, *140*(8), 4423–4439. https://doi.org/10.1172/JCI131656

Lee, J. E., & Gleeson, J. G. (2011). Cilia in the nervous system: Linking cilia function and neurodevelopmental disorders. *Current Opinion in Neurology*, *24*(2), 98–105. https://doi.org/10.1097/WCO.0b013e3283444d05

Lessard, F., Morin, F., Ivanchuk, S., Langlois, F., Stefanovsky, V., Rutka, J., & Moss, T. (2010). The ARF Tumor Suppressor Controls Ribosome Biogenesis by Regulating the RNA Polymerase I Transcription Factor TTF-I. *Molecular Cell*, *38*(4), 539–550. https://doi.org/10.1016/j.molcel.2010.03.015

Lewis, S. A., Lee, M. G. S., & Cowan, N. J. (1985). Five mouse tubulin isotypes and their regulated expression during development. *Journal of Cell Biology*, *101*(3), 852–861. https://doi.org/10.1083/jcb.101.3.852

Li, C., Wang, J., Hao, J., Dong, B., Li, Y., Zhu, X., Ding, J., Ren, S., Zhao, H., Wu, S., Tian, Y., & Wang, G. Q. (2016). Reduced cytosolic carboxypeptidase 6 (CCP6) level leads to accumulation of serum polyglutamylated DNAJC7 protein: A potential biomarker for renal cell carcinoma early detection. *Oncotarget*, *7*(16), 22385–22396. https://doi.org/10.18632/oncotarget.8107

Li, J., Gu, X., Ma, Y., Calicchio, M. L., Kong, D., Teng, Y. D., Yu, L., Crain, A. M., Vartanian, T. K., Pasqualini, R., Arap, W., Libermann, T. A., Snyder, E. Y., & Sidman, R. L. (2010). Nna1 mediates Purkinje cell dendritic development via lysyl oxidase propeptide and NF-κB signaling. *Neuron*, *68*(1), 45–60. https://doi.org/10.1016/j.neuron.2010.08.013

Liang, C. C., Park, A. Y., & Guan, J. L. (2007). In vitro scratch assay: A convenient and inexpensive method for analysis of cell migration in vitro. *Nature Protocols*, *2*(2), 329–333. https://doi.org/10.1038/nprot.2007.30

Lindemann, C. B., & Lesich, K. A. (2010). Flagellar and ciliary beating: The proven and the possible. *Journal of Cell Science*, *123*(4), 519–528. https://doi.org/10.1242/jcs.051326

Liu, B., Ye, B., Zhu, X., Huang, G., Yang, L., Zhu, P., Du, Y., Wu, J., Meng, S., Tian, Y., & Fan, Z. (2017). IL-7Rα glutamylation and activation of transcription factor Sall3 promote group 3 ILC development. *Nature Communications*, *8*(1). https://doi.org/10.1038/s41467-017-00235-x

Loncarek, J., & Bettencourt-Dias, M. (2018). Building the right centriole for each cell type. *Journal of Cell Biology*, *217*(3), 823–835. https://doi.org/10.1083/JCB.201704093

Long, H., & Huang, K. (2020). Transport of Ciliary Membrane Proteins. In *Frontiers in Cell and Developmental Biology* (Vol. 7, p. 381). Frontiers. https://doi.org/10.3389/fcell.2019.00381

López-Otín, C., & Overall, C. M. (2002). Protease degradomics: A new challenge for proteomics. In *Nature Reviews Molecular Cell Biology* (Vol. 3, Issue 7, pp. 509–519). Nat Rev Mol Cell Biol. https://doi.org/10.1038/nrm858

Lyons, P. J., Callaway, M. B., & Fricker, L. D. (2008). Characterization of carboxypeptidase A6, an extracellular matrix peptidase. *Journal of Biological Chemistry*, *283*(11), 7054–7063. https://doi.org/10.1074/jbc.M707680200

Lyons, P. J., Sapio, M. R., & Fricker, L. D. (2013). Zebrafish cytosolic carboxypeptidases 1 and 5 are essential for embryonic development. *Journal of Biological Chemistry*, *288*(42), 30454–30462. https://doi.org/10.1074/jbc.M113.497933

Madhurantakam, C., Varadamsetty, G., Grütter, M. G., Plückthun, A., & Mittl, P. R. E. (2012). Structure-based optimization of designed Armadillo-repeat proteins. *Protein Science*, *21*(7), 1015–1028. https://doi.org/10.1002/pro.2085

Magiera, M. M., Bodakuntla, S., Žiak, J., Lacomme, S., Marques Sousa, P., Leboucher, S., Hausrat, T. J., Bosc, C., Andrieux, A., Kneussel, M., Landry, M., Calas, A., Balastik, M., & Janke, C. (2018). Excessive tubulin polyglutamylation causes neurodegeneration and perturbs neuronal transport. *The EMBO Journal*, *37*(23). https://doi.org/10.15252/embj.2018100440

Magiera, M. M., & Janke, C. (2013). Investigating tubulin posttranslational modifications with specific antibodies. In *Methods in Cell Biology* (Vol. 115, pp. 247–267). Methods Cell Biol. https://doi.org/10.1016/B978-0-12-407757-7.00016-5

Maiato, H., & Logarinho, E. (2014). Mitotic spindle multipolarity without centrosome amplification. *Nature Cell Biology 2014 16:5*, *16*(5), 386–394. https://doi.org/10.1038/NCB2958

Maimouni, S., Lee, M. H., Sung, Y. M., Hall, M., Roy, A., Ouaari, C., Hwang, Y. S., Spivak, J., Glasgow, E., Swift, M., Patel, J., Cheema, A., Kumar, D., & Byers, S. (2019). Tumor suppressor RARRES1 links tubulin deglutamylation to mitochondrial metabolism and

cell survival. *Oncotarget*, *10*(17), 1606–1624. https://doi.org/10.18632/oncotarget.26600

Mandelkow, E., & Mandelkow, E. M. (1995). Microtubules and microtubule-associated proteins. *Current Opinion in Cell Biology*, *7*(1), 72–81. https://doi.org/10.1016/0955-0674(95)80047-6

Mansfield, S. G., & Gordon-Weeks, P. R. (1991). Dynamic post-translational modification of tubulin in rat cerebral cortical neurons extending neurites in culture: Effects of taxol. *Journal of Neurocytology*, *20*(8), 654–666. https://doi.org/10.1007/BF01187067

Mariani, M., Karki, R., Spennato, M., Pandya, D., He, S., Andreoli, M., Fiedler, P., & Ferlini, C. (2015). Clas- III β-tubulin in normal and cancer tissues. In *Gene* (Vol. 563, Issue 2, pp. 109–114). Elsevier. https://doi.org/10.1016/j.gene.2015.03.061

McKean, P. G., Vaughan, S., & Gull, K. (2001). The extended tubulin superfamily. *Journal of Cell Science*, *114*(15), 2723–2733.

McKinnon, P. J. (2004). ATM and ataxia telangiectasia. *EMBO Reports*, *5*(8), 772–776. https://doi.org/10.1038/SJ.EMBOR.7400210

Meghwanshi, G. K., Kaur, N., Verma, S., Dabi, N. K., Vashishtha, A., Charan, P. D., Purohit, P., Bhandari, H. S., Bhojak, N., & Kumar, R. (2020). Enzymes for pharmaceutical and therapeutic applications. *Biotechnology and Applied Biochemistry*, *67*(4), 586–601. https://doi.org/10.1002/BAB.1919

Mellacheruvu, D., Wright, Z., Couzens, A. L., Lambert, J.-P., St-Denis, N. A., Li, T., Miteva, Y. V, Hauri, S., Sardiu, M. E., Low, T. Y., Halim, V. A., Bagshaw, R. D., Hubner, N. C., al-Hakim, A., Bouchard, A., Faubert, D., Fermin, D., Dunham, W. H., Goudreault, M., … Nesvizhskii, A. I. (2013). The CRAPome: a contaminant repository for affinity purification–mass spectrometry data. *Nature Methods 2013 10:8*, *10*(8), 730–736. https://doi.org/10.1038/nmeth.2557

Meyer, M. A. (2014). Highly expressed genes in human high grade gliomas: Immunohistochemical analysis of data from the Human Protein Atlas. *Neurology International*, *6*(2), 5348. https://doi.org/10.4081/ni.2014.5348

Miller, K. E., & Heald, R. (2015). Glutamylation of Nap1 modulates histone H1 dynamics and chromosome condensation in Xenopus. *Journal of Cell Biology*, *209*(2), 211–220. https://doi.org/10.1083/jcb.201412097

Mirvis, M., Stearns, T., & James Nelson, W. (2018). Cilium structure, assembly, and disassembly regulated by the cytoskeleton. *Biochemical Journal*, *475*(14), 2329–2353. https://doi.org/10.1042/BCJ20170453

Misteli, T., Cáceres, J. F., & Spector, D. L. (1997). The dynamics of a pre-mRNA splicing factor in living cells. *Nature*, *387*(6632), 523–527. https://doi.org/10.1038/387523a0

Morley, S. J., Qi, Y., Iovino, L., Andolfi, L., Guo, D., Kalebic, N., Castaldi, L., Tischer, C., Portulano, C., Bolasco, G., Shirlekar, K., Fusco, C. M., Asaro, A., Fermani, F., Sundukova, M., Matti, U., Reymond, L., de Ninno, A., Businaro, L., … Heppenstall, P. A. (2016). Acetylated tubulin is essential for touch sensation in mice. *ELife*, *5*(DECEMBER2016), 25. https://doi.org/10.7554/eLife.20813

Moskowitz, P. F., & Oblinger, M. M. (1995). Sensory neurons selectively upregulate synthesis and transport of the β(III)-tubulin protein during axonal regeneration. *Journal of Neuroscience*, *15*(2), 1545–1555. https://doi.org/10.1523/jneurosci.15-02-01545.1995

Mullen, R., Eicher, E., & Sidman, R. (1976). Purkinje cell degeneration, a new neurological mutation in the mouse. *Proceedings of the National Academy of Sciences of the United States of America*, *73*(1), 208–212. https://doi.org/10.1073/pnas.73.1.208

Murphy, G., & Nagase, H. (2008). Reappraising metalloproteinases in rheumatoid arthritis and osteoarthritis: Destruction or repair? In *Nature Clinical Practice Rheumatology* (Vol. 4, Issue 3, pp. 128–135). Nat Clin Pract Rheumatol. https://doi.org/10.1038/ncprheum0727

Nalivaeva, N., Fisk, L., Belyaev, N., & Turner, A. (2008). Amyloid-Degrading Enzymes as Therapeutic Targets in Alzheimers Disease. *Current Alzheimer Research*, *5*(2), 212–224. https://doi.org/10.2174/156720508783954785

Nehlig, A., Molina, A., Rodrigues-Ferreira, S., Honoré, S., & Nahmias, C. (2017). Regulation of end-binding protein EB1 in the control of microtubule dynamics. In *Cellular and Molecular Life Sciences* (Vol. 74, Issue 13, pp. 2381–2393). Birkhauser Verlag AG. https://doi.org/10.1007/s00018-017-2476-2

Niwa, S., Takahashi, H., & Hirokawa, N. (2013). β-Tubulin mutations that cause severe neuropathies disrupt axonal transport. *EMBO Journal*, *32*(10), 1352–1364. https://doi.org/10.1038/emboj.2013.59

O'Hagan, R., Piasecki, B. P., Silva, M., Phirke, P., Nguyen, K. C. Q., Hall, D. H., Swoboda, P., & Barr, M. M. (2011). The tubulin deglutamylase CCPP-1 regulates the function and stability of sensory cilia in C. elegans. *Current Biology*, *21*(20), 1685–1694. https://doi.org/10.1016/j.cub.2011.08.049

Okada, M., Hozumi, Y., Ichimura, T., Tanaka, T., Hasegawa, H., Yamamoto, M., Takahashi, N., Iseki, K., Yagisawa, H., Shinkawa, T., Isobe, T., & Goto, K. (2011). Interaction of nucleosome assembly proteins abolishes nuclear localization of DGKζ by attenuating its association with importins. *Experimental Cell Research*, *317*(20), 2853–2863. https://doi.org/10.1016/J.YEXCR.2011.09.014

Okada, Y., Takeda, S., Tanaka, Y., Belmonte, J. C. I., & Hirokawa, N. (2005). Mechanism of nodal flow: A conserved symmetry breaking event in left-right axis determination. *Cell*, *121*(4), 633–644. https://doi.org/10.1016/j.cell.2005.04.008

References

Ori-McKenney, K. M., McKenney, R. J., Huang, H. H., Li, T., Meltzer, S., Jan, L. Y., Vale, R. D., Wiita, A. P., & Jan, Y. N. (2016). Phosphorylation of β-Tubulin by the Down Syndrome Kinase, Minibrain/DYRK1a, Regulates Microtubule Dynamics and Dendrite Morphogenesis. *Neuron*, *90*(3), 551–563. https://doi.org/10.1016/j.neuron.2016.03.027

Otero, A. (2014). *Characterization of two metallocarboxypeptidases of M14D subfamily from bacterial and human origin*.

Otero, A., Rodríguez de la Vega, M., Tanco, S., Lorenzo, J., Avilés, F. X., & Reverter, D. (2012). The novel structure of a cytosolic M14 metallocarboxypeptidase (CCP) from Pseudomonas aeruginosa : a model for mammalian CCPs. *The FASEB Journal*, *26*(9), 3754–3764. https://doi.org/10.1096/fj.12-209601

Pala, R., Alomari, N., & Nauli, S. M. (2017). Primary cilium-dependent signaling mechanisms. In *International Journal of Molecular Sciences* (Vol. 18, Issue 11). Int J Mol Sci. https://doi.org/10.3390/ijms18112272

Parisi, M. A. (2009). Clinical and molecular features of Joubert syndrome and related disorders. In *American Journal of Medical Genetics, Part C: Seminars in Medical Genetics* (Vol. 151, Issue 4, pp. 326–340). Am J Med Genet C Semin Med Genet. https://doi.org/10.1002/ajmg.c.30229

Patel, N., Aldahmesh, M. A., Alkuraya, H., Anazi, S., Alsharif, H., Khan, A. O., Sunker, A., Al-mohsen, S., Abboud, E. B., Nowilaty, S. R., Alowain, M., Al-Zaidan, H., Al-Saud, B., Alasmari, A., Abdel-Salam, G. M. H., Abouelhoda, M., Abdulwahab, F. M., Ibrahim, N., Naim, E., … Alkuraya, F. S. (2016). Expanding the clinical, allelic, and locus heterogeneity of retinal dystrophies. *Genetics in Medicine*, *18*(6), 554–562. https://doi.org/10.1038/gim.2015.127

Pathak, N., Austin-Tse, C. A., Liu, Y., Vasilyev, A., & Drummond, I. A. (2014). Cytoplasmic carboxypeptidase 5 regulates tubulin glutamylation and zebrafish cilia formation and function. *Molecular Biology of the Cell*, *25*(12), 1836–1844. https://doi.org/10.1091/mbc.E13-01-0033

Paturle-Lafanechère, L., Manier, M., Trigault, N., Pirollet, F., Mazarguil, H., & Job, D. (1994). Accumulation of delta 2-tubulin, a major tubulin variant that cannot be tyrosinated, in neuronal tissues and in stable microtubule assemblies. *Journal of Cell Science*, *107*(6), 1529–1543.

Paulson, H. L., & Miller, V. M. (2005). Breaks in Coordination: DNA Repair in Inherited Ataxia. *Neuron*, *46*(6), 845–848. https://doi.org/10.1016/J.NEURON.2005.05.025

Pejler, G., Knight, S. D., Henningsson, F., & Wernersson, S. (2009). Novel insights into the biological function of mast cell carboxypeptidase A. In *Trends in Immunology* (Vol. 30, Issue 8, pp. 401–408). Trends Immunol. https://doi.org/10.1016/j.it.2009.04.008

Peterfi, L., Banyai, D., Yusenko, M. V., Bjercke, T., & Kovacs, G. (2020). Expression of RARRES1 and AGBL2 and progression of conventional renal cell carcinoma. *British Journal of Cancer*, *122*(12), 1818–1824. https://doi.org/10.1038/s41416-020-0798-6

Poole, C. A., Flint, M. H., & Beaumont, B. W. (1985). Analysis of the morphology and function of primary cilia in connective tissues:A cellular cybernetic probe? *Cell Motility*, *5*(3), 175–193. https://doi.org/10.1002/cm.970050302

Prosser, S. L., & Pelletier, L. (2017). Mitotic spindle assembly in animal cells: A fine balancing act. In *Nature Reviews Molecular Cell Biology* (Vol. 18, Issue 3, pp. 187–201). Nature Publishing Group. https://doi.org/10.1038/nrm.2016.162

Puente, X. S., Sánchez, L. M., Gutiérrez-Fernández, A., Velasco, G., & López-Otín, C. (2005). A genomic view of the complexity of mammalian proteolytic systems. *Biochemical Society Transactions*, *33*(2), 331–334. https://doi.org/10.1042/BST0330331

Pumroy, R. A., & Cingolani, G. (2015). Diversification of importin-α isoforms in cellular trafficking and. In *Biochemical Journal* (Vol. 466, Issue 1, pp. 13–28). Portland Press Ltd. https://doi.org/10.1042/BJ20141186

Puvion-Dutilleul, F., Mazan, S., Nicoloso, M., Pichard, E., Bachellerie, J. P., & Puvion, E. (1992). Alterations of nucleolar ultrastructure and ribosome biogenesis by actinomycin D. Implications for U3 snRNP function. *European Journal of Cell Biology*, *58*(1), 149–162. https://europepmc.org/article/med/1386570

Qiao, H., Li, Y., Feng, C., Duo, S., Ji, F., & Jiao, J. (2018). Nap1l1 Controls Embryonic Neural Progenitor Cell Proliferation and Differentiation in the Developing Brain. *Cell Reports*, *22*(9), 2279–2293. https://doi.org/10.1016/j.celrep.2018.02.019

Ramamurthy, V., & Cayouette, M. (2009). Development and disease of the photoreceptor cilium. In *Clinical Genetics* (Vol. 76, Issue 2, pp. 137–145). Clin Genet. https://doi.org/10.1111/j.1399-0004.2009.01240.x

Rani, K., Rana, R., & Datt, S. (2012). Review on latest overview of proteases. *International Journal of Current Life Sciences*, *2*(1), 12–18. https://www.researchgate.net/publication/265865007

Rao, K. N., Anand, M., & Khanna, H. (2016). The carboxyl terminal mutational hotspot of the ciliary disease protein RPGRORF15 (retinitis pigmentosa GTPase regulator) is glutamylated in vivo. *Biology Open*, *5*(4), 424–428. https://doi.org/10.1242/bio.016816

Raška, I., Koberna, K., Malínský, J., Fidlerová, H., & Mašata, M. (2004). The nucleolus and transcription of ribosomal genes. *Biology of the Cell*, *96*(8), 579–594. https://doi.org/10.1016/J.BIOLCEL.2004.04.015

References

Rawlings, N. (2020). Twenty-five years of nomenclature and classification of proteolytic enzymes. *Biochimica et Biophysica Acta - Proteins and Proteomics*, *1868*(2). https://doi.org/10.1016/j.bbapap.2019.140345

Rawlings, N., & Barrett, A. (1993). Evolutionary families of peptidases. *Biochemical Journal*, *290*(1), 205–218. https://doi.org/10.1042/bj2900205

Rawlings, N., & Barrett, A. (1999). MEROPS: The Peptidase Database. *Nucleic Acid Research*, *27*(1), 325–331. https://pubmed.ncbi.nlm.nih.gov/9847218/?from_term=MEROPS%3A+the+peptidase+database&from_pos=8

Rawlings, N., Barrett, A., & Bateman, A. (2011). Asparagine peptide lyases: A seventh catalytic type of proteolytic enzymes. *Journal of Biological Chemistry*, *286*(44), 38321–38328. https://doi.org/10.1074/jbc.M111.260026

Rawlings, N., & Salvesen, G. (2013). Handbook of Proteolytic Enzymes. In *Handbook of Proteolytic Enzymes* (Vols. 1–3). Elsevier Ltd. https://doi.org/10.1016/C2009-1-60990-4

Rawlings, N., Tolle, D., & Barrett, A. (2004). Evolutionary families of peptidase inhibitors. *Biochemical Journal*, *378*(3), 705–716. https://doi.org/10.1042/BJ20031825

Rawlings, N., Waller, M., Barrett, A., & Bateman, A. (2014). MEROPS: the database of proteolytic enzymes, their substrates and inhibitors. *Nucleic Acid Research*, *42*(1), 503–509. https://doi.org/10.1093/nar/gkt953

Redeker, V., Levilliers, N., Schmitter, J. M., le Caer, J. P., Rossier, J., Adoutte, A., & Bré, M. H. (1994). Polyglycylation of tubulin: A posttranslational modification in axonemal microtubules. *Science*, *266*(5191), 1688–1691. https://doi.org/10.1126/science.7992051

Regnard, C., Desbruyères, E., Denoulet, P., & Eddé, B. (1999). Tubulin polyglutamylase: isozymic variants and regulation during the cell cycle in HeLa cells. *Journal of Cell Science*, *112 (Pt 2*, 4281–4289. http://www.ncbi.nlm.nih.gov/pubmed/10564646

Regnard, C., Desbruyères, E., Huet, J. C., Beauvallet, C., Pernollet, J. C., & Eddé, B. (2000). Polyglutamylation of nucleosome assembly proteins. *The Journal of Biological Chemistry*, *275*(21), 15969–15976. https://doi.org/10.1074/jbc.M000045200

Reznik, S. E., & Fricker, L. D. (2001). Carboxypeptidases from A to Z: Implications in embryonic development and Wnt binding. In *Cellular and Molecular Life Sciences* (Vol. 58, Issues 12–13, pp. 1790–1804). Birkhauser Verlag Basel. https://doi.org/10.1007/PL00000819

Rhee, H. W., Zou, P., Udeshi, N. D., Martell, J. D., Mootha, V. K., Carr, S. A., & Ting, A. Y. (2013). Proteomic mapping of mitochondria in living cells via spatially restricted

enzymatic tagging. *Science*, *339*(6125), 1328–1331. https://doi.org/10.1126/science.1230593

Riazuddin, S. A., Vasanth, S., Katsanis, N., & Gottsch, J. D. (2013). Mutations in AGBL1 cause dominant late-onset Fuchs corneal dystrophy and alter protein-protein interaction with TCF4. *American Journal of Human Genetics*, *93*(4), 758–764. https://doi.org/10.1016/j.ajhg.2013.08.010

Rimsa, V., Eadsforth, T. C., Joosten, R. P., & Hunter, W. N. (2014). High-resolution structure of the M14-type cytosolic carboxypeptidase from Burkholderia cenocepacia refined exploiting PDB-REDO strategies. *Acta Crystallographica Section D: Biological Crystallography*, *70*(2), 279–289. https://doi.org/10.1107/S1399004713026801

Robak, P., & Robak, T. (2019). Bortezomib for the Treatment of Hematologic Malignancies: 15 Years Later. In *Drugs in R and D* (Vol. 19, Issue 2, pp. 73–92). Springer International Publishing. https://doi.org/10.1007/s40268-019-0269-9

Rodríguez de la Vega, M., Lorenzo, J., Tort, O., Avilés, F. X., & Bautista, J. M. (2013). Functional segregation and emerging role of cilia-related cytosolic carboxypeptidases (CCPs). *FASEB Journal*, *27*(2), 424–431. https://doi.org/10.1096/fj.12-209080

Rodriguez de la Vega, M., Sevilla, R. G., Hermoso, A., Lorenzo, J., Tanco, S., Diez, A., Fricker, L. D., Bautista, J. M., & Avilés, F. X. (2007). Nna1-like proteins are active metallocarboxypeptidases of a new and diverse M14 subfamily. *The FASEB Journal*, *21*(3), 851–865. https://doi.org/10.1096/fj.06-7330com

Rodriguez, P., Munroe, D., Prawitt, D., Chu, L. L., Bric, E., Kim, J., Reid, L. H., Davies, C., Nakagama, H., Loebbert, R., Winterpacht, A., Petruzzi, M. J., Higgins, M. J., Nowak, N., Evans, G., Shows, T., Weissman, B. E., Zabel, B., Housman, D. E., & Pelletier, J. (1997). Functional characterization of human nucleosome assembly protein-2 (NAP1L4) suggests a role as a histone chaperone. *Genomics*, *44*(3), 253–265. https://doi.org/10.1006/geno.1997.4868

Rodriguez, P., Ruiz, M. T., Price, G. B., & Zannis-Hadjopoulos, M. (2004). NAP-2 is part of multi-protein complexes in Hela cells. *Journal of Cellular Biochemistry*, *93*(2), 398–408. https://doi.org/10.1002/JCB.20163

Rogowski, K., Juge, F., van Dijk, J., Wloga, D., Strub, J. M., Levilliers, N., Thomas, D., Bré, M. H., van Dorsselaer, A., Gaertig, J., & Janke, C. (2009). Evolutionary Divergence of Enzymatic Mechanisms for Posttranslational Polyglycylation. *Cell*, *137*(6), 1076–1087. https://doi.org/10.1016/j.cell.2009.05.020

Rogowski, K., van Dijk, J., Magiera, M. M., Bosc, C., Deloulme, J. C., Bosson, A., Peris, L., Gold, N. D., Lacroix, B., Bosch Grau, M., Bec, N., Larroque, C., Desagher, S., Holzer, M., Andrieux, A., Moutin, M. J., & Janke, C. (2010). A family of protein-deglutamylating enzymes associated with neurodegeneration. *Cell*, *143*(4), 564–578. https://doi.org/10.1016/j.cell.2010.10.014

References

Ross, P. L., Cheng, I., Liu, X., Cicek, M. S., Carroll, P. R., Casey, G., & Witte, J. S. (2009). Carboxypeptidase 4 gene variants and early-onset intermediate-to-high risk prostate cancer. *BMC Cancer*, *9*. https://doi.org/10.1186/1471-2407-9-69

Roux, K. J., Kim, D. I., Raida, M., & Burke, B. (2012). A promiscuous biotin ligase fusion protein identifies proximal and interacting proteins in mammalian cells. *The Journal of Cell Biology*, *196*(6), 801–810. https://doi.org/10.1083/jcb.201112098

Rusconi, F., Potier, M. C., le Caer, J. P., Schmitter, J. M., & Rossier, J. (1997). Characterization of the chicken telokin heterogeneity by time-of-flight mass spectrometry. *Biochemistry*, *36*(36), 11021–11026. https://doi.org/10.1021/BI970752E

Saillour, Y., Broix, L., Bruel-Jungerman, E., Lebrun, N., Muraca, G., Rucci, J., Poirier, K., Belvindrah, R., Francis, F., & Chelly, J. (2014). Beta tubulin isoforms are not interchangeable for rescuing impaired radial migration due to Tubb3 knockdown. *Human Molecular Genetics*, *23*(6), 1516–1526. https://doi.org/10.1093/hmg/ddt538

Satir, P., & Christensen, S. T. (2007). Overview of structure and function of mammalian cilia. In *Annual Review of Physiology* (Vol. 69, pp. 377–400). Annual Reviews. https://doi.org/10.1146/annurev.physiol.69.040705.141236

Schechter, I., & Berger, A. (1967). On the size of the active site in proteases. I. Papain. *Biochemical and Biophysical Research Communications*, *27*(2), 157–162. https://doi.org/10.1016/S0006-291X(67)80055-X

Schilling, O., Huesgen, P. F., Barré, O., Auf Dem Keller, U., & Overall, C. M. (2011). Characterization of the prime and non-prime active site specificities of proteases by proteome-derived peptide libraries and tandem mass spectrometry. *Nature Protocols*, *6*(1), 111–120. https://doi.org/10.1038/nprot.2010.178

Schmidt, T. G. M., & Skerra, A. (2007). The Strep-tag system for one-step purification and high-affinity detection or capturing of proteins. *Nature Protocols*, *2*(6), 1528–1535. https://doi.org/10.1038/nprot.2007.209

Scholey, J. M. (2008). Intraflagellar transport motors in cilia: moving along the cell's antenna. *Journal of Cell Biology*, *180*(1), 23–29. https://doi.org/10.1083/JCB.200709133

Shang, Y., Li, B., & Gorovsky, M. A. (2002). Tetrahymena thermophila contains a conventional γ-tubulin that is differentially required for the maintenance of different microtubule-organizing centers. *Journal of Cell Biology*, *158*(7), 1195–1206. https://doi.org/10.1083/jcb.200205101

Shashi, V., Magiera, M. M., Klein, D., Zaki, M., Schoch, K., Rudnik-Schöneborn, S., Norman, A., Lopes Abath Neto, O., Dusl, M., Yuan, X., Bartesaghi, L., de Marco, P., Alfares, A. A., Marom, R., Arold, S. T., Guzmán-Vega, F. J., Pena, L. D., Smith, E. C., Steinlin, M., … Senderek, J. (2018). Loss of tubulin deglutamylase CCP 1 causes infantile-onset neurodegeneration. *The EMBO Journal*, *37*(23). https://doi.org/10.15252/embj.2018100540

Sheffer, R., Gur, M., Brooks, R., Salah, S., Daana, M., Fraenkel, N., Eisenstein, E., Rabie, M., Nevo, Y., Jalas, C., Elpeleg, O., Edvardson, S., & Harel, T. (2019). Biallelic variants in AGTPBP1, involved in tubulin deglutamylation, are associated with cerebellar degeneration and motor neuropathy. *European Journal of Human Genetics*, 1. https://doi.org/10.1038/s41431-019-0400-y

Sia, P. I., Wood, J. P. M. M., Chidlow, G., Sharma, S., Craig, J., & Casson, R. J. (2016). Role of the nucleolus in neurodegenerative diseases with particular reference to the retina: A review. *Clinical and Experimental Ophthalmology*, *44*(3), 188–195. https://doi.org/10.1111/ceo.12661

Singla, V., Romaguera-Ros, M., Garcia-Verdugo, J. M., & Reiter, J. F. (2010). Ofd1, a Human Disease Gene, Regulates the Length and Distal Structure of Centrioles. *Developmental Cell*, *18*(3), 410–424. https://doi.org/10.1016/j.devcel.2009.12.022

Sirajuddin, M., Rice, L. M., & Vale, R. D. (2014). Regulation of microtubule motors by tubulin isotypes and post-translational modifications. *Nature Cell Biology*, *16*(4), 335–344. https://doi.org/10.1038/ncb2920

Sobell, H. M. (1985). Actinomycin and DNA transcription. *Proceedings of the National Academy of Sciences*, *82*(16), 5328–5331. https://doi.org/10.1073/PNAS.82.16.5328

Sperry, R. W. (1963). Chemoaffinity in the orderly growth of nerve fiber pattern and connections. *Proceedings of the National Academy of Sciences of the United States of America*, *50*(4), 703–710. https://doi.org/10.1073/pnas.50.4.703

Srsen, V., Gnadt, N., Dammermann, A., & Merdes, A. (2006). Inhibition of centrosome protein assembly leads to p53-dependent exit from the cell cycle. *Journal of Cell Biology*, *174*(5), 625–630. https://doi.org/10.1083/jcb.200606051

Sui, H., & Downing, K. H. (2010). Structural basis of interprotofilament interaction and lateral deformation of microtubules. *Structure*, *18*(8), 1022–1031. https://doi.org/10.1016/j.str.2010.05.010

Suryavanshi, S., Eddé, B., Fox, L. A., Guerrero, S., Hard, R., Hennessey, T., Kabi, A., Malison, D., Pennock, D., Sale, W. S., Wloga, D., & Gaertig, J. (2010). Tubulin Glutamylation Regulates Ciliary Motility by Altering Inner Dynein Arm Activity. *Current Biology*, *20*(5), 435–440. https://doi.org/10.1016/j.cub.2009.12.062

Tachiwana, H., Osakabe, A., Kimura, H., & Kurumizaka, H. (2008). Nucleosome formation with the testis-specific histone H3 variant, H3t, by human nucleosome assembly proteins in vitro. *Nucleic Acids Research*, *36*(7), 2208. https://doi.org/10.1093/NAR/GKN060

Tanaka, T., Hozumi, Y., Martelli, A. M., Iino, M., & Goto, K. (2019). Nucleosome assembly proteins NAP1L1 and NAP1L4 modulate p53 acetylation to regulate cell fate. *Biochimica et Biophysica Acta - Molecular Cell Research*, *1866*(12). https://doi.org/10.1016/j.bbamcr.2019.118560

References

Tanco, S., Tort, O., Demol, H., Aviles, F. X., Gevaert, K., Van Damme, P., & Lorenzo, J. (2015). C-terminomics Screen for Natural Substrates of Cytosolic Carboxypeptidase 1 Reveals Processing of Acidic Protein C termini. *Molecular & Cellular Proteomics : MCP*, *14*(1), 177–190. https://doi.org/10.1074/mcp.M114.040360

Tas, R. P., Chazeau, A., Cloin, B. M. C., Lambers, M. L. A., Hoogenraad, C. C., & Kapitein, L. C. (2017). Differentiation between Oppositely Oriented Microtubules Controls Polarized Neuronal Transport. *Neuron*, *96*(6), 1264-1271.e5. https://doi.org/10.1016/j.neuron.2017.11.018

Taylor, M. S., Altukhov, I., Molloy, K. R., Mita, P., Jiang, H., Adney, E. M., Wudzinska, A., Badri, S., Ischenko, D., Eng, G., Burns, K. H., Fenyö, D., Chait, B. T., Alexeev, D., Rout, M. P., Boeke, J. D., & LaCava, J. (2018). Dissection of affinity captured LINE-1 macromolecular complexes. *ELife*, *7*. https://doi.org/10.7554/eLife.30094

Thakar, K., Karaca, S., Port, S. A., Urlaub, H., & Kehlenbach, R. H. (2013). Identification of CRM1-dependent Nuclear Export Cargos Using Quantitative Mass Spectrometry. *Molecular & Cellular Proteomics : MCP*, *12*(3), 664–678. https://doi.org/10.1074/mcp.M112.024877

Tillement, V., Remy, M.-H., Raynaud-Messina, B., Mazzolini, L., Haren, L., & Merdes, A. (2009). Spindle assembly defects leading to the formation of a monopolar mitotic apparatus. *Biology of the Cell*, *101*(1), 1–11. https://doi.org/10.1042/BC20070162

Tort, O., Tanco, S., Rocha, C., Bièche, I., Seixas, C., Bosc, C., Andrieux, A., Moutin, M. J., Avilés, F. X., Lorenzo, J., & Janke, C. (2014). The cytosolic carboxypeptidases CCP2 and CCP3 catalyze posttranslational removal of acidic amino acids. *Molecular Biology of the Cell*, *25*(19), 3017–3027. https://doi.org/10.1091/mbc.E14-06-1072

Trask, D. K., & Muller, M. T. (1988). Stabilization of type I topoisomerase-DNA covalent complexes by actinomycin D. *Proceedings of the National Academy of Sciences*, *85*(5), 1417–1421. https://doi.org/10.1073/PNAS.85.5.1417

Turk, B. (2006). Targeting proteases: Successes, failures and future prospects. In *Nature Reviews Drug Discovery* (Vol. 5, Issue 9, pp. 785–799). https://doi.org/10.1038/nrd2092

Valenstein, M. L., & Roll-Mecak, A. (2016). Graded Control of Microtubule Severing by Tubulin Glutamylation. *Cell*, *164*(5), 911–921. https://doi.org/10.1016/j.cell.2016.01.019

Valero, J., Berciano, M. T., Weruaga, E., Lafarga, M., & Alonso, J. R. (2006). Pre-neurodegeneration of mitral cells in the pcd mutant mouse is associated with DNA damage, transcriptional repression, and reorganization of nuclear speckles and Cajal bodies. *Molecular and Cellular Neurosciences*, *33*(3), 283–295. https://doi.org/10.1016/j.mcn.2006.08.002

van der Laan, S., Dubra, G., & Rogowski, K. (2019). Tubulin glutamylation: A skeleton key for neurodegenerative diseases. In *Neural Regeneration Research* (Vol. 14, Issue 11, pp. 1899–1900). Wolters Kluwer Medknow Publications. https://doi.org/10.4103/1673-5374.259611

van Dijk, J., Miro, J., Strub, J.-M. M., Lacroix, B., van Dorsselaer, A., Edde, B., & Janke, C. (2008). Polyglutamylation is a post-translational modification with a broad range of substrates. *The Journal of Biological Chemistry*, *283*(7), 3915–3922. https://doi.org/10.1074/jbc.M705813200

van Dijk, J., Rogowski, K., Miro, J., Lacroix, B., Eddé, B., & Janke, C. (2007). A targeted multienzyme mechanism for selective microtubule polyglutamylation. *Molecular Cell*, *26*(3), 437–448. https://doi.org/10.1016/j.molcel.2007.04.012

Varela, I., Cadiñanos, J., Pendás, A. M., Gutiérrez-Fernández, A., Folgueras, A. R., Sánchez, L. M., Zhou, Z., Rodríguez, F. J., Stewart, C. L., Vega, J. A., Tryggvason, K., Freije, J. M. P., & López-Otín, C. (2005). Accelerated ageing in mice deficient in Zmpste24 protease is linked to p53 signalling activation. *Nature*, *437*(7058), 564–568. https://doi.org/10.1038/nature04019

Vendrell, J., Querol, E., & Avileés, F. X. (2000). Metallocarboxypeptidases and their protein inhibitors: Structure, function and biomedical properties. *Biochimica et Biophysica Acta - Protein Structure and Molecular Enzymology*, *1477*(1–2), 284–298. https://doi.org/10.1016/S0167-4838(99)00280-0

Verdone, L., Caserta, M., & di Mauro, E. (2005). Role of histone acetylation in the control of gene expression. *Biochemistry and Cell Biology = Biochimie et Biologie Cellulaire*, *83*(3), 344–353. https://doi.org/10.1139/O05-041

Verhey, K. J., & Gaertig, J. (2007). The tubulin code. In *Cell Cycle* (Vol. 6, Issue 17, pp. 2152–2160). Taylor and Francis Inc. https://doi.org/10.4161/cc.6.17.4633

Villagrá, N. T., Berciano, J., Altable, M., Navascués, J., Casafont, I., Lafarga, M., & Berciano, M. T. (2004). PML bodies in reactive sensory ganglion neurons of the Guillain- Barré syndrome. *Neurobiology of Disease*, *16*(1), 158–168. https://doi.org/10.1016/j.nbd.2004.02.005

Vogel, P., Hansen, G., Fontenot, G., & Read, R. (2010). Tubulin tyrosine ligase-like 1 deficiency results in chronic rhinosinusitis and abnormal development of spermatid flagella in mice. *Veterinary Pathology*, *47*(4), 703–712. https://doi.org/10.1177/0300985810363485

Walker, R. A., O'Brien, E. T., Pryer, N. K., Soboeiro, M. F., Voter, W. A., Erickson, H. P., & Salmon, E. D. (1988). Dynamic instability of individual microtubules analyzed by video light microscopy: rate constants and transition frequencies. *The Journal of Cell Biology*, *107*(4), 1437–1448. https://doi.org/10.1083/jcb.107.4.1437

References

Wang, L. L., Jin, X. H., Cai, M. Y., Li, H. G., Chen, J. W., Wang, F. W., Wang, C. Y., Hu, W. W., Liu, F., & Xie, D. (2018). AGBL2 promotes cancer cell growth through IRGM-regulated autophagy and enhanced Aurora A activity in hepatocellular carcinoma. *Cancer Letters*, *414*, 71–80.

Wang, R., Lin, L., Zheng, Y., Cao, P., Yuchi, Z., & Wu, H. Y. (2020). Identification of 2-PMPA as a novel inhibitor of cytosolic carboxypeptidases. *Biochemical and Biophysical Research Communications*, *533*(4), 1393–1399. https://doi.org/10.1016/j.bbrc.2020.10.029

Willsey, J. J., & State, M. W. (2015). Autism spectrum disorders: From genes to neurobiology. In *Current Opinion in Neurobiology* (Vol. 30, pp. 92–99). Elsevier Ltd. https://doi.org/10.1016/j.conb.2014.10.015

Wloga, D., Webster, D. M., Rogowski, K., Bré, M. H., Levilliers, N., Jerka-Dziadosz, M., Janke, C., Dougan, S. T., & Gaertig, J. (2009). TTLL3 Is a Tubulin Glycine Ligase that Regulates the Assembly of Cilia. *Developmental Cell*, *16*(6), 867–876. https://doi.org/10.1016/j.devcel.2009.04.008

Wu, H. Y., Rong, Y., Correia, K., Min, J., & Morgan, J. I. (2015). Comparison of the enzymatic and functional properties of three cytosolic carboxypeptidase family members. *The Journal of Biological Chemistry*, *290*(2), 1222–1232. https://doi.org/10.1074/jbc.M114.604850

Wu, H. Y., Wang, T., Li, L., Correia, K., & Morgan, J. I. (2012). A structural and functional analysis of Nna1 in Purkinje cell degeneration (pcd) mice. *FASEB Journal*, *26*(11), 4468–4480. https://doi.org/10.1096/fj.12-205047

Wu, H. Y., Wei, P., & Morgan, J. I. (2017). Role of Cytosolic Carboxypeptidase 5 in Neuronal Survival and Spermatogenesis. *Scientific Reports*, *7*(1), 1–14. https://doi.org/10.1038/srep41428

Wu, J., & Akhmanova, A. (2017). Microtubule-Organizing Centers. *Annual Review of Cell and Developmental Biology*, *33*(1), 51–75. https://doi.org/10.1146/annurev-cellbio-100616-060615

Wu, S., Zhang, C., Xu, D., & Guo, H. (2010). Catalysis of carboxypeptidase A: Promoted-water versus nucleophilic pathways. *Journal of Physical Chemistry B*, *114*(28), 9259–9267. https://doi.org/10.1021/jp101448j

Wu, X., Xiang, X., & Hammer, J. A. (2006). Motor proteins at the microtubule plus-end. In *Trends in Cell Biology* (Vol. 16, Issue 3, pp. 135–143). Trends Cell Biol. https://doi.org/10.1016/j.tcb.2006.01.004

Xia, P., Ye, B., Wang, S., Zhu, X., Du, Y., Xiong, Z., Tian, Y., & Fan, Z. (2016). Glutamylation of the DNA sensor cGAS regulates its binding and synthase activity in antiviral immunity. *Nature Immunology*, *17*(4), 369–378. https://doi.org/10.1038/ni.3356

Xiong, Z., Xia, P., Zhu, X., Geng, J., Wang, S., Ye, B., Qin, X., Qu, Y., He, L., Fan, D., Du, Y., Tian, Y., & Fan, Z. (2020). Glutamylation of deubiquitinase BAP1 controls self-renewal of hematopoietic stem cells and hematopoiesis. *The Journal of Experimental Medicine*, *217*(2). https://doi.org/10.1084/jem.20190974

Yamada, M., Sato, T., Shimohata, T., Hayashi, S., Igarashi, S., Tsuji, S., & Takahashi, H. (2001). Interaction between neuronal intranuclear inclusions and promyelocytic leukemia protein nuclear and coiled bodies in CAG repeat diseases. *American Journal of Pathology*, *159*(5), 1785–1795. https://doi.org/10.1016/S0002-9440(10)63025-8

Yang, W. T., Hong, S. R., He, K., Ling, K., Shaiv, K., Hu, J. H., & Lin, Y. C. (2021). The Emerging Roles of Axonemal Glutamylation in Regulation of Cilia Architecture and Functions. In *Frontiers in Cell and Developmental Biology* (Vol. 9, p. 429). Frontiers. https://doi.org/10.3389/fcell.2021.622302

Ye, B., Li, C., Yang, Z., Wang, Y., Hao, J., Wang, L., Li, Y., Du, Y., Hao, L., Liu, B., Wang, S., Xia, P., Huang, G., Sun, L., Tian, Y., & Fan, Z. (2014). Cytosolic carboxypeptidase CCP6 is required for megakaryopoiesis by modulating Mad2 polyglutamylation. *Journal of Experimental Medicine*, *211*(12), 2439–2454. https://doi.org/10.1084/jem.20141123

Ye, B., Liu, B., Hao, L., Zhu, X., Yang, L., Wang, S., Xia, P., Du, Y., Meng, S., Huang, G., Qin, X., Wang, Y., Yan, X., Li, C., Hao, J., Zhu, P., He, L., Tian, Y., & Fan, Z. (2018). Klf4 glutamylation is required for cell reprogramming and early embryonic development in mice. *Nature Communications*, *9*(1), 1261. https://doi.org/10.1038/s41467-018-03008-2

Zhang, H., Ren, Y., Pang, D., & Liu, C. (2014). Clinical implications of AGBL2 expression and its inhibitor latexin in breast cancer. *World Journal of Surgical Oncology*, *12*(1), 142. https://doi.org/10.1186/1477-7819-12-142

Zhao, X., Onteru, S. K., Dittmer, K. E., Parton, K., Blair, H. T., Rothschild, M. F., & Garrick, D. J. (2012). A missense mutation in AGTPBP1 was identified in sheep with a lower motor neuron disease. *Heredity*, *109*(3), 156–162. https://doi.org/10.1038/hdy.2012.23

Zhu, X., & Kaverina, I. (2013). Golgi as an MTOC: Making microtubules for its own good. In *Histochemistry and Cell Biology* (Vol. 140, Issue 3, pp. 361–367). Springer. https://doi.org/10.1007/s00418-013-1119-4